HAL
open science

Properties of suspension plasma sprayed zirconia coatings using different plasma torches

Pawel Sokolowski

To cite this version:

Pawel Sokolowski. Properties of suspension plasma sprayed zirconia coatings using different plasma torches. Materials. Université de Limoges; Uniwersytet Wroclawski, 2016. English. NNT : 2016LIMO0133 . tel-01953309

HAL Id: tel-01953309

https://theses.hal.science/tel-01953309

Submitted on 12 Dec 2018

HAL is a multi-disciplinary open access archive for the deposit and dissemination of scientific research documents, whether they are published or not. The documents may come from teaching and research institutions in France or abroad, or from public or private research centers.

L'archive ouverte pluridisciplinaire **HAL**, est destinée au dépôt et à la diffusion de documents scientifiques de niveau recherche, publiés ou non, émanant des établissements d'enseignement et de recherche français ou étrangers, des laboratoires publics ou privés.

Thèse de doctorat

Université de Limoges

Université de Limoges

École Doctorale Sciences et Ingénierie en Matériaux, Mécanique, Énergétique et Aéronautique (ED 522)

Laboratoire Sciences des Procédés Céramiques et Traitements de Surface

Thèse pour obtenir le grade de

Docteur de l'Université de Limoges

Discipline / Spécialité :Sciences des Matériaux

Présentée et soutenue par

Paweł Sokołowski

Le 25 novembre 2016

Properties of suspension plasma sprayed zirconia coatings using different plasma torches

Thèse dirigée par

Professeur Lech Pawłowski et Professeur Andrzej Ambroziak

JURY :

Président du jury

M. Zbigniew MIRSKI, Professeur, Politechnika Wrocławska (Pologne)

Rapporteurs

M. Robert VASSEN, Professeur, Forschungszentrum Jülich (Allemagne)

M. Igor SMUROV, Professeur, École Nationale d'Ingénieurs de Saint-Etienne (France)

M. Thomas LAMPKE, Professeur, Technische Universität Chemnitz (Allemagne)

Membres du jury

M. Andrzej AMBROZIAK, Professeur, Politechnika Wrocławska (Pologne)

M. Lech PAWŁOWSKI, Professeur, Université de Limoges (France)

Wrocław University of Science and Technology
Faculty of Mechanical Engineering

and

University of Limoges
Faculty of Science and Technology
Laboratory of Science of Ceramic Processing and Surface Treatments

Properties of suspension plasma sprayed zirconia coatings using different plasma torches

PhD thesis

Paweł Sokołowski

Scientific supervisors:

Prof. Andrzej Ambroziak (Wrocław University of Science and Technology)

Prof. Lech Pawłowski (University of Limoges)

Additional supervisor:

Dr. Stefan Kozerski (Wrocław University of Science and Technology)

Wrocław 2016

To my beloved wife and family…

GENERAL INTRODUCTION

In this PhD thesis several scientific issues regarding Suspension Plasma Sprayed (SPS) zirconia coatings were studied. The coatings were analyzed mainly in terms of the application as insulating top-coat of Thermal Barrier Coatings (TBC's). These multi-layer coatings are applied onto the metallic parts of e.g. gas turbines to protect them against high temperature loads caused by the hot exhaust gases. But the initial assessment of the possibility of the use of Suspension Plasma Spraying to produce electrolyte layer in Solid Oxide Fuel Cells was done also. SOFC's seem to be the most promising fuel cell types currently. (*See Chapter 1-2 with the literature review)*

The first important research goal was to analyze the possibility of producing coatings being various in terms of the microstructure. The main aim was to obtain coatings characterized by very porous and irregular structure (called columnar-like) but also very dense and homogeneous coatings with typical two-zones microstructure. For this purpose two zirconia powders were used: (i) fully yttria-stabilized zirconia and (ii) ytrria-ceria-stabilized zirconia. The powders had different chemical composition, particle size and morphology. These powders were used for a suspension formulation. The other variable in the spray process was suspension concentration. The suspension with a solid content in range of 2.5 and 30 wt. % were prepared and sprayed. All suspensions were home-produced. A very important concept of this work was the use of four various, commercially-available, plasma torches, namely: (i) SG-100, (ii) TriplexPro-200, (iii) Axial III and (iv) WSP-H 500. The torches were different in terms of design, electric power, plasma stabilization mode and the suspension injection angle. Due to the big differences between plasma torches and SPS set-ups the spray process parameters were chosen in each case individually. The last variable in the experiment design was the topography and roughness of substrate in order to evaluate its influence on the coatings growth-up mechanisms. The substrates were prepared prior to spraying by: (i) grit-blasting, (ii) laser-treatment and by (iii) grinding. The wide

spray experiment allowed complex analysis of SPS coatings microstructure, coatings growth-up mechanisms and the development of SPS process itself. (*All details are described in Chapters 3-4*)

In the next step the careful microstructure characterization was performed, starting from the basic studies of thickness, porosity, phase and chemical composition. Then, more advanced studies were performed like for example: the quantitative phase analysis, crystal lattice parameters determination and the studies of grain size, morphology and orientation. The analysis of coating free-surface was also performed. The qualitative investigations of coating roughness and the observations of coating topographies were carried-out. The studies enabled to analyze the formation mechanisms of columnar-like and two-zones coatings in Suspension Plasma Spraying. (*Please, see Chapter 6.1 with the coating microstructure analysis*)

In the following part of studies the selected properties of various zirconia coatings were determined. The main goal was to analyze thermal transport properties as these one's are one of the most important in case of Thermal Barrier Coatings. The studies were performed by indirect laser flash method (LFA). But in case of LFA analysis there is a need to specify many different material properties prior to the measurements. In this work all necessary thermophysical properties (density, specific heat capacity and thermal dilatation) were determined experimentally for the purpose of LFA. The thermal transport properties were also verified by the use of analytical method called "response method". At the end of experimental work, the preliminary analysis of mechanical properties (Young's modulus and Martens hardness) was performed. (*The results of the analysis of coating properties are described in Chapter 6.2*).

The studies allowed to analyze the influence of spray parameters on the coating microstructure. The correlation of coating properties and coating microstructure was also possible. Finally, the ideas for further works were proposed. (*Conclusions are collected in Chapter 7*).

At the end of this PhD thesis the set of five articles is presented. These papers were prepared based on the mentioned studies. (S*ee Appendix*).

The presented PhD thesis is a result of collaboration between Wroclaw University of Science and Technology (Poland) and University of Limoges (France). The studies were

supported by French Embassy in Warsaw (Poland) and were realized under joint PhD program, namely “co-tutelle”. The work was financed by the research grant provided by National Science Centre in Poland in term of Grant “Sonata” (UMO-2013/11/D/ST8/03400). The studies were performed in an international cooperation with different research teams:

- spraying by Axial III was performed at the University West in a research group of prof. Per Nylen and with help of Eng. Stefan Bjorklund,
- spraying by WSP-H500 was realized at Institute of Plasma Physics in a research group of prof. Thomas Chraska and with help of Dr. Radek Musalek,
- Electron Backscatter Diffraction studies were carried-out at Chemnitz University of Technology in a research group of prof. Thomas Lampke and with help of Dr. Dagmar Dietrich,
- Instrumental Indentation Testing was done at University of Lille in a research group of prof. Didier Chicot and help of Dr. Alberto Meijas.

WPROWADZENIE

W rozprawie doktorskiej podjęto kilka istotnych problemów badawczych dotyczących powłok ceramicznych wytwarzanych metodą natryskiwania plazmowego z zawiesin (Suspension Plasma Spraying, SPS). Obiektem badań były powłoki na bazie stabilizowanego tlenku cyrkonu, które analizowane były głównie pod kątem zastosowania ich jako zewnętrznej warstwy izolacyjnej w powłokowych barierach cieplnych. Te wielowarstwowe systemy używane są w turbinach gazowych, głównie do ochrony elementów metalicznych przed działaniem wysokiej temperatury powstającej w czasie procesu spalania. Wykonano też wstępną ocenę możliwości zastosowania powłok jako elektrolitu w stałotlenkowych ogniwach paliwowych. *(Rozdział 1-2)*

Pierwszym z podjętych zagadnień badawczych było określenie możliwości modyfikowania mikrostruktury powłok poprzez zastosowanie różnych parametrów w procesie natryskiwania. Główny cel stanowiło osiągnięcie powłok zróżnicowanych pod względem budowy wewnętrznej w porównaniu do klasycznej, dwustrefowej, struktury. W tym celu wykorzystano dwa różne rodzaje proszków stabilizowanego tlenku cyrkonu. Użyte proszki to: (i) tlenek cyrkonu stabilizowany tlenkiem itru oraz (ii) tlenek cyrkonu stabilizowany tlenkiem itru oraz tlenkiem ceru. Proszki różniły się składem chemicznym, wielkością oraz morfologią cząsteczek. Na bazie opisanych proszków przygotowano zawiesiny. Jako kolejny parametr w procesie przyjęto zawartość fazy stałej w zawiesinie. W procesie SPS zostały użyte zawiesiny o koncentracji od 2.5 do 30 % wag. Zawiesiny zostały przygotowane indywidualnie w laboratorium. Bardzo istotnym założeniem projektu było wykorzystanie czterech różnych palników plazmowych, tj. SG-100, TriplexPro-200, Axial III oraz WSP-H 500. Palniki te różnią się konstrukcją, generowaną mocą elektryczną, rodzajem stabilizacji łuku plazmowego, a także sposobem wstrzeliwania zawiesiny w strumień plazmy. W związku z różną konfiguracją stanowisk oraz różnicami w budowie wspomnianych palników konieczne było dobranie odpowiednich parametrów procesu indywidualnie

dla każdego stanowiska. Ostatnim parametrem w procesie było zastosowanie podłoży charakteryzujących się różną topografią powierzchni oraz chropowatością w celu oceny ich wpływu na formowanie struktury powłoki. Wykorzystano podłoża stalowe, które przed procesem natryskiwania zostały oddane obróbce: (i) strumieniowo-ściernej, (ii) szlifowaniu, (iii) mikroobróbce laserowej. Szeroki plan eksperymentu umożliwił kompleksową ocenę mikrostruktury powłok, mechanizmu formowania powłok oraz możliwości rozwoju metody natryskiwania plazmowego z zawiesin (SPS). *(Rozdział 3-5)*

W dalszej części wykonano badania mikrostruktury natryskanych powłok, począwszy od podstawowych własności m.in. grubości, porowatości, morfologii, składu fazowego, czy składu chemicznego. W dalszej kolejności przeprowadzono zaawansowaną analizę, m. in. ilościową analizę fazową, określenie parametrów komórek elementarnych, wielkości, czy orientacji ziaren w strukturze powłok. Dodatkowo wykonane zostały badania topografii powierzchni oraz jakościowa ocena chropowatości powłok. Badania te posłużyły do analizy osadzania się cząsteczek proszku na powierzchni podłoża oraz oceny mechanizmów formowania różnych typów powłok w procesie natryskiwania plazmowego z zawiesin (SPS). *(Rozdział 6.1)*

Kolejnym punktem badań było określenie wybranych własności powłok o zróżnicowanej budowie wewnętrznej. Najważniejszym elementem była analiza dyfuzyjności i przewodnictwa cieplnego powłok. Badania te zostały wykonane z użyciem pośredniej laserowej metody impulsowej (Laser Flash Analysis, LFA). Metoda ta wymaga określenia wielu danych materiałowych. W celu możliwie dokładnego określenia własności cieplnych wykonano szereg badań własności termofizycznych, tj. analiza gęstości powłok, pomiary pojemności cieplnej, czy liniowej rozszerzalności cieplnej. Otrzymane wyniki własności cieplnych zostały zweryfikowane również analitycznie z użyciem tzw. response method. W końcowej fazie prac wykonano także badania wybranych własności mechanicznych powłok, tj. twardości oraz modułu Younga, które są uzupełnieniem wiedzy na temat powłokowych barier cieplnych wytwarzanych metodą SPS. *(Rozdział 6.2)*

Przeprowadzenie badań pozwoliło na określenie wpływu budowy wspomnianych powłok na ich własności użytkowe, a także ocenę potencjału aplikacyjnego metody SPS oraz proponowanych rozwiązań w przemyśle. *(Rozdział 7)*

Pracę kończy zbiór artykułów, które zostały przygotowane oraz opublikowane na podstawie przeprowadzonych badań. *(Załaczniki)*

Niniejsza praca została zrealizowana we współpracy pomiędzy Politechniką Wrocławską, a Uniwersytetem Limoges we Francji. Całość praca realizowana była pod opieką Ambasady Francji w Warszawie w ramach programu podwójnego dyplomowania „*Co-tutelle*". Prace były finansowane z projektu "Sonata" (UMO-2013/11/D/ST8/03400) przyznanego przez Narodowe Centrum Nauki. Badania były realizowane w międzynarodowej współpracy z różnymi zespołami badawczymi:

- natryskiwanie z użyciem palnika Axial III odbyło się na University West w grupie badawczej prof. Pera Nylena oraz z pomocą inż. Stefana Bjorklunda,
- natryskiwanie z użyciem palnika WSP-H 500 odbyło się w Institute of Plasma Physics w grupie badawczej prof. Thamasa Chraski z pomocą dr Radka Musalka,
- badania metodą dyfrakcji elektronów wstecznie rozproszonych (EBSD) przeprowadzone zostały na Chemnitz University of Technology w grupie badawczej prof. Thomasa Lampke z pomocą dr Dagmar Dietrich,
- badania z wykorzystaniem metody nanoindentacji zostały przeprowadzone na University of Lille w grupie badawczej prof. Didiera Chicot z pomocą dr Alberto Meijasa.

RÉSUMÉ

Dans cette thèse plusieurs questions scientifiques concernant la projection plasma de suspensions (SPS) revêtements de zircone ont été étudiées. Les revêtements ont été analysées principalement en termes de l'application comme isolant top-coat des revêtements de barrière thermique (TBC). Ces revêtements multicouches sont appliqués sur les parties métalliques par exemple, Les turbines à gaz pour les protéger contre les charges thermiques élevées provoquées par les gaz d'échappement chauds. Mais l'évaluation initiale de la possibilité de l'utilisation de la projection plasma de suspensions pour produire la couche d'électrolyte en pile à combustible à oxyde solide (SOFC) a été fait aussi. SOFC semblent être les types de piles à combustible les plus prometteurs actuellement. (Voir le chapitre 1-2 de la revue de la littérature).

Le premier objectif de recherche important était d'analyser la possibilité de produire des revêtements étant différents en termes de la microstructure. L'objectif principal était d'obtenir des revêtements caractérisés par une structure très poreuse et irrégulière (appelé colonnaires-like), mais aussi des revêtements très denses et homogènes avec typique, deux zones microstructure. A cet effet, les deux poudres de zircone ont été utilisées: (i) l'oxyde de zirconium entièrement stabilisé à l'yttria et (ii) de la zircone yttria-oxyde de cérium stabilisé. Les poudres ont des compositions chimiques différentes, la taille des particules et leur morphologie. Ces poudres ont été utilisées pour une formulation de suspension. L'autre variable dans le procédé de pulvérisation est la concentration de la suspension. La suspension avec une teneur en matières solides dans la gamme de 2,5 et 30 en poids % ont été préparées et projetée. Toutes les suspensions ont été produites au laboratoire. Un concept très important de ce travail est l'utilisation de quatre différents, disponibles dans le commerce, des torches à plasma, à savoir: (i) SG-100, (ii) TriplexPro-200, (iii) Axial III et (iv) WSP-H 500. Les torches étaient différentes en termes de conception, l'énergie électrique, le mode de stabilisation du plasma et l'angle d'injection de suspension. En raison des grandes

différences entre les torches à plasma et SPS set-ups les paramètres du procédé de pulvérisation ont été choisis dans chaque cas individuellement. La dernière variable dans la conception de l'expérience était la topographie et la rugosité du substrat afin d'évaluer son influence sur les revêtements des mécanismes de croissance-up. Les substrats ont été préparés avant la projection par: (i) le grenaillage, (ii) le traitement au laser et par (iii) le broyage. L'expérience de projection large a permis une analyse complexe de SPS revêtements microstructure, des mécanismes de croissance des revêtements et le développement de processus SPS lui-même. (Tous les détails sont décrits dans les chapitres 3-4)

Dans l'étape suivante, la caractérisation de la microstructure minutieuse a été réalisée à partir des études de base d'épaisseur, la porosité, la phase et la composition chimique. Ensuite, des études plus poussées ont été réalisées comme par exemple: l'analyse quantitative de phase, les paramètres de maille cristalline de détermination et les études de la taille des grains, de la morphologie et l'orientation. L'analyse du revêtement de surface libre a également été réalisée. Les enquêtes qualitatives de la rugosité du revêtement et les observations des topographies de revêtement ont été-out. Les études ont permis d'analyser les mécanismes de formation des revêtements colonnaires-like et-deux zones en suspension pulvérisation de plasma. (S'il vous plaît, voir le chapitre 6.1 avec l'analyse de la microstructure de revêtement)

Dans la suite des études des propriétés sélectionnées de divers revêtements de zircone ont été déterminées. L'objectif principal était d'analyser les propriétés de transport thermiques ces ses sont l'un des plus importants dans le cas des revêtements de barrière thermique. Les études ont été réalisées par la méthode flash laser indirecte (LFA). Mais dans le cas de l'analyse LFA, il est nécessaire de préciser de nombreuses différentes propriétés des matériaux avant les mesures. Dans ce travail, toutes les propriétés thermodynamiques nécessaires (densité, capacité thermique spécifique et dilatation thermique) ont été déterminées expérimentalement dans le but de LFA. Les propriétés de transport thermique ont également été vérifiées par l'utilisation de la méthode d'analyse dite «méthode de réponse." A la fin du travail expérimental, l'analyse préliminaire des propriétés mécaniques (le module d'élasticité de Young et de dureté Martens) a été réalisée. (Les résultats de l'analyse des propriétés de revêtement sont décrits dans le chapitre 6.2).

Les études ont permis d'analyser l'influence des paramètres de pulvérisation sur la microstructure du revêtement. La corrélation de revêtement des propriétés et le revêtement microstructure est également possible. Enfin, les idées pour d'autres travaux ont été proposées. (Conclusion sont collectées au chapitre 7).

A la fin de cette thèse l'ensemble des cinq articles est présenté. Ces documents ont été préparés sur la base des études mentionnées. (Voir l'annexe).

La thèse de doctorat présentée est le résultat d'une collaboration entre l'Université de Wroclaw de Science et Technologie (Pologne) et de l'Université de Limoges (France). Les études ont été réalisées sous la supervision de l'ambassade française à Varsovie (Pologne) et le programme de doctorat conjoint, à savoir “co-tutelle”. Le travail a été financé par la subvention de recherche fourni par le Centre national de la science en Pologne en terme de Grant "Sonata" (UMO 2013/11 / D / ST8 / 03400). Les études ont été réalisées dans une coopération internationale avec les différentes équipes de recherche:

- Pulvérisation par Axial III a été réalisée à l'Université de l'Ouest dans un groupe de recherché de prof Per Nylen et avec l'aide de Stefan Bjorklund,

- Pulvérisation par WSP-H500 a été réalisée à l'Institut de physique des plasmas dans un groupe de recherché de prof Thomas Chraska et avec l'aide du Dr Radek Musalek,

- Études Electron rétrodiffusion Diffraction ont été réalisées-out à l'Université de Technologie de Chemnitz dans un groupe de recherché de prof Thomas Lampke et avec l'aide du Dr Dagmar Dietrich,

- Instrumental Test indentation a été fait à l'Université de Lille dans un groupe de recherché de prof Didier Chicot et aide du Dr Alberto Meijas.

ACKNOWLEDGEMENTS

The PhD studies were a life-changing experience for me. During this period I had a possibility to meet many great people who supported and guidance me. I would like to express my special thanks to these people.

I would like to acknowledge first my PhD supervisors. Prof. Lech Pawłowski (University of Limoges), who gave me the possibility to work on this topic and shared with me his great experience in thermal spraying. When I had too many ideas in my mind he kept me going forward and straight with my studies, saying "finish first you PhD". Prof. Andrzej Ambroziak (Wroclaw University of Technology) for his enthusiasm and constant support. He learned me that "you will not succeed If you do not try". I would like to acknowledge also help of my additional supervisor, Dr Stefan Kozerski (Wroclaw University of Technology). He travelled with me around Europe in order to help with spraying. I learned from him many practical aspects about thermal spraying.

During my PhD studies I visited different laboratories and research groups. They were very open for me, helped me a lot with my work and allowed learning many interesting things about thermal spraying. So I would like to acknowledge their help, in particular:

- prof. Per Nylen, Mr. Stefan Bjorklund and Mr. Jonas Olsson (Univesrity West, Sweden) for their help with spraying by Axial III,
- prof. Thomas Chraska, Dr. Radek Musalek, Mr. Marek Janata, Mr. Tomas Tesar, Jan Medricky, Zdenek Pala and Frantisek Lukac (Institute of Plasma Physics in Prague, Czech Republic) for their help with spraying by WSP-H500 and XRD studies,
- prof. Thomas Lampke and Dr. Dagmar Dietrich (Chemnitz University of Technology, Germany) for their help with Electron Backscatter Diffraction studies

- prof. Didier Chicot and Dr. Alberto Meijas (University of Lille, France) for their help with Instrumental Indentation Testing.

My sincere thanks to all my friends from Wrocław and Limoges for great atmosphere and for helping me with the organization of all travels during my PhD thesis. First to my friend Rolando T. Candidato Jr., for all long days and funny moments in our laboratory. I learned a lot from you! Special thanks to Leszek Łatka, Marcin Winnicki and Aleksnadra Małachowska who were my "emergency group" at my home University. Małgorzata Piechowiak, Joanna Krówka and Jayanth Channagiri are acknowledged for their great support and friendship that I received in Limoges. The list of my friends that I would like acknowledge is much longer of course: Olivier Noguera, Jess Gambe, Andrzej Warchał, Marcin Korzeniowski, Ewa Harapińska, Tomasz Piwowarczyk, Tomasz Wojdat, Paweł Kustroń, Kasia Żegleń, Monika Michalak, Salyani Mahmod, Mohammed Reda Zaki, Karolina Kazak, Robert Kaczmarek, Irmina Gutkowski, I could always count on you guys, thanks so much!

But my special thanks are dedicated to my family and my wife. My parents, Ewa and Artur, my brother Jakub and my lovely wife Małgosia, who support me every single day and are proud that I am doing what I am doing. In fact it is me, who is proud and very lucky to have such great family.

Finally, I would like to acknowledge French Embassy in Warsaw (Poland) for great joint PhD program, namely "co-tutelle" and your scholarship. I thank also the financial support from National Science Centre in Poland in term of Grant "Sonata" (UMO-2013/11/D/ST8/03400).

CONTENTS

ABBREVIATIONS **1**

SYMBOLS **3**

LIST OF FIGURES **5**

LIST OF TABLES **9**

CHAPTER 1. INTRODUCTION **10**

1.1. Gas turbines and Thermal Barrier Coatings **10**

1.2. Solid Oxide Fuel Cells **13**

CHAPTER 2. SUSPENSION PLASMA SPRAYING **16**

2.1. Powders and suspensions **17**

2.2. Modes of suspension injection **25**

2.3. Commercially available plasma torches **30**

2.4. Physical phenomena at spraying **32**

2.5. Key process parameters **32**

CHAPTER 3. Materials **34**

3.1. Fully yttria-stabilized zirconia **34**

3.2. Yttria-ceria-stabilized zirconia **36**

CHAPTER 4. THE AIM OF RESEARCH WORK **39**

CHAPTER 5. EXPERIMENTAL PROCEDURES **41**

5.1. Suspension manufacturing **41**

5.1.1. Powder characteristics 41

5.1.2. Suspension formulation 46

5.1.3. Zeta potential 47

5.2. Substrate preparation **48**

5.3. Thermal spraying **50**

5.3.1. Plasma torches and spray set-ups 50

5.3.2. Spray process parameters 57

5.3.3. Spray process design 59

5.4. Characterization of coatings **61**
5.4.1. Light microscopy (LM) 61
5.4.2. Scanning Electron Microscopy and Energy Dispersive X-Ray Spectrometry (SEM/EDS) 61
5.4.3. X-Ray Diffraction (XRD) and Rietveld refinement 62
5.4.4. Electron Backscatter Diffraction (EBSD) 63
5.4.5. Laser Scanning Confocal Microscopy (LSCM) 65
5.4.6. Shape From Shading (SFS) 65
5.4.7. Density measurements 66
5.4.8. Dilatometry (DIL) 67
5.4.9. Differential Scanning Calorimetry (DSC) 68
5.4.10. Laser Flash Analysis (LFA) 70
5.4.11. Instrumented Indentation Testing (IIT) 72

CHAPTER 6. RESULTS AND DISCUSSION **75**

6.1. Microstructure and growth-up mechanisms **75**
6.1.1, Coating morphology 75
6.1.2, Coating free-surface 82
6.1.3. Coating phase and chemical composition 84
6.1.4. Formation of columnar-like coatings 88
6.1.5 Formation of two-zones coatings 92

6.2. Properties of coatings **95**
6.2.1. Density 96
6.2.2. Specific heat capacity 97
6.2.3. Thermal expansion 98
6.2.4. Thermal transport properties 101
6.2.5. Hardness and Young modulus 105

CHAPTER 7. CONCLUSIONS **108**
7.1. Coatings microstructure 108
7.2. Coatings properties 110
7.3. Further works 111

REFERENCES **113**

APPENDIX **125**

ABBREVIATIONS

APS -Atmospheric Plasma Spraying

BC - Bond-Coat

BSE - Backscattered Electrons

CHFS - Continuous Hydrothermal Flow Synthesis

CI - Confidence Index

CMOS - Complementary Metal–Oxide–Semiconductor

CS - Cold Spraying

DSC - Differential Scanning Calorimetry

EBSD - Electron Back Scatter Diffraction

EDS - Energy-Dispersive X-Ray Spectroscopy

FEG - Field Emission Gun

FEPA - Federation Of The European Producers Of Abrasives

FS - Flame Spraying

HM - Martens Hardness

HVOF - High Velocity Oxygen Fuel

IEP - Isoelectric Point

IIT - Instrumented Indentation Testing

IQ - Image Quality

JCPDS - Joint Committee Of Powder Diffraction Standards

LFA - Laser Flash Analysis

LSCM - Laser Scanning Confocal Microscopy

MA - Mechanical Alloying

MDSC - Modulated Differential Scanning Calorimetry

MEK - Methylethylketone

MM - Mechanical Milling

PPS - Powder Plasma Spraying

RT - Room Temperature

SE - Secondary Electrons

SEM - Scanning Electron Microscope

SFS - Shape From Shading

SPS - Suspension Plasma Spraying

TBC - Thermal Barrier Coatings

TC - Top-Coat

TGO - Thermally Grown Oxide

XRD - X-Ray Diffraction

SYMBOLS

A - contact area [nm^2]

a - solid particle size [m]

A_2 - surface area corresponding to thermal diffusion time [-]

C - total compliance [-]

C_f - instrument compliance [-]

Cp - specific heat capacity [J/kg·K]

d_1 - substrate thicknesses [m]

d_2 - coating thicknesses [m]

dn_{10} - particle size; 10 % of powder particles (by number) below this particle size [μm]

dn_{50} - median particle size by number [μm]

dn_{90} -particle size; 90 % of powder particles (by number) below this particle size [μm]

dv_{10} - particle size; 10 % of powder particles (by volume) below this particle size [μm]

dv_{50} - median particle size by volume [μm]

dv_{50} - particle size; 90 % of powder particles (by volume) below this particle size [μm]

E_R - reduced elastic modulus [GPa]

fi - mass of the i-th constituent [%]

g - constant of gravity [m/s^2]

h – displacement of the indenter [nm]

HM - Martens Hardness [GPa]

n - total number of constituents [-]

P – applied load [mN]

P - porosity [%]

Ra - roughness parameter, mean roughness [μm]

Rz - roughness parameter, mean roughness depth [μm]

T - temperature [°C]

V - sedimentation speed [m/s]

α - thermal diffusivity [m2/s]

β - geometrical correction factor [-]

γ - geometrical correction factor depends on the Poisson's coefficient [-]

ΔL/L - thermal expansion [-]

ζ - zeta potential [mV]

η - dynamic viscosity [Pa·s]

λ - thermal conductivity [W/m·K]

π - 3.14159265 [-]

ρ - true density [kg/m^3]

ρ_{300} - bulk density at 300K [kg/m^3]

F_A - adhesion force [N]

F_D - drag force [N]

LIST OF FIGURES

Figure 1 The scheme of gas turbine main parts [2] 10
Figure 2 The influence of turbine inlet temperature on the turbine core power and efficiency (T_4 - turbine inlet temperature) [3] 11
Figure 3 The Thermal Barrier Coating System (by Sokołowski and Pawłowski [5]) 12
Figure 4 The scheme of the microstructural features of EB-PVD and APS zirconia coatings (by Sokołowski and Pawłowski [5]) 13
Figure 5 The operating principle of Solid Oxide Fuel Cell (by Sokołowski and Pawłowski[5], [9], inspired by [9]) 14
Figure 6 The relationship between Zeta potential and suspension behavior [59] 23
Figure 7 Two kinds of zirconia suspension: (a) well-stabilized suspension, (b) poorly-stabilized suspension (by Sokołowski and Pawłowski [5]) 24
Figure 8 The comparison of liquid stream injection (a) and atomization (b) [65] 26
Figure 9 The scheme presenting effective SPS process parameters (by Sokołowski and Pawłowski [5], inspired by [86]) 33
Figure 10 The phase diagram of ZrO_2 - Y_2O_3 system (with detailed version up to 10 mol. % of Y_2O_3) [89], [90] 35
Figure 11 Isothermal section of CeO2-Y2O3-ZrO2 ternary system at 1250°C [94] 36
Figure 12 Isothermal section of CeO2-Y2O3-ZrO2 ternary system at 1500°C [95] 37
Figure 13 The research methodology used in this PhD project 40
Figure 14 The morphology of YSZ powder produced by Tosoh (FEG-SEM, SE) [99] 41
Figure 15 YSZ powder particle size diagram: (a) volume-based particle size distribution and (b) number-based particle size distribution 42
Figure 16 The XRD diagram presenting the phase composition of YSZ powder in as-produced state 43
Figure 17 The morphology of YCeSZ powder produced by Oerlikon Metco (SEM, SE) 44
Figure 18 The SEM micrograph of milled YCeSZ powder (SEM, SE) 44

Figure 19 YCeSZ powder particle size diagram: (a) volume-based particle size distribution and (b) number-based particle size distribution 45
Figure 20 The XRD diagram of YCeSZ powder in initial stage 46
Figure 21 Suspension preparation procedure (powder pre-treatment applied if necessary) 47
Figure 22 The 3D substrate topography view after: grit-blasting (a), laser treatment (b) and grinding (c) 48
Figure 23 The substrates profiles: (a) grit- blasted, (b) laser treated (c) and grinded 49
Figure 24 SG-100 plasma torch with internal injection [102] 51
Figure 25 The SPS set-up equipped with SG-100 plasma torch; a – pneumatic system for suspension injection, b – plasma torch and sample fixture (University of Limoges) 51
Figure 26 TriplexPro-200 plasma torch design [103] (a) and the feedstock injection optimization of materials having high-melting point [104] (b) 52
Figure 27 The SPS set-up equipped with TriplexPro-200 plasma torch; a – pneumatic system for suspension injection, b – plasma torch and sample fixture (University of Limoges) 53
Figure 28 Axial III plasma torch with axial injection [105] 54
Figure 29 The SPS set-up equipped with Axial III plasma torch; a – commercial NanoFeed suspension injection system with peristaltic pump, b – plasma torch and sample fixture (University West, Trollhättan) 54
Figure 30 WSP-H 500 plasma torch operating principle [84] 55
Figure 31 The SPS set-up equipped with WSP-H 500 plasma torch; a – pneumatic system for suspension injection, b – plasma torch and sample fixture (Institute of Plasma Physics CAS, Prague) 56
Figure 32 The optimization of radial injection point by changing the injection pressure (by shadowgraphy): (a) 2.8 bars, (b) 3.0 bars, (c) 3.2 bars 56
Figure 33 The control of plasma jet, solvent flow and suspension injection 57
Figure 34 The example of the temperature history recorded during spraying (blue color - substrate rear surface and red color - at the sample front face) 59
Figure 35 The methodology of samples labeling 60
Figure 36 The example of coating thickness measured by the light microscopy (only one region of sample) 61

Figure 37 The example of porosity calculations by image analysis method (SEM, SE micrograph edited using ImageJ, sample WT101) 62
Figure 38 The interaction between the electron beam and polycrystalline material in EBSD method [107] 64
Figure 39 Shape From Shading technique: the procedure to reconstruct coating surface (a), 3D model of coating (b) (by Sokolowski et. al [99]) 66
Figure 40 The microstructure of YSZ powder plasma sprayed coating used for thermal expansion analysis (a) and the arrangement of measurements relative to the coating microstructure (b) (by Sokołowski et al. [109]) 68
Figure 41 The application range of Laser Flash method [111] 70
Figure 42 The methodology of thermal conductivity calculations in high-temperature range (up to 1000°C) 71
Figure 43 The interpretation of areal heat diffusion time used in response method that bases on LFA signal [114] 72
Figure 44 The multicycle nanoindentation test 73
Figure 45 The cross-sections of selected YSZ coatings deposited by SG-100 and TriplexPro-200 plasma torches (SE mode, 200x and 400x) 77
Figure 46 The cross-sections of selected YCeSZ coatings deposited by SG-100 and TriplexPro-200 plasma torches (SE, 200x and 400x) 78
Figure 47 The cross-sections of selected YSZ coatings deposited by Axial III and WSP-H500 plasma torches (SE, 200x and 400x) 79
Figure 48 The cross-sections of selected YCeSZ coatings deposited by Axial III and WSP-H500 (SE, 200x and 400x) 80
Figure 49 The deposition rate (thickness/pass) values obtained during spraying 81
Figure 50 The 3D views of columnar coatings surfaces reconstructed by Shape from Shading method (a - ST23, b - WT103, c - ST52) 83
Figure 51 The 3D views of two-zones coatings surfaces reconstructed by Shape from Shading method (a - TC102, b - AT203) 83
Figure 52 XRD diagram presenting phase composition of selected YSZ coatings 85
Figure 53 XRD diagram presenting phase composition of selected YCeSZ coatings 85
Figure 54 The different forms of stabilized zirconia [90] 87
Figure 55 The examples of EDS spectra of YSZ (a) and YCeSZ (b) coatings 88
Figure 56 The columnar-like coatings: WT101 (a) and WT103 (b) [109] 89

Figure 57 The forces acting particle at the plasma jet/substrate interface (a), mechanism of columnar-like coating growth at rough substrate (b) [33] 89
Figure 58 The EBSD analysis of columnar-like ST52 sample sprayed onto laser-treated substrate: (a) selection of area, (b) detailed crystallographic orientation map and (c) grain size distribution (volume-based) [99] 90
Figure 59 The growth of columns on the flat substrate (1,2,3 - subsequent stages of columns formation) [99] 91
Figure 60 EBSD analysis of columnar-like ST23 sprayed onto grinded substrate crystallographic orientation of grains (a), and texture analysis (b) [99] 91
Figure 61 The coatings characterized by two-zones microstructure: WC101 (a) and AC203 (b) [109] 92
Figure 62 The formation of conventional two-zone structure in Suspension Plasma Spraying [66] 92
Figure 63 EBSD analysis of two-zones TC102 coating: selection of test area (a), Inverse Pole Figure (b) and grain size distribution (c) [99] 93
Figure 64 EBSD analysis of two-zones AT102 coating: selection of test area (a), Inverse Pole Figure (b) and grain size distribution (c) [109] 94
Figure 65 The influence of the injection angle on the coating growth-up mechanism [109] 95
Figure 66 The evaluation of specific heat capacity values of YSZ(a), YCeSZ (b) [131] 98
Figure 67 The results of thermal expansion measurements of YSZ (a) and YCeSZ (b) coatings [131] 100
Figure 68 The YSZ samples selected for thermal transport properties studies [131] 101
Figure 69 Figure 55 The YCeSZ samples selected for thermal transport properties studies [131] 101
Figure 70 Thermal conductivity values of YSZ (a) and YCeSZ (b) coatings [131] 102
Figure 71 Analytical validation of thermal conductivity values. The example of YSZ (a) and YCeSZ (b) coating [131] 104
Figure 72 Examples of inverse of the contact stiffness versus reciprocal of the contact area for coatings having various microstructures 105
Figure 73 E-modulus vs. porosity for YSZ and YCeSZ coatings 106
Figure 74 Martens hardness vs. porosity for YSZ and YCeSZ coatings 107

LIST OF TABLES

Table 1 The summary of bottom-up and top-down processing methods (by Sokołowski and Pawłowski [5], inspired by [28]) 18
Table 2 The summary of mechanical and atomization injection modes based on the literature (by Sokołowski and Pawłowski [5]) 27
Table 3 The characteristic of suspension used for spraying 47
Table 4 The summarized characteristic of plasma torches that were used for the coating production (by Sokołowski and Pawłowski [5]) 57
Table 5 The detailed list of spray process parameters used for the coating production 58
Table 6 The design of experiment and coating nomenclature 60
Table 7 The thickness and porosity of coatings (red color - coatings having columnar-like microstructure; * - coatings that were not deposited correctly) 75
Table 8 The roughness parameters of obtained coatings (red color - coatings having columnar-like microstructure) 84
Table 9 The lattice parameters of YSZ coatings sprayed by Axial III and WSP-H 500 86
Table 10 The lattice parameters of YCeSZ coatings sprayed by SG-100 and TriplexPro-200 [33] 86
Table 11 The results of density measurements [131] 97

CHAPTER 1. INTRODUCTION

1.1. Gas turbines and Thermal Barrier Coatings

The gas turbine engines are internal combustion units. They produce the energy from fuel and then convert it into mechanical energy. But in fact, the air is used as a working fluid to drive the engine. The working cycle [1] is as follows:

- the pressure and temperature of air is mechanically increased by the compressor (1),
- fuel and air are combusted in the combustion chamber and heat energy is generated (2),
- hot gases moves through the turbine section and spin the turbine blades. Then the blades rotate the shaft and compressor blades (3),
- exhaust gases are accelerated in a convergent nozzle and the jet thrust propel e.g. the airplane forward (4).

The gas turbine engines are used in transportation (mostly aviation) and energy sectors as well. The scheme of a typical gas turbine engine used in aviation industry is presented in Figure 1 [2].

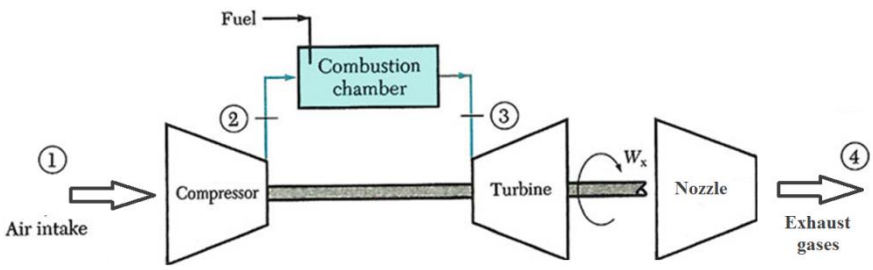

Figure 1 The scheme of gas turbine main parts [2]

Based on the literature the gas turbine core power and its efficiency is directly influenced by the temperature of gases entering the turbine section (Figure 2) [3], [4]. These parameters are important from the economical point of view, especially in the aviation industry. The increase in the energy efficiency improves the thrust-to-weight ratio. This causes that the continuous increase of gas turbine engines operating temperature occurs. The operating temperature of turbines reached currently the point far above the melting temperature of materials that are used for parts fabrication (mainly nickel superalloys) and exceeds even 1500°C - 1600°C. However, another problem is the rapid change of the temperature during the gas turbine service. While the turbine starts or stops operating the great difference in the temperature occurs. The temperature can jump between 0 °C and 1500°C - 1600°C in a very short time and hence the thermal stresses arise also in the turbine elements. Therefore, there is a big need to protect metallic parts placed inside the hot section of gas turbine against high heat loads. At the same time the high thermal shock resistance should be ensured.

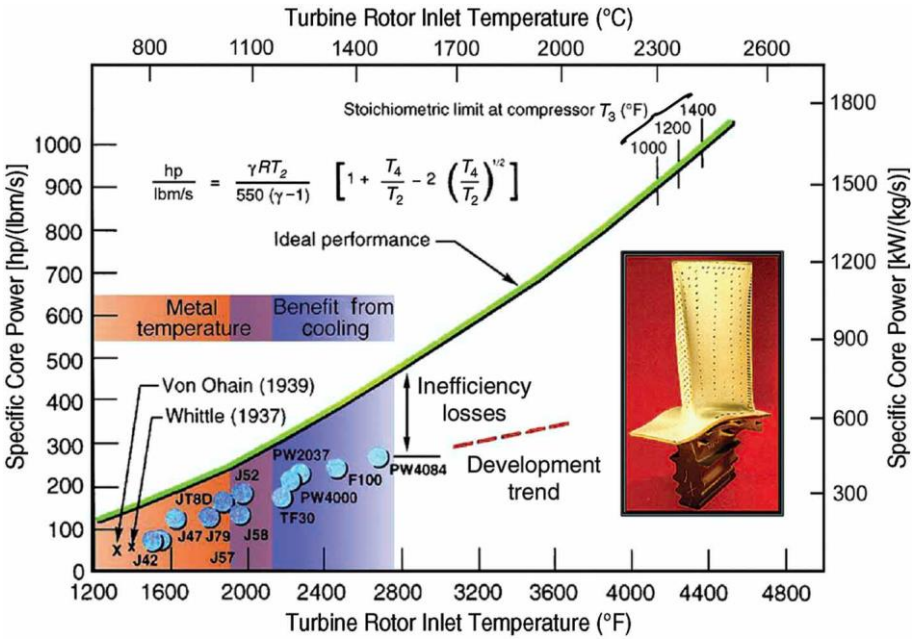

Figure 2 The influence of turbine inlet temperature on the turbine core power and efficiency (T_4 - turbine inlet temperature) [3]

The turbine inlet temperature can be increased by the use of internal cooling systems (for example cooling of turbine blades). But this solution influences negatively the gas turbine engine efficiency (see Figure 2). The other approach is the use of Thermal Barrier Coatings (TBC's). TBC's are complex, systems that protect the gas turbine parts against heat, solids and corrosives. To overcome mentioned loads the multilayer

structure of TBC is needed. The currently used TBC's are consisting from: ceramic top-coat (TC), thermally grown oxides (TGO's) and metallic bond-coat (BC). Each layer (as presented in Figure 3) has an important role in order to provide sufficient protection of gas turbine parts. Thermal Barrier Coating is one of the key technologies related to gas turbines - both in the aviation industry as well as power plants. Two different reasons of their application can be distinguished: the possibility to extend the turbine lifetime at desired operating temperature and the need to increase operating temperature and thus the turbine efficiency as mentioned above.

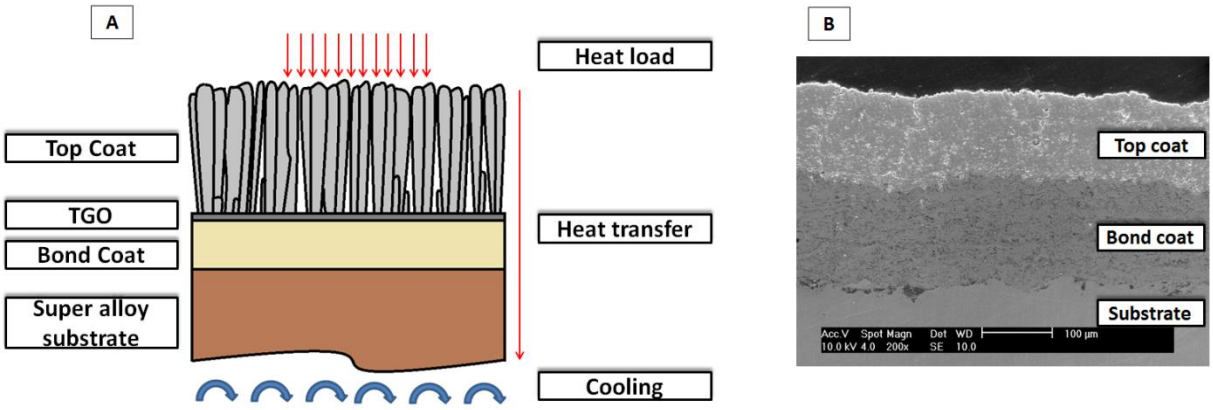

Figure 3 The Thermal Barrier Coating System (by Sokołowski and Pawłowski [5])

The critical part of TBC's is undoubtedly the external coating, as it is directly exposed to very complex loads (thermal, thermomechanical, mechanical, chemical etc.). This layer should provide sufficient thermal insulation and thus protect the internal materials. The ceramic materials (usually zirconia-based) are mainly used to produce the top-coat layer. So the high thermal shock resistance is another key property in case of ceramic top-coat. Unfortunately, with existing technology it is difficult to produce described ceramic coatings having both beneficial characteristics in one. On the one hand, the Electron Beam Physical Vapor Deposition (EB-PVD) method enables producing columnar microstructure. The strain accommodation in columnar coatings occurs during cyclic temperature change because they are characterized by low in-plane modulus. Afterwards, the thermal expansion mismatch between bond coat layer and top coat layer can be reduced [6]. Furthermore, EB-PVD technology enables to obtain coatings having controlled, desired, properties. The free-surface of such coating is smooth, the cooling holes closure is avoided and an aerodynamic design of the blades is maintained also. However, this is one of the most expensive coating technologies

(in terms of set-up investment and production as well), so the application of EB-PVD is usually limited to the critical and relatively small parts of the turbines. The bigger and less fragile parts are produced nowadays using well-established powder plasma spraying (PPS) method [7], [8]. The ceramic coatings produced by PPS are characterized by brick-wall microstructure with horizontally oriented lamellas. Furthermore, the conventional PPS coating consist also of many gaps, pores and horizontal defects between the splats. This is beneficial in TBC applications for the reduction of heat transport and improving thermal insulation. The negative effect of such lamellar structure is much lower thermal shock resistance when comparing to coatings produced by EB-PVD.

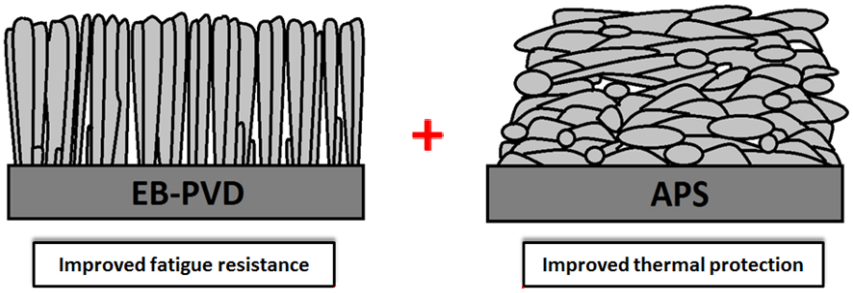

Figure 4 The scheme of the microstructural features of EB-PVD and APS zirconia coatings (by Sokołowski and Pawłowski [5])

The best compromise will be to join advantages of these two mentioned methods and coating microstructures (high thermal shock resistance of columnar-like EB-PVD coatings and low thermal conductivity, high deposition rate, inexpensive manufacturing of PPS coatings) to be produced in one single process (see Figure 4). In order to produce such ceramic coatings for Thermal Barrier Coatings application the Suspension Plasma Spraying was tested in this PhD project.

1.2. Solid Oxide Fuel Cells

The other field, where the thermal spray processes are used more and more often, is the production of Solid Oxides Fuel Cells (SOFC's). Starting with a short introduction of Solid Oxides Fuel Cells technology it should be mentioned that these are power devices that can convert fuel into the electricity. They can be classified as highly efficient units having many different advantages over other types of fuel cells. They use easily available fuels

(biomass, alcohols or natural gases); instead of a typical combustion process the energy is produced in an electrochemical way; the emissions of toxic gases like CO_X, NO_X, SO_2 is very limited and they have modular structure [9]. The operating principle of SOFC is presented in Figure 5 [5], [9]. In case of plasma spraying the most possible and beneficial can be a production of dense electrolytes. This application will be discussed here more in details.

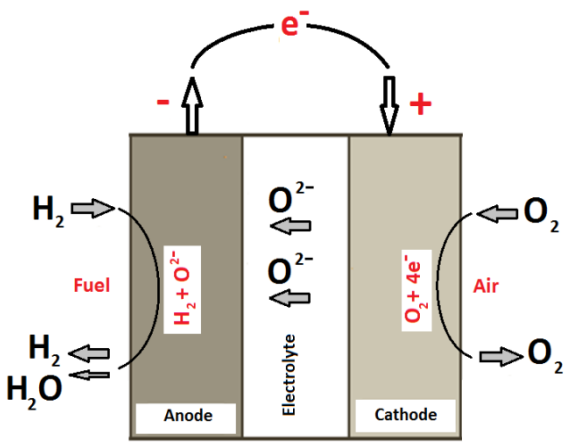

Figure 5 The operating principle of Solid Oxide Fuel Cell (by Sokołowski and Pawłowski[5], [9], inspired by [9])

The core of Solid Oxide Fuel Cell is a gas tight electrolyte that prevents mixing of oxidizing and reducing gases. The charge is transported by O_2–ions in electrolyte layer. So the electrolyte should enable high ionic conductivity and low electronic conductivity also. The mentioned properties can be improved by changing the electrolyte microstructure or by the development of new electrolyte materials. In case of microstructure the following trends can be distinguished:

- deposition of thin electrolyte layers (the oxygen ions have reduced travelling distance and the electrolyte resistance can be reduced),
- production of fine grained structures (they seem to be less resistance and have higher strength also).

In case of material selection the ones having fluorite structure are preferred for electrolyte production. This is caused by the high oxide ion conductivity of these structures (according to van Gool criterion [10]). So among the most popular materials yttria-stabilized zirconia (YSZ), scandia-doped zirconia (ScSZ) or rare earth-doped ceria

can be mentioned. The studies with perovskites and oxides characterized by hexagonal structure are carried out currently also. Their ionic conductivity is high enough to be considered for Solid Oxide Fuel Cells applications [11]. However, the material change is not considered in this work, so the material approach will be not discussed here in details.

Many different technologies exist that allow producing of electrolytes for SOFC's. The most popular are:

- wet ceramic processing techniques [12],
- spray pyrolysis [13],
- vapor deposition methods (PVD, CVD, EVD) [14], [15],
- magnetron sputtering [16],
- powder plasma spraying (APS) [17].

As can be easy seen the production of electrolytes by mentioned methods is mostly limited by the high manufacturing costs or difficulties in meeting the microstructural requirements (like thickness, density or strength) [18]. Therefore, the new manufacturing methods are tested for SOFC's manufacturing. The goal is to produce improved systems having higher performance and reduce the manufacturing costs at the same time. One of potential methods can be Suspension Plasma Spraying (SPS), especially for zirconia-based electrolytes.

CHAPTER 2. SUSPENSION PLASMA SPRAYING

Concerning the limitations of vapor condensation processes (long deposition time, high set-up costs etc.) many attempts were conducted in order to produce nanometer coatings by cheaper and more effective thermal spraying processes. The conventional powder plasma spraying (PPS) was tested mainly for this purpose. But due to the difficulties associated with feeding, injection and then transportation of fine powder particles in a hot plasma jet, the studies did not bring the expected results. The main problem is caused by the low weight of fine powder particles. As a result they do not have enough momentum at the outlet of the injector to fully penetrate the hot region of plasma jet [19], [20]. The first idea proposed to solve this issue was to perform a pre-treatment of nano-powders prior to the plasma spraying. The additional step of powder preparation was supposed to provide thermally spray able feedstock. Lima and Marple [21] proposed the use of agglomerated nanostructured particles for powder plasma spraying. Marcinauskas [22] granulated alumina nanoparticles, dried in a furnace and then sieved the powders to keep particles smaller than 50μm. This powder was then well deposited by PPS process. Chen and Ding [23] decided to perform spray drying of zirconia nano-powder prior to spraying and thereby to preserve their fine grained structure in a coating microstructure. Spray drying was also proposed by Shaw et al., who achieved composite Al_2O_3-TiO_2 nano-coatings by powder plasma spraying [24]. In fact, a very narrow parameter window is necessary to obtain nanostructured coatings by thermal spraying of pre-processed nano-powders. Especially the in-flight particle temperature should be controlled carefully to do not fully melt nano-feedstock. The mixed structure, partially nanometer, can be achieved only if the powder particles can be maintained in a semi-molten state during spraying.

The other innovative idea was proposed by the research group from Sherbrook University in Canada in 1997. Gitzhofer et al. [25] assumed that instead of the micrometer-sized powders, the liquid feedstocks can be used in plasma spraying. As a result fine powders suspended in water, alcohol or their mixtures can form droplets having enough mass and momentum to be introduced into the plasma flame. The transportation of liquid feedstock from feeder to the injector is also easier than in case of dry powders. Furthermore, the solvent provides the protection for fine powder particles against the hot plasma gases and the melting of powder material takes place after the evaporation of solvent from the suspension droplet. This approach allowed to develop a new thermal spraying method, called Suspension Plasma Spraying (SPS)[25]. This dynamically evolving process will be discussed in details in this chapter.

2.1. Powders and suspensions

When analyzing the suspension preparation for SPS method it should be emphasized at the beginning that this process is not only limited to a mixing of a solid powder with liquid solvent. This multistep process requires the knowledge about the colloid chemistry. Furthermore, the suspension preparation can highly influence the spray process and coating microstructure, so each component of suspension will be discussed in details.

Powder preparation

The quality of powder material directly influences the quality of deposited coating [26]. The two main ways that enables the preparation of fine-grained powders for SPS process can be mentioned: (i) the production of submicrometer- or even nano-sized powders or (ii) the pre-processing (mainly by milling) of coarse powders designed for conventional plasma spraying. In general, two well-known approaches called: (i) bottom-up and (ii) top-down are used for the powder preparation. These two approaches are usually classified in accordance to the state of the precursor used for powder formulation (see Table 1). The precursors can be in a form of: gas, liquid or solid as well [27], [28].

In case of "bottom-up" processing a continuous progress can be noticed. Under this approach there are many various methods which allow producing the fine powders. The use of liquid precursors in powder manufacturing is commonly classified as quite simple method. The powders can be precipitated in a non-complicated chemical way, usually from a solution [29]. The calcination of chemically precipitated precursors is used for example by MEL Chemicals Inc. to produce both: zirconia nano-powders and nano-suspensions. Carpio et al. [30] successfully deposited in his work mentioned zirconia suspension and obtained finely-grained coatings. But the "bottom-up" processing can be sometimes also very complex, often multistage. This takes place of submicrometer zirconia powders manufactured by Tosoh Corp. The following stages can be distinguished in their procedure: hydrolysis of chemical precursors, drying, calcination, milling and finally spray drying [31]. This zirconia powder was already deposited by SPS for the purpose of Solid Oxide Fuel Cell's [32] and Thermal Barrier Coatings [33].

Table 1 The summary of bottom-up and top-down processing methods (by Sokołowski and Pawłowski [5], inspired by [28])

Precursor	Processing	Approach
Gas	Physical vapor deposition	Bottom-up
	Chemical vapor deposition	
	Aerosol processing	
Liquid	Sol–gel process	Bottom-up
	Wet chemical synthesis	
Solid	Mechanical alloying Mechanical milling[1] Mechanochemical synthesis Sonication	Top-down
Combined	Vapor–liquid–solid	Bottom-up

In case of "top-down" approach, the powder preparation process is much different [29]. It assumes a breakdown of the coarse, micrometer sized, powders into fine particles. As

[1] The most popular process nowadays for a preparation of powders for Suspension Plasma Spraying

a base material for “top-down” processing the powders manufactured for other thermal spraying processes (like APS, FS, HVOF, CS etc.) can be used [19]. The breakdown of powder particles is realized mainly mechanically - by using well-established ball-milling method. Two most popular methods can be mentioned, called “low energy” and “high energy” milling. The difference between them is the amount of mechanical energy transferred to the powder material and kinetic of the process as well [34]. Both can be classified as efficient and low-cost methods, enabling the production of nanostructured powders at low temperatures. These methods can be used to pre-process all kinds of advanced materials (even very ductile, brittle or hard compounds) [35]. The ball milling is very popular for the preparation of feedstock for SPS method. Kassner et al. applied ball-milling to pre-process alumina powders [36], Chen et al. crushed and mixed by ball-milling the composite powder of Al-ZrO_2 [37], Łatka et al. used mechanical-milling to reduce the size of various zirconia powders [38], Jaworski et al. of hydroxyapatite powders [39], whereas Berghaus et al. of cermet WC-Co [40].

The mentioned methods can be used for mechanical milling (MM), but there is also a possibility to apply them for mechanical alloying (MA). MA process usually needs higher temperature and kinetic energy than milling. This is necessary to ensure high atomic mobility [41]. Mechanically alloyed powders (like YSZ-NiCrAlY, YSZ-Ni, Ni-Al etc.) [42]–[44] become to be an interesting option for the use in liquid feedstock spraying.

Solid content

Beside the powder preparation, the important parameter is also the content of solid phase in the suspension. It was noticed in the literature that the amount of powder has an important influence on the rheological properties of liquid feedstock [45]. Afterwards, the viscosity of suspension is one of key property affecting the droplet formulation in the plasma jet [46]. The size of droplet and the distribution of powder inside single droplet influence the droplet heat treatment in the plasma jet [47]. According to the literature, the amount of the solid particles in the suspension droplet has an effect on coating microstructural features, like: porosity, surface topography and morphology [33], [45], [47]. Furthermore, the suspension concentration can be a crucial parameter in case of suspension transport from feeder to the plasma torch. In the industrial practice the feeder is placed usually outside of the spray booth, so the total length of the installation can exceed several meters. On the other hand, the use of highly

concentrated suspensions is in the interest of industry, as the higher solid load is equal to greater "thickness per pass" ratio in SPS practice.

Solvent

The suspension droplet consist of powder particles that are surrounded by the solvent. The pure water, pure alcohol or the mixture of water and alcohol can be used for the suspension formulation. The ethanol is primarily used among alcohols. But other kinds of alcohols like: methanol, methylethylketone (MEK, butanone) [48] were also investigated for the purpose of Suspension Plasma Spraying.

The selection of solvent can be influenced by few factors, e.g. its properties, economical and environment aspects etc. But the characteristics of liquid feedstock is influenced mainly by two properties of solvents, namely surface tension and evaporation time.

The influence of the surface tension on the spray process was investigated by Rampon et al. [48]. By using tensiometry method they showed that aqueous suspension is characterized by has much higher surface tension than ethanol based suspension. The authors suggested also that the surface tension preserve liquid feedstock against the change of its surface area and is the main property that influence the break-up and size of suspension droplets. Furthermore, it was shown that the change of surface tension cannot be achieved by the addition of chemical agents but only by the solvent. The same effect was observed by Toma et al. [49]. It this work a faster and more efficient fragmentation of ethanol based liquid feedstock than aqueous one were observed also due to the lower surface tension of ethanol when comparing to the water. Afterwards, the size of droplet affects its velocity and residence time in the plasma jet, and its temperature also (it can be estimated that big droplet = higher velocity = lower temperature). This can have an influence on the coating microstructure. If the particles have a high speed and kinetic energy during the impact on the substrate they will tend to form denser microstructures.

The role of surface tension and evaporation time in case of Solution Precursor Plasma Spraying (SPPS) was discussed by Chen et al. [50]. They reported that the evaporation of solvent and formulation of solid particles in the plasma jet can be incomplete when droplets have high surface tension and high boiling point. On the other hand, the solution droplets that are formed by solvent characterized by lower surface tension and

boiling point can be processed more rapidly. These droplets undergo complete heat treatment in the plasma jet. The issues related to the droplet evaporation were studied deeply in the work of Kaβner et al. [51]. The evaporation time of droplets was calculated using of the model considering the latent and specific heats. The droplets of alcohol and aqueous based suspensions having various sizes were taken into account. The studies confirmed that water based droplets were evaporated after nearly three-times longer time in the plasma jet (as the vaporization enthalpy of water is almost three times higher comparing to ethanol; 2.3×10^6 J·kg^{-1} versus 0.8×10^6 J·kg^{-1} [52]).

The solvent type determines also the min. velocity of droplets that is necessary to penetrate the plasma jet by the feedstock (as discussed by Pawlowski [53]). The aqueous suspensions need lower velocity to reach the core of plasma jet. This is due to higher density of water than that of ethanol and should be considered particularly for torches operating with radial injection. They need a careful optimization of injection.

The viscosity of suspension is another property that can be also influenced by the solvent type. This is caused by the difference in viscosity rate between alcohols and water. However, this can be controlled more easily by the addition of chemical agents (so called plasticizers). Their role is discussed in details later.

The application of "green suspensions" is mentioned in the literature also. The deionized water is a solvent and a reagent here. There is no need to add stabilizers to ensure suspension stability. As an example the nano-titania suspension were prepared [54]. As suggested by the authors, the limitation of toxic organic solvents and chemical agents should be considered as they can be wasteful for the environment. However, that kind of suspension needs a dedicated powder production method (continuous hydrothermal flow synthesis, CHFS) [54].

The security, e.g. fire risk, should be considered also when alcohol based suspensions are used. Furthermore, the economic reasons suggest that even a small replacement of alcohol by water makes the suspension cheaper and more attractive for the industry.

Chemical agents

In order to provide stable and reproducible SPS process, there is a demand to formulate homogeneous and stable suspension. This becomes to be especially important when

very fine powders are used as a solid fraction. As denoted in the literature, the nanoparticles show a high reactivity and agglomerate easily, because of their high specific areas. [28]. The change and control of rheological properties of suspension can be done by the addition of chemical agents.

The rheology of suspension is a complex function of physical properties of powders (particle size, particle shape, density etc.) and interactions occurring between powder particles [55]. Wang et al. analyzed the interplay between individual solid particles but also the effect when liquid and solid phases separate (so called flocculation). This takes place when the Van der Waals forces overcome the electrostatic repulsion [56]. The detailed description of forces affecting the behavior of colloids was presented by Ring [57]. As an example 1μm TiO_2 particle in water was given. The different forces (electrical, Van der Waals attraction force, viscous, gravitational and inertial force) were referred to the Brownian force that was used as a denominator. All forces excluding inertial force showed impact higher (the ratio between electrical force and Brownian force was even 10^3) or equal to Brownian force. Finally, Larson [58] suggested that the particle size have a significant influence on suspension stability. Following, the powder particle size influence the approach that should be applied to formulate stable suspension. The gravitational force is dominant when coarser powders are used. For fine (submicrometer sized and smaller) Brownian force overcomes the gravity force effect.

As mentioned above, to maintain the stability of fine grained suspensions the Brownian motion approach can be used. The possible way to prevent the particles against sticking to each other is to ensure inter-particle repulsion. This can be done by increasing of the net value of so called zeta potential (ζ). Zeta potential can be described as the difference of potentials between the thin layer of solvent surrounding the particle and its eternal slipping plane. To ensure suspension stability ζ should be over the values of +/- 30mV. The change of ζ can be achieved by the addition of dispersant agents (called also flocculating agents). Finely grained suspension should be optimized in a way to ensure a long range electrostatic repulsion. But the addition of the flocculating agent should be controlled carefully. Dispersant can also strongly negate the particles' surface charge and influences the formation of floccules (see Figure 6) [59].

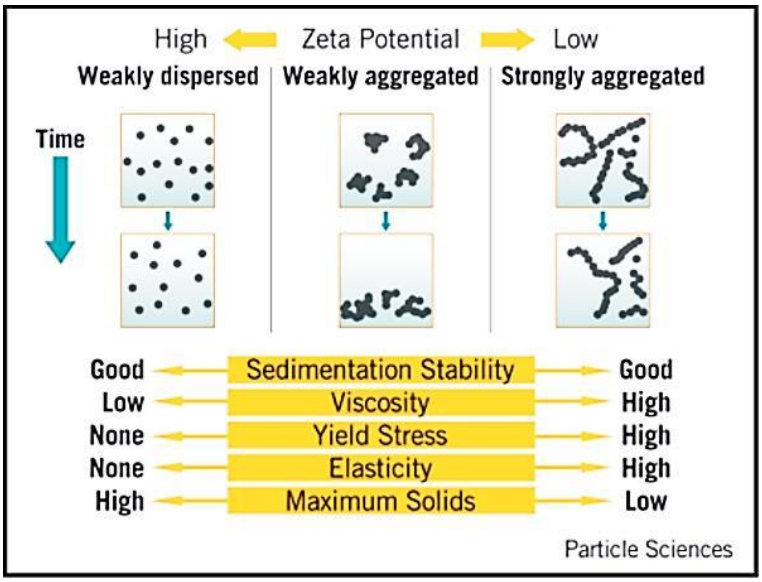

Figure 6 The relationship between Zeta potential and suspension behavior [59]

The sedimentation of finely grained suspension is influenced also by its viscosity, η. The sedimentation speed can be evaluated by using the Stokes equation:

$$V = \frac{2\Delta\rho g a^2}{9\eta} \qquad (1)$$

The Stokes equation suggests that the sedimentation speed can be decreased by: (i) application of finer solids, a, (ii) using dispersed and continuous phases having as much comparable densities as possible, so Δρ is small, (iii) increasing the value of "low shear viscosity", η. But in fact, the low shear viscosity is very often the only one Stoke's variable and can be modified by the application of viscosity enhancers (called thickeners or plasticizers also). It is important also that the low shear viscosity can increase when the zeta potential increases. The control of both parameters is usually required. This was discussed in the studies of Waldbillig and Kesler. They tested various dispersants and observed their influence on the suspension rheology. According to their studies, the use of optimal concentration of dispersant agent allows to obtain the lowest viscosity of suspension. Otherwise the effect can be reversed and as a result the viscosity can be changed strongly. Following, this can influences negatively the Suspension Plasma Spraying efficiency and can cause clogging of the injector during spraying [60]. But in such cases the addition of plasticizers can preserve the proper viscosity of suspension, as mentioned above [48].

The other approach is needed when the submicrometer particles are used for suspension formulation, especially powders characterized by not fully monomodal powder particle size distribution. In such situation, the gravitational force exceeds the Brownian motion. Then, the suspension sedimentation can be preserved by approaching an isoelectric point (IEP). So called IEP is defined as a state when the electrostatic forces are equal to zero for a specific pH value. Afterwards, when electrostatic forces are minimized, then there is a possibility to produce a "secondary minimum". If its value is big enough the suspension can be defined as strong reversible flocculated network. Furthermore, to decrease the sedimentation rate of micrometer sized suspension the idea suggesting increasing of low shear viscosity can be applied also as suggested for finely grained suspensions.

Finally, the practical examples of proper application of flocculating agents can be find in the literature, e.g. for zirconia suspensions [61]–[63]. The comparison of well- and poorly- stabilized zirconia suspension is presented in Figure 7 [5].

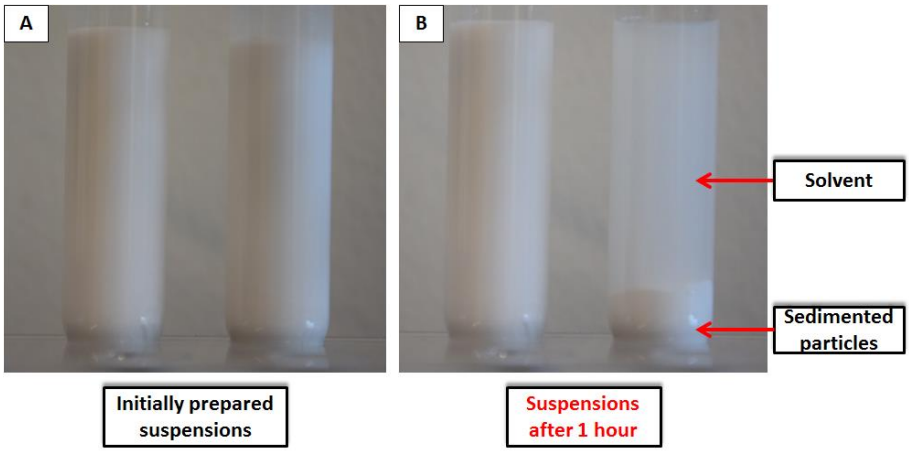

Figure 7 Two kinds of zirconia suspension: (a) well-stabilized suspension, (b) poorly-stabilized suspension (by Sokołowski and Pawłowski [5])

Based on the information presented in this chapter the three main steps can be distinguished during the suspension formulation:

1 – preparation and characterization of powder particles,

2 – suspension formulation, homogenization, determination of rheological properties and stabilization test,

3 – suspension re-dispersion just prior to spraying.

There is a possibility to use commercially available suspensions also. They become more popular nowadays, because long and complex suspension preparation process can be avoided and there is no need to prepare long-term laboratory tests to examine the suspension properties. The feedstock is delivered in a premixed form – with solvent and chemical agents and there is only a need to well re-disperse the mixture prior to spraying. However, there are two main reasons that limit the use of commercial suspensions: their cost and availability. The price of a kilogram of 20 wt. % loaded suspension is comparable to price of a kilogram of powder material that was used to formulate that suspension. So the price of commercial and house-made feedstock is roughly 5:1, as the powder material is the most expensive component. Furthermore, only suspensions that can be applied soon in the industry are available on the market. The most popular ones are zirconia-based suspensions at this moment.

2.2. Modes of suspension injection

When liquid slurry is prepared and well-optimized there is a need to transport it to the plasma torch. The feedstock transportation from container to the injector is usually provided by compressed air (pressurized system) or mechanically (by using of peristaltic pump). The transportation system should provide a constant flow of slurry with a set value of its feed rate (measured in ml x min^{-1} or mg x min^{-1}). Then, the injection of liquid feedstock to the plasma takes place. The basic role of transportation and injection systems is to ensure dynamic pressure of a liquid greater than that of the plasma jet. This allows the proper penetration of the jet by the slurry [53]. Suspension injection is one of the key factors in Suspension Plasma Spraying as it influences the droplets formulation and then the heat treatment of the slurry. In the following section the various types of injection modes will be analyzed.

Continuous stream injection vs. atomization

The mechanical injection, which is called also a liquid stream injection, is probably the most often used in Suspension Plasma Spraying. It can be performed radially or axially but also internally or externally with regard to the torch design. In mechanical injection, the feedstock is pushed through a nozzle having fixed diameter and shape. Another

characteristic appearance for mechanical injection is that the atomization of the slurry takes place only in the plasma jet. The fragmentation of slurry is caused by the various external factors, like plasma jet velocity, plasma temperature, force of gravity, resistance of surrounding gases etc. The mathematical approach of the fragmentation of slurry that occurs in the plasma was presented in details in the literature already (see e.g. the work of Pawłowski [64]).

The other possibility of the feedstock injection is its atomization (Figure 8) [65]. It means that the formulation of droplets takes place before the feedstock contacts the plasma jet. The atomization occurs usually in two steps: (i) first, low velocity slurry is pre-injected to a nozzle, (ii) where by using of other external energy (flow of gas or other fluid, kinetic energy, acoustic energy) is fragmented into droplets. In SPS practice usually simple atomizers are used, where the fragmentation of droplets is forced by the gas flow. In this case, the gases characterized by high specific mass (like for example argon) are very often used. The type of external energy defines the type of atomizer and more information can be found here [64]. The droplet formulation is much more complex than in case of mechanical injection. It is influenced by the design of atomizer, external energy but also by the properties of liquid slurry. The phenomena were discussed in the literature already. Furthermore, the atomizers are used usually only with external or radial injection modes, eventually co-axial atomization is possible also.

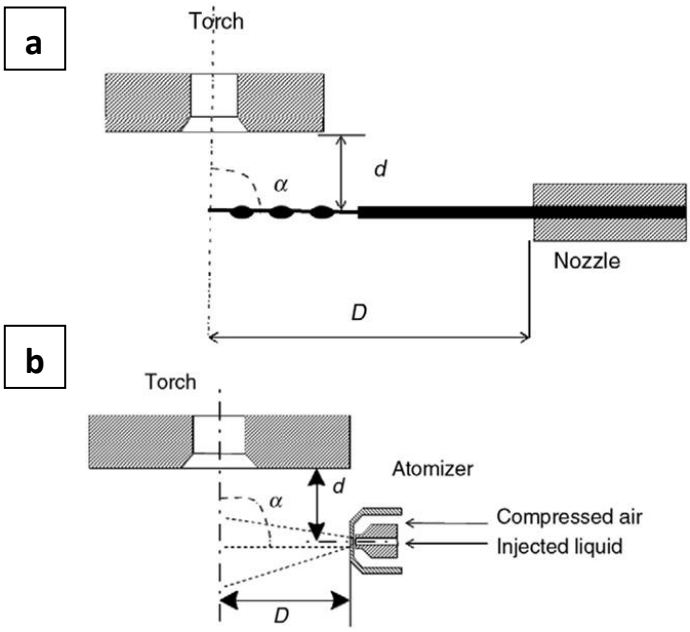

Figure 8 The comparison of liquid stream injection (a) and atomization (b) [65]

The influence of injection mode on the coatings microstructure was already studied in the literature. The comparison of two mentioned injection modes was done e.g. by Kozerski et al. [66], [67]. In this study, the use of atomizer resulted in uniform, finely grained microstructure. The splats were not deformed and preserved spherical shape. The molting and solidification of powder particles occurred before the solids reached and hit the substrate. Much more complex microstructure was observed when the mechanical injection mode was used. So called two-zones microstructure was observed, where well molten lamellas but also loosely bounded sintered particles were present. The stronger deformation of grains was observed also by authors when mechanical injection was used.

The different practical information regarding mentioned injection systems can be found in the literature. The short comparison is presented in the Table 2 [5].

Table 2 The summary of mechanical and atomization injection modes based on the literature (by Sokołowski and Pawłowski [5])

Continuous stream injection	Atomization
- avoids the plasma jet perturbation caused by the atomization gases [68], [69], - injection with fixed velocity, no dispersion of droplet trajectories and sizes [68] - through the use of a precise positioning system of the injector the droplets can be injected at the chosen location in plasma plume [68], - droplets are more effectively injected into the core of the plasma jet [69], - higher thickness per pass ratio [70], - the use of ink jet printer as injector allows the formulation of uniform and small droplets with constant spacing of droplets in plasma [71].	- good control of the atomization, generation of high velocities of droplets at low feeding rates [72], - atomization produces small, well-defined and uniform droplets influencing formation of fine splats [69], - reduction of unmelted particles in the coating structure [36], - possibility to design atomizer in a way that limits the problems associated with injector's clogging and agglomeration of suspensions in injector/nozzle [73].

Radial injection vs. axial injection

The discussion on the use of radial or axial injection mode is very common nowadays. However the choice is in this case defined by the design of the plasma torch itself.

In radial injection the feedstock is introduced perpendicularly to the plasma jet axis. This kind of introducing feedstock material is still the most popular in the plasma spraying practice. This is caused by the fact that the construction of plasma torches usually do not allow to install injector axially. Concerning the information presented in previous paragraphs, the radial injection in SPS can be realized by: (i) atomizer or, (ii) mechanical injector. In each case the slurry should reach the high temperature core of plasma jet. Otherwise the heat treatment of feedstock material will be incomplete and this will implicate different problems with the formation of good quality coating. The problem becomes complex when powder particles or suspension droplets are very inhomogeneous in terms of their size. After they are introduced into the plasma jet, the difference of size and mass of particles implicates their momentums and influence the possibility of penetration the plasma jet. The injection optimization is a way to find compromise here, as there are always: (i) particles that reach only the periphery of the plasma jet (the ones being to light or having to low momentum), (ii) particles that goes into the core of plasma (having optimal mass and momentum) and (iii) particles that pass through the plasma jet (to heavy particles or the ones having to high momentum).

The plasma torch with axial injection mode becomes more and more popular currently. The first trials with one-cathode torch having co-axial injection were done. But the millage point was the application of multi-cathode torch for this purpose (Axial III of Mettech). In Axial III torch there are three independent plasma jets formed by three electric arcs. The feedstock material is injected just inside the center of the place, where three plasma jets converge into one. That unique idea allows also introducing slurry exactly in the same direction as the plasma flow occurs. Comparing to the radial injection there is no problem with the adjustment of powder/droplet trajectory. A very narrow dispersion angle of droplets causes that the heat treatment of feedstock material is uniform. But when using the axial injection mode, then the optimization of spray parameters connected with suspension injection is limited. The location of the injector is fixed so there are only few variables, like: injector diameter and injection pressure. The injector is long and has usually small internal diameter (such design is caused by the

torch construction) can implicate problems with back-pressure or clogging during e.g. spraying of high-viscous suspensions.

The direct comparisons of plasma torches having radial and axial injections were already done in the literature. Ozturk et al. used mathematical modeling to prove that big differences in the plasma temperature and velocity fields occurred when using different injection types in SPPS. The droplets introduced axially were heated-up much faster and the precipitation of zirconia solution could be observed much earlier. Afterwards, the solid grains formulated in plasma jet were more homogeneous in case of axial injection [74]. The experimental work in this topic was performed by Killinger et al. [69]. The effect of the injection type (transverse and axial) on the SPPS sprayed coating microstructure was studied. But a very similar behavior of solution droplet processing was observed. The use of axial injection mode allowed the formulation of fine droplets that underwent rapid heat treatment in plasma. Furthermore, full pyrolysis of droplets allowed creating uniform coating microstructure.

External injection mode vs. internal injection mode

The choice of external or internal injection mode is influenced mainly by the design of the plasma torch, similarly as in the case of axial vs. radial injection. There are plasma torches (like SG-100 of Praxair or Axial III of Mettech) that give the possibility to place injector internally and externally also. On the other hand, many plasma torches have to be used with external injection mode (Triplex and F4 of Oerlikon). Furthermore, it is possible to find few practical information in the literature discussing advantages and disadvantages of both injection modes.

The advantage of internal injection is undoubtedly the fact that the slurry can be introduced directly into the hottest zones of plasma flame. A good heat treatment of particles is in this case ensured. This is especially important for high melting point materials which need high temperature to be melted but the importance of this parameter was already discussed in this chapter. This type of injection does not require also long process of injection point selection and the problems with instability of injection are limited. However, there is no possibility to experimentally observe the first step of feedstock injection and fragmentation, which occurs inside the plasma torch. Etchart-Salas et al. [75] recommended the use of external transverse injection mode as it

is less sensitive for the nozzle clogging. The clogging of Axial torch injector was discussed in [76] for APS process. The authors suggested also that the erosion of hot cathode can occur as a result of injection of powder particles inside the torch. The negative influence of internal injection system on the torch lifetime was found by Gotô and Atsuya when using acid solution [77]. The copper electrode was slightly dissolved by the acidic slurry. This should be always considered when using acids for suspension stabilization or in case of SPPS method, where acids are commonly used to prepare various solutions. The use of internal, especially axial, injection mode can seriously limit the operation time of the cathodes.

2.3. Commercially available plasma torches

Many aspects regarding the plasma torches design were discussed above. In this section a short comparison of plasma torches that are used widely for the purpose of SPS process is prepared. The plasma torches can be classified based on many different aspects. Here, the torches were divided into two groups, depending on the electric power that torch generates and the mode of plasma stabilization.

The main group of plasma torches, which is used in plasma spraying, is basically DC, gas-stabilized and one cathode-one anode construction. The properties of gas-stabilized plasma are mainly influenced by plasma torch design, properties of plasma gases and their flow rate and power input. The generated power is usually less than 50kW but this is enough to generate the temperature that can exceed 15000°C (depending on parameters). This is the temperature that allows spraying most of the engineering materials. The main problem of such simple construction is the instability of the arc. The electrode life and thermal efficiency of plasma set-up was found to be strongly related to the nature of arc fluctuations. This was discussed extensively in the literature [78]. The idea to limit fluctuations of the gas-stabilized arc was proposed in Triplex torch, where three cathodes (supplied separately) create three arcs striking one single anode. These long arcs having high voltage allow reducing significantly fluctuations comparing to conventional plasma torches. The power level during the operation using Triplex is similar or slightly higher than that of conventional plasma torches. However, the injection point of feedstock should be carefully optimized in accordance to the three

high-energy areas produced by Triplex that arranged in a triangle [36], [79]. Alternatively, another multi-cathode design was proposed recently in the market. Axial III torch is composed of three cathodes and three anodes. The operated power is ensured by three independent power suppliers (each can generate up to 50 kW). To my knowledge this is one of the most powerful gas-stabilized torch designed for plasma spraying currently. The higher power input influence the increase of temperature, velocity of particles and the number of particles which can be molten in the plasma jet. This allows achieving higher deposition rates and higher productivity. However, the economics aspect should be mentioned. The multi-cathode systems tend to be bigger, more complex and more expensive. They require much bigger gas flow rates also. Furthermore, the change of the cathodes is takes more time when comparing to single cathode torches and there is often a need to change all cathodes at the same time to keep uniform and stable arc [76].

Alternative idea to design high-power plasma torch was achieved by the use of so called Gerdien arc principle, so basically by the change of the arc stabilization method. In this development a water channel inside plasma torch is burnt by the electric arc. The vapors stabilize the arc, whereas the water flow protects internal parts of the torch against overheating. Oxygen-hydrogen plasma is formed by the products of water vortex vaporization and ionization. Plasma jet produced by water stabilized plasma torch (WSP) thanks to the high arc power and low mass flow rate is characterized by very high enthalpy (even 10 times higher than for conventional plasma torches), increased value of the temperature (up to 30000 K) and gas velocity (even 5-7 km/s). Thermodynamic and thermophysical properties of water vapor plasma enable to increase also the heat transfer to the feedstock material. As a result high-molting point materials can be sprayed (including refractory materials) but also higher process rates can be achieved (hundreds of grams of powders per minute or more than hundred milliliters of suspension per minute). But the interaction of plasma jet with surrounding atmosphere and high turbulences, which occur due to the high velocity of gases and low plasma density [80], [81]. Furthermore, the use of external - rotational anode impedes the operating (the turning on of the plasma) and can causes the plasma asymmetry also [82].

As an upgrade version a new type of torch with mixed stabilization mode has been designed also. Hybrid WSP (WSPH-500 torch) bases on both principles of arc stabilization - by water vortex, as well as by the gas flow. An important advantage of the new, hybrid, version is the possibility to regulate the plasma jet properties by changing the flow rate and kind of secondary plasma gas, which was unobtainable for conventional WSP [83], [84]. As a secondary plasma forming gas argon is mainly applied. Due to its high mass the increase in plasma density is observed. But this implies a decrease of the gas velocity in the hybrid WSP [84]. The use of additional gas simplifies also the operating of hybrid WSP plasma gun comparing to conventional version of WSP. Though many important advantages regarding thermophysical properties of plasma produced by water-stabilized plasma torches the complex design and operating principles of WSP and hybrid WSP torch still limit their application in the industry. The large construction of torch cause also that the application possibilities are mainly for big parts, where big area should be coated.

2.4. Physical phenomena at spraying

The application of liquid feedstock, instead of using of dry powder, causes a change of the features of plasma deposition. The spray process becomes much more complex than the conventional powder plasma spraying. The phenomena, which occur in plasma jet during SPS process, are well characterized already. The following mechanisms take place right after suspension is injected into the plasma plume: (i) aerodynamic break-up of suspension stream and formulation of droplets, (ii) evaporation of solvent, (iii) sintering of very fine powders, (iv) melting of fine powders, sintered solids and powder agglomerates, (v) the evaporation of very fine particles and (vi) deposition of molten powder particles on the substrate and formulation of coating [65], [85].

2.5. Key process parameters

Although Suspension Plasma Spraying was successfully applied for various types of engineering materials, the deposition parameters selection is a complex issue.

Furthermore, the spray process parameter window for desired microstructure type (dense or porous; columnar-like or typical two-zone microstructure etc.) is quite narrow. All process variables that can influence the microstructure of SPS coatings are schematically shown on Figure 9 [5].

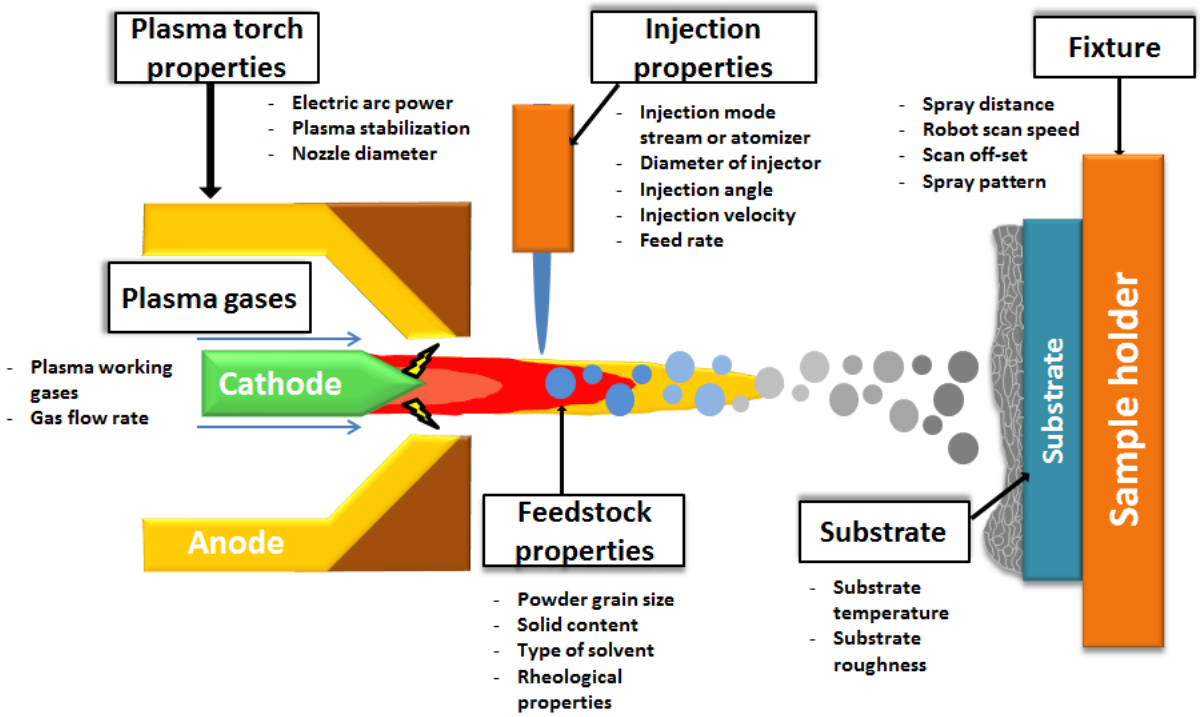

Figure 9 The scheme presenting effective SPS process parameters (by Sokołowski and Pawłowski [5], inspired by [86])

CHAPTER 3. Materials

In this PhD project the attention is paid mostly on the modification of the microstructure of insulating ceramic layer of TBC's. However, the other approach that is studied by many researchers is to find new materials that can provide improved properties of TBC's. The stabilized zirconia is one of the most popular studied ceramic materials thanks to its unique properties. It is also one of the materials, which is the most often tested for Suspension Plasma Spraying. Usually, in the industrial practice, a doped zirconia is actually used. This is caused by the fact that pure ZrO_2 has three crystal phases, namely monoclinic, tetragonal and cubic. Monoclinic (M) is stable below 1170°C, tetragonal (T) is stable between 1170 and 2370°C and cubic (C) is stable above 2370°C [87]. The phase transformation between mentioned crystal structures is followed by the volume change. The stresses are then generated in the material and the material fracture can occur. The most critical is a rapid T → M transformation, where the volume change exceeds even more than 4 %. But the doping of zirconia allows stabilizing a desire structure in this material.

Many different oxides of rare-earth elements (like Gd, Yt, Ce, La etc.) are tested in order to replace conventional 8 wt. % yttria-stabilized zirconia in the industrial practice, mainly because of their low thermal conductivity [88]. In this work two materials were tested: fully yttria-stabilized zirconia (8 mol. % of Y_2O_3) and ytrria-ceria-stabilized zirconia (ZrO_2 + 24 wt. % CeO_2 + 2.5 wt. % Y_2O_3). A short theoretical background about these two materials is given in this chapter.

3.1. Fully yttria-stabilized zirconia

The conventional TBC topcoat is usually composed of zirconia partially stabilized by the addition of 3-5 mol. % of Y_2O_3 (PSZ). The zirconia powder having higher content (8 mol.

%) of Y_2O_3 was tested in this study. The content of the yttrium oxide highly affect the structure and properties of zirconia.

According to the ZrO_2 - Y_2O_3 phase diagram (see Figure 10) [89], [90], the doping of ZrO_2 by Y_2O_3 in concentrations higher than 8 mol. %, fully stabilizes YSZ structure in cubic form. As mentioned by Scott [91], the lattice parameters of YSZ are also influenced by the content of Y_2O_3 dopant. The Zr^{4+} ions are slightly smaller than Y^{3+} (ionic radius of 0.82 Å and 0.96 Å respectively), so the increase in yttrium oxide causes the increase in lattice volume.

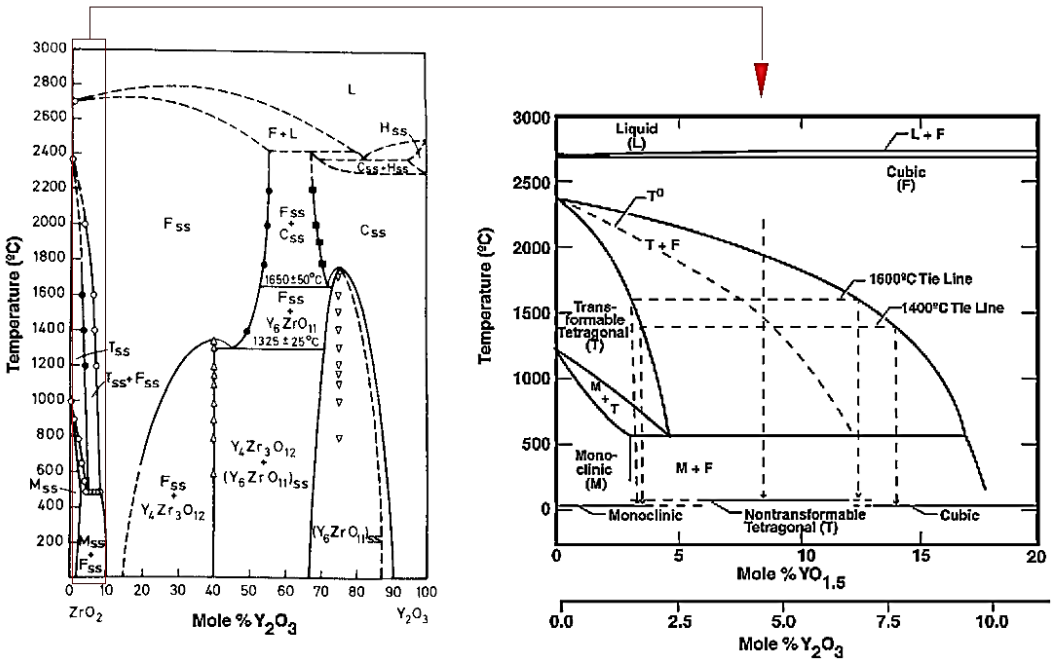

Figure 10 The phase diagram of ZrO_2 - Y_2O_3 system (with detailed version up to 10 mol. % of Y_2O_3) [89], [90]

The higher content of Y_2O_3 means that more big Y^{3+} ions is entrapped in the YSZ structure. According to the studies of Gong et al. [92] the thermal conductivity decrease when the interatomic distances in the YSZ structure are bigger. This means, that the heightened implementation of big and heavy Y^{3+} (comparing to Zr^{4+}) ions can improve the thermal transport properties of zirconia coatings. In the fully-stabilized YSZ the oxygen vacancies provide also a sufficient ionic conductivity, which is import in SOFC's. Furthermore, in case of fully stabilized YSZ the transition between cubic and monoclinic does not occur. FSZ is not subjected to high internal stresses associated with the phase change and the micro-cracking when working in wide temperature range.

As mentioned above, the increase in Y_2O_3 causes that the additional oxygen vacancies are created in the YSZ structure. This means that the oxygen transport through the ceramic TBC layer can be more effective and can cause higher oxidation of metallic bond coat. Moreover, the fully stabilization of zirconia causes that the strengthening mechanism, which is common for partially stabilized zirconia, disappears. The more monoclinic phase is created in front of the propagating crack, then the higher the compressive stresses are. As a result the high strain energy can arrest the propagating crack and provide better thermal shock resistance [93].

The choice of 8 mol. % YSZ was also caused mainly by the potentially better thermal transport properties and high ionic conductivity. The interesting feature of powder, which was used for spraying, was also important. This is described in details in the following chapters.

3.2. Yttria-ceria-stabilized zirconia

The yttria-stabilized zirconia is used in the aviation industry for longer than 30-40 years. The new materials are tested that can replace conventional YSZ. Among these materials the zirconia stabilized by other effective dopants is tested. One of the most promising materials is yttria-ceria-stabilized zirconia.

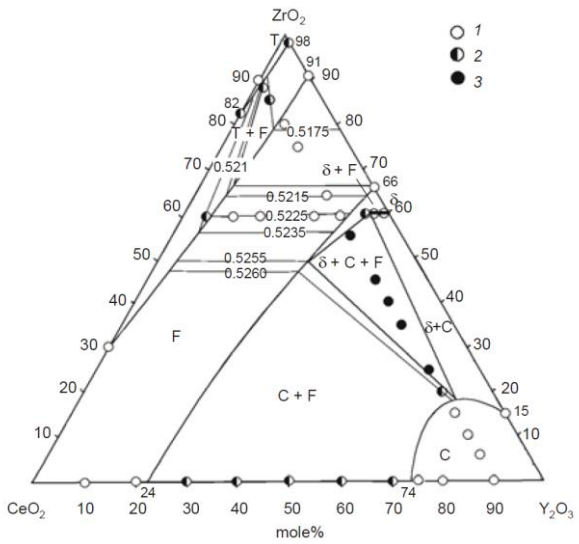

Figure 11 Isothermal section of CeO2-Y2O3-ZrO2 ternary system at 1250°C [94]

The preparation and investigation of ternary systems (like ZrO_2 - Y_2O_3 - CeO_2) is more complex issue than in case of binary systems. So-called Gibbs phase diagrams are used to describe the phase composition of systems composed of ternary mixtures. In each case, the Gibbs diagram is prepared for specified temperature and pressure. The example of Gibbs diagram of ZrO_2 - Y_2O_3 - CeO_2 at 1250°C [94] and at 1500°C [95] is given in Figure 11 and Figure 12 respectively.

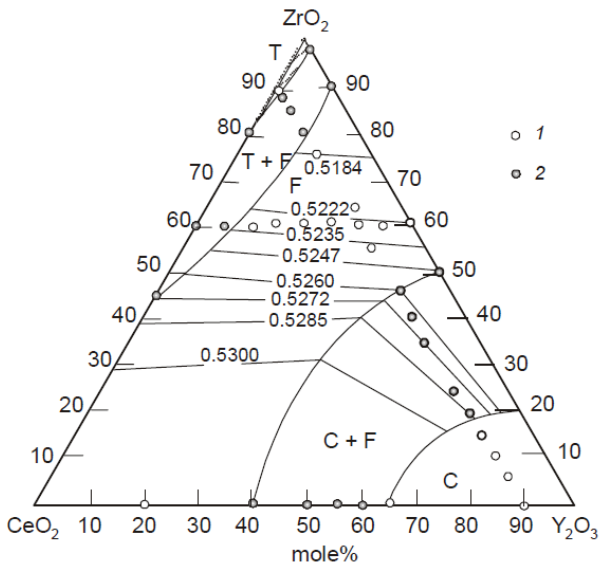

Figure 12 Isothermal section of CeO2-Y2O3-ZrO2 ternary system at 1500°C [95]

The phase diagrams in two mentioned temperatures differ slightly. The solid solution fields of T-ZrO_2, F-ZrO_2, and C-Y_2O_3 were observed in two temperatures. But these fields vary in mentioned temperatures, the same as homogeneity fields of other phases. It can be observed also that for lower temperature the homogeneity ranges of tetragonal and fluorite phases decrease. At the same time the ranges of two or even three phases increase [94].

The zirconia having a composition of ZrO_2 - Y_2O_3 - CeO_2 was not studied very intensively yet. But its properties can be evaluated basing on the first initial research or analyzing the studies focused on binary CeO_2- ZrO_2 and Y_2O_3- ZrO_2 systems. The very useful property of CeO_2 doped ZrO_2 materials is high stability, even under thermal and chemical conditions [95]. This is in agreement to experimental work [96], [97], where the high corrosion resistance and high phase stability was mentioned also. The thermal conductivity seems to be lower in case of YCeSZ also. This effect can be associated with the change of internal structure of such stabilized zirconia. Cerium atoms, which are

bigger and heavier than yttrium influence the material lattice. The interatomic distances change and the transport of heat can be limited. The improvement of thermal transport properties of 56.6 % when compared to conventional YSZ coating was obtained in the study [92]. But it should be mentioned also, that YCeSZ material was characterized by much finer microstructure than YSZ in mentioned work. YCeSZ is characterized also by slightly higher thermal expansion when comparing to conventional YSZ. This should provide improvement of thermal shock resistance [88]. Furthermore, the YCeSZ was found to possess high fracture toughness according to [95].

On the other hand, ZrO_2 - CeO_2 systems are characterized by much lower ionic conductivity and electronic conductivity (in reducing medias) than ZrO_2 - Y_2O_3. So the application of ZrO_2 - Y_2O_3 - CeO_2 systems in SOFC's is rather dubious. The hardness of YCeSZ is also lower than in case of YSZ. Due to the vaporization or reduction of CeO_2 the stoichiometry of the whole system can slightly change during the operation [98]. The material was selected for this study because of the perspective thermal transport properties and the possibility of application in TBC's. The powder had completely different morphology than YSZ, what is described in following chapters.

CHAPTER 4. THE AIM OF RESEARCH WORK

The literature review of gas turbines technology showed that there is a constant need to increase the combustion temperature in the jet engines. The higher inlet turbine temperature increase the efficiency of the engine. The amount of toxic substances in the exhaust gases can be decreased also. But together with the increase of combustion temperature the insulating properties of Thermal Barrier Coatings should be improved. Based on these information, the research hypothesis of this work was that:

Due to the appropriate selection of SPS spray process parameters it is possible to modify the zirconia coating microstructure and improve thermal transport properties of Thermal Barrier Coatings.

The useful goal of this work was *to test the commercially available torches with zirconia suspensions in view of possible applications as thermal barriers and electrolyte in SOFC's* (SG-100, Triplex, Axial III and WSP-H 500). The torches were different in the term of plasma stabilization mode, electric power, feedstock injection etc. It was necessary to find appropriate spray conditions for each torch in order to produce high-quality coatings. The idea was to prepare coatings very different in the term of their morphology (namely columnar coatings or two-zones coatings) with varied content of pores in the coating structure.

The analysis of the growth-up mechanisms in Suspension Plasma Spraying method as well as *the characterization of selected properties of SPS zirconia coatings deposited with different spray parameters* were a scientific goals of this PhD project. Finally, the correlations between microstructure and properties of coatings were investigated and discussed also.

The methodology and scheme of performed studies are presented in Figure 13.

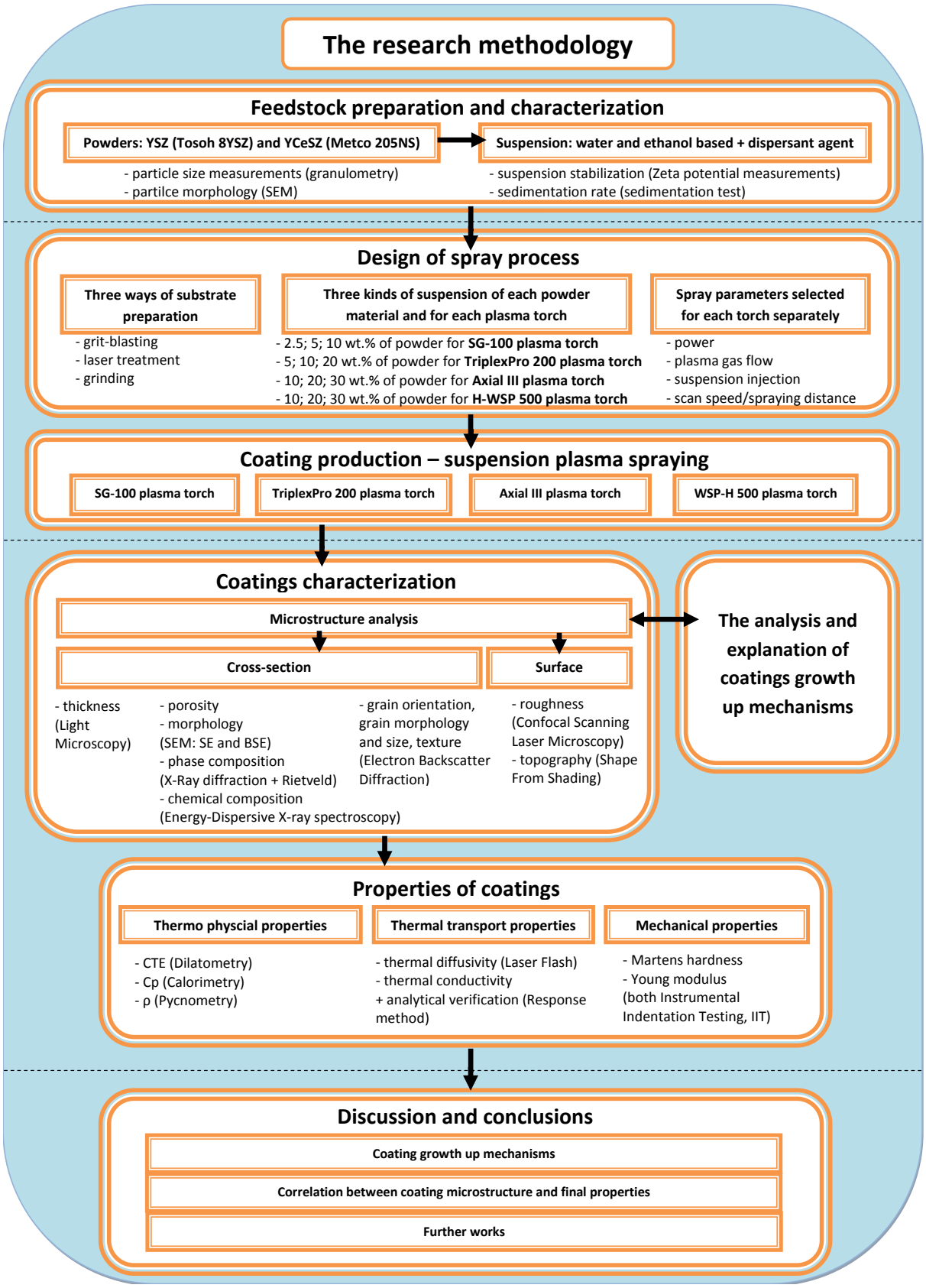

Figure 13 The research methodology used in this PhD project

CHAPTER 5. EXPERIMENTAL PROCEDURES

5.1. Suspension manufacturing

5.1.1. Powder characteristics

Yttria-stabilized zirconia (YSZ) and yttria/ceria-stabilized zirconia (YCeSZ) powders were used for coating production. The main features of powders were as follows:

YSZ powder

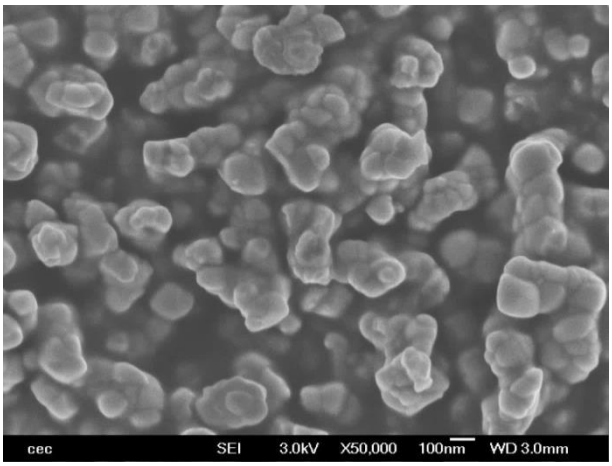

Figure 14 The morphology of YSZ powder produced by Tosoh (FEG-SEM, SE) [99]

The submicrometer-sized powder produced by Tosoh (Tosoh TZ-8YS, Tokio, Japan) with a chemical composition of ZrO_2 + 14 wt. % Y_2O_3. The powder is manufactured in a multi-step procedure, starting with hydrolysis of chemical precursors, followed by drying, calcination, milling and finally spray drying [31]. The morphology of YSZ powder was characterized using Scanning Electron Microscope equipped with Field Emission Gun (JEOL JSM 7400F, Tokyo, Japan) and showed irregular microstructural features of YSZ

powder. The powder particles formed longitudinal and heterogeneous aggregates (see Figure 14 [99]).

The powder particle size was measured by the means of Dynamic Light Scattering (DLS) technique using Zetasizer Nano ZS (Malvern Instruments Ltd, Worcestershire, UK). The method allows to measure submicrometer- or even nanometer-sized (even down to 1nm) particles. This method determines in fact the particles motion from the detected fluctuations of scattered light. Then the particle motion can be converted to the particles size by the Stokes-Einstein relationship. According to the measurements the powder particles were equal to dv_{10}=0.36 μm, dv_{50}=0.53 μm, and dv_{90}=0.95 μm. The particle size distribution diagrams are presented in Figure 15.

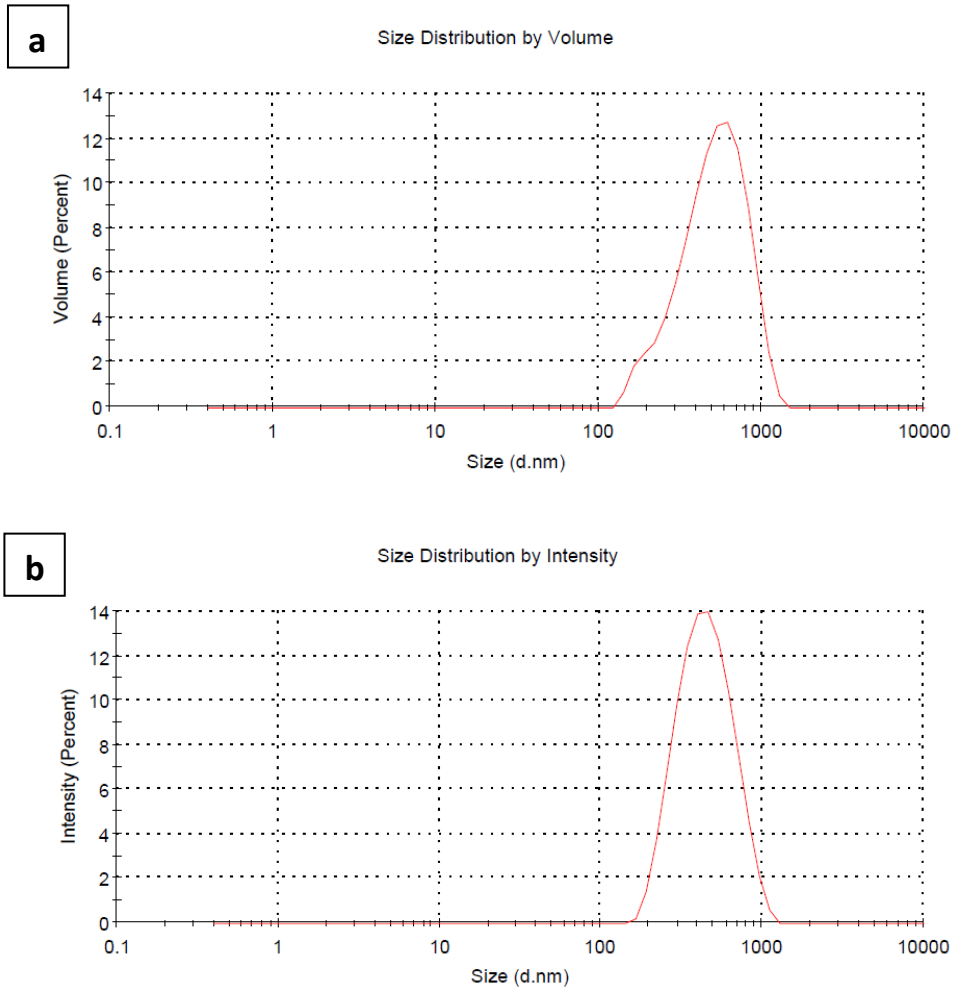

Figure 15 YSZ powder particle size diagram: (a) volume-based particle size distribution and (b) number-based particle size distribution

The XRD measurements were prepared to verify the phase composition of powders used for spraying process. The conventional powder X-Ray diffractometer Bruker D8 Advance

(Bruker, Billerica, MA, USA) operating under Bragg-Brentano geometry with Cu Kα1 radiation was used for this purpose. The measurements were carried out at 2θ angle in the range 15–120° with the step size of 0.03°. The diffractograms were analyzed with dedicated Diffrac+ EVA Software and JCPDS-ICDD database. In the case of YSZ powder produced by Tosoh, the XRD studies showed that powder had fully cubic structure (see Figure 16) [33]. The 01-078-5501 file (Yttrium Zirconium Oxide) of the JCPDS data base was used to describe the phase composition of Tosoh powder.

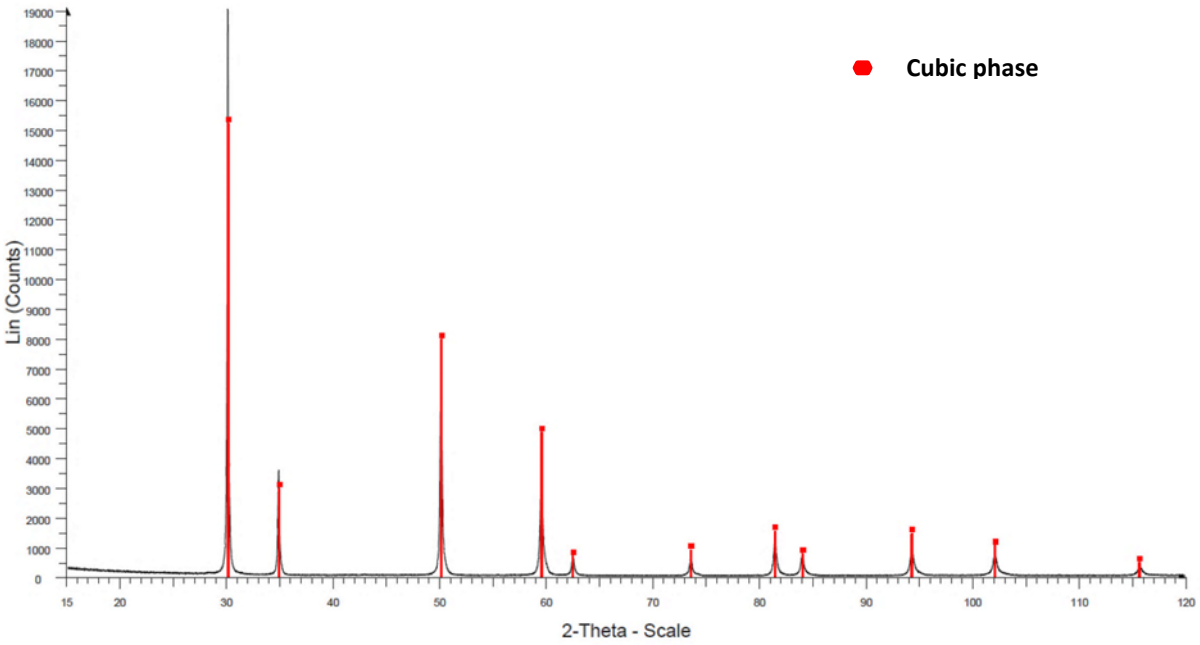

Figure 16 The XRD diagram presenting the phase composition of YSZ powder in as-produced state

YCeSZ powder

The powder produced by Oerlikon Metco with a chemical composition of ZrO_2 + 24 wt. % CeO_2 + 2.5 wt. % Y_2O_3 (Metco 205NS, Winterthur, Switzerland). The solid particles were prepared by spray drying and heat treatment. In fact, the powder was originally designed for conventional Powder Plasma Spraying. The particles were coarse, micrometer-sized, and spherical in the as-produced state (see Figure 17). According to the product data sheet the powder particle were in range of -125 +11 µm.

The particles were to coarse to be sprayed by Suspension Plasma Spraying. Therefore, the powder was pre-treated prior to the suspension formulation. The YCeSZ powder

underwent 3-hours mechanical milling performed by using agitator ball-mill moliNEx system (Netzsch, Selb, Germany).

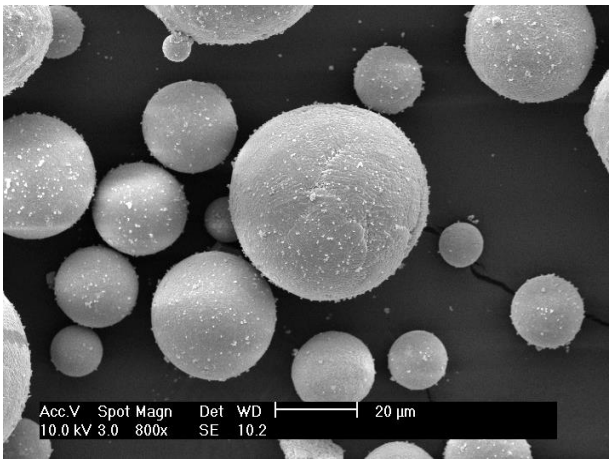

Figure 17 The morphology of YCeSZ powder produced by Oerlikon Metco (SEM, SE)

This high-energy method enables to crush powder materials having different hardness and reduce their size even up to submicrometer. In this case, the process was performed in an ethanol bath and 2 mm zirconia balls were used as a grinding medium. The process allowed to obtain fine and irregular YCeSZ powder particles as show in Figure 18. The final powder particles were angular and non-agglomerated [100].

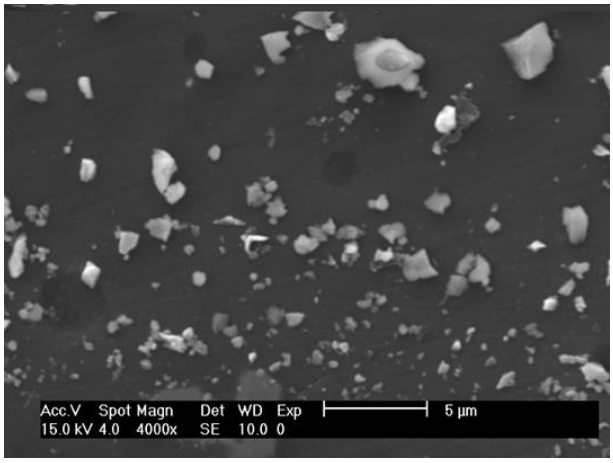

Figure 18 The SEM micrograph of milled YCeSZ powder (SEM, SE)

The laser diffraction method was applied in order to evaluate the YCeSZ powder particle size. In this case, the variation in the intensity of light being scattered by powder particles in a function of scattering angles is measured. The particles having different size scatter the light at different angles, e.g. the bigger particle, the lower is the angle. The particle size is a direct function of the scattered light and scattering angle and can be

calculated using the Mie theory [101]. In comparison to DLS method, the laser diffraction technique is dedicated for slightly coarser powders, starting from micrometer-sized powders up to subicrometer ones. The granulometry test was performed by Horiba Partica LA-950 V2 (Horiba Ltd., Kyoto, Japan). The powder particle size distribution of crushed powder showed monomodal feature but much wider than in case of YSZ powder (see Figure 19). The results of granulometry test were as follows: dv_{10}=0.41 µm, dv_{50}=0.75 µm, and dv_{90}=1.80 µm.

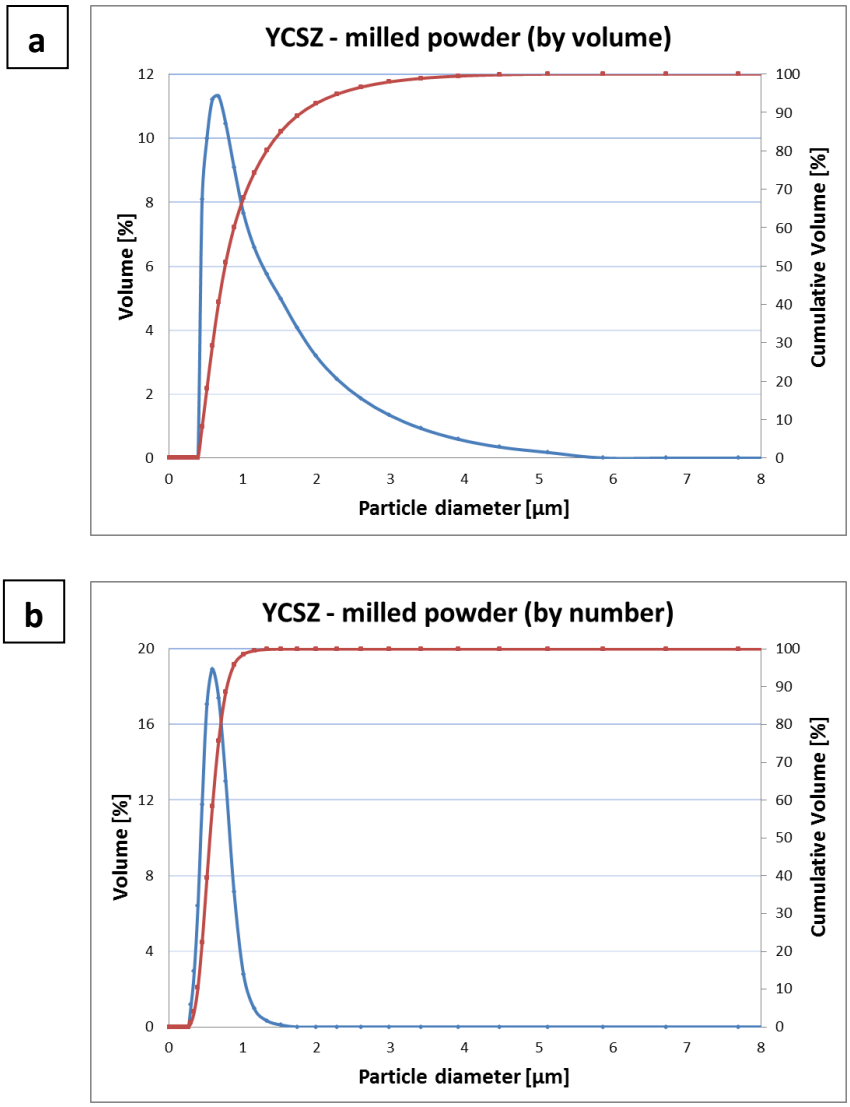

Figure 19 YCeSZ powder particle size diagram: (a) volume-based particle size distribution and (b) number-based particle size distribution

The XRD studies showed that powder had complex phase composition (mostly tetragonal but the appearance of cubic and monoclinic components was observed also) [33]. The XRD diagram is presented in Figure 20.

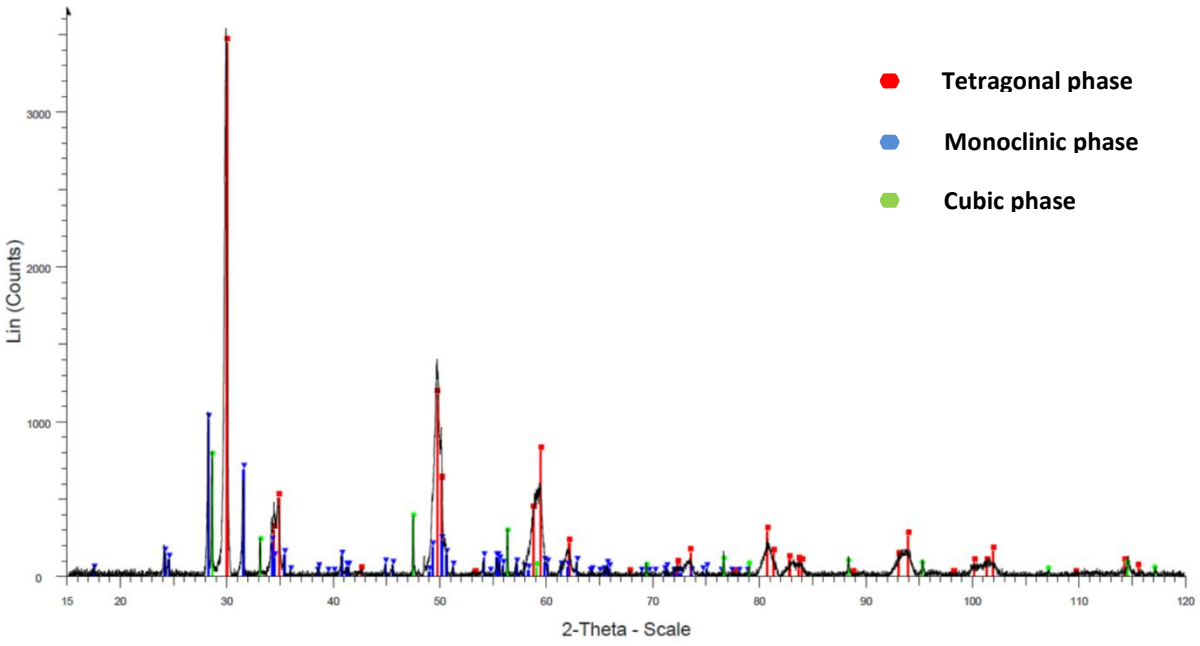

Figure 20 The XRD diagram of YCeSZ powder in initial stage

The phase composition of YCeSZ powder was found to be a mixture of:

- tetragonal phase of Cerium Yttrium Zirconium Oxide (04-013-9723 file of the JCPDS data base) - this was a dominating phase;
- monoclinic phase of Baddeleyite, ZrO2 (00-037-1484 file of the JCPDS data base);
- cubic phase of Cerium Yttrium Oxide (04-016-4629 file of the JCPDS data base).

5.1.2. Suspension formulation

After the characterization of zirconia powders the suspensions were prepared. The liquid feedstock was a mixture of powder material, solvent and dispersant agent. The procedure of suspension formulation is presented in Figure 21. As a solid phase the as-produced YSZ and ball-milled YCeSZ powders were used. Three different amounts of solid phase were used depending on the plasma torch and spray parameters:

- 2.5, 5, 10 wt. % – SG-100;
- 5, 10, 20 wt. % - Triplex;
- 10, 20, 30 wt. % – Axial III and WSP-H 500.

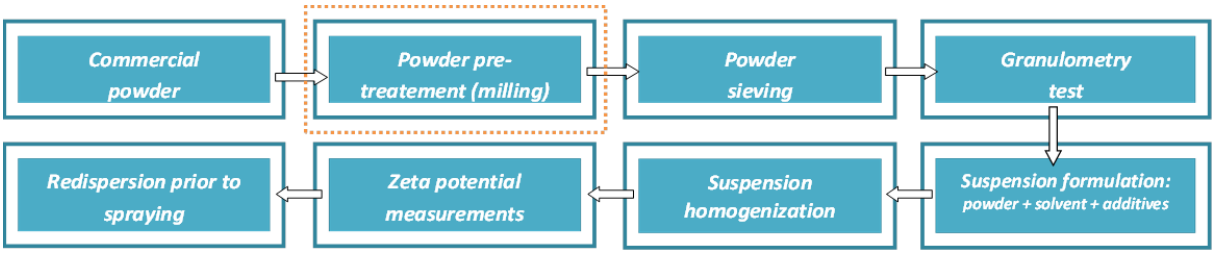

Figure 21 Suspension preparation procedure (powder pre-treatment applied if necessary)

Afterwards, the powders were mixed with a water/ethanol (50 vol. %/50 vol. %) based solvent. Furthermore, the suspensions were homogenized and stabilized by the addition of dispersant agent. The phosphate ester agent namely Beycostat C213 (CECA, France) was used to ensure electrostatic stabilization of suspension. The most important features of liquid feedstocks used for spraying are summarized in Table 3.

Table 3 The characteristic of suspension used for spraying

Suspension details	Powder dv_{10} (µm)	Powder dv_{50} (µm)	Powder dv_{90} (µm)	Suspension concentration (wt. % of solid)	Solvent type	Chemical agent
YSZ based suspension	0.36	0.53	0.95	2.5 ; 5 ; 10 (SG-100) 5 ; 10 ; 20 (TriplexPro-200) 10 ; 20 ; 30 (Axial III; WSP-H500)	water / ethanol (50:50)	Beycostat C213
YCeSZ based suspension	0.41	0.75	1.80	2.5 ; 5 ; 10 (SG-100) 5 ; 10 ; 20 (TriplexPro-200) 10 ; 20 ; 30 (Axial III; WSP-H500)	water / ethanol (50:50)	Beycostat C213

5.1.3. Zeta potential

The formulation of suspensions is a part of colloid chemistry and the main aim of this process is to prepare a stable suspension. By the means of suspension's stability the sedimentation rate should be minimized. In case of suspensions for SPS the particle dispersability should be improved and rheological properties should be enhanced also. The stability and dispersion of colloids can be prevented for example by electrostatic

repulsion. The strength of this force can be described by the Zeta potential (ζ). The higher is the force better is the suspension stability. The detailed information about Zeta potential and suspension stabilization methods were given in the part of literature review (Chapter 2).

As mentioned in previous paragraph, in order to prevent the powder particles against agglomeration and sedimentation the dispersant agent was used (Beycostat C213). The Zeta potential measurements were performed to optimize the liquid feedstock and predict its behavior during spraying. The measurements were performed by Zetasizer Nano ZS (Malvern Instruments Ltd, Worcestershire, UK). The best obtained values of Zeta potential (ζ) for mentioned suspension were as follows:

- ζ = 82.5 mV for the YSZ suspension,
- ζ = −12.9 mV for YCeSZ suspension.

5.2. Substrate preparation

The substrate preparation is a one of the crucial sub-process in the coating technology. This substrate pre-treatment strongly influence the quality and adhesion of deposited coating. But in this study the idea was to check the influence of the substrate topography on the coating microstructure and coating growth-up mechanisms.

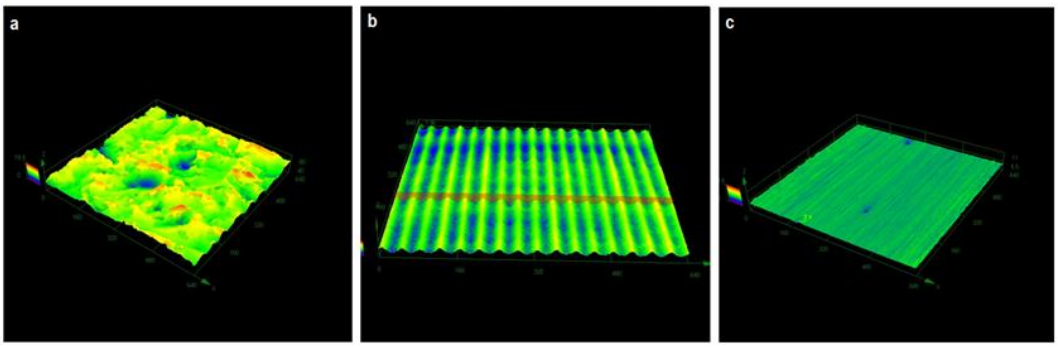

Figure 22 The 3D substrate topography view after: grit-blasting (a), laser treatment (b) and grinding (c)

For this purpose three different technologies were applied to form the substrate surfaces having different roughness and features: (i) grit- blasting, (ii) grinding, (iii) laser treatment. Grit-blasted substrates were the most rough (Ra=5.5-7.8 μm) and

they had very irregular surface. The white corundum with the size of F36 (particles between 500-600μm according to the FEPA standards) was used for grit-blasting. The laser-treated substrates were having medium roughness (Ra=3.2-3.9 μm) but the surface peaks were distributed very regularly when comparing to grit-blasted substrates. The laser texturing allowed creating of fine grooves on the substrate surface (one-dimensional linear pattern). The treatment was performed by using Duetto picosecond laser (Time-Bandwidth Products, Zürich, Switzerland). Finally, the grinding process was performed with 320 grit SiC abrasive paper. The grinded substrates were at the same time the smoothest ones (Ra=0.1-0.5 μm).

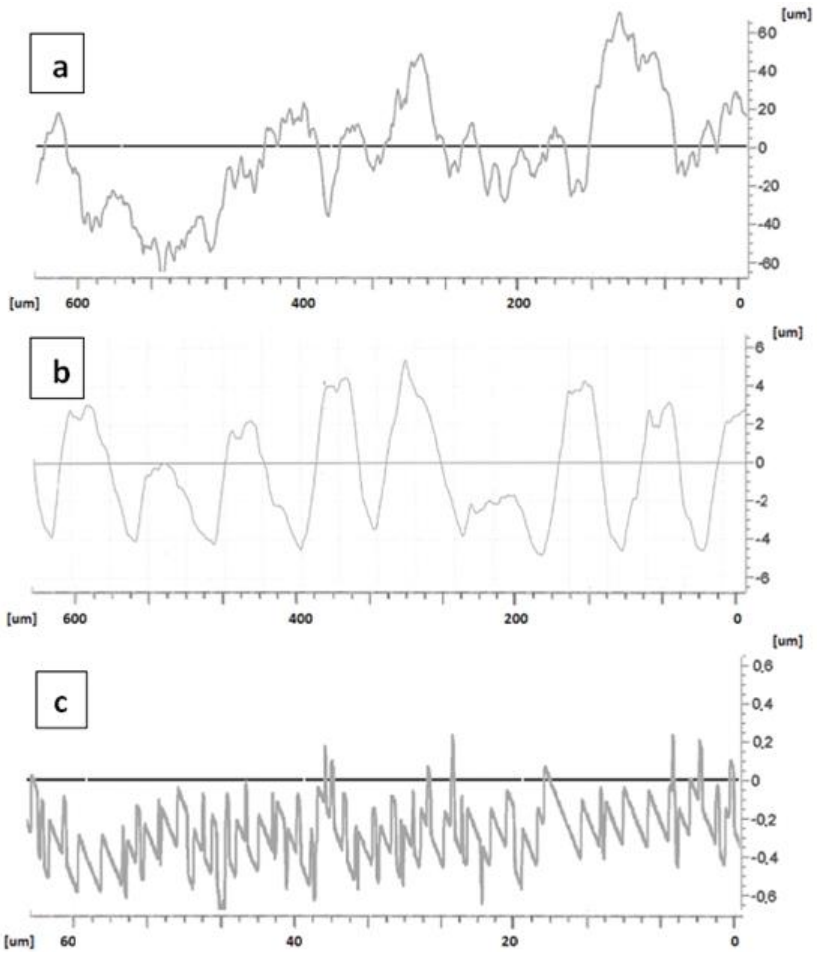

Figure 23 The substrates profiles: (a) grit- blasted, (b) laser treated (c) and grinded

The 3D views of substrates topographies were prepared by confocal laser scanning microscopy (Lext OLS4000, Olympus, Tokyo, Japan) and are presented in Figure 22. The roughness measurements were made with the use of stylus profilometer FORM TALYSURF 120L (Rank Taylor Hobson Ltd, Leicester, UK). The substrate profiles are shown on Figure 23 and the roughness values were as follows:

- Sand-blasted substrate Ra=5.5-7.8 μm, Rz=32.4-38.9 μm,
- Laser treated substrate Ra=3.2-3.9 μm, Rz=16.7-18.6 μm,
- Grinded substrate Ra=0.1-0.5 μm, Rz=0.5-0.9 μm.

Two kinds of substrates were used. The coupons with the diameter of 25mm manufactured from 2 mm thick 304L stainless steel were used for microstructural characterization of coatings. For the purpose of studies that were performed at relatively high temperatures the temperature-resistant nickel super alloy (Inconel 600, UNS N06600) substrate were used also. The substrates were 2mm thick and 10x10mm square-shaped. All substrates were cleaned in the ultrasonic bath in ethanol prior to spraying.

5.3. Thermal spraying

5.3.1. Plasma torches and spray set-ups

The spray process was performed with the use of four different plasma torches. They had different design, power, plasma stabilization mode, feedstock injection etc. Following, the plasma set-ups were also slightly different what influenced the arrangement of the deposition process. The main characteristic of each plasma torch and each set-up is discussed below. The detailed discussion focused on advantages and disadvantages of different types of plasma torches was presented already in the literature review part.

SG-100

The basic torch that was used for coating production having simple stick-type (called also rod-shaped) cathode design and conical anode. The internal suspension injection mode together with the continuous-stream injector were used during spraying. The injector was mounted inside the anode so the optimization of feedstock injection point was not necessary here. The SG-100 torch (Figure 24) was developed by Praxair (Indianapolis, IN, USA) [102].

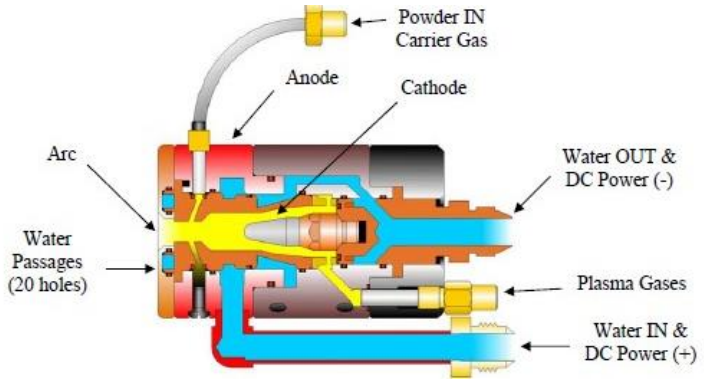

Figure 24 SG-100 plasma torch with internal injection [102]

The SG-100 plasma torch was mounted on an arm of 5-axis industrial robot of ABB (Zurich, Switzerland). The robot was used to move the plasma torch and scan the substrates' surface. The samples were mounted on the flat table which was connected to the vacuum pump. The vacuum system was necessary to keep the substrates in one position on the table during spraying. This kind of sample fixture enabled to use substrates having various shape and size without the need to design different samples holders. The whole spray-set up equipped with SG-100 plasma torch is presented in Figure 25b. The suspension transportation was ensured by the pneumatic system. The liquid was mixed in the pressurized container by the magnetic stirrer in order to prevent particle sedimentation. The feedstock injection pressure was controlled during spraying by the analog manometer (Figure 25a).

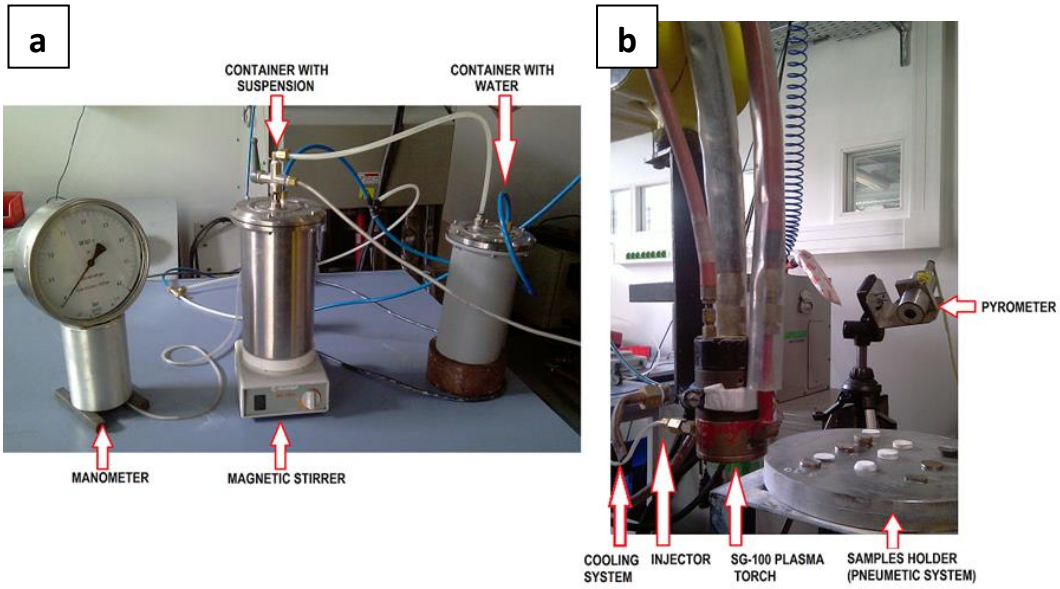

Figure 25 The SPS set-up equipped with SG-100 plasma torch; a – pneumatic system for suspension injection, b – plasma torch and sample fixture (University of Limoges)

Triplex

The second spray set-up was equipped in more advanced TriplexPro-200 torch of Oerlikon Metco (Wohlen, Switzerland). The torch is characterized by three parallel cathodes and one anode. The cathodes and anode are separated by electrically insulated rings what prolongs and stabilizes the arc (Figure 26a). The design of torch makes impossible to use internal injection of feedstock material. The injector was mounted outside of the torch, radially to the plasma jet. The suspension injection point was set based on the own experience of the laboratory. The feedstock was injected using one continuous liquid stream injector. The angle was set in a way, that the injected liquid could go through the one of the plasma peaks (in term of plasma temperature, enthalpy etc.). The peaks are generated by the cathodes and they are shown in dark gray in Figure 26b. The injection pressure was high enough in order to penetrate the plasma jet.

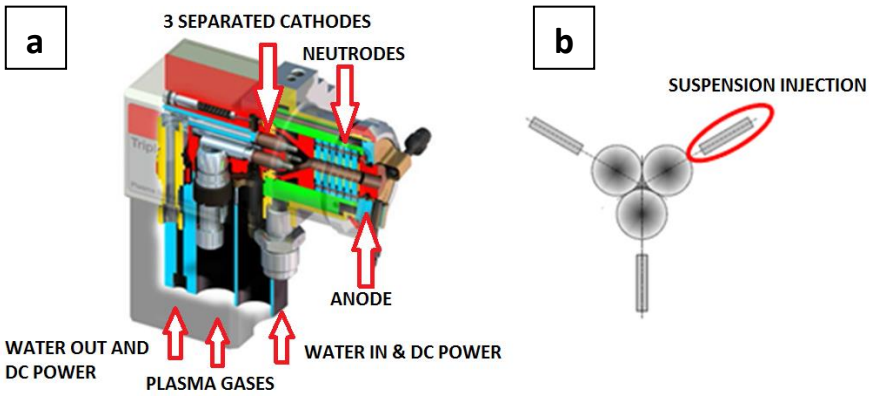

Figure 26 TriplexPro-200 plasma torch design [103] (a) and the feedstock injection optimization of materials having high-melting point [104] (b)

The whole set-up arrangement was slightly different then in case of SG-100 plasma torch. The plasma torch was fixed and the movement of substrates was realized by the reciprocating and rotating sample fixture (Figure 27b). The substrates were mounted on the sample fixture by the use of vacuum system (vacuum pump connected to the fixture, similarly as in case of SG-100 set-up) or mechanically by screws. The rotation of samples allowed more effective cooling of samples when comparing to the flat table used in the previously described set-up. The pressurized system was used for the suspension injection (Figure 27a). The containers with the feedstock material were equipped with the magnetic stirring system and pressure control system also.

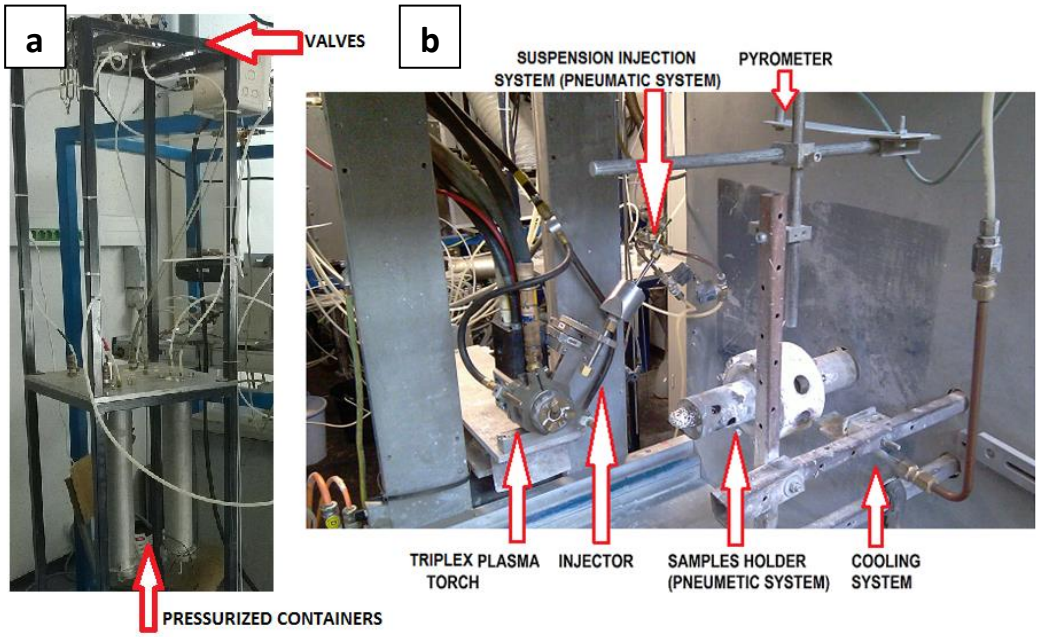

Figure 27 The SPS set-up equipped with TriplexPro-200 plasma torch; a – pneumatic system for suspension injection, b – plasma torch and sample fixture (University of Limoges)

Axial III

The next plasma torch applied for coating deposition was multi-cathode and multi-anode gas-stabilized Axial III (Northwest Mettech Corp., North Vancouver, Canada). Thanks to the use of three independent DC arcs supplied by three power sources, the torch can reach much higher electric power then in the case of other gas-stabilized plasma units. The torch enables also an internal and fully axial injection of liquid slurry (see Figure 28). Furthermore, in this patented solution, the feedstock is introduced directly in the hot center of three plasma jets, which joint in an exit nozzle of the torch. The material is entrapped in the hot plasma jet, so the optimization of the suspension injection point was not necessary for Axial III.

The spray set-up arrangement was semi-industrial one in case of Axial III (in contrast to typical laboratory set-ups equipped with SG-100 and Triplex torches). The configuration of the spray system was as follow: the torch was mounted on a 6-axis industrial robot of ABB (Zurich, Switzerland) and the substrates were fixed to the carousel. The carousel was screwed to the thermal spray turntable. The rotation of the table corresponded to the torch scan speed velocity. Afterwards, the linear movement of the torch (up and down) defined at the same time the scan off-set and the trajectory of the torch (Figure 29b).

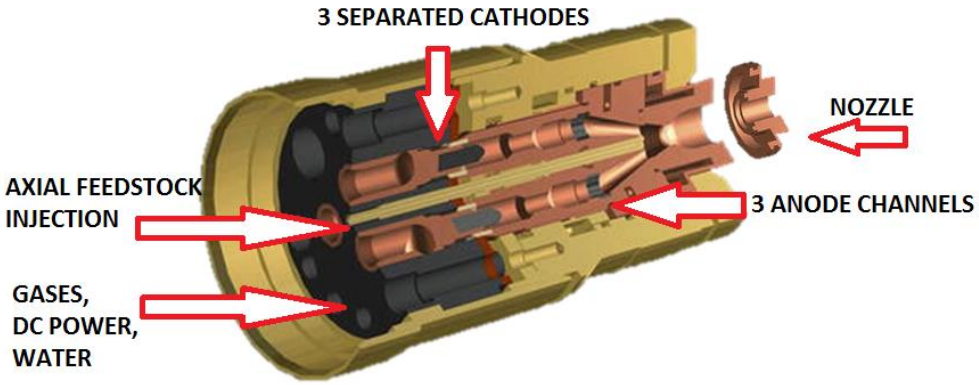

Figure 28 Axial III plasma torch with axial injection [105]

The suspension transportation was realized by the NanoFeed system dedicated for Axial III plasma torch (Figure 29a). The system was equipped with peristaltic pump and Coriolis mass flow meter, so the feed rate was measured and controlled on-line during spraying. The system allowed also to observe the injection back-pressure value in order to eliminate any problems related to the feedstock introduction into the plasma jet. Furthermore, the suspension was mixed inside the suspension feeder by the internal mechanical stirrer.

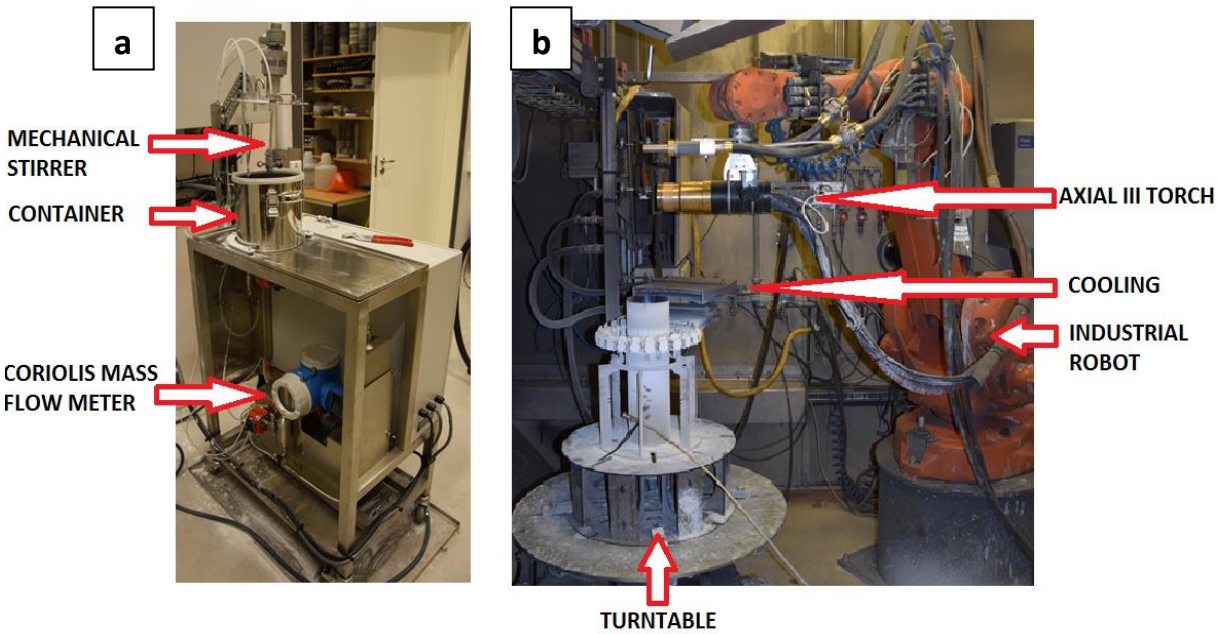

Figure 29 The SPS set-up equipped with Axial III plasma torch; a – commercial NanoFeed suspension injection system with peristaltic pump, b – plasma torch and sample fixture (University West, Trollhättan)

WSP-H500

The last of applied torches (Figure 30) [84] was a hybrid version of water stabilized plasma torch (WSP). The torch operates in dual, gas and water, stabilization mode. As a result the torch can use a very low working gas flow rate (only a few to a dozen slpm of Ar). But the unit consumes also a few liters of pure water (per hour). The water is decomposed into hydrogen, oxygen and OH groups and these gases form together with working gases the plasma jet. At the same time the torch provided also the highest electric power among all units that were tested in this PhD project. This resulted in the higher temperature and enthalpy of plasma jet (when comparing to gas stabilized torches).

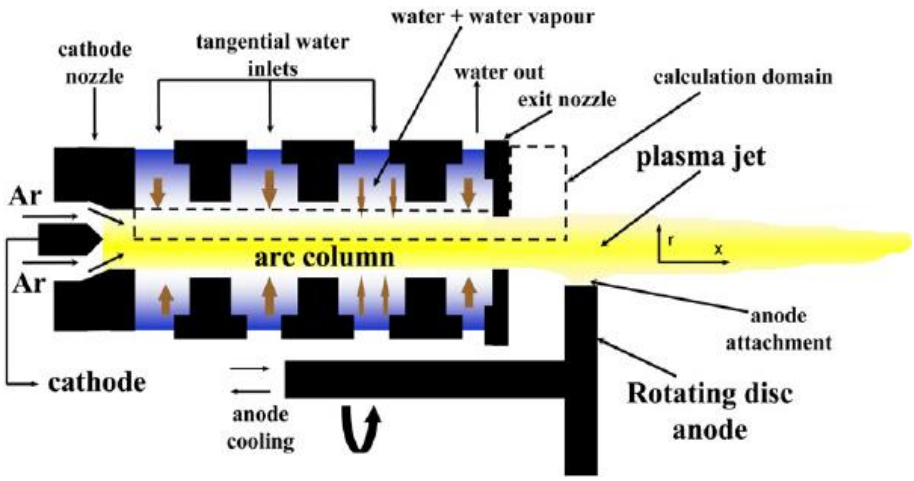

Figure 30 WSP-H 500 plasma torch operating principle [84]

The plasma torch was mounted on an arm of 6-axis industrial robot, whereas the substrates were mounted on a rotational carousel. The linear movement of the robot arm determined the spraying path and the offset between consecutive plasma torch passes. Afterwards, the rotation of the carousel corresponded to the plasma torch scan speed. The arrangement of spray set-ups is presented in Figure 31b.

The suspension transportation was realized using conventional pneumatic system (similar as in case of SG-100 and TriplexPro-200). The containers were equipped with magnetic stirrer and sonotrode. The slurry was introduced to the plasma jet by the external injection mode. The suspension injection system is shown in Figure 31a.

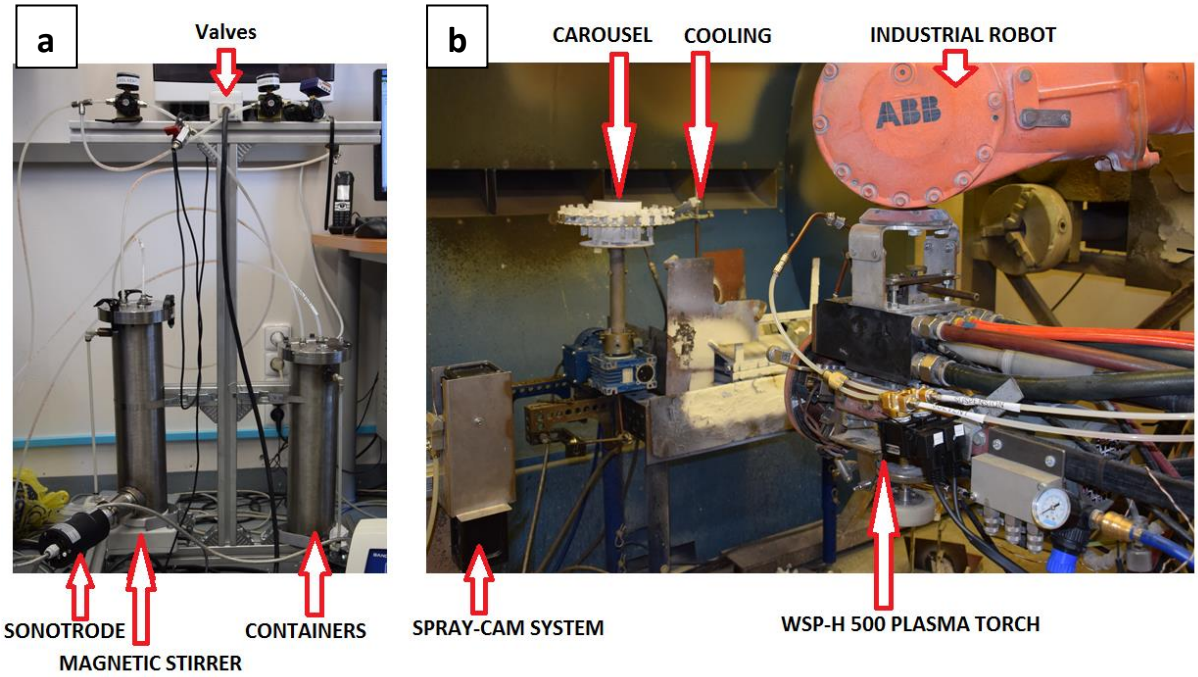

Figure 31 The SPS set-up equipped with WSP-H 500 plasma torch; a – pneumatic system for suspension injection, b – plasma torch and sample fixture (Institute of Plasma Physics CAS, Prague)

The optimization of appropriate injection angle and pressure was done by using the shadowgraphy method. The diagnostic system was basing on SprayCam camera (Control Vision Inc., Sahuarita, USA) and was used also for a visualization of the liquid feedstock stream break-up and droplets fragmentation in the plasma jet (Figure 32)[5]. The injection pressure was adjusted depending on the powder material and suspension concentration.

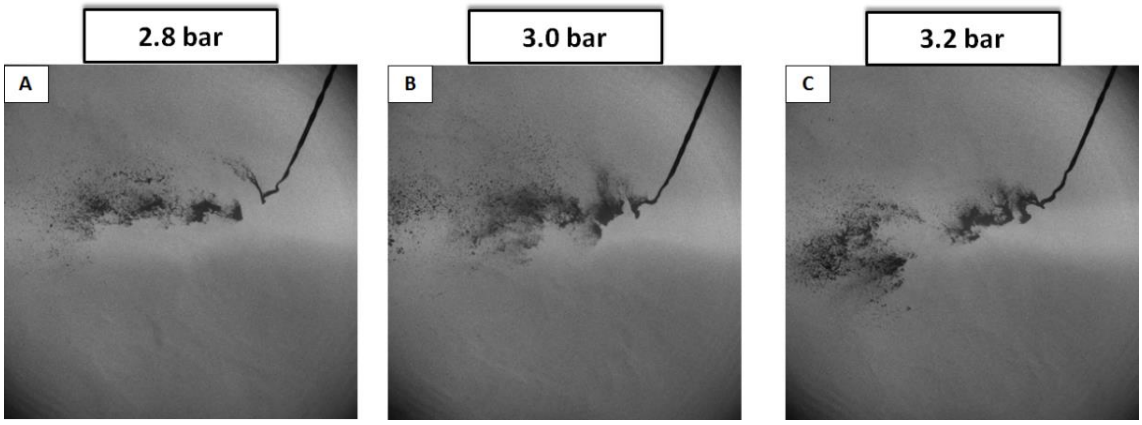

Figure 32 The optimization of radial injection point by changing the injection pressure (by shadowgraphy): (a) 2.8 bars, (b) 3.0 bars, (c) 3.2 bars

Before starting of each spray run the plasma jet, solvent flow, as well as appropriate suspension flow were controlled also by conventional camera equipped with CMOS image sensor as presented in Figure 33.

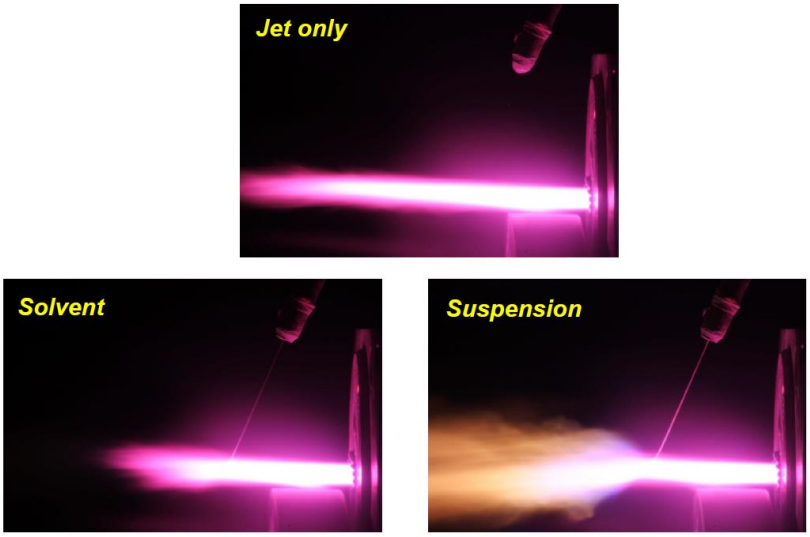

Figure 33 The control of plasma jet, solvent flow and suspension injection

5.3.2. Spray process parameters

The very big differences between the spray set-ups that were described in the previous paragraph (and are summarized in Table 4)[5] caused that the spray parameters had to be optimized for each plasma torch separately.

Table 4 The summarized characteristic of plasma torches that were used for the coating production (by Sokołowski and Pawłowski [5])

Torch	Injector	Injection angle	Electric power (kW)	Arc stabilization mode
SG-100	Internal	Radial	Low (40kW)	Gas
Triplex	External	Radial	Low (45kW)	Gas
Axial III	Internal	Axial	High (120kW)	Gas
WSP-H500	External	Radial	High (150kW)	Water

The detailed spray process parameters for each set-up are collected in the Table 5. The two plasma torches operated at relatively low electric power 40-45kW (SG-100 and TriplexPro-200), whereas Axial III and WSP-H500 generated much greater electric power (120kW and 150kW, respectively). Furthermore, the working gas composition and gas flow rates were much different for each torch. This influenced the stand-off distance (bigger power = bigger spray distance), spraying speed, plasma torch trajectory (offset between the torch passes). Depending on the torch power, the suspension injection feed rate could be optimized also (bigger power = bigger suspension flow rate).

Table 5 The detailed list of spray process parameters used for the coating production

Torch	SG-100	TriplexPro-200	WSP-H 500	Axial III
Process parameters, units	Values	Values	Values	Values
Electric power, kW	40	45	~150	~120
Working gases composition	Ar + H_2	Ar	Ar + H_2O decomposition products*	Ar + H_2 + N_2
Total plasma gases flow rate, slpm	50	70	15 of Ar + H_2O decomposition products*	245
Stand-off distance, mm	40	70	100	75
Relative torch scan speed velocity, mm/s	500	1000	~900	~1000
Offset between plasma torch passes, mm	3	10	30	5
Nozzle injector internal diameter, mm	0.50	0.15	0.35	0.50
Suspension injection system	Pneumatic system; continuous stream injector	Pneumatic system; continuous stream injector	Pneumatic system; continuous stream injector	Peristaltic pomp; continuous stream injector
Suspension injection rate, ml/min	35	40	90-100**	45

* H_2, O_2 and OH groups formed from the water vortex ionization (the torch consumed 2-3 liters of water per hour)

** Depending on the feeding pressure optimized by SprayCam system

The stand-off distance in Suspension Plasma Spraying is much shorter when comparing to conventional Powder Plasma Spraying. This causes that the temperature control is a very important element in SPS manufacturing. The sample temperature should be controlled in order to avoid overheating of substrate or coating. In this study, each spray set-up was equipped with the temperature control system. The measurements were conducted by the use of infrared pyrometer, thermocamera or thermocouple attached to the substrate rear surface. The selection of the equipment depended on the set-up arrangement. The example of temperature history (WSP-H500, temperature measured by thermocamera and thermocouple) is presented in Figure 34.

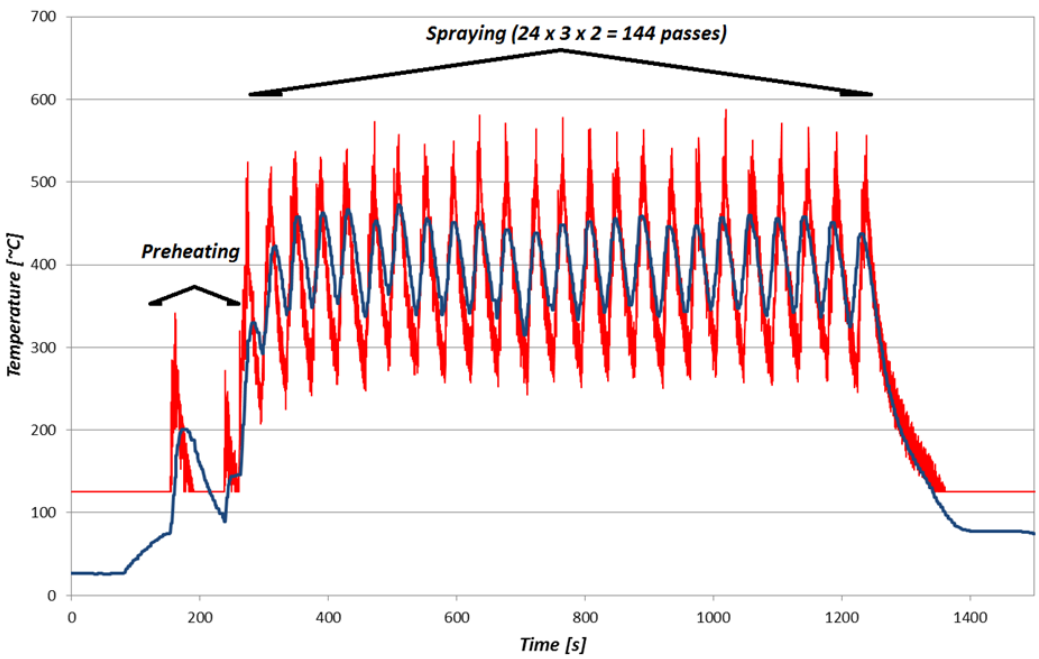

Figure 34 The example of the temperature history recorded during spraying (blue color - substrate rear surface and red color - at the sample front face)

5.3.3. Spray process design

The coatings were prepared in a multi-parameter spray process experiment. The key process parameters were selected based on the preliminary tests. These parameters seemed to have a great influence on the internal microstructure and the build-up mechanism of coatings. Based on the information mentioned in previous paragraphs, the spray variables were as follows: (i) powder material (size and morphology), (ii) suspension concentration, (iii) substrate topography, and finally, (iv) plasma torch.

Table 6 The design of experiment and coating nomenclature

Powder	Substrate	Suspension concentration [%]	SG-100 sample	Suspension concentration [%]	TriplexPro-200 sample	Suspension concentration [%]	Axial III sample	Suspension concentration [%]	WSP-H 500 sample
YSZ	GB	2.5	ST21	5	TT51	10	AT101	10	WT101
YSZ	LT	2.5	ST22	5	TT52	10	AT102	10	WT102
YSZ	G	2.5	ST23	5	TT53	10	AT103	10	WT103
YSZ	GB	5	ST51	10	TT101	20	AT201	20	WT201
YSZ	LT	5	ST52	10	TT102	20	AT202	20	WT202
YSZ	G	5	ST53	10	TT103	20	AT203	20	WT203
YSZ	GB	10	ST101	20	TT201	30	AT301	30	WT301
YSZ	LT	10	ST102	20	TT202	30	AT302	30	WT302
YSZ	G	10	ST103	20	TT203	30	AT303	30	WT303
YCeSZ	GB	2.5	SC21	5	TC51	10	AC101	10	WC101
YCeSZ	LT	2.5	SC22	5	TC52	10	AC102	10	WC102
YCeSZ	G	2.5	SC23	5	TC53	10	AC103	10	WC103
YCeSZ	GB	5	SC51	10	TC101	20	AC201	20	WC201
YCeSZ	LT	5	SC52	10	TC102	20	AC202	20	WC202
YCeSZ	G	5	SC53	10	TC103	20	AC203	20	WC203
YCeSZ	GB	10	SC101	20	TC201	30	AC301	30	WC301
YCeSZ	LT	10	SC102	20	TC202	30	AC302	30	WC302
YCeSZ	G	10	SC103	20	TC203	30	AC303	30	WC303

In total, 72 different spray runs were carried out using YSZ and YCeSZ based suspensions. The full list of samples is collected in Table 6 and the methodology of samples labeling is shown in the Figure 35.

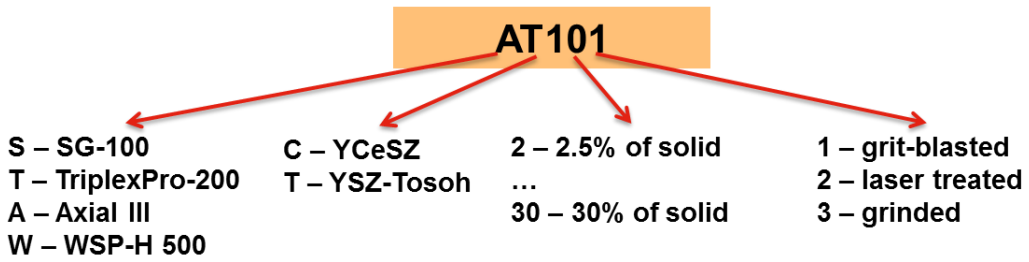

Figure 35 The methodology of samples labeling

5.4. Characterization of coatings

5.4.1. Light microscopy (LM)

The thickness of coatings was estimated on metallographically prepared cross-section of samples as shown in Figure 36. The samples were observed using the light microscope Nikon Eclipse LV100 (Nikon Instruments, Amsterdam, Netherlands). The mean thickness of coatings was found from 15 measurements that were taken in different region of coatings (five local measurements in three different regions of each sample). As a result the average thickness value and standard deviation were calculated.

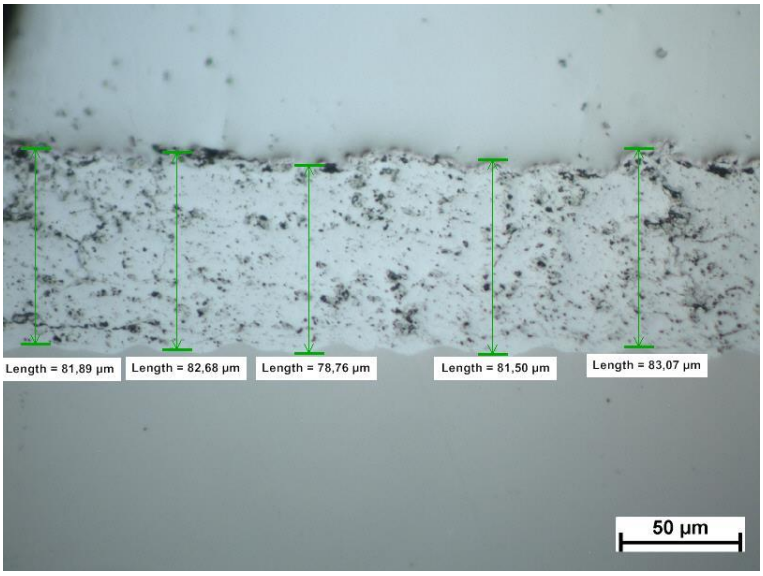

Figure 36 The example of coating thickness measured by the light microscopy (only one region of sample)

5.4.2. Scanning Electron Microscopy and Energy Dispersive X-Ray Spectrometry (SEM/EDS)

Scanning Electron Microscopy (SEM) is a well-known method that enables the microstructural characterization of coatings at high magnifications. The method was used in the study to investigate the morphology of deposited coatings. The micrographs of the coating surface as well as of the coating cross-section were taken. Different SEM microscopes were used during studies: Philips XL30 (Eindhoven, Netherlands), Leo

1455VP (Carl Zeiss GmbH, Oberkochen, Germany) and Neon 40ESB (Carl Zeiss GmbH, Oberkochen, Germany). The SEM analysis was made with the use of secondary electrons (SE) detector and backscattered electrons (BSE) detector also.

SEM micrographs were used also for a calculation of the coating porosity. First, a few images of each sample were taken at constant magnification (1600x). Then, the micrographs were edited using ImageJ free software and total area of pores was calculated (Figure 37). The porosity of coatings was analyzed in at least five different regions of samples and then the average value and standard deviation were calculated.

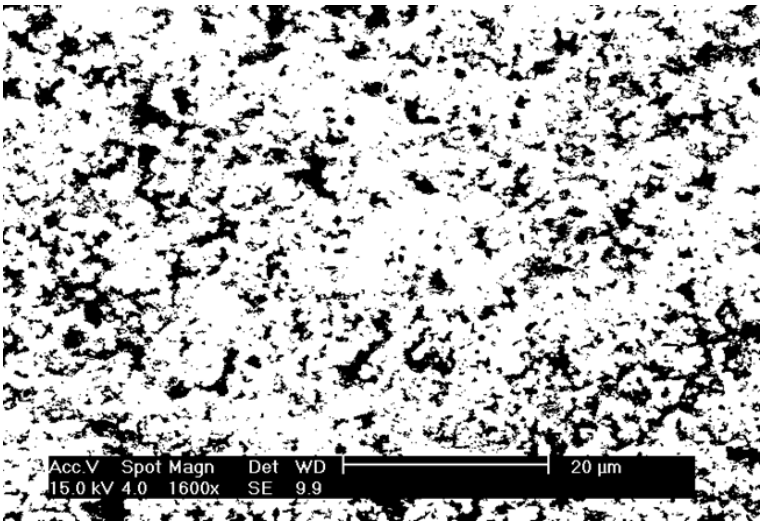

Figure 37 The example of porosity calculations by image analysis method (SEM, SE micrograph edited using ImageJ, sample WT101)

Afterwards, the energy-dispersive spectroscopy (EDS) studies were performed in order to qualitatively evaluate chemical composition of deposits. The investigations were performed by using Philips XL30 microscope equipped with INCA energy-dispersive spectrometer (Oxford Instruments, Oxfordshire, UK) and Leo 1455VP microscope with Metek EDS detector (EDAX Inc., Mahwah, NJ, USA).

5.4.3. X-Ray Diffraction (XRD) and Rietveld refinement

The qualitative analysis of the phase composition of coatings was determined with X-ray Diffraction (XRD) method. The measurements were performed by using Bruker D8 Advance diffractometer (Billerica, MA, USA) operating under Bragg-Brentano geometry

(theta-2 theta). The CuKα1 radiation and a range of 2θ angles from 15° to 120° were used. The phases were identified using Diffrac+ Eva software using JCPDS database.

Using XRD data and Rietveld refinement method the quantitative analysis of YSZ and YceSZ coatings was carried out. The method allowed to calculate the content of phases that were defined using Diffrac+ Eva software. The lattice parameters of different phases that were identified in the coating structures were calculated also. The studies were carried out using TOPAS V4.1 software.

5.4.4. Electron Backscatter Diffraction (EBSD)

The microstructural-crystallographic analysis was followed by the electron back-scattered diffraction (EBSD) studies. EBSD is conducted in scanning electron microscopes. The method enables a quantitative analysis of different microstructural feature of crystalline materials. In this work, the EBSD studies allowed to observe the crystallographic orientation of grains. The shape, size and boundaries of grains were investigated also.

In this method the electron beam is directed at the surface of highly tilted sample (the angle between the beam and sample surface is usually ~70°). Then the electrons are scattered by the atoms that form the material structure and they undergo different interactions with single crystals. The electrons that were back scattered accordingly to the well-known Bragg's law can be recorded on electron-sensitive detector in a form of strong lines. These lines are called Kikuchi patterns and they are associated with the crystal plane from which they arise. The ones that were not Bragg scattered (and have lower energy) produce a background for Kikuchi patterns. In fact, EBSD is a technique basing on the discovery of diffractions patterns observed together by Nishikawa and Kikuchi in 1928 [106]. Those patterns were called firstly "p-type" or "patterns of the fourth kind". The formation of Kikuchi lines can be observed in Figure 38 [107].

In order to have a qualitative data about the material, the sample is scanned point by point with an adjusted step size. Then the point results are combined and presented in a form of map of the tested area. The method became very useful since the high-

performance SEM microscopes are available and the data acquisition/processing systems are fast enough to ensure reasonable time of analysis.

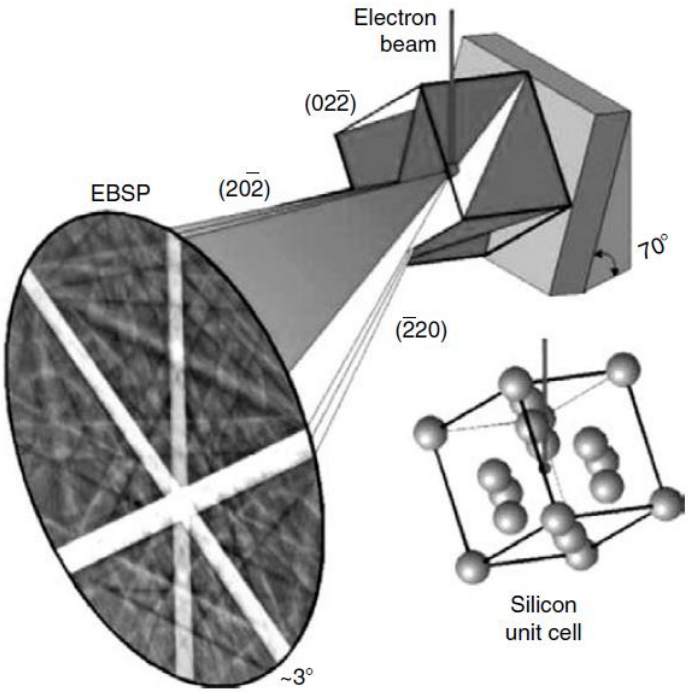

Figure 38 The interaction between the electron beam and polycrystalline material in EBSD method [107]

The EBSD method requires a very careful metallographic preparation of samples. The samples were mounted in electrically conductive Bakelite resin together with the carbon filler (Polyfast Struers). The samples were then ground and carefully polished with fine colloidal silica (OPS Struers). After cleaning in an ethanol bath the samples were coated with a very thin carbon layer.

Due to the fine grained microstructure of SPS coatings, the appropriate selection of EBSD acquisition parameters was necessary in order to ensure high resolution and high quality of results. The parameters were as follows:

- the proper test area was chosen based on the SEM observations
- step size of about 100nm (max. of 150nm for biggest test areas)
- beam voltage of 15kV and aperture of 60μm
- acquisition speed of about 6-10 points per second

The measurements were done using SEM Neon 40ESB equipped with DigiView EBSD camera (EDAX Inc, Mahwah, NJ, USA). Then, the recorded data were analyzed using dedicated OIM Analysis 6.1 software. The EBSD data were filtered each time in order to minimize noises, which are unavoidable for this kind of analysis. The data filtering was performed by using of two types of filters - confidence index (CI > 0.12) or image quality (IQ).

5.4.5. Laser Scanning Confocal Microscopy (LSCM)

Then, the analysis of the coating surface topography was performed. The roughness of the samples was evaluated by Laser Scanning Confocal Microscopy (LSCM). The measurements were carried out using Olympus LEXT OLS4000 (Olympus Co. Ltd., Tokyo, Japan). For each sample five measurements were performed. Then, the average value and standard deviation of Ra and Rz roughness parameters were calculated and compared.

The roughness was evaluated qualitatively only - the coatings were compared between each other. Finally, the influence of the substrate roughness and SPS deposition parameters on the surface roughness of the coatings was analyzed.

5.4.6. Shape From Shading (SFS)

The coating free-surface topography was also characterized by Shape From Shading (SFS) method. The way to build 3D model of coating results from the assembling of four local 2D images of the coating surface and well-known shadowing effect [108]. The local SEM micrographs are taken by the symmetrically located BSD detectors (see Figure 39 [99]).

The analysis was performed on Phenom G2 pro SEM microscope (Phenom-World B.V., Eindhoven, Netherlands). The 3D models of the coating free-surfaces that were obtained by SFS method gave another insight on the coating formation mechanisms, surface profile and coating roughness.

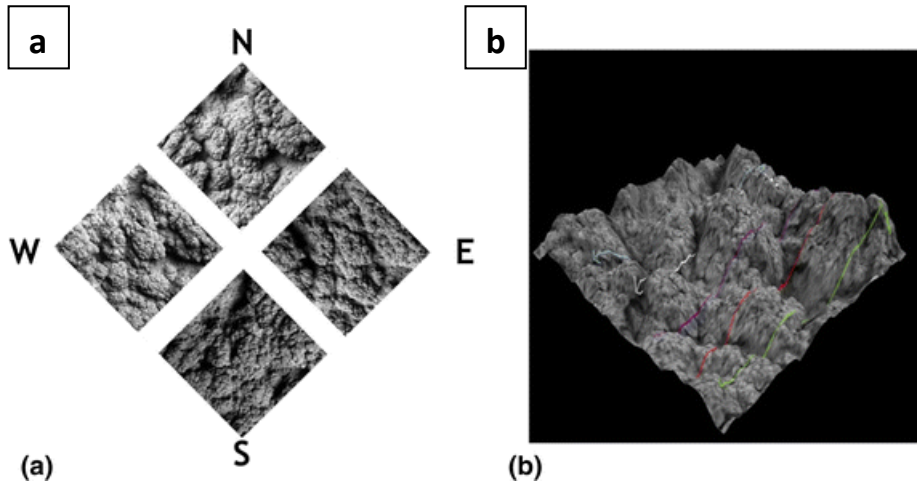

Figure 39 Shape From Shading technique: the procedure to reconstruct coating surface (a), 3D model of coating (b) (by Sokolowski et. al [99])

5.4.7. Density measurements

One of the key property, which should be known in order to evaluate thermal diffusivity and thermal conductivity is a true density of material. In this study, the gas pycnometry method was used (AccuPyc II 1340 Pycnometer, Micromeritics Corp., GA, USA) to determine this property. In this gas displacement method, the volume of material is measured very precisely. This is possible by using helium as a working (called also replacement) gas and its small molecules size. Then, basing on the well-known "mass to volume" ratio the density of materials can be calculated.

The closed porosity of materials can be an important factor in pycnometry analysis. In order to eliminate the effect of internal pores, the densities of:

- powders in as-produced state,
- powders after ball-milling (in case of YCeSZ),
- mechanically crushed coatings

were determined and compared. For each powder 10 measurements were performed and then average values were calculated. The density of Inconel 600, which was used as a substrate for high-temperature LFA test was determined using the same procedure. All materials were dried before pycnometry test.

Finally, based on true density determined by pycnometry, the bulk density of each coating was calculated by the following equation:

$$\rho = \rho_0 \cdot (1 - P) \qquad (2)$$

5.4.8. Dilatometry (DIL)

Another property of coatings analyzed prior to the studies of thermal transport properties was the thermal expansion of YSZ and YCeSZ deposits. The well-known push-rod dilatometry was used to measure dilatation and contraction of zirconia coatings (Netzsch DIL 402 C, Selb, Germany). The temperature cycle was as follows: room temperature RT – 1200 °C – RT. The measurements were carried using argon as a shielding gas. The heating and cooling rates were both 2°C/min. The correction values for DIL 402 C dilatometer were obtained by measuring alumina standard sample first. The data were analyzed by using dedicated Proteus® software.

The main goal was to determine the value of thermal expansion and contraction of SPS coating itself. It means that there was a need to separate the coating from the substrate and then cut a rigid sample from the coating material. However, due to the limited thickness of samples that was possible to obtain in the laboratory and due to the high adhesion of coatings, this approach was not successful. Therefore, the coatings for dilatometry test were sprayed by conventional powder plasma spraying method (and SG-100 plasma torch) and by using coarser powders. The powders were as follows:

- YSZ - Metco 204NS with a composition of ZrO2 + 8 wt. % of Y_2O_3 (powder had slightly different composition the powder that was used for suspension spraying. Unfortunately, YSZ powder containing 8 mol. % of Y_2O_3 dedicated for APS was not available at the moment on the market).

- YCeSZ - Metco 205NS (the base powder that was used for ball-milling and the preparation of submicrometer-sized YCeSZ powder for SPS).

The aimed thickness of both APS sprayed coatings was equal to 2mm. This allowed to cut cubic samples having the diameter 2x2x2mm for dilatometry measurements (the size of cubes was limited by the thickness of coatings). Then, the samples were analyzed

in two directions - in-plane (parallel to the substrate) and out-of-plane (perpendicular to the substrate). This methodology enabled to measure thermal expansion and distortion with the same accuracy in two directions and to see if there is any anisotropy of thermal elongation in coatings deposited by plasma spraying. The microstructure of coatings and the arrangement of dilatometry measurements relative to the coating orientation can be seen in Figure 40[109] (the example of YSZ coating is given only). The powder plasma sprayed coatings were used only for the purpose of dilatometry test.

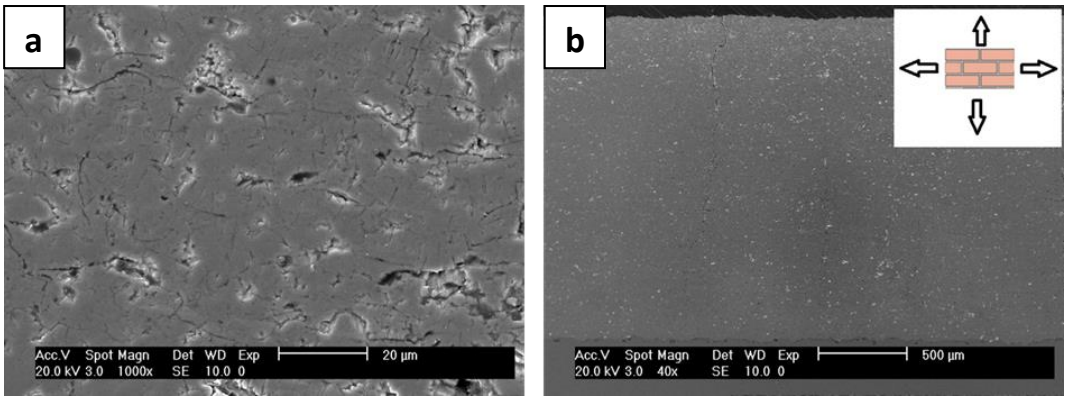

Figure 40 The microstructure of YSZ powder plasma sprayed coating used for thermal expansion analysis (a) and the arrangement of measurements relative to the coating microstructure (b) (by Sokołowski et al. [109])

But the accuracy of dilatometry test can be highly influenced by the length of the sample. Therefore, the 10 mm long samples were measured also in in-plane position to validate the results (just one measurement direction due to the limited thickness of coatings).

The dilatometry test was carried out also for Inconel 600 substrates with the same test conditions.

5.4.9. Differential Scanning Calorimetry (DSC)

Two methods (experimental and theoretical) were applied to examine specific heat capacity of YSZ and YCeSZ coating materials. First, the differential scanning calorimetry method (DSC) was used. Two different calorimeters were used in the following temperature ranges:

- from 40°C to 200°C by using Setaram C80 (SETARAM Instrumentation, Caluire, France). The machine uses a 3D Calvet sensor, which surrounds the crucible with

sample material. This causes that the accuracy of Cp measurements is very high for this kind of equipment. Furthermore, the relatively large-volume crucible is another advantage influencing the precision of Setaram C80 equipment. It was possible to measure from 10 to even 20 g of the YSZ and YCeSZ material with a heating rate of 0.2 °C/min;

- from 30°C to 500°C by Q1000 calorimeter (TA Instruments, DE, USA). The modulated DSC (MDSC) mode was used during measurements as it enhances the sensitivity of measurements (due to the separation of material properties from their thermal history). MDSC mode is recommended for evaluation of complex materials [110]. The modulation of ± 1°C every 100 s was used. The conventional hermetic, alumina pan was used. The pan allowed to measure from 5 to 8 g of coating material.

Both SPS sprayed zirconia coatings (YSZ and YCeSZ) were removed from the substrates and crushed. Then, the coating materials, having a form of powder, were able to fill well DSC crucibles. This procedure allowed to improve the heat flow through the analyzed material. The materials were dried prior to the DSC experiments. Furthermore, both calorimeters were also calibrated prior to the measurements by using sapphire samples.

The DSC measurements allowed determining Cp values in relatively low temperature. The theoretical approach was used in order to calculate specific heat capacity values of YSZ and YCeSZ coatings in much higher temperature. The calculations were done using Kopp's law (known also as "rule of mixtures"). Based on the chemical composition of coatings the Cp values were evaluated using the formula:

$$c_p(T) = \sum_{i=1}^{n} c_{pi}(T) \cdot f_i \qquad (3)$$

Finally, the general chart presenting Cp that were evaluated experimentally and theoretically was plotted for comparison.

5.4.10. Laser Flash Analysis (LFA)

Laser Flash method is a well-established method that is widely used for a characterization of thermal diffusivity and then for a calculation of thermal conductivity of coatings. In this technique the energy pulse is generated by xenon lamp or laser and is applied to the bottom side of the sample. Then, the change of the temperature in a function of time is detected on the top side by the infrared detector (in a form of electric signal). The higher the thermal diffusivity of material is, the faster the change of temperature can be observed. The LFA has many important advantages, like: simple operating rule, wide range of thermal diffusivities that can be detected by this method (see Figure 41 [111]) etc.

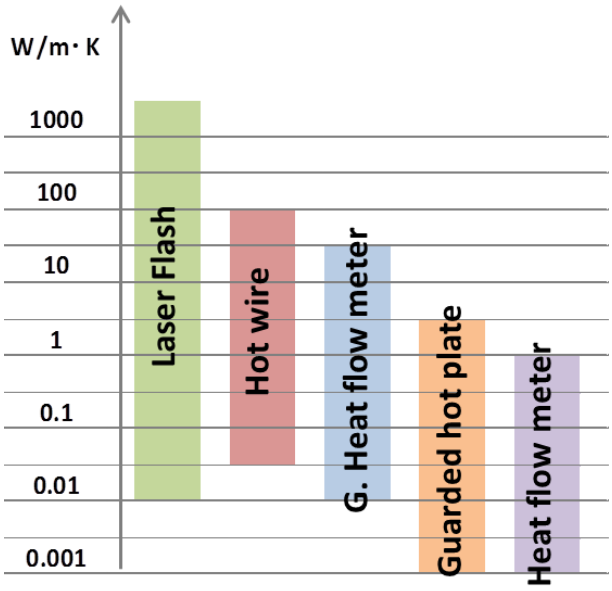

Figure 41 The application range of Laser Flash method [111]

But LFA does not investigate the thermal diffusivity and thermal conductivity directly, as this is an indirect measurement method. Moreover, there is a need to determine many different material properties in order to obtain a satisfying accuracy. As mentioned in previous paragraphs, all necessary thermophysical properties of substrates and coatings were evaluated experimentally. The properties were then used to measure thermal diffusivity by LFA and calculate thermal conductivity by the equation given below. The chart presenting the whole procedure used to investigate thermal transport properties of YSZ and YCeSZ coatings is given in Figure 42.

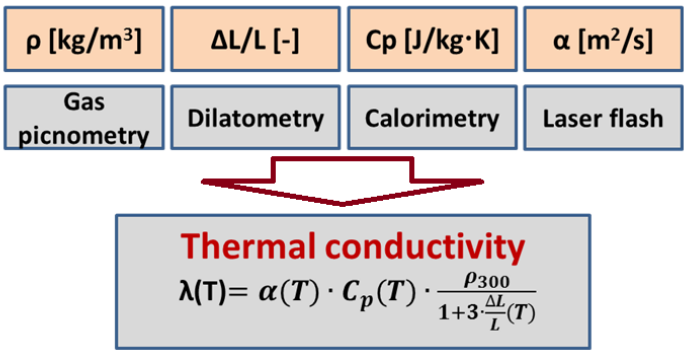

Figure 42 The methodology of thermal conductivity calculations in high-temperature range (up to 1000°C)

Laser Flash Analysis was performed using Netzsch LFA 427 (Netzsch, Selb, Germany). In this high-temperature set-up the laser pulse is used to generate the energy at the substrate surface. The temperature change was observed on the ceramic coating surface. The measurements were conducted with the following parameters:

- Inconel 600 substrate was investigated by using one layer Cape & Lehman model [112]. The model considers the heat losses during the measurement, the finite pulse duration and transient heat transfer also. The measurements were carried out up to 1000°C;

- The zirconia coatings were measured and considered as two-layer systems (coating + substrate material). The two-layer model that included corrections resulting from: heat losses, finite pulse duration and did not consider the thermal contact resistance between mentioned layers. The LFA test was performed up to 1000°C in case of YSZ coatings and up to 800°C in case of YCeSZ coatings. The difference was caused by the fact that YCeSZ coatings reacted together with graphite layer and alumina crucibles of the equipment. In order to avoid the pollution of expensive alumina parts the temperature was limited. This phenomenon is still under investigation.

Prior to the experiments the both sides of each sample were coated with the thin graphite layer. This provides uniform heat distribution, increases the energy absorbed from laser pulse and improve the quality of temperature signal on the detector side.

The analysis of very heterogeneous materials or multi-layer systems by LFA is still quite complex issue. Therefore, the verification of thermal conductivity values was done.

The approach called response method introduced by Baba et al. [113] was used to confirm the accuracy of thermal conductivity values obtained by laser flash analysis. The method bases on the LFA signal obtained during the experimental work. Then the following procedure is applied:

- normalization of the electrical signal value in a way that the max. value is always "1" and initial temperature is "0". In this way different measurements can be compared;
- finding the max value (=1 on the Y scale after the normalization);
- calculation of the "areal heat diffusion time" (see Figure 43 [114])

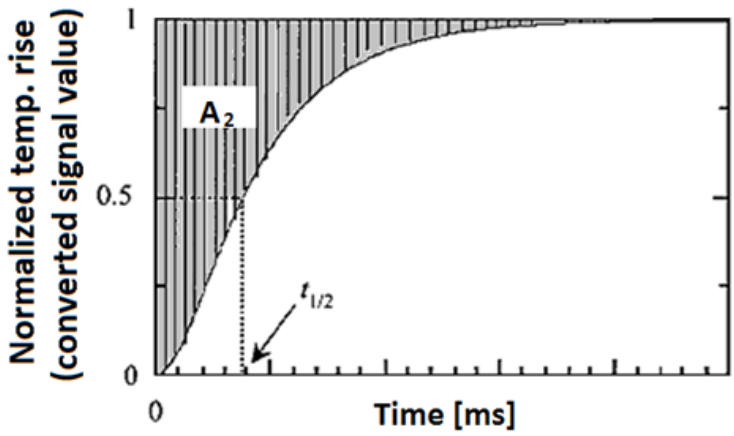

Figure 43 The interpretation of areal heat diffusion time used in response method that bases on LFA signal [114]

Then, using the following formula, the thermal conductivity value can be calculated. Similarly as in case of LFA method the exact (experimentally obtained) values of thermophysical properties of coatings were used to evaluate thermal conductivity:

$$\lambda_2 = \frac{d_2^2 C_{p2}\rho_2\left(3d_1C_{p1}\rho_1 + d_2C_{p2}\rho_2\right)}{6A_2\left(d_1C_{p1}\rho_1 + d_2C_{p2}\rho_2\right) - d_1^2C_{p1}\rho_1\left(d_1C_{p1}\rho_1 + 3d_2C_{p2}\rho_2\right)/\lambda_1}$$

5.4.11. Instrumented Indentation Testing (IIT)

The investigations of basic mechanical properties (elastic modulus and hardness) of zirconia coatings were performed by Instrumented Indentation Test (IIT).

The measurements were carried-out by the use of micro-hardness tester CSM 2-107 (CSM Instruments, Peseux, Switzerland). The equipment has resolution of 100 μN for load measurement and 0.3 nm for indenter displacement measurements. The set-up was equipped with a diamond Berkovich indenter. The selected samples were analyzed in as-sprayed condition (without any pre-treatment) and the measurements were performed at the free-surface of coatings. The measurements were realized using multicycle loading and unloading scheme (see Figure 44).

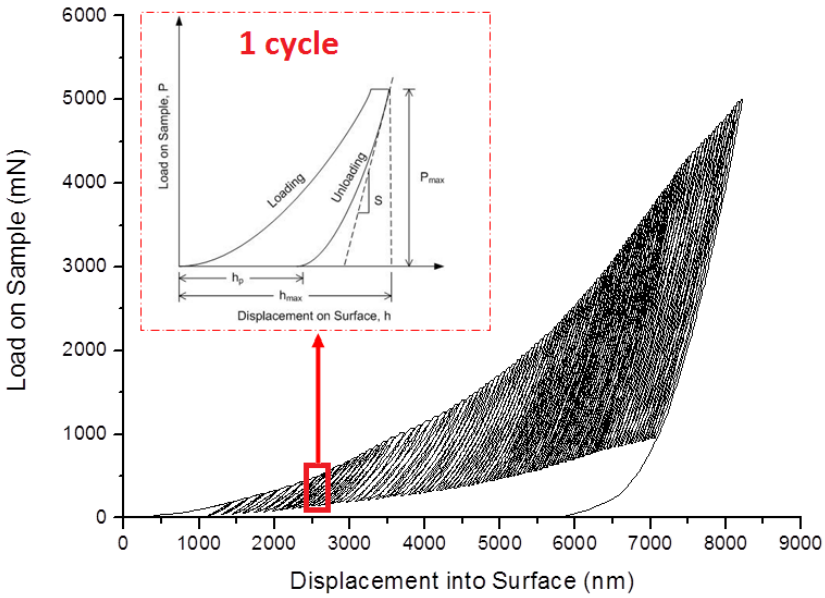

Figure 44 The multicycle nanoindentation test

The measurements were carried-out in accordance with ASTM E92-82 [115] standard. The parameters were as follows:

- 100 loading/unloading cycles per one test,
- loading rate (mN/min) was set as twice as the value of the maximum applied load. This guaranteed that all cycles took the same time [116],
- increasing loading values in the range of 200mN (first cycle) - 5000mN (last cycle),
- increasing unloading value, set as20 % of loading value,
- dwell time of 15s used for each maximum/minimum load.

Elastic Modulus by IIT

The method of using IIT for evaluation of reduced elastic modulus was given by Olivier and Pharr [117]. They used the unloading part of the IIT curve and applied the following formula in order determinate the E-modulus:

$$E_R = \frac{1}{\beta}\frac{\sqrt{\pi}}{2}\frac{1}{\sqrt{A}}\frac{1}{C} \qquad (4)$$

But when considering different measurement conditions, then many various effects can occur. During the years many different correction factors were proposed in order to improve conventional methodology, for example:

- correction factor (β) for various geometries of indenters [118]–[120],
- contact area (A) influenced by the indentation depth, type of the indenter and tip deformation/defect. The deformation around the indentation (so called sinking-in or piling-up) should be took into account also [121]–[124],
- instrument compliance (C_f), when the displacement of indenter may be overestimated due to the deflection of equipment parts ,
- geometrical correction factor (γ) as a function of Poisson's coefficient [125].

As a result the following form of Olivier and Pharr equation was used to evaluate elastic modulus of coatings:

$$E_R = \frac{1}{\beta\gamma}\frac{\sqrt{\pi}}{2}\frac{1}{\sqrt{A}}\frac{1}{C - C_f} \qquad (5)$$

Hardness by IIT

The Martens hardness (HM) was used to describe the hardness of zirconia coatings. It can be calculated using following formula:

$$HM = \frac{P}{26.43h^2} \qquad (6)$$

HM was expressed as the ratio of applied load value and the contact area between Berkovich indenter and tested material.

CHAPTER 6. RESULTS AND DISCUSSION

6.1. Microstructure and growth-up mechanisms

6.1.1. Coating morphology

As mentioned in a previous chapter, due to the extensive experiment design 72 different coatings were produced (see Table 7). All of them were characterized in term of the microstructure and they were used to analyze the coating growth-up mechanisms.

Table 7 The thickness and porosity of coatings (red color - coatings having columnar-like microstructure; * - coatings that were not deposited correctly)

SG-100 sample	Thickness [µm]	Porosity [%]	TriplexPro-200 sample	Thickness [µm]	Porosity [%]	Axial III sample	Thickness [µm]	Porosity [%]	WSP-H 500 sample	Thickness [µm]	Porosity [%]
ST21	66.1	21.4	TT51	77.4	16.0	AT101	139.5	10.3	WT101	176.0	21.0
ST22	-	-	TT52	-	-	AT102	-	-	WT102	-	-
ST23	-	-	TT53	-	-	AT103	-	-	WT103	-	-
ST51	82.6	18.1	TT101	90.9	13.1	AT201	160.4	16.1	WT201	165.6	16.3
ST52	-	-	TT102	-	-	AT202	-	-	WT202	-	-
ST53	-	-	TT103	-	-	AT203	-	-	WT203	-	-
ST101	115.9	15.2	TT201	139.5	11.8	AT301	166.1	15.8	WT301	179.2	13.1
ST102	-	-	TT202	-	-	AT302*	-	-	WT302	-	-
ST103	-	-	TT203	-	-	AT303*	-	-	WT303	-	-
SC21	54.9	19.0	TC51	74.0	18.0	AC101	161.7	5.2	WC101	145.4	11.3
SC22	-	-	TC52	-	-	AC102	-	-	WC102	-	-
SC23	-	-	TC53	-	-	AC103	-	-	WC103	-	-
SC51	105.2	15.5	TC101	91.2	15.9	AC201	168.6	5.2	WC201	152.1	12.2
SC52	-	-	TC102	-	-	AC202	-	-	WC202	-	-
SC53	-	-	TC103	-	-	AC203*	-	-	WC203	-	-
SC101	96.5	13.2	TC201	147.9	12.4	AC301	186.6	5.6	WC301	186.4	7.9
SC102	-	-	TC202	-	-	AC302	-	-	WC302	-	-
SC103	-	-	TC203	-	-	AC303*	-	-	WC303	-	-

Four different set-ups were used for Suspension Plasma Spraying. So the coating morphology will be discussed for each torch separately.

SG-100

The micrographs of YSZ coatings sprayed by SG-100 plasma torch are collected in Figure 45. It can be seen, that a wide range of process parameters allowed producing coatings characterized by contrasting microstructures. When the low concentrated suspension was sprayed, then very irregular coatings were formulated. The coatings were having columnar-like feature. On the other hand, much more dense and homogeneous coatings were deposited by using suspensions containing more solid. The porosity of YSZ coatings was in a range of 15 up to 21 %. The substrate preparation had also an influence on the coating morphology. The coatings were more heterogeneous when greater the roughness of substrate was. The YSZ coatings showed a limited number of defects in the structure and the interfaces between coatings and substrates was free of any discontinuities.

YCeSZ coatings were much more dense and homogeneous than YSZ coatings (see Figure 46). The coatings had typical two-zones microstructure, which is composed of well molten lamella and small unmelted or sintered powder particles. The porosity was also lower than in case of YSZ (13 to 19 %) and depended on the suspension concentration. However, the pores were greater and had tendency to form aggregates. The substrate preparation method did not have such great effect on the coating microstructure like in the case of fine yttria-stabilized powder.

TriplexPro-200

YSZ coatings that were sprayed by TriplexPro-200 torch (Figure 45) were much denser and homogeneous comparing to those deposited by SG-100 torch. The porosity was also lower, in a range of 12-16 %. Only the coatings that were sprayed onto laser-treated substrates showed columnar-like features, but not in case, when the most concentrated suspension were used (20 wt. % of powder). In that case much denser coatings were obtained. Furthermore, the filling of laser-treated patterns by feedstock material was not ideal and the pores at the substrate/coating interface were observed. The other spraying conditions caused formulation of dense, two-zones, structures. The coating

density was then influenced by the suspension concentration. The pores seemed to be slightly bigger than in case of SG-100.

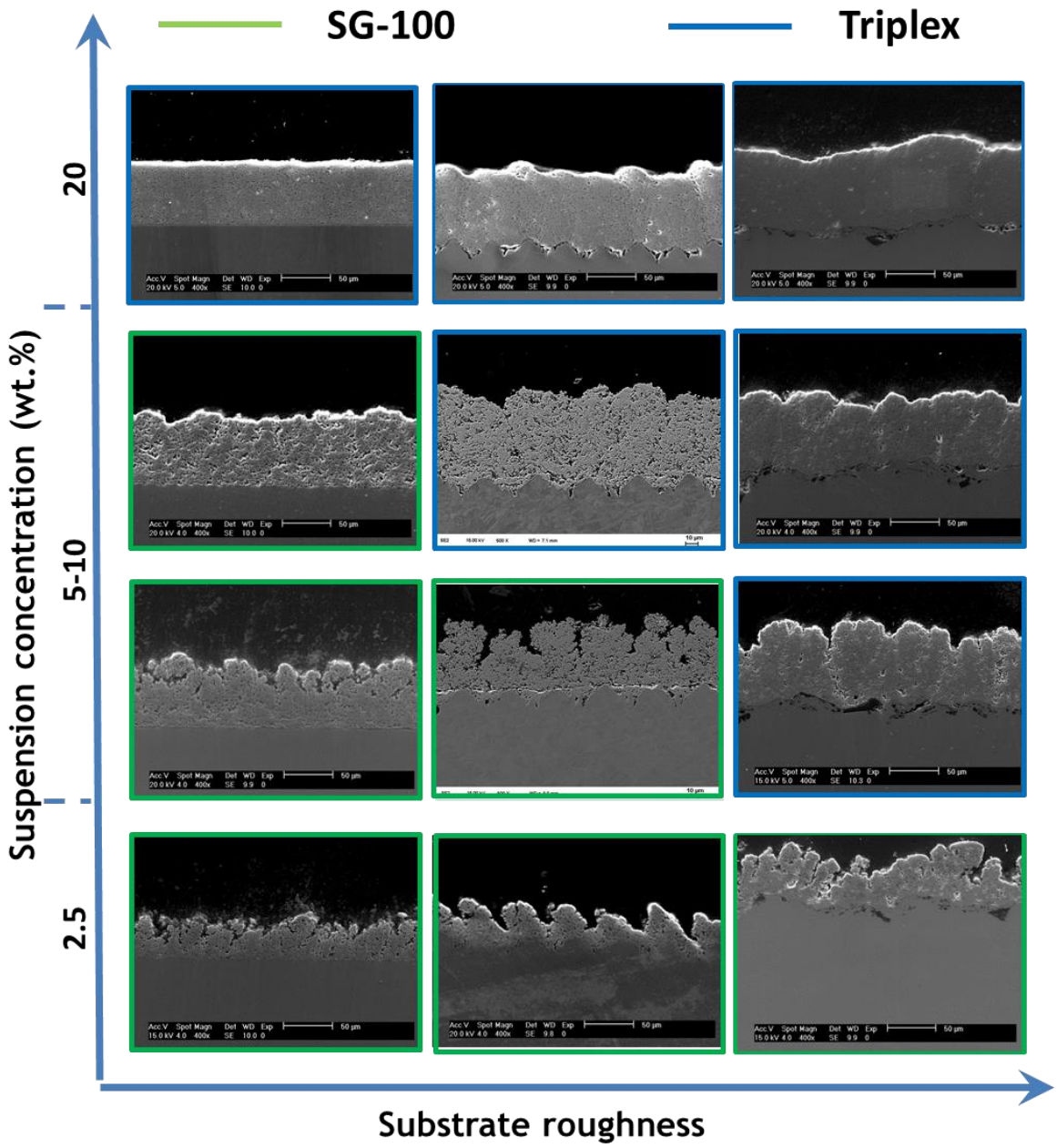

Figure 45 The cross-sections of selected YSZ coatings deposited by SG-100 and TriplexPro-200 plasma torches (SE mode, 200x and 400x)

The spraying of YCeSZ suspensions using TriplexPro-200 (Figure 46) allowed producing only two-zones coatings and with various porosity. The most dense deposits had porosity of 12 % and the most porous of 18 %. The coating density was also highly affected by the suspension concentration. The increase in the amount of solid phase in the suspension resulted in the increase in YCeSZ coating density. The coatings showed

also a single microcracks and pore aggregates. But based on SEM micrographs, the bonding of coatings was proper with no defects at the interface.

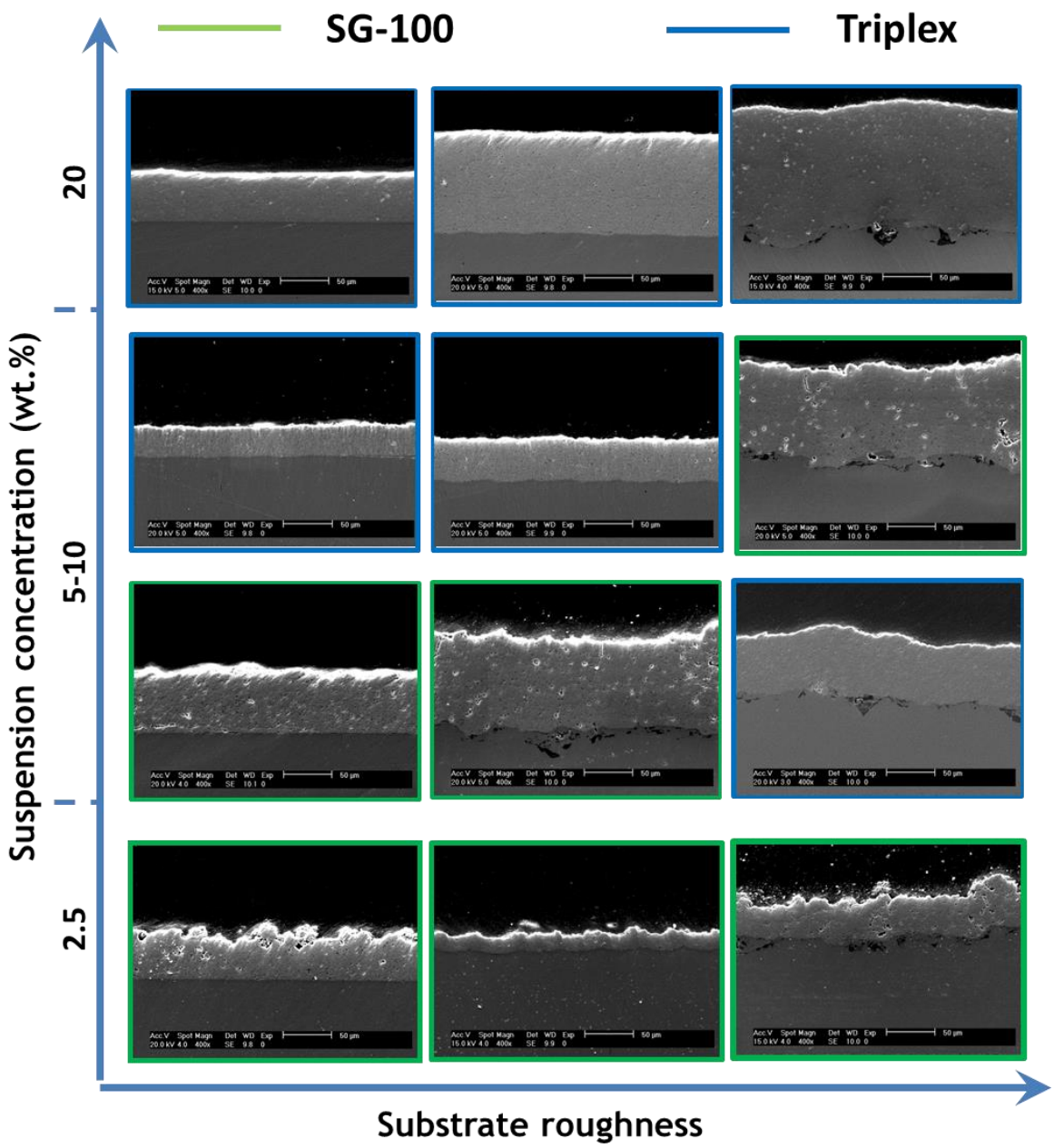

Figure 46 The cross-sections of selected YCeSZ coatings deposited by SG-100 and TriplexPro-200 plasma torches (SE, 200x and 400x)

Axial III

All YSZ coatings that were sprayed by Axial III were characterized by similar porosity and morphology. The suspension preparation and substrate topography did not have a big influence on the coating microstructure (Figure 47). The columnar-like morphology

was not obtained for Axial III, even for fine YSZ powder. The coatings had the porosity in the range between 10 and 16 %. Furthermore, the pores were homogenously distributed in the coating and were also very fine (hundreds of nanometers). The coating-substrate interface did not show any defects when grit-blasted substrates were used. But when coatings were sprayed onto laser treated or grinded substrates, then coating adhesion was much lower. The careful metallographic preparation was needed as YSZ coatings had a tendency to delaminate during e.g. cutting.

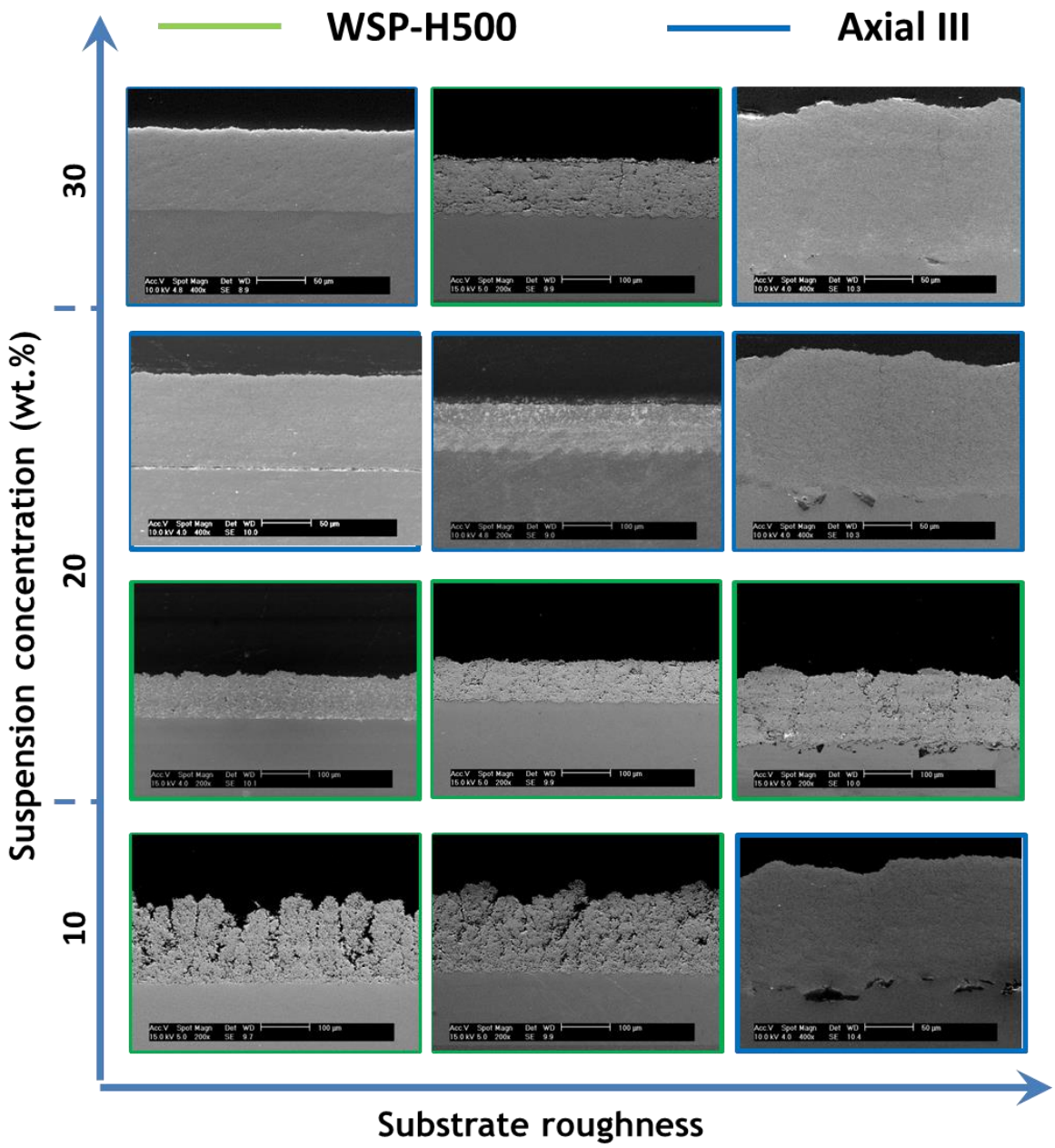

Figure 47 The cross-sections of selected YSZ coatings deposited by Axial III and WSP-H500 plasma torches (SE, 200x and 400x)

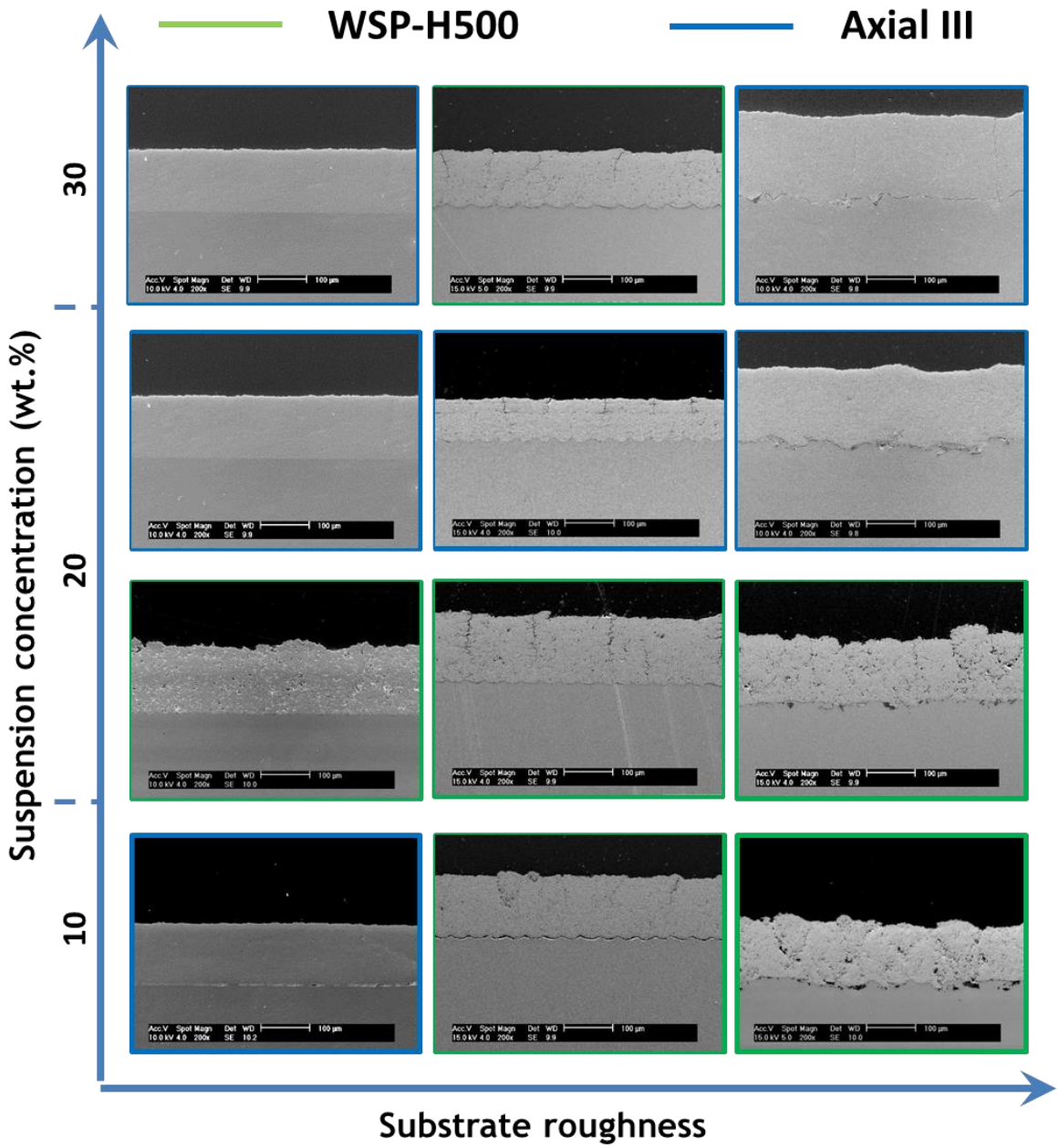

Figure 48 The cross-sections of selected YCeSZ coatings deposited by Axial III and WSP-H500 (SE, 200x and 400x)

The YCeSZ coatings deposited by using Axial III torch were characterized by the highest density among all produced coatings (Figure 48). These YCeSZ coatings were also the most homogeneous with porosity of around 5 % (Table 7). The single and very fine pores were mostly spherical and did not create bigger aggregates like in case of other plasma torches. The effect of suspension and substrate preparation on the coating morphology was not so obvious as in the case of other plasma torches. The coatings were well-deposited, the interface was free of defects.

WSP-H500

Two various types of coatings were produced when spraying fine YSZ suspension by WSP-H500 torch (Figure 47). The columnar-like structures characterized by typical intercolumnar voids were achieved for suspension with the lowest content of powder (10 wt. %). The height and width of single columns was not uniform. Furthermore, it should be stressed that these coatings were obtained for all kinds of substrate topographies, including flat, grinded, substrate. The appropriate substrate interface, without any signs of delamination, was also achieved for all columnar-like coatings. On the other hand, when more concentrated YSZ suspensions were used, then the produced coatings were much denser and had two-zones microstructure. The single micro-cracks were observed also. In case of coatings deposited using the most loaded (30 wt. %) suspension onto polished or laser treated substrates a discontinuity at the coating-substrate interface appeared. The YSZ coatings had porosity ranging from 13 to 21 % depending on the coating morphology. The single pores were fine, nanometric or submicrometric, but the aggregates reached the size of a few micrometers.

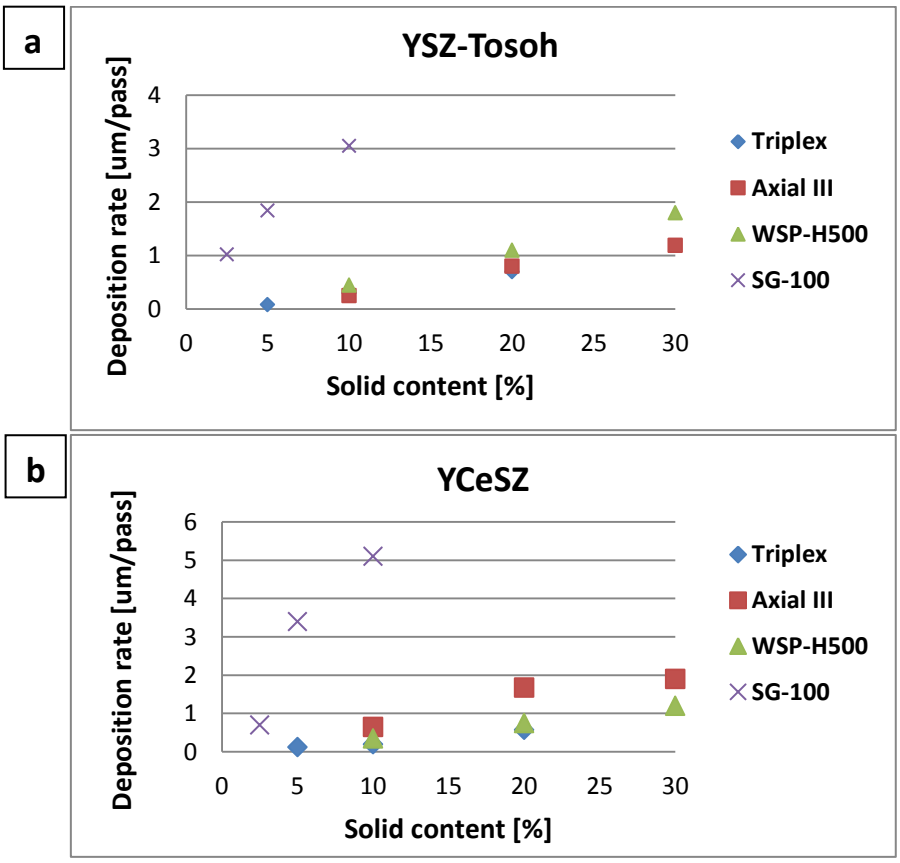

Figure 49 The deposition rate (thickness/pass) values obtained during spraying

The YCeSZ coatings sprayed by WSP-H500 torch had typical two-zones structure. The coatings showed well-melted lamellas with single powder aggregates. The columnar-like coatings were not achieved. The coatings were characterized by various porosity ranged from 13 to 14 %. The porosity was lower for coatings sprayed by more concentrated suspension, similarly as in case of YSZ. The single clusters of pores were observed in the microstructure of coatings sprayed by 10 wt. % suspension. They did not occur for 20 and 30 wt. % suspension and pores seemed to be smaller also. But the single microcracks appeared at the same time, especially for grinded or laser-treated substrates.

The deposition rate (μm/pass) that was obtained using mentioned set-ups is also an important information about Suspension Plasma Spraying experiment. The deposition rates were evaluated based on the grit-blasted samples that were carefully characterized. As can be seen in Figure 49, the deposition rates were different for each torch. This was caused by the differences between set-up designs and plasma torch features. It was not possible to use the same spray parameters each time. Following, the results of thickness per pass ratios cannot be compared directly (for example the offset between plasma torch passes was 3 mm in case of SG-100 and 30 mm for WSP-H 500). The results do not consider also the coating porosity, which affects the deposition rate expressed as μm/pass. But, regardless to the plasma torch, the deposition rates of a few microns per pass were achieved. These results of deposition rate clearly show that Suspension Plasma Spraying method may be an effective technology and can be a very competitive process to other technologies enabling production of fine-grained coatings.

6.1.2. Coating free-surface

The analysis of coating free-surfaces is presented for columnar-like and two-zones microstructures separately. These two different morphologies were identified based on SEM analysis made at the coatings cross-sections.

Columnar-like coatings

It was clearly seen that the most irregular surface was a domain of columnar-like coatings, which had even two times greater roughness than the other coatings (Table 8).

Another observations were performed by Shape From Shading (SFS) method. The 3D models of the coating surfaces were reconstructed and investigated. This technique was found to be a very useful tool in order to analyze columnar-like coatings (see Figure 50). By using SFS, the column high and width were easily measured. The width of columns was in a range of 70 to 90 µm.

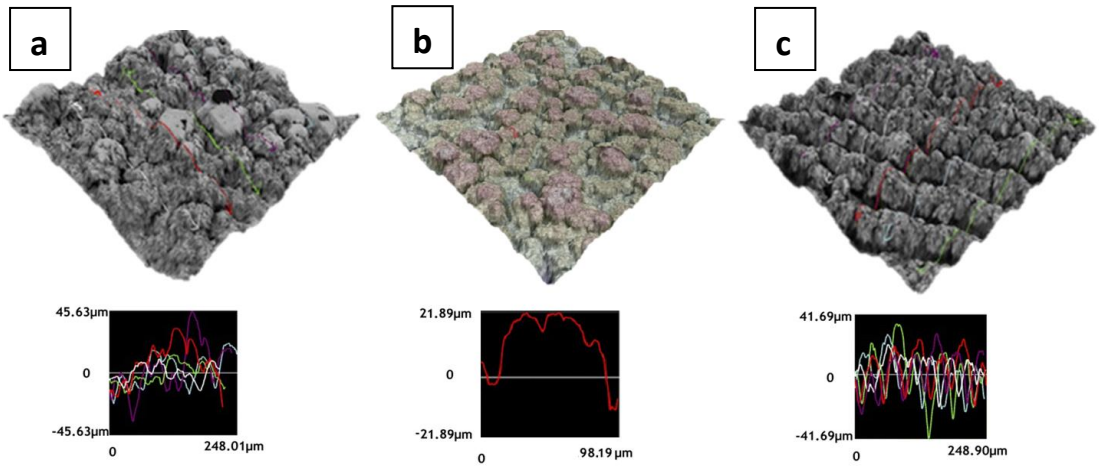

Figure 50 The 3D views of columnar coatings surfaces reconstructed by Shape from Shading method (a - ST23, b - WT103, c - ST52)

Two-zones microstructures

The surfaces of coatings characterized by two-zones microstructure corresponded to the coating morphology. When the porosity was relatively high and coating structure was not very homogeneous, then the surface was also irregular. But on the other hand, the surfaces of very dense structures (like YSZ coatings sprayed by Axial III) were very smooth (see Figure 51).

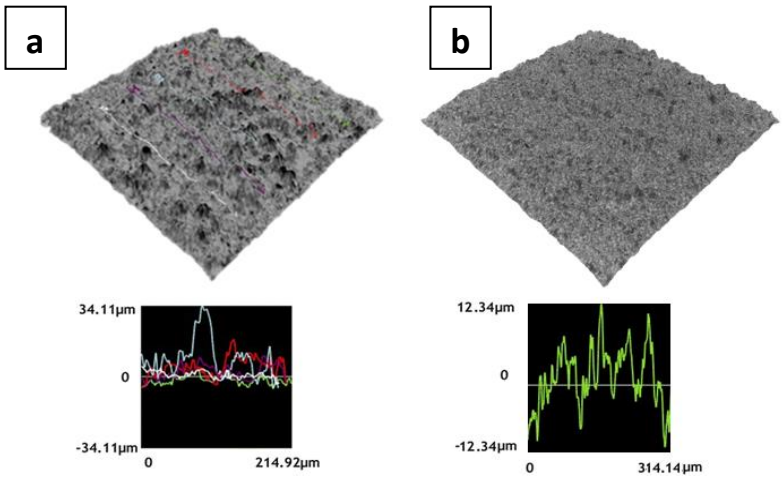

Figure 51 The 3D views of two-zones coatings surfaces reconstructed by Shape from Shading method (a - TC102, b - AT203)

Generally, the coating roughness was highly influenced by the suspension concentration. This phenomenon was observed for YSZ and YCeSZ powders as well. The higher amount of solid in suspension resulted in smoother and more uniform coating surface. The substrate preparation was another important parameter affecting the coating structure. The highest Ra values of the coating surfaces were observed for the most irregular, grit-blasted, substrates. The substrate topography had much greater influence on YSZ coatings than on YCeSZ (for Axial III even negligible in case of YCeSZ).

Table 8 The roughness parameters of obtained coatings (red color - coatings having columnar-like microstructure)

SG-100 sample	Roughness Ra [µm]	Standard dev. [µm]	TriplexPro-200 sample	Roughness Ra [µm]	Standard dev. [µm]	Axial III sample	Roughness Ra [µm]	Standard dev. [µm]	WSP-H 500 sample	Roughness Ra [µm]	Standard dev. [µm]
ST21	10.7	1.6	TT51	6.9	1.1	AT101	4.5	0.5	WT101	14.1	1.6
ST22	8.2	0.4	TT52	6.0	0.6	AT102	1.9	0.2	WT102	6.4	0.8
ST23	7.9	1.5	TT53	2.9	0.4	AT103	2.0	0.3	WT103	9.7	0.3
ST51	10.6	1.2	TT101	6.1	0.8	AT201	3.9	0.6	WT201	6.0	0.4
ST52	7.4	0.9	TT102	6.5	1.3	AT202	1.8	0.2	WT202	3.9	0.4
ST53	5.7	0.4	TT103	2.3	0.3	AT203	1.6	0.1	WT203	3.7	0.4
ST101	7.2	0.7	TT201	5.1	1.0	AT301	3.1	0.5	WT301	3.9	0.6
ST102	5.9	0.6	TT202	3.5	0.8	AT302	1.9	0.2	WT302	3.3	0.2
ST103	3.9	0.7	TT203	2.2	0.3	AT303	1.7	0.2	WT303	4.2	0.4
SC21	8.3	0.8	TC51	3.8	0.6	AC101	2.4	0.4	WC101	9.0	1.5
SC22	4.0	0.4	TC52	2.5	0.4	AC102	2.1	0.3	WC102	3.1	0.1
SC23	5.5	0.7	TC53	2.1	0.2	AC103	1.9	0.2	WC103	6.2	0.6
SC51	6.8	0.7	TC101	3.5	0.5	AC201	2.6	0.2	WC201	6.3	0.4
SC52	3.7	0.6	TC102	3.2	0.4	AC202	1.9	0.2	WC202	3.5	0.5
SC53	4.2	0.7	TC103	2.9	0.3	AC203	1.8	0.3	WC203	4.9	1.1
SC101	6.7	0.7	TC201	3.5	0.7	AC301	2.5	0.4	WC301	6.7	0.7
SC102	3.6	0.6	TC202	2.4	0.1	AC302	2.0	0.2	WC302	3.1	0.4
SC103	4.2	0.5	TC203	2.7	0.4	AC303	2.0	0.3	WC303	3.3	0.5

6.1.3. Coating phase and chemical composition

The results of XRD and EDS studies are presented for a few different coatings together in a just one chart. There was no significant difference in the phase composition for coatings deposited by various plasma torches.

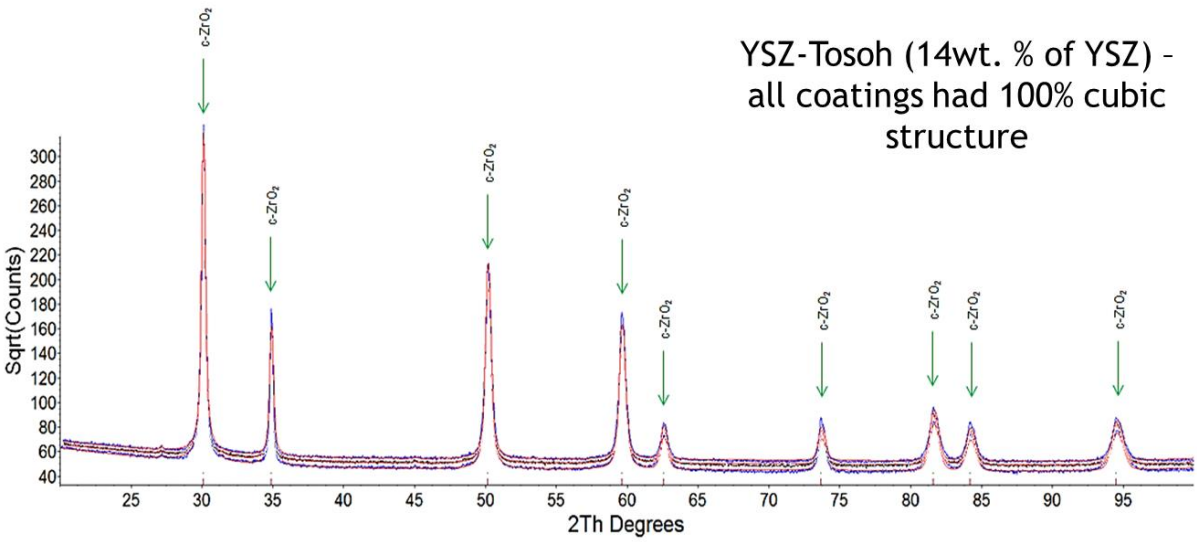

Figure 52 XRD diagram presenting phase composition of selected YSZ coatings

The phase composition of YSZ and YCeSZ coatings was almost not changing when comparing to the raw powder material and deposited coatings. According to XRD analysis, the YSZ coatings were still characterized by fully-cubic structure. This phase remained unchanged. The full XRD diagram is presented in Figure 52.

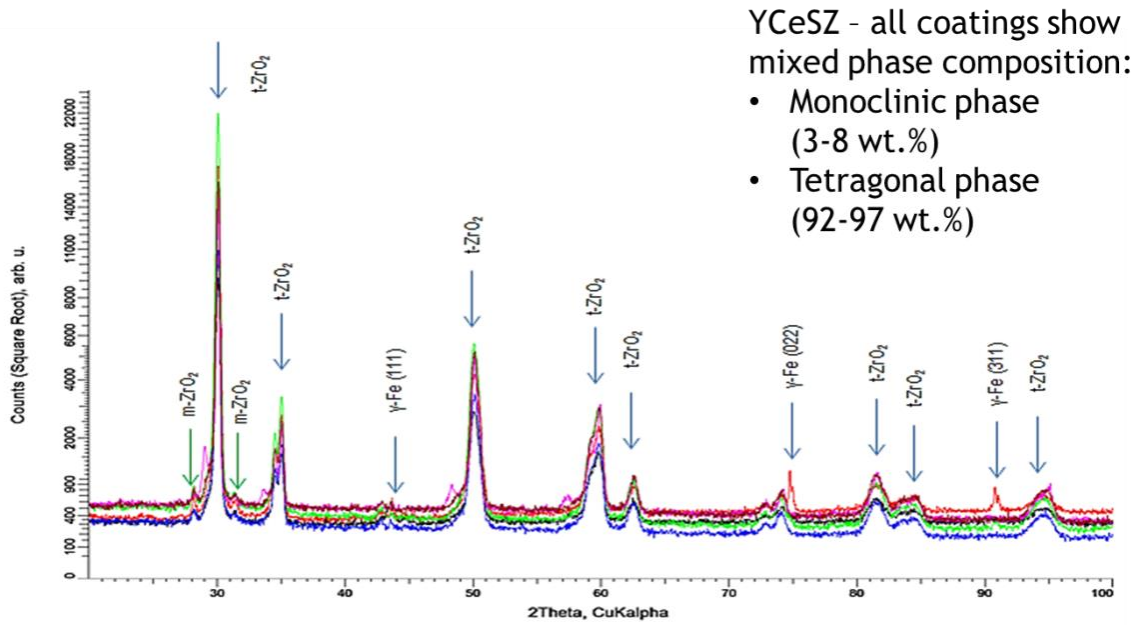

Figure 53 XRD diagram presenting phase composition of selected YCeSZ coatings

YCeSZ coatings crystalized in tetragonal lattice with a very small contribution of monoclinic ZrO_2 (Figure 53). Based on the qualitative analysis of X-ray diffractogram the

cubic phase was not distinguished. It means there was a small phase change of YCeSZ during spraying.

Table 9 The lattice parameters of YSZ coatings sprayed by Axial III and WSP-H 500

	YSZ coatings	
Sample	**Cubic phase**	
	content, wt. %	***a*, Å**
AT101	100	5.1396
AT201	100	5.1398
AT301	100	5.1390
WT101	100	5.1409
WT201	100	5.1414
WT301	100	5.1406

The Rietveld refinement method was used to evaluate more precisely the phase composition of coatings. The content of each phase is showed in Figure 52 and Figure 53. The lattice parameters were calculated also and the results are presented in Table 9 and Table 10 [33].

Table 10 The lattice parameters of YCeSZ coatings sprayed by SG-100 and TriplexPro-200 [33].

	YCSZ coatings					
Sample	**Tetragonal phase**			**Monoclinic phase**		
	content, wt. %	***a*, Å**	***c*, Å**	**content, wt. %**	***a, b*, Å**	***c*, Å; *γ*, °**
SC21	97.45	3.6401	5.2133	2.55	5.1570 5.2601	5.2590 99.165
SC51	97.10	3.6406	5.2160	2.90	5.1532 5.2719	5.2551 99.064
SC101	97.30	3.6382	5.2097	2.70	5.1535 5.2545	5.2574 99.090
TC51	92.62	3.6351	5.2167	7.38	5.1884 5.2783	5.2077 98.799
TC101	96.02	3.6358	5.2146	3.98	5.1867 5.2983	5.2033 98.834
TC201	94.54	3.6353	5.2161	5.46	5.1932 5.2993	5.2046 98.818

Based on the lattice parameters the calculation of $c/a\sqrt{2}$ ratio was done. As suggested by Viazzi et al. [90], using this formula the accurate evaluation of tetragonal phase of stabilized zirconia can be done (see Figure 54). The ratio could be directly calculated for YCeSZ coatings. In case of YSZ coatings the fitting of XRD data with tetragonal phase was done also. In case of YSZ the ratio was nearly 1. This means that the coatings were cubic in fact. In case of YCeSZ the ratio was in range of 1.013-1.015. So the tetragonal phase in YCeSZ coatings was probably transformable. But the more advanced studies are performed currently to confirm these results.

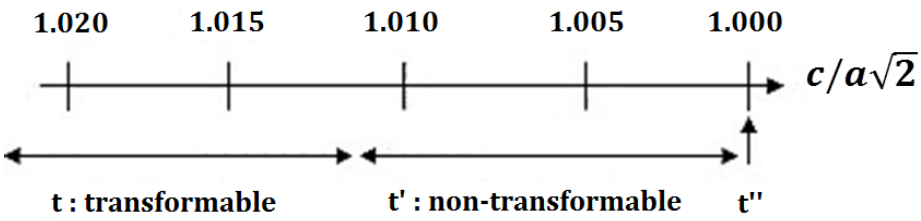

Figure 54 The different forms of stabilized zirconia [90]

The qualitative EDS analysis of the samples sprayed using suspension was made in two steps. First, the analysis of coatings deposited by low-power plasma torches (SG-100 and TriplexPro-200) was done, and then the evaluation of coatings sprayed by high-energy plasma torches was performed (Axial III and WSP-H500). The contents of the elements were as follows:

SG-100 and TriplexPro-200:

- YSZ: (i) 14-18 wt. % of yttrium, (ii) 53-58 wt. % of zirconium and (iii) 25-30 wt. % of oxygen;
- YCeSZ: (i) 5-6 wt. % of yttrium, (ii) 15-18 wt. % of cerium, (iii) 56-63wt. % of zirconium and (iv) 18-23 wt. % of oxygen;

Axial III and WSP-H500:

- YSZ: (i) 13-17 wt. % of yttrium, (ii) 56-60 wt. % of zirconium and (iii) 23-28 wt. % of oxygen;
- YCeSZ: (i) 3-5 wt. % of yttrium, (ii) 16-20 wt. % of cerium, (iii) 58-63 wt. % of zirconium and (iv) 20-22 wt. % of oxygen;

and the initial chemical composition of powder was:

- YSZ: (i) 25 wt. % of oxygen, (ii) 11 wt. % of yttrium and (iii) 64 wt. % of zirconium;
- YCeSZ: (i) 21 wt. % of oxygen, (ii) 20 wt. % of cerium, (iii) 2 wt. % of yttrium and (iv) 47 wt. % of zirconium.

The EDS studies showed that the spraying did not introduce significant changes to the chemical composition of coatings when comparing to the powder materials that were used for suspension formulation. There was also no significant differences in the chemical compositions between coatings. The examples of EDS spectra of YSZ and YCeSZ coatings are presented in Figure 55.

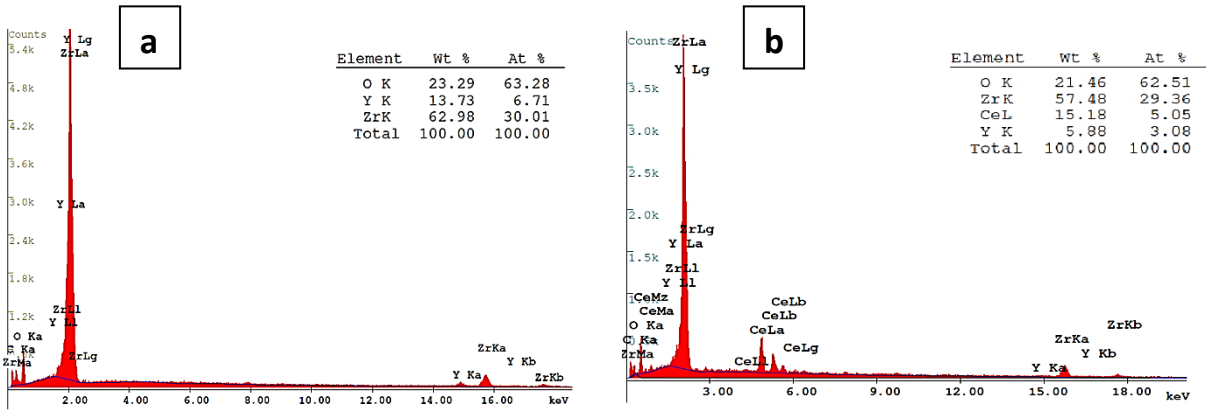

Figure 55 The examples of EDS spectra of YSZ (a) and YCeSZ (b) coatings

6.1.4. Formation of columnar-like coatings

As mentioned in the previous paragraphs, some of the process parameters caused the growth of columnar-like microstructures. The more detailed micrographs of selected coatings having columnar features are presented in Figure 56 [109].

First columnar-like coatings were obtained when rough (laser-treated in particular) substrates were used. The mechanism of coatings growth can be associated to the particles which follow the hot gas swirls and adhere mainly to the peaks of substrate or previous deposits and then form columnar-like microstructure. The behavior of powder particles that came into a contact with substrate resulted from equilibrium of forces:

(i) F_D — drag force pushing fine solids together with plasma jet swirls and (ii) adhesion force F_A keeping the particles on the substrate surface.

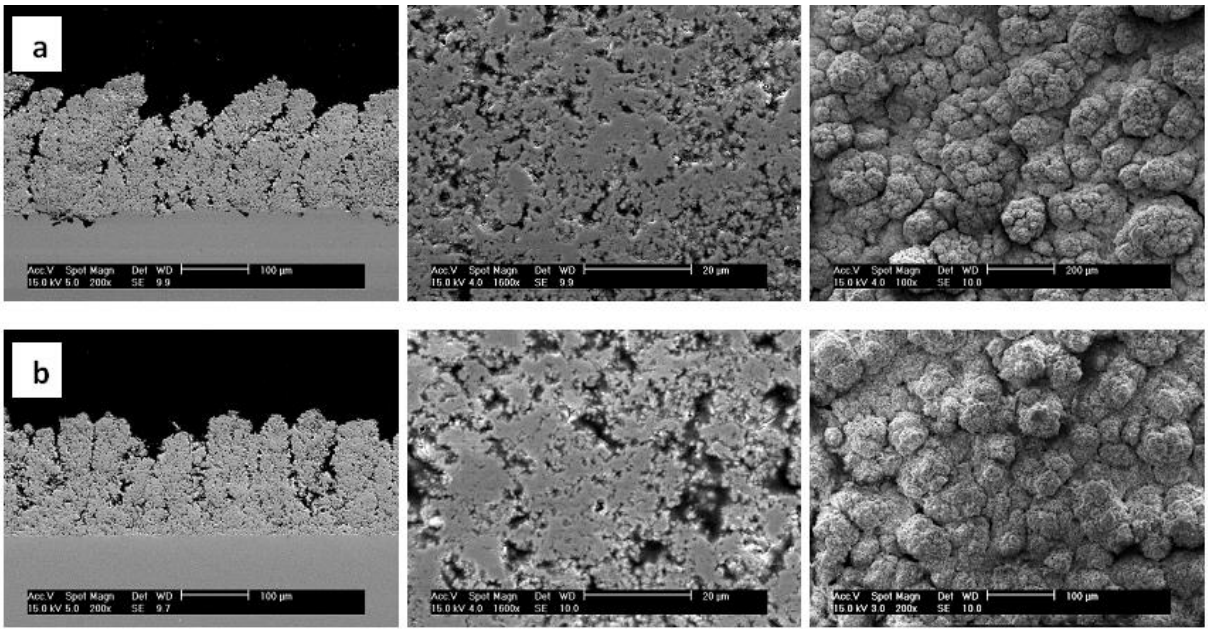

Figure 56 The columnar-like coatings: WT101 (a) and WT103 (b) [109]

Afterwards, the powder particles can adhere directly to the substrate or move parallel to its surface - depending on which of the force dominates. The $F_A > F_D$ relation is valid for coarser particles moving close to the center of plasma jet. But inside the coatings, the fractions of fine, unmelted, grains were noticed also. They are generated by the particles moving in the external and much colder regions of plasma. And then, the balance of forces change and, consequently, $F_D > F_A$. Subsequently, these particles move parallel to the substrate surface and adhere to the substrate peak that they meet first (Figure 57) [33]. So the effect is strengthened by morphology of substrate surface and the size of powder particles.

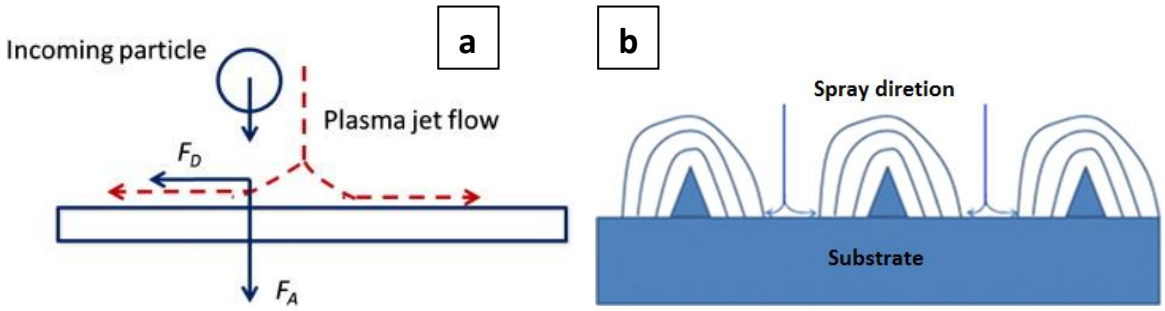

Figure 57 The forces acting particle at the plasma jet/substrate interface (a), mechanism of columnar-like coating growth at rough substrate (b) [33]

The concept of columns growth-up mechanisms was investigated and confirmed by EBSD analysis. The test area was chosen in a way that the "peaks and valleys" were analyzed simultaneously (Figure 58). The analysis showed that the deposition mechanism is not the same in the two analyzed regions of the sample. The grains which adhered just above the substrate peak (see Figure 58b), were rather spherical. Whereas, the grains that were deposited between two peaks were deformed, i.e., thin and more perpendicular to the substrate. The deformed grains are the ones following the plasma swirls. The analysis of grain size proved fine-grained feature of SPS coatings. The main size of grains was of about 600 nm (see Figure 58c). But many finer grains (with the size of about 250-300 nm) were observed also.

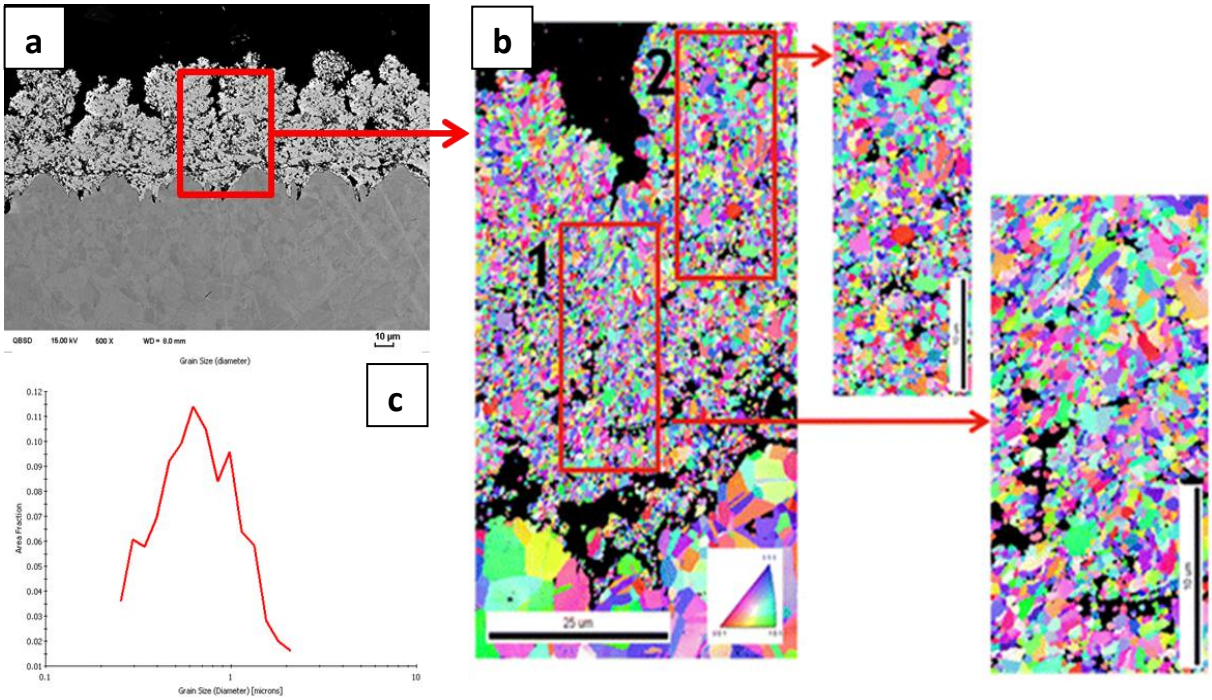

Figure 58 The EBSD analysis of columnar-like ST52 sample sprayed onto laser-treated substrate: (a) selection of area, (b) detailed crystallographic orientation map and (c) grain size distribution (volume-based) [99]

A slightly more complex mechanism takes place, when the columnar-like coatings are formed on flat, e.g. grinded, substrate. The growth of columns on the flat surface is possible only if single irregularities ("peaks") are created on the substrate surface first. In this work, it was possible when lowest concentration of suspension was used. Consequently, there was a low number of particles in the suspension droplet being introduced into plasma. These particles form mentioned peaks. Then the procedure is the same as in case of laser-treated substrate (see Figure 59).

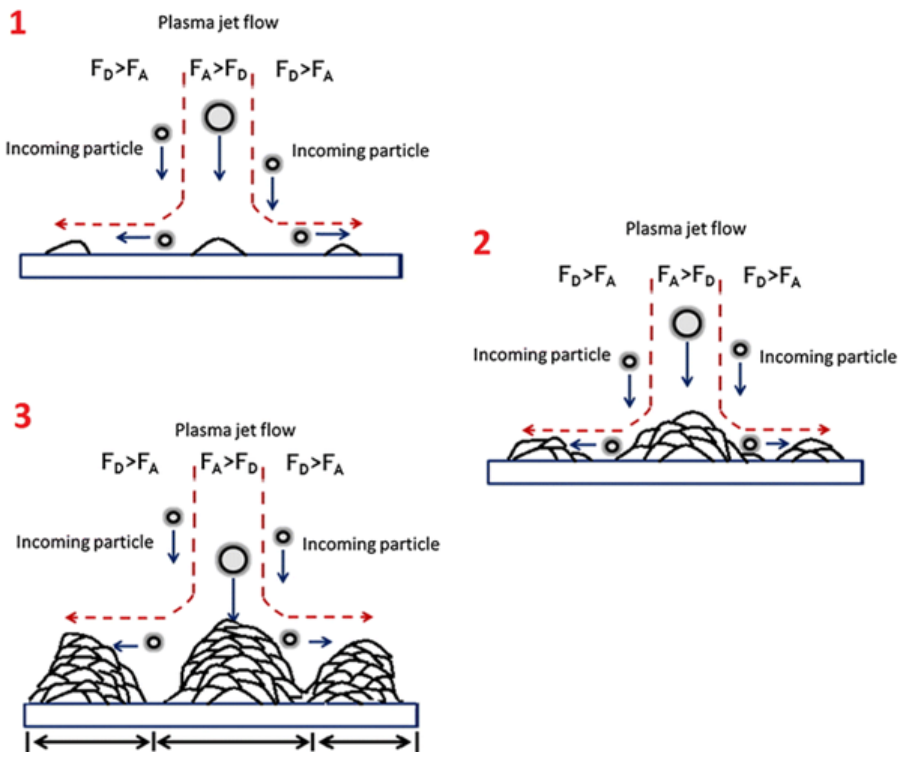

Figure 59 The growth of columns on the flat substrate (1,2,3 - subsequent stages of columns formation) [99]

However, much more irregular columns are formed (see Figure 60a). Furthermore, the texture analysis was performed in case of columnar like coatings (Figure 60b). But in each case the differences between grain orientations were very big and it was not possible to find any preferred directions of crystal growth.

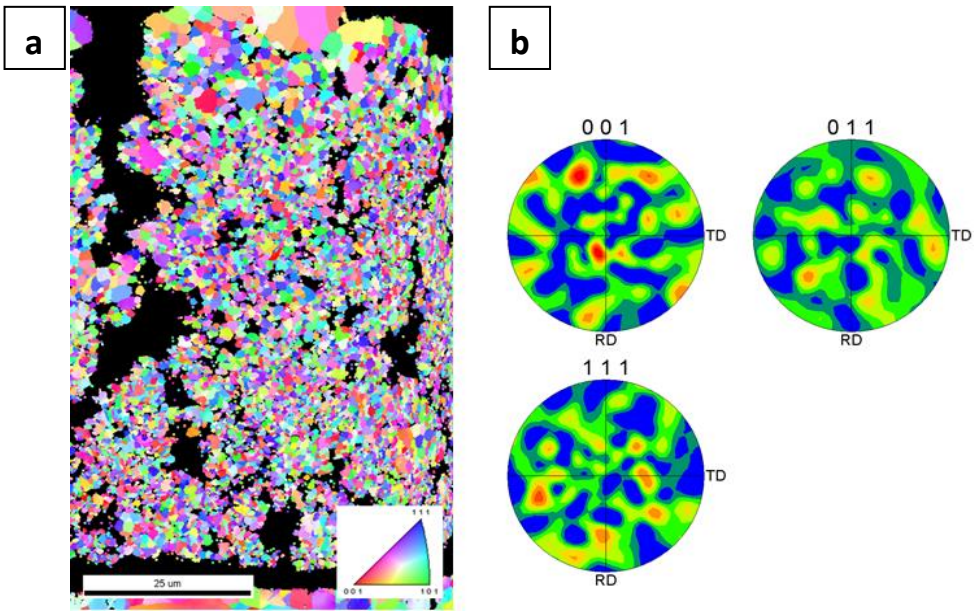

Figure 60 EBSD analysis of columnar-like ST23 sprayed onto grinded substrate crystallographic orientation of grains (a), and texture analysis (b) [99]

6.1.5. Formation of two-zones coatings

The coatings characterized by two-zones microstructure were obtained in most cases. The detailed micrographs of this type of coatings are presented in Figure 61.

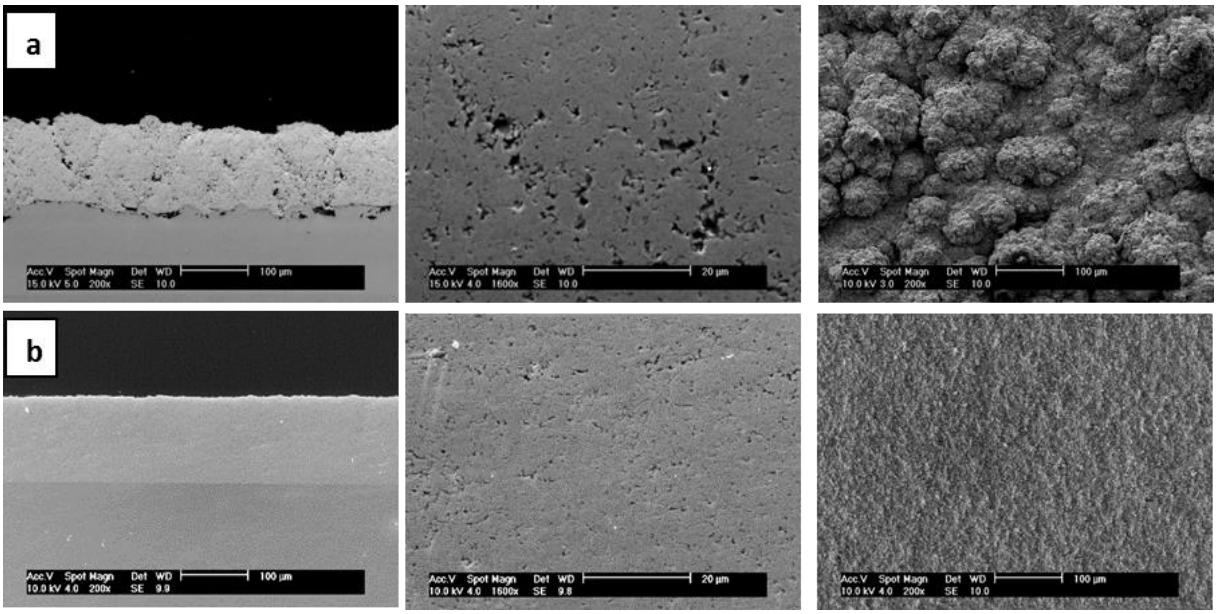

Figure 61 The coatings characterized by two-zones microstructure: WC101 (a) and AC203 (b) [109]

The formulation of typical two-zones coatings was described in details by Kozerski et al. [66]. The growth of complex lamellar microstructure results from the heat treatment of powders in the plasma jet. Some of powder particles are well-melted and form lamellas. But there are also fine sintered/unmelted powders in the coating structure which travelled in colder regions of plasma. The mechanism is presented in the Figure 62 [66].

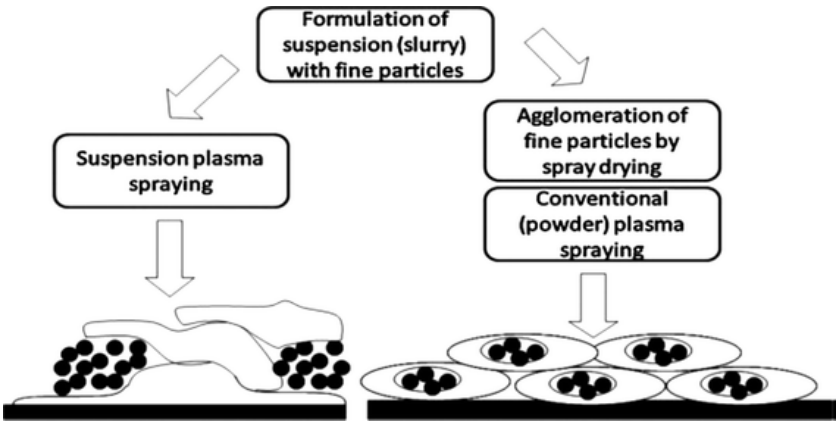

Figure 62 The formation of conventional two-zone structure in Suspension Plasma Spraying [66]

The lamellar microstructure was observed for YSZ and YCeSZ coatings sprayed by suspensions having higher concentration of solid phase, mainly when the suspension had 20-30 wt. % of solid phase. The microstructure of these coatings was much denser than in case of columnar-like coatings. The EBSD investigation showed that inside some coatings (deposited by SG-100) the thin layer of columnar grains appeared. This was especially visible near the substrate and was caused probably by the low temperature of substrate during first passes (Figure 63b). The substrate was only slightly preheated prior to spraying. The grain size investigations, that were carried out for TC102 sample, enabled to find the main size of about 450 nm, and the main number grain size was below 300 nm.

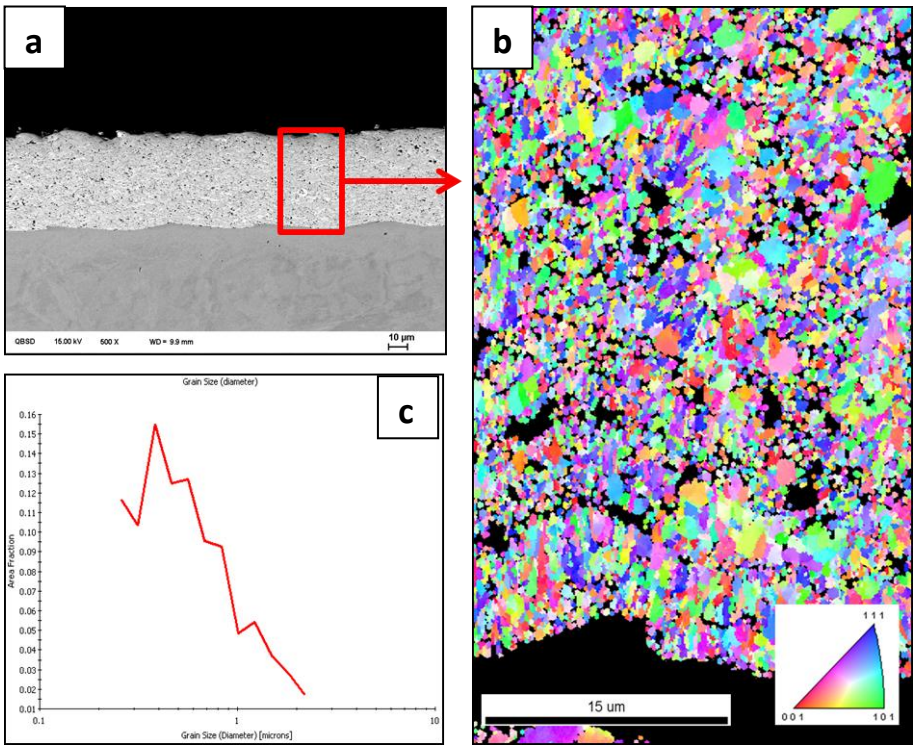

Figure 63 EBSD analysis of two-zones TC102 coating: selection of test area (a), Inverse Pole Figure (b) and grain size distribution (c) [99]

The EBSD studies confirmed also that some two-zones coatings were having very fine grained and uniform structure, especially the coatings deposited by Axial III torch. The inverse pole figure (IPF) presented in Figure 64 shows the homogeneous shape and size of grains. Even the use of laser treated substrates did not affect the grain morphology. Only the fine, spherical grains can be noticed in the coating microstructure. The volume-based mean grain size was of about 800 nm (Figure 64c) and number-based mean size of around 570 nm.

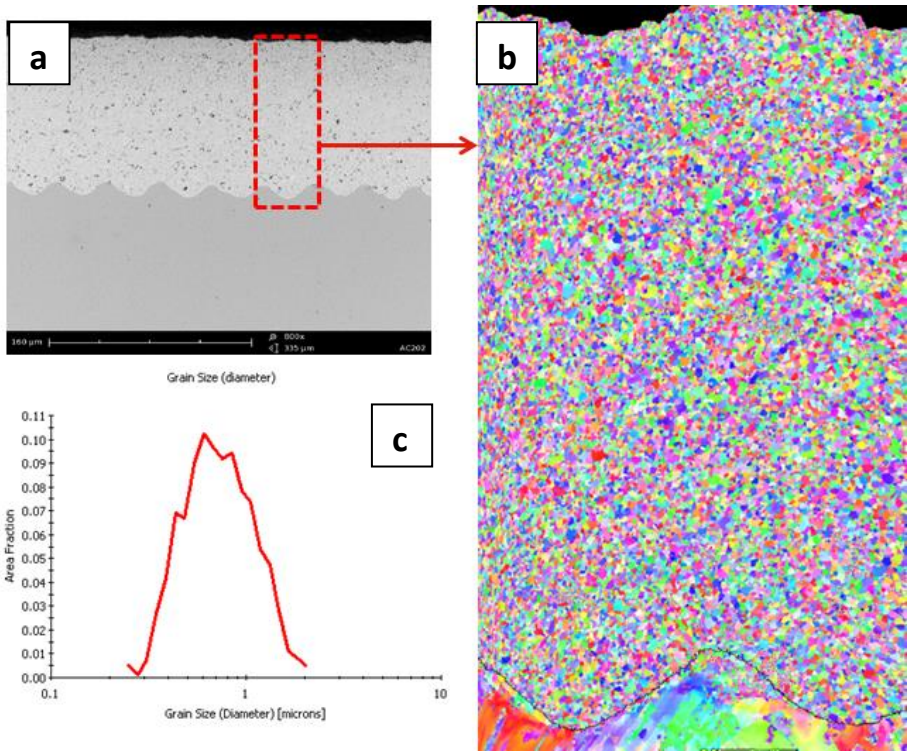

Figure 64 EBSD analysis of two-zones AT102 coating: selection of test area (a), Inverse Pole Figure (b) and grain size distribution (c) [109]

A very dense coatings were obtained for Axial III torch. Even the laser-treated substrate had no influence on the coating growth-up mechanisms. The characteristic deformations of grains observed in previous cases when laser-treated substrates were used (see for example sample ST52 and longitudinal grains in the coating structure) did not occur in coatings sprayed with axial suspension injection. This proves that the particles travel mostly in the hot regions of plasma and do not follow the plasma swirls. The formation of very dense coatings in case of the axial injection mode (Axial III) in comparison to radial injection can be explained by the Figure 65. If the injection is realized fully axially (as for Axial III torch), then the suspension can be introduced exactly in the same direction as the plasma flow occurs. The dispersion angle of the particles travelling in the plasma jet is very narrow. Following, there is much less powder particles travelling in the plasma periphery, so the particles flow together in a small space of narrow plasma jet [86], [126]. As a result, the fragmentation of liquid stream into fine droplets may be less effective than in the case of radial injection mode, where much more pronounced shearing of the liquid occurs. The mentioned phenomena cause that fine powders can easily interact with one another in the plasma jet. Consequently, they can form bigger aggregates. Moreover, it was presented already [33], [99] that the interactions between

powder particles and plasma jet but also plasma particles and substrate are influenced by the adhesion and drag forces. The big particles travelling in the core of plasma jet would have the balance of forces $F_A > F_D$. For smaller, moving in the plasma periphery, the relationship is reversed and $F_D > F_A$. In case of axial injection the adhesion force seems to be much greater than drag force. As a result, the molten particles having narrow distribution of temperature and velocity hit the substrate and form a dense and homogeneous structure (in this study).

The key process parameters, which can enable the formation of columnar coatings by using Axial III torch, seem to be the powder particle size and the powder size distribution. As presented by Curry et al. [45], the decrease in the powder particle size promotes the growth of the columnar coatings [127]. The smaller the particles are, the harder for them to keep the trajectory in the core of plasma jet. The particles that travel in the plasma periphery and then follow the drag force seem to be an important factor to obtain columnar-like coatings.

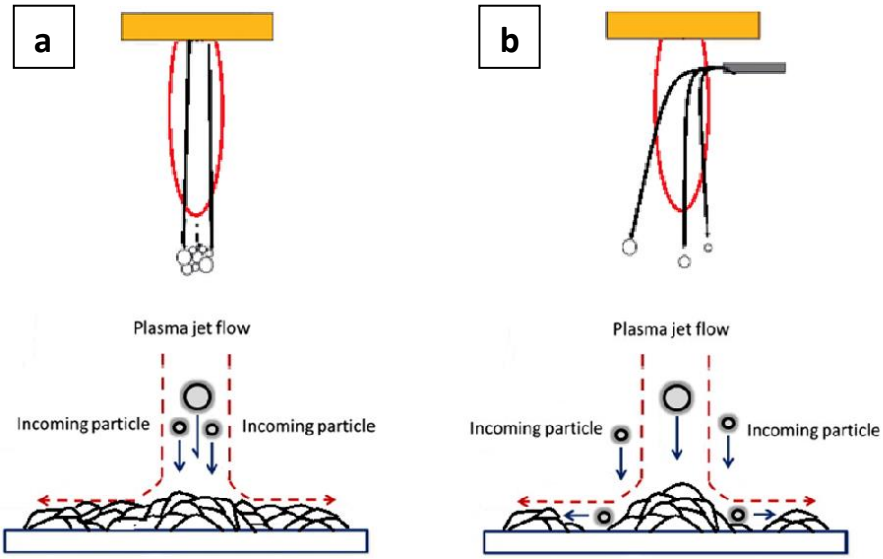

Figure 65 The influence of the injection angle on the coating growth-up mechanism [109]

6.2. Properties of coatings

After spraying and characterization of coating microstructures, the selection of coatings was carried out. The coatings with strongly contrasting microstructural features,

namely:

- columnar-like or lamellar;
- homogeneous or heterogeneous;
- dense or very porous microstructure,

were chosen for further studies. Furthermore, only the samples sprayed onto grit-blasted substrates were selected for further tests (the evaluation of selected coating properties). This was caused by the fact that this substrate preparation technology is widely used in the industrial practice currently.

6.2.1. Density

The first property necessary for thermal diffusivity and thermal conductivity studies is true (called also theoretical) density of material. By using this value the apparent (called also bulk) density in ambient temperature (ρ_{300}) can be evaluated. The measurements carried-out by pycnometry method showed that the densities of coatings were significantly higher than that of initial powders that were used for spraying (Table 11). The greatest difference occurred for YCeSZ material. The coarse, as-produced, YCeSZ powder had the smallest density (5.507 g/cm^3). This is an effect of production method (spray-drying followed by heat treatment) so the resulting Metco 205NS powder particles are very often hollow inside. The hollows were opened during milling and as a result the density of fine pre-processed powders was greater. Finally, the porosity was completely eliminated after spraying and then crushing of coating. This way the true density could be estimated by pycnometry method.

The obtained values of true coating density corresponded well to the values reported in the literature, where the theoretical approach is very often used [128]. The true density of stabilized zirconia is influenced by the type of stabilizer, its content and usually is estimated by the rule of mixtures. The theoretical density of ZrO_2 is equal to 6200 kg/m^3 (according to the X-ray density from ASTM pattern 27-997), of Y_2O_3 is 5031 kg/m^3 (using X-ray density from ASTM pattern 25-1200) and of CeO_2 is equal to 7647 kg/m^3 [129], [130]. The literature values are in agreement with obtained densities of YSZ

coating. In case of YCeSZ coatings, the theoretical values are higher. The crucial seems to be the CeO_2 content having the greatest mass. But the approach considering also the complex phase composition and arrangement of atoms in the crystal structure should be applied to evaluate theoreticaly the density of complex YCeSZ coatings more precisely.

Table 11 The results of density measurements [131]

Material	Average density value [g/cm³]	Standard deviation [g/cm³]
YSZ - powder as-produced	6.000	0.004
YSZ - crushed coating[2]	6.099	0.005
YCeSZ - powder as-produced	5.507	0.003
YCeSZ - powder after milling	5.825	0.005
YCeSZ - crushed coating[3]	6.108	0.009
Inconel 600	8.415	0.003

6.2.2. Specific heat capacity

The specific heat capacity of YSZ and YCeSZ coatings was evaluated experimentally (in low temperature range) and then also extrapolated for high temperatures by using Kopp's law. The chart comparing both c_p values is presented in Figure 66 [131]. The DSC measurement results and the values obtained by Kopp's law are presented together. The difference between the results was not greater than 10 %. The specific heat values that were calculated by the rule of mixtures lies between the two curves obtained experimentally by DSC. In case of YSZ coatings the values found from Kopp's law were almost an average of c_p values measured with the two DSC experimental set-ups. The difference between the results of specific heat capacity that were obtained using two DSC set-ups can be explained by various operational protocols and procedures but also by different quantity of powdered coating materials that was measured. Barros et al. [132] mentioned that the use of too low sample mass reduces the precision of c_p measurements using modulated DSC approach. There are many other factors that influences the precision of Differential Scanning Calorimetry method (e.g. related to the instrument itself, sample characteristics, calibration method and standard material etc.).

[2] this value was taken for apparent coating density calculations of YSZ coatings
[3] this value was taken for apparent coating density calculations of YCeSZ coatings

The structure of the material can slightly affects the value of specific heat capacity, e.g. grain size, crystallographic structure, dislocation density etc. [133]. Anyway, the results were satisfactory, also when comparing to the other literature data [134]. Finally, in the view in all c_p results, the conclusion is that values of specific heat values that were calculated using Kopp's law are enough precise to be used for LFA. So the values determined by rule of mixture were used for thermal diffusivity and conductivity evaluation.

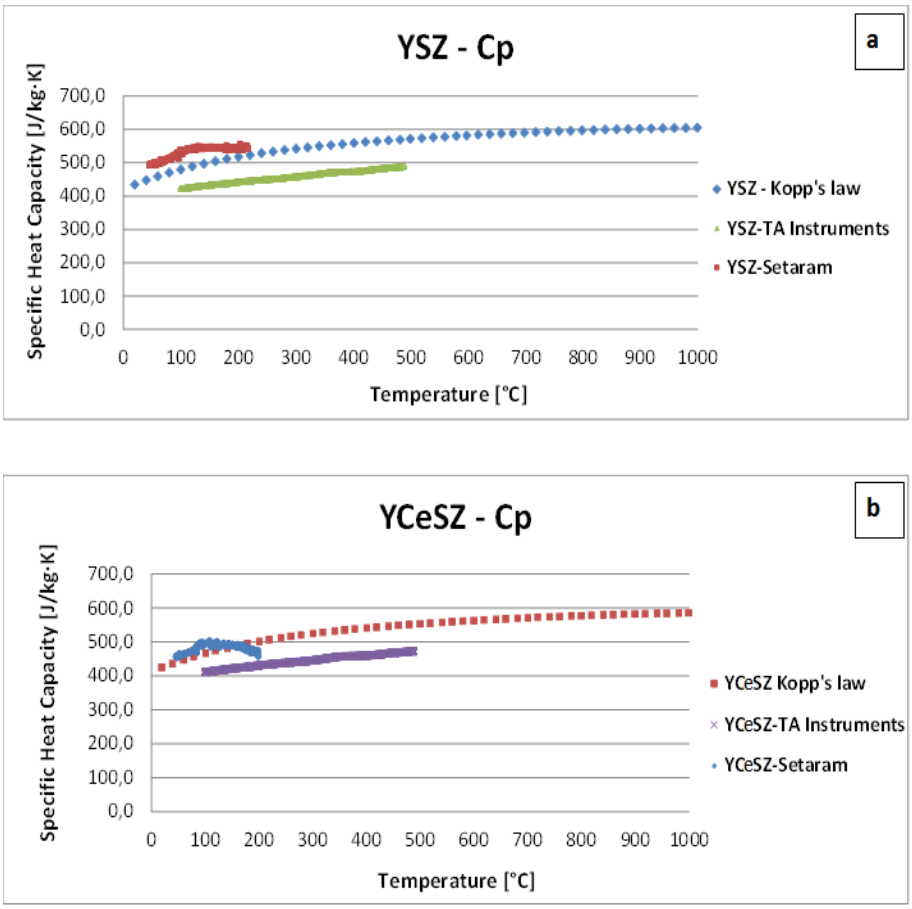

Figure 66 The evaluation of specific heat capacity values of YSZ(a), YCeSZ (b) [131]

6.2.3. Thermal expansion

The studies were followed by thermal expansion investigations. The coatings for dilatometry were prepared by Powder Plasma Spraying instead of Suspension Plasma Spraying. The microstructure of SPS sprayed coatings can be somehow comparable to the PPS one, especially for dense structures [66]. Both types of coatings include lamellas

that are formed by molten solid particles and create a brick-wall structure of coating. The most important difference is the size of single lamellas (these are much greater in case of PPS) and the coating morphology. Especially in case, when columnar-like was produced by SPS. But the proposed approach seems to be more accurate than the use of literature data, where the bulk or sintered zirconia is measured usually.

The anisotropy of $\Delta L/L$ values was observed in zirconia coatings (Figure 67). This effect was reported in the literature for powder plasma sprayed coatings by e.g. Berndt et al. [135] or Ilavsky et al. [136]. This phenomenon can be caused by many different factors. The brick-wall like structure i.e. lamellar structure combined with the extensive network of cracks, voids and pores preferentially oriented according to the spraying direction can highly influence thermal dilatation of coating [137]. Furthermore the multiphase composition of coatings can have a slight effect also [138].

Both, YSZ and YCeSZ, coatings showed higher values of thermal expansion in a horizontal direction (parallel to the substrate). The anisotropy of thermal expansion of plasma sprayed coatings was not fully understood yet, so the phenomena can be analyzed based on other mechanical properties, like stiffness or elastic modulus. Sevostianov and Kachanov [139] used the term of "inverse anisotropy". It means that the values of elastic modulus and stiffness of deposits were higher in the perpendicular direction according to the substrate as a result of scattering of pores orientation in the thermally sprayed coatings. Consequently, the lower thermal expansion is observed in materials having higher stiffness [140]. But in other studies, it was observed that the Young modulus may be even two greater in the in-plane direction (parallel to the coating surface) than in vertical direction (perpendicular to the coating's surface) [136], [137]. This phenomenon is still not fully understood and needs more studies to be confirmed. In this work, the $\Delta L/L$ values that were estimated perpendicularly to the substrate material (the lower values) were chosen for further LFA test. This was caused by the fact, that the heat flow direction was the same.

The thermal expansion values were different during cooling and heating. As the $\Delta L/L$ was found to be anisotropic, so the dimensional changes were not uniform and the same in the coating material. As a consequence the micro-stresses and micro-cracks could have been generated during heating and the thermal expansion during cooling could change. This effect was less visible in case of YCeSZ samples, which are more fatigue-

resistant than YSZ. The very short length of the sample (only 2 mm) could influence also the accuracy of measurements and cause some instabilities during measurements. The measurements of 10mm long sample (done as a verification) did not show such significant differences of thermal expansion when samples were heated and cooled.

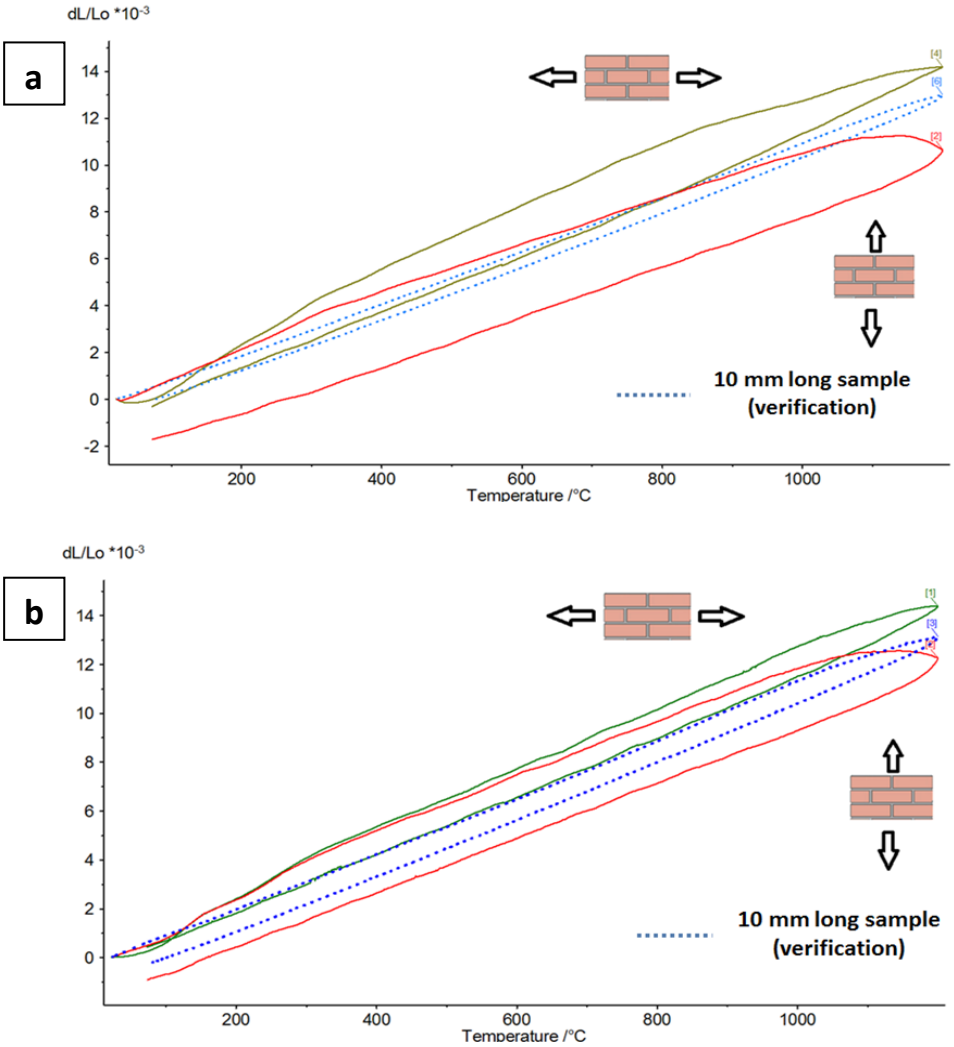

Figure 67 The results of thermal expansion measurements of YSZ (a) and YCeSZ (b) coatings [131]

The values obtained by using dilatometry method were in a good agreement with literature values of thermal expansion for both zirconia materials. Many studies suggest that YCeSZ exhibits slightly greater expansion than YSZ. This was confirmed, especially when comparing the values determined perpendicularly to the substrate [134], [141], [142]. Furthermore, the results obtained for substrate material, Inconel 600, (in fact only 10-15 % higher than that of YSZ and YCeSZ coatings) were in an agreement with the literature and values given by the manufacturer.

6.2.4. Thermal transport properties

The thermal transport properties evaluation were started by the thermal diffusivity measurements. The following samples were selected for this purpose. In case of YSZ coatings, the samples having columnar-like microstructure and two-zones microstructure were selected as well. The porosity of YSZ coatings selected for LFA test was between 10.3 and 21.4 % (Figure 68).

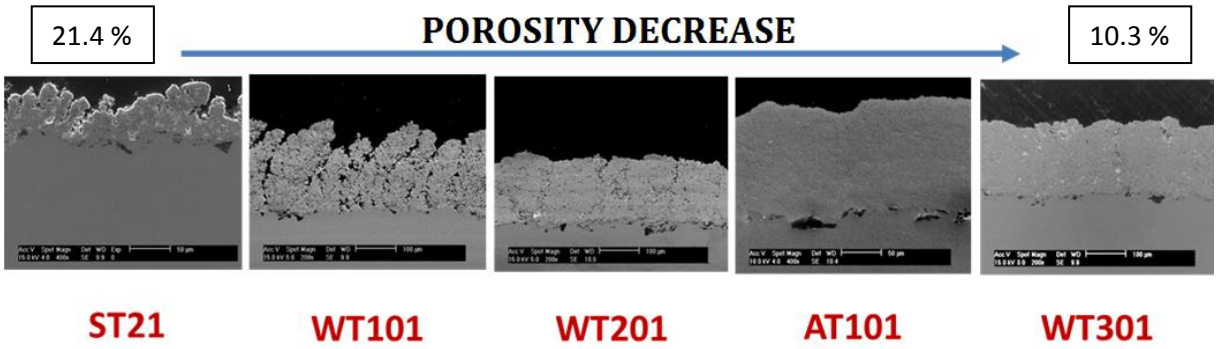

Figure 68 The YSZ samples selected for thermal transport properties studies [131]

The columnar-like coatings were not obtained for YCeSZ powder. So the samples were selected based on the porosity that was in range of 5.2 up to 15.5 % (Figure 69)

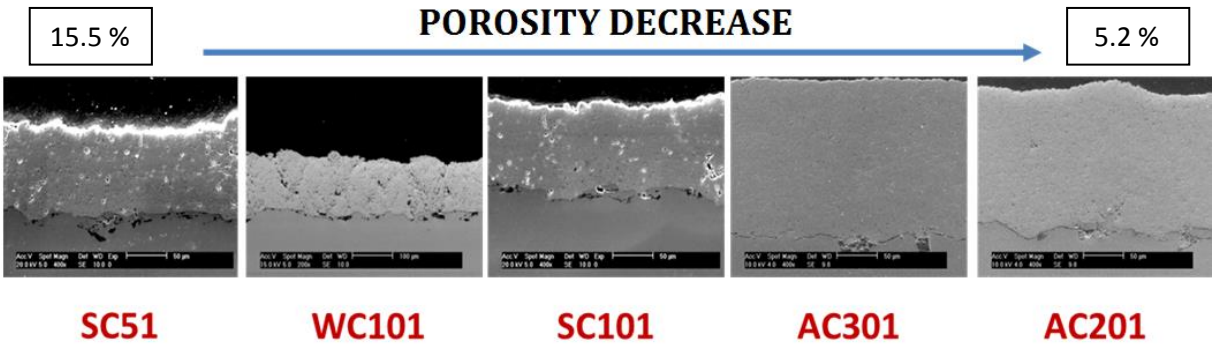

Figure 69 Figure 55 The YCeSZ samples selected for thermal transport properties studies [131]

The obtained values of thermal diffusivity allowed to calculate thermal conductivity of coatings according to the mentioned methodology. Thermal conductivity values were in a range from 0.63 to 0.99 [W/m·K] for YSZ samples (Figure 70a) and between 0.82 and 1.37 [W/m·K] in the case of YCeSZ (Figure 70b). Thermal conductivity was influenced by the coatings' porosity and microstructure. The samples ST21 and WT101 had the highest porosity and the lowest thermal conductivity values. In the case of YCeSZ

coatings the correlation was not that clear. Sample AC301 was characterized by the smallest λ values at low temperatures. This sample was characterized by very low porosity. On the other hand at high temperatures, the samples with the highest porosity had the lowest thermal conductivity.

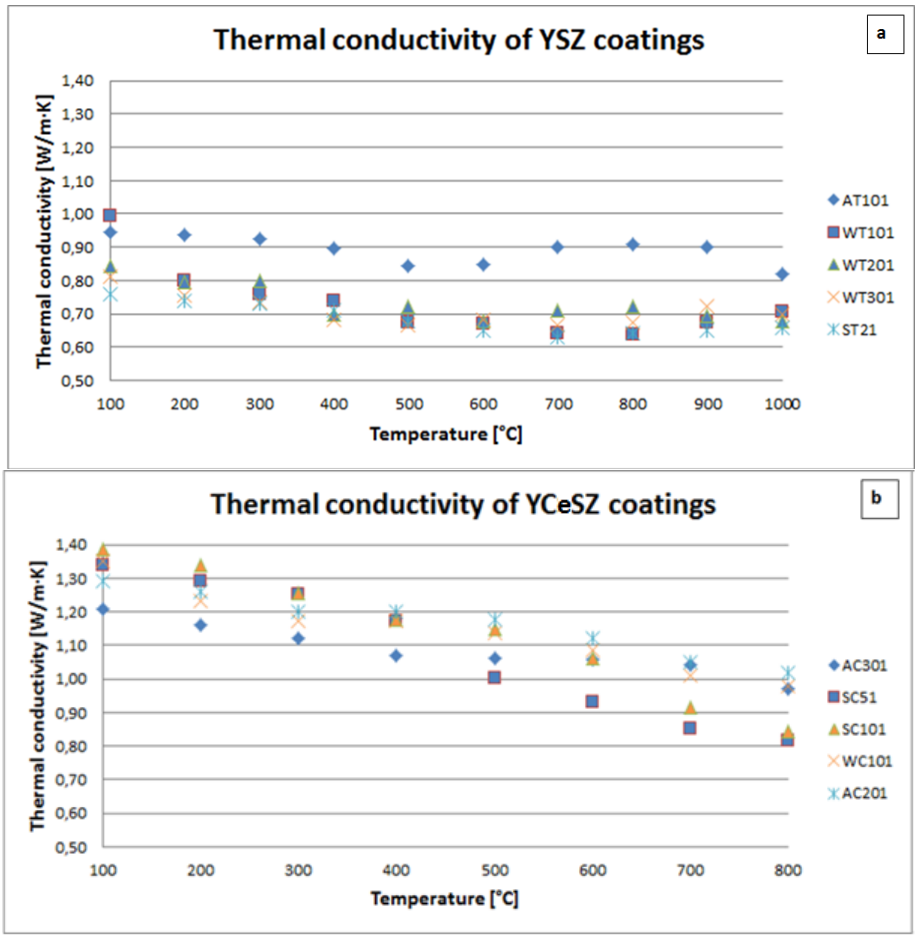

Figure 70 Thermal conductivity values of YSZ (a) and YCeSZ (b) coatings [131]

YSZ coatings were characterized by lower thermal conductivity, especially in a low temperature range. The difference between YSZ and YCeSZ became much smaller in the highest temperatures. The preliminary studies (only up to 300°C by LFA equipped with xenon lamp and presented in the Appendix) showed the thermal conductivity values of YSZ and YCeSZ were much more similar [100]. It should be mentioned that in this studies, the LFA machine was equipped with InSb detector, which is more precise at higher temperatures. Furthermore, the increase of thermal conductivity values of porous samples was observed at high temperatures. This effect could have been caused by the radiative heat transport mechanism at high temperatures [143].

When analyzing the thermal transport properties of YSZ and YCeSZ coatings it should be stated first that thermal conductivity values are much lower than in case of bulk zirconia. This is typical for thermally sprayed coatings and was mentioned already in the literature [144]. But the SPS coatings are characterized also by significantly better thermal transport properties EB-PVD columnar-like zirconia coatings or dense APS coatings. The coatings produced by vapor deposition methods have more homogenous and uniform microstructure but, on the other hand, they have longitudinal pores which may hamper the heat flow in the direction parallel to the substrate [145].

The low values of thermal conductivity of SPS coatings can be explained by microstructural features of these coatings, mainly: (i) porosity and (ii) fine grained microstructure.

The porosity is an important factor when analyzing thermal transport properties. Thermal conductivity of gases (which fill in fact pores trapped in coating structure) is much lower than that of the ceramic materials (e.g. for air is 0.026W/m·K)[146]. So thermal conductivity of materials can be significantly decreased by high porosity. However, the shape, size, orientation and total volume of pores may also play an important factor [147]. If the pores are oriented parallel according to the heat flow, then they can hamper the transport of thermal flux. If the pores have some preferential orientation then thermal conductivity can be also anisotropic [139]. However, the quantitative analysis of pores morphology is difficult. The existing methods of direct porosity measurements, such as mercury intrusion porosimetry, are useful to find open porosity of coating. On the other hand, image analysis method is limited to a few cross-sections of one sample.

Another factors influencing thermal transport properties are microstructural effects. The mean free path of heat carriers is controlled by phonon-phonon interactions and depends on the: (i) material grain size, (ii) the scattering by defects and (iii) the crystallographic disorder. As described in details in previous studies, both suspension sprayed YSZ and YCeSZ coatings have submicrometer grain size of approximatively 500 nm [99]. Some other studies focused on SPS method used nano-suspensions, e.g. the work of Carpio et al. [148]. The size of grains would have the greatest effect on the heat flow if their size were similar size to the mean free path of phonon scattering. Consequently, thermal conductivity of such coatings would be drastically decreased

[92]. It should be mentioned also that the structure of SPS coatings have a high number of various defects that can scatter phonons and impede the heat flow [143]. Moreover, YSZ and YCeSZ ceramics have internal point defects being oxygen vacancies resulting from incorporation of yttria or ceria into zirconia lattice. Finally, the implementation of big and heavy atoms (like Y or Ce) into the structure of ZrO_2 can decrease thermal conductivity too [92].

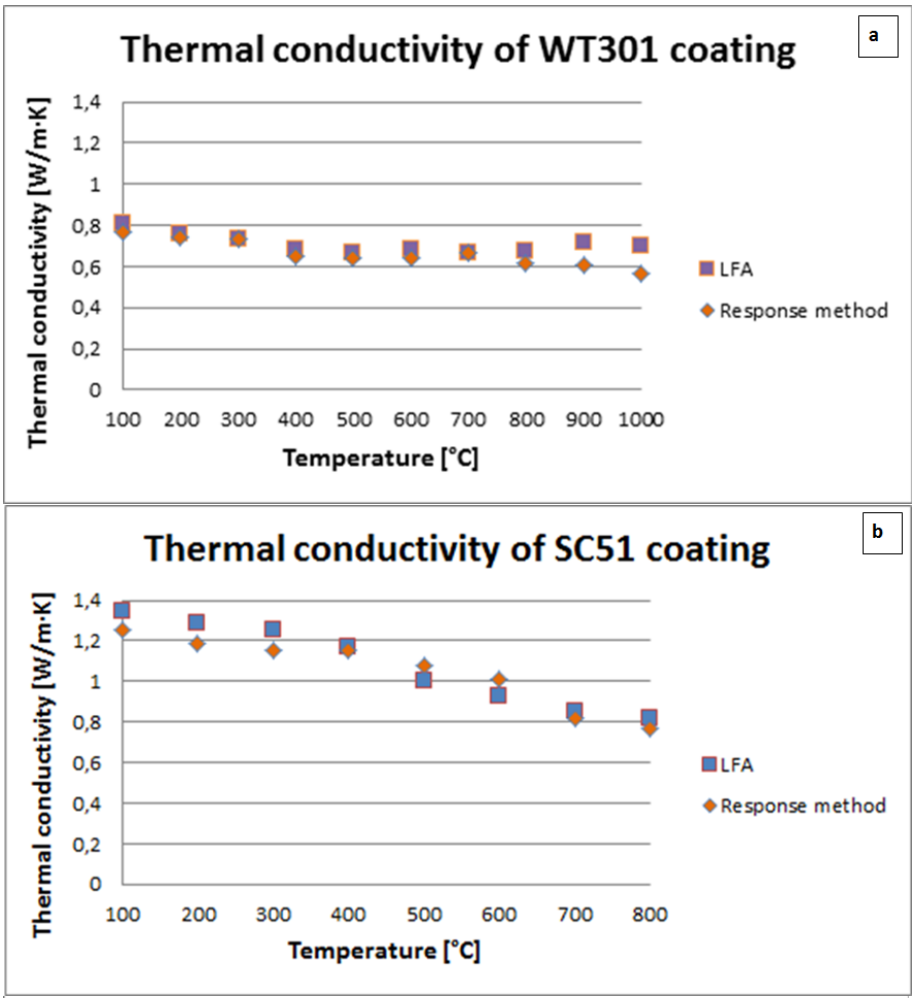

Figure 71 Analytical validation of thermal conductivity values. The example of YSZ (a) and YCeSZ (b) coating [131]

Laser Flash Analysis is an indirect method, quite sensitive and also having some limitations. The analytical validation of results was performed using response function method (see Figure 71). One example of each type of coating is presented in full temperature range. The calculations were made for each sample in each temperature. The difference between thermal conductivity values usually did not exceed ±15 %. In the case of coating WT101 and AC301 was ±20 % but in the lowest temperatures only.

Thermal conductivity of WT101 obtained by laser flash method in 100°C seemed to be too high, whereas the empirical data for AC301 seemed to be too low in the temperatures between 100°C and 400°C. But generally, the results obtained by response method are very satisfactory and can be an alternative to Finite Elements Method (FEM), where the calculations take more time and the model computation needs sometimes very high processing power. The response method is quite well-known actually and was applied to estimate thermal conductivity of different materials already. However, the FEM analysis gives more possibilities and more complex data, as in the case of previous analysis [100].

6.2.5. Hardness and Young modulus

Elastic modulus

In order to determine elastic modulus in accordance to the mentioned methodology the inverse of the contact stiffness vs. the inverse of the square root of the contact area was plotted (as shown on Figure 72). Afterwards, the Young modulus values were calculated using the method suggested by Olivier and Pharr as described above. This was done using the unloading part of the indentation curve.

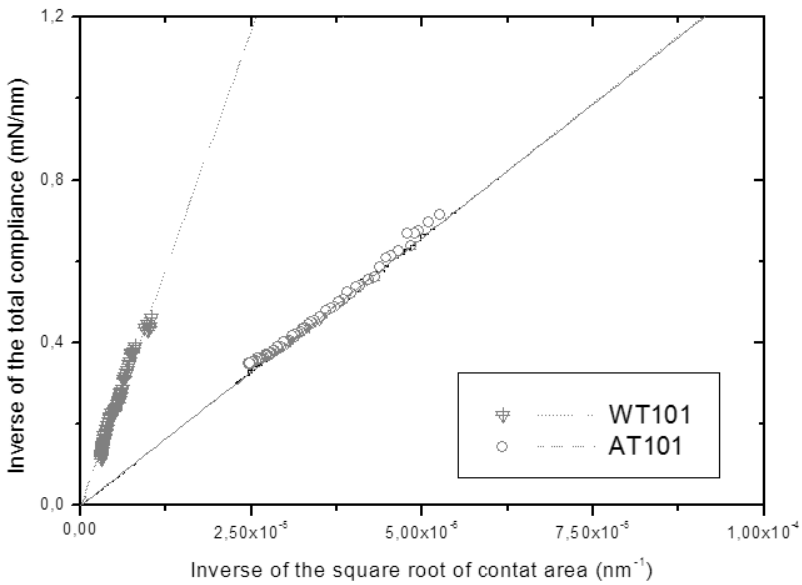

Figure 72 Examples of inverse of the contact stiffness versus reciprocal of the contact area for coatings having various microstructures

The results of elastic modulus calculations are presented in the Figure 73. The Young modulus is strongly influenced by the coating microstructure, mainly porosity. YSZ and YCeSZ coatings having the highest porosity and very irregular morphology (ST21, WT101) show the lowest values of elastic modulus. Whereas the samples that were dense, uniform with a homogeneous distribution of pores in the structure present the much higher values (AY301, AC201) of elastic modulus.

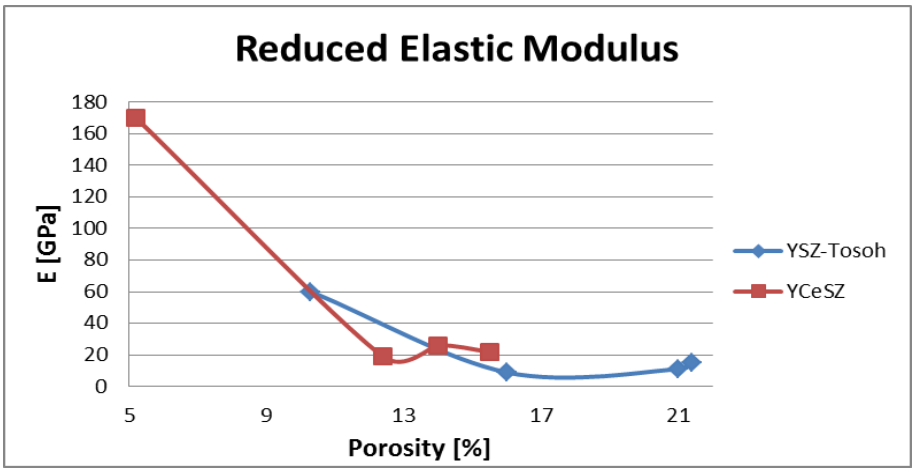

Figure 73 E-modulus vs. porosity for YSZ and YCeSZ coatings

As presented and discussed already, the slope of the elastic modulus was constant when the indentation depth increases (Figure 72). It was observed in each measuring point and each point consists of 100 cycles. Therefore, a very small standard deviation of elastic modulus values was observed. The values of standard deviation of around 10 % in each measuring point suggested also that the indentation did not cause probably any local fracture of the coating during IIT testing. But to confirm this, the analysis of the load-displacement curve together with detailed microscopic studies of the indentations should be carried out.

The values of elastic modulus strongly vary between different measuring points. This can be an effect of the microstructural feature of plasma sprayed coatings. They are highly disordered in the term of their microstructures. The splats have different size, orientation. The coatings consist of sintered or not properly melted particles also. Carpio et al. [30] observed also the bimodal distribution of mechanical properties of SPS coatings that were determined by IIT method. But these are only preliminary studies that will be continued to deeply examine and understand the mechanical properties of SPS coatings.

Hardness

The values of HM hardness of coatings are presented in the Figure 74. The calculated values vary between 0.04 and 5.18 GPa. A similar behavior as in case of Young modulus was observed. The higher values of HM hardness were obtained for coatings having more uniform microstructure. At the same time, the most heterogeneous coatings (in the term of their morphology and porosity) exhibit much lower hardness. When analyzing the hardness in single measuring point then the standard deviation is usually not greater than 15 % (for 100 cycles). But the results vary when different measuring points are considered and analyzed and this is a result of the microstructure also, as discussed for elastic modulus.

The microhardness of homogeneous and dense coatings corresponds to the work presented by Łatka et al. [149]. Furthermore, a very low values of hardness (obtained for irregular and very porous coatings) may be also a result of very weak interfaces between splats as suggested by Lima et al. [150].

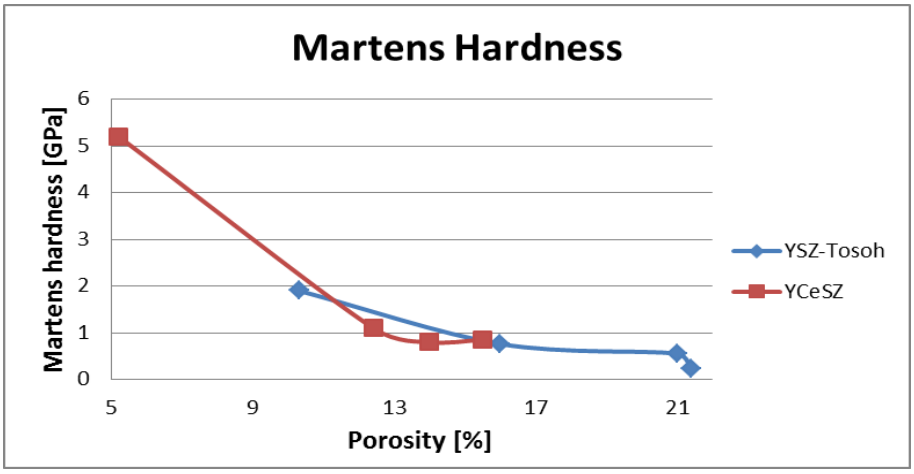

Figure 74 Martens hardness vs. porosity for YSZ and YCeSZ coatings

CHAPTER 7. CONCLUSIONS

7.1. Coatings microstructure

Microstructure modification

In these studies different variables were tested to produce coatings having different microstructures by Suspension Plasma Spraying. Based on the microstructural characterization of coatings the following findings can be mentioned:

- Suspension Plasma Spraying allows producing coatings having various microstructures. Columnar-like coatings, as well as two-zones microstructures were obtained. The coatings were characterized also by different porosity, starting from very dense microstructures up to very porous.
- Through the use of different plasma spray torches different coatings' morphologies can be obtained. The suspension injection angle (radial and axial injection modes were used) was found to be one of the crucial in term of the microstructure modification.
- The suspension preparation seems to be another important factor that has an effect on the coating growth-up. The lower concentration of the suspension is, then the coating microstructure and topography is more irregular also. The lowest suspension concentration (2.5 wt. %) allowed producing of columnar-like coatings on even a flat substrates. The reverse effect was observed for high-concentrated suspensions.
- The powder particle size is also one of the key parameters in SPS. It was observed that the use of fine-grained powder (YSZ) allowed obtaining coatings having columnar-like microstructure, whereas the coarser powder (YCeSZ) influenced

formation of dense two-zone microstructure. This is caused by the transportation of powder particles in the plasma jet. The small one's have a tendency to travel in the plasma periphery, whereas the coarser ones near to the plasma core. The fine powders following the plasma swirls seem to be very important in formation of columnar-like coatings.

- The substrate topography influences also the coating growth-up mechanisms, especially for fine powder particles and low concentrated suspensions. This can be explained by the shadowing effect, which is more effective when rougher substrates are used during spraying.

- Suspension Plasma Spraying method may be an effective coating technology. The obtained spray process deposition rate (defined here as thickness per pass ratio) was up to few microns/pass. This clearly shows that SPS can be a very competitive process for other technologies enabling production of fine-grained coatings (like PVD or CVD).

Finally, using SPS process a coating microstructure can be, to a degree, designed for specific application or desirable final property. After the use of different plasma torches and spray set-ups it can be stated that there are already sufficient tools that can be applied in the industrial production. Especially the application of high-power plasma torches seems to be possible in a near future. They provide enough power to well heat the suspension inside the plasma flame - evaporate the solvent and melt the solid phase. High suspension injection rates can be used also. Based on these studies two important applications can be mentioned:

Application in Thermal Barrier Coatings

Based on the microstructural studies can be stated that Suspension Plasma Spraying is a promising method for Thermal Barrier Coatings applications. The method is currently the best compromise between EB-PVD and APS coatings. Using SPS it is possible to deposit columnar-like coatings with a high deposition rate. Furthermore, the coatings are characterized by fine-grained microstructure with a high closed porosity. The fine, spherical, pores that are trapped in the coating structure can be an effective barrier for heat transport. So the columnar-like coatings that can be produced by Suspension

Plasma Spraying seem to join high thermal shock resistance and effective thermal insulation, which are the most important in TBC's.

Applications in Solid Oxide Fuel Cells

There are many advantages of SPS sprayed components for the purpose of SOFC's when comparing to other deposition processes. The fine powders, which are used in SPS, can produce smaller splats in the coatings. This leads to the formation of fine grained microstructure having controlled pore distribution. Afterwards, there is no need to use "pore making" agents and perform heat treatment of coating, which is common in SOFC's practice. Furthermore, the microstructural control during spraying and the possibility to produce coatings in wide range of thicknesses are big advantages of SPS. An important issue is that coatings produced by Suspension Plasma Spraying are characterized by relatively high mechanical properties. If needed (as in case of SOFC's electrolyte), the process conditions can be optimized in a way to produce very dense coatings.

7.2. Coatings properties

In this study the Thermal Barrier Coating application was prioritized. The experimental methods were selected in order to get a complex information about thermal transport properties of YSZ and YCeSZ coatings. The most important idea was to obtain experimentally all thermophysical properties that are necessary for the determination of thermal conductivity by laser flash method:

- The density measurements showed that there is a need to investigate the coating material itself. Any simplification and the use of powder's density can lead to a big error, depending on the feedstock preparation method.
- Specific heat capacity measurements showed that the Kopp's law can be a sufficient tool for the extrapolation of Cp values. However, the experimental verification is needed also, especially for complex materials.
- Thermal expansion measurements of SPS coatings remain still unsolved problem. In this study the thick Powder Plasma Sprayed coatings were deposited and measured. SPS and PPS coatings exhibit many similarities in terms of the

microstructure. The obtained values should provide more accurate values than in case of literature data that are usually obtained for bulk or sintered zirconia. The coatings showed also anisotropy of thermal dilatation, which was much more visible for YSZ coatings then in case of YCeSZ.

- Finally, the thermal conductivity of Suspension Plasma Sprayed zirconia coatings seems to be lower than that of EB-PVD coatings or PPS coatings. The values far below 1[W/m·K] were obtained. The low thermal conductivity of SPS coatings can be explained by the high amount of fine pores in the coating structure but also other microstructural effects, like fine-grained structure.

- The basic evaluation of mechanical properties showed that there is a correlation between coating porosity and Young modulus and Martens Hardness. As expected, the increase in the porosity causes the decrease in mechanical properties of coatings.

7.3. Further works

In this work the two main research issues were investigated: (i) the formation and modification of coating microstructure in Suspension Plasma Spraying method and (ii) the determination of thermal transport properties of produced zirconia coatings. The studied samples were two-layer systems of substrate and zirconia coating. This allowed analyzing zirconia coatings with higher accuracy.

But in accordance to the information presented in the Introduction chapter, the typical Thermal Barrier Coatings is a three layer system with zirconia coating as a topcoat. After the optimization of zirconia coatings, the studies on the complete TBC systems will be undertaken. The thermomechanical and thermophysical properties, like thermal shock resistance, isothermal oxidation or CMAS attack resistance seem to be crucial in term of TBC lifetime prediction.

The dense coatings that were obtained in this study will be tested for the purpose of Solid Oxide Fuel Cell application.

The laser pre-treatment gave many interesting results in this work. The studies focused on the modification of zirconia coating microstructure by using laser treatment will be continued also.

REFERENCES

[1] D. R. Greatrix, "Gas Turbine Engines: Fundamentals," in *Powered Flight*, Springer London, 2012, pp. 147–231.

[2] J. R. Simões-Moreira, "Fundamentals of Thermodynamics Applied to Thermal Power Plants," in *Thermal Power Plant Performance Analysis*, G. F. M. de Souza, Ed. London: Springer London, 2012, pp. 7–39.

[3] D. M. Dimiduk and J. H. Perepezko, "Mo-Si-B Alloys: Developing a Revolutionary Turbine-Engine Material," *MRS Bull.*, vol. 28, no. 9, pp. 639–645, Sep. 2003.

[4] D. R. Clarke, M. Oechsner, and N. P. Padture, "Thermal-barrier coatings for more efficient gas-turbine engines," *MRS Bull.*, vol. 37, no. 10, pp. 891–898, Oct. 2012.

[5] P. Sokołowski and L. Pawlowski, "Review of Recent Studies on Suspension Plasma Sprayed ZrO2 Coatings," in *Advances in Materials Science Research*, vol. Volume 26, M. C. Wythers, Ed. Nova Science Publishers, 2016.

[6] R. Darolia, "Thermal barrier coatings technology: critical review, progress update, remaining challenges and prospects," *Int. Mater. Rev.*, vol. 58, no. 6, pp. 315–348, Aug. 2013.

[7] R. A. Miller, "Current status of thermal barrier coatings — An overview," *Surf. Coat. Technol.*, vol. 30, no. 1, pp. 1–11, Jan. 1987.

[8] D. J. Wortman, B. A. Nagaraj, and E. C. Duderstadt, "Proceedings of the 2nd International Symposium on High Temperature Corrosion of Advanced Materials and CoatingsThermal barrier coatings for gas turbine use," *Mater. Sci. Eng. A*, vol. 120, pp. 433–440, Dec. 1989.

[9] H. A. Taroco, J. A. F. Santos, R. Z. Domingues, and T. Matencio, "Ceramic Materials for Solid Oxide Fuel Cells," in *Advances in Ceramics - Synthesis and Characterization, Processing and Specific Applications*, C. Sikalidis, Ed. InTech, 2011.

[10] M. Mogensen, D. Lybye, N. Bonanos, P. V. Hendriksen, and F. W. Poulsen, "Factors controlling the oxide ion conductivity of fluorite and perovskite structured oxides," *Solid State Ion.*, vol. 174, no. 1–4, pp. 279–286, Oct. 2004.

[11] T. Ishihara, N. M. Sammes, and O. Yamamoto, "Chapter 4 - Electrolytes," in *High Temperature and Solid Oxide Fuel Cells*, Amsterdam: Elsevier Science, 2003, pp. 83–117.

[12] D. Waldbillig and O. Kesler, "Effect of suspension plasma spraying process parameters on YSZ coating microstructure and permeability," *Surf. Coat. Technol.*, vol. 205, no. 23–24, pp. 5483–5492, Sep. 2011.

[13] T. Setoguchi, M. Sawano, K. Eguchi, and H. Arai, "Application of the stabilized zirconia thin film prepared by spray pyrolysis method to SOFC," *Solid State Ion.*, vol. 40–41, Part 1, pp. 502–505, Aug. 1990.

[14] J. Seydel, M. Becker, E. Ivers-Tiffée, and H. Hahn, "Granular nanocrystalline zirconia electrolyte layers deposited on porous SOFC cathode substrates," *Mater. Sci. Eng. B*, vol. 164, no. 1, pp. 60–64, Aug. 2009.

[15] L. Mingde, Y. Bo, W. Mingfen, C. Jing, X. Jingming, and Z. Yuchun, "The Fabrication Technique of YSZ Electrolyte Film," *Prog. Chem.*, vol. 20, no. 708, pp. 1222–1232, 2008.

[16] R. Nédélec, S. Uhlenbruck, D. Sebold, V. A. C. Haanappel, H.-P. Buchkremer, and D. Stöver, "Dense yttria-stabilised zirconia electrolyte layers for SOFC by reactive magnetron sputtering," *J. Power Sources*, vol. 205, pp. 157–163, May 2012.

[17] M. Scagliotti, F. Parmigiani, G. Chiodelli, A. Magistris, G. Samoggia, and G. Lanzi, "Plasma-sprayed zirconia electrolytes," *Solid State Ion.*, vol. 28–30, Part 2, pp. 1766–1769, Sep. 1988.

[18] D. Waldbillig and O. Kesler, "Electrochemical testing of suspension plasma sprayed solid oxide fuel cell electrolytes," *J. Power Sources*, vol. 196, no. 13, pp. 5423–5431, Jul. 2011.

[19] L. Pawlowski, *The Science and Engineering of Thermal Spray Coatings, 2nd Edition*. Wiley.

[20] P. Fauchais, G. Montavon, and G. Bertrand, "From Powders to Thermally Sprayed Coatings," *J. Therm. Spray Technol.*, vol. 19, no. 1–2, pp. 56–80, Dec. 2009.

[21] R. S. Lima and B. R. Marple, "Thermal Spray Coatings Engineered from Nanostructured Ceramic Agglomerated Powders for Structural, Thermal Barrier and Biomedical Applications: A Review," *J. Therm. Spray Technol.*, vol. 16, no. 1, pp. 40–63, Mar. 2007.

[22] L. Marcinauskas, "Deposition of alumina coatings from nanopowders by plasma spraying," *Medziagotyra*, vol. 16, no. 1, pp. 47–51, 2010.

[23] H. Chen and C. X. Ding, "Nanostructured zirconia coating prepared by atmospheric plasma spraying," *Surf. Coat. Technol.*, vol. 150, no. 1, pp. 31–36, Feb. 2002.

[24] L. L. Shaw *et al.*, "The dependency of microstructure and properties of nanostructured coatings on plasma spray conditions," *Surf. Coat. Technol.*, vol. 130, no. 1, pp. 1–8, Aug. 2000.

[25] F. Gitzhofer, E. Bouyer, and M. I. Boulos, "Suspension plasma spray," US5609921 A, 1997.

[26] C. C. Berndt, “Materials Production for Thermal Spray Processes,” in *Handbook of Thermal Spray Technology*, J. R. Davis, Ed. ASM International, 2004.

[27] M. Sopicka-Lizer, *High-Energy Ball Milling: Mechanochemical Processing of Nanopowders*. Elsevier, 2010.

[28] S. C. Tjong and H. Chen, “Nanocrystalline materials and coatings,” *Mater. Sci. Eng. R Rep.*, vol. 45, no. 1–2, pp. 1–88, Sep. 2004.

[29] S. Banerjee and D. A. K. Tyagi, *Functional Materials: Preparation, Processing and Applications*. Elsevier, 2012.

[30] P. Carpio *et al.*, “Microstructure and indentation mechanical properties of YSZ nanostructured coatings obtained by suspension plasma spraying,” *Surf. Coat. Technol.*, vol. 220, pp. 237–243, Apr. 2013.

[31] TOSOH CORPORATION, “Zirconia,” Tokyo, Japan.

[32] M. Marr, J. Kuhn, C. Metcalfe, J. Harris, and O. Kesler, “Electrochemical performance of solid oxide fuel cells having electrolytes made by suspension and solution precursor plasma spraying,” *J. Power Sources*, vol. 245, pp. 398–405, Jan. 2014.

[33] P. Sokołowski, S. Kozerski, L. Pawłowski, and A. Ambroziak, “The key process parameters influencing formation of columnar microstructure in suspension plasma sprayed zirconia coatings,” *Surf. Coat. Technol.*, vol. 260, pp. 97–106, Dec. 2014.

[34] B. Movahedi, “A Solid State Approach to Synthesis Advanced Nanomaterials for Thermal Spray Applications,” in *Advanced Plasma Spray Applications*, H. Salimi Jazi, Ed. InTech, 2012.

[35] C. C. Koch, “Synthesis of nanostructured materials by mechanical milling: problems and opportunities,” *Nanostructured Mater.*, vol. 9, no. 1–8, pp. 13–22, 1997.

[36] H. Kassner, R. Siegert, D. Hathiramani, R. Vassen, and D. Stoever, “Application of Suspension Plasma Spraying (SPS) for Manufacture of Ceramic Coatings,” *J. Therm. Spray Technol.*, vol. 17, no. 1, pp. 115–123, Dec. 2007.

[37] D. Chen, E. H. Jordan, and M. Gell, “Suspension plasma sprayed composite coating using amorphous powder feedstock,” *Appl. Surf. Sci.*, vol. 255, no. 11, pp. 5935–5938, Mar. 2009.

[38] L. Łatka *et al.*, “Mechanical Properties of Yttria- and Ceria-Stabilized Zirconia Coatings Obtained by Suspension Plasma Spraying,” *J. Therm. Spray Technol.*, vol. 22, no. 2–3, pp. 125–130, Dec. 2012.

[39] R. Jaworski, C. Pierlot, L. Pawlowski, M. Bigan, and M. Quivrin, “Synthesis and Preliminary Tests of Suspension Plasma Spraying of Fine Hydroxyapatite Powder,” *J. Therm. Spray Technol.*, vol. 17, no. 5–6, pp. 679–684, Oct. 2008.

[40] J. O. Berghaus, B. Marple, and C. Moreau, “Suspension plasma spraying of nanostructured WC-12Co coatings,” *J. Therm. Spray Technol.*, vol. 15, no. 4, pp. 676–681, Dec. 2006.

[41] C. Suryanarayana, “Mechanical alloying and milling,” *Prog. Mater. Sci.*, vol. 46, no. 1–2, pp. 1–184, Jan. 2001.

[42] F. Fernandes, A. Ramalho, A. Loureiro, J. M. Guilemany, M. Torrell, and A. Cavaleiro, “Influence of nanostructured ZrO2 additions on the wear resistance of Ni-based alloy coatings deposited by APS process,” *Wear*, vol. 303, no. 1–2, pp. 591–601, Jun. 2013.

[43] B. Movahedi and M. H. Enayati, “Thermal spray coatings of Ni–10 wt-%Al composite powder synthesised by low energy mechanical milling,” *Surf. Eng.*, vol. 25, no. 4, pp. 276–283, 2009.

[44] Z. L. Dong and K. A. Khor, “Microstructure formation in plasma-sprayed functionally graded NiCoCrAlY/yttria-stabilized zirconia coatings,” *Surf. Coat. Technol.*, vol. 114, no. 2–3, pp. 181–186, 1999.

[45] N. Curry, K. VanEvery, T. Snyder, J. Susnjar, and S. Bjorklund, “Performance Testing of Suspension Plasma Sprayed Thermal Barrier Coatings Produced with Varied Suspension Parameters,” *Coatings*, vol. 5, no. 3, pp. 338–356, Jul. 2015.

[46] O. Marchand, P. Bertrand, J. Mougin, C. Comminges, M.-P. Planche, and G. Bertrand, “Characterization of suspension plasma-sprayed solid oxide fuel cell electrodes,” *Surf. Coat. Technol.*, vol. 205, no. 4, pp. 993–998, Nov. 2010.

[47] P. Fauchais, R. Etchart-Salas, V. Rat, J. F. Coudert, N. Caron, and K. Wittmann-Ténèze, “Parameters Controlling Liquid Plasma Spraying: Solutions, Sols, or Suspensions,” *J. Therm. Spray Technol.*, vol. 17, no. 1, pp. 31–59, Feb. 2008.

[48] R. Rampon, O. Marchand, C. Filiatre, and G. Bertrand, “Influence of suspension characteristics on coatings microstructure obtained by suspension plasma spraying,” *Surf. Coat. Technol.*, vol. 202, no. 18, pp. 4337–4342, Jun. 2008.

[49] F.-L. Toma *et al.*, “Microstructure and environmental functionalities of TiO2-supported photocatalysts obtained by suspension plasma spraying,” *Appl. Catal. B Environ.*, vol. 68, no. 1–2, pp. 74–84, Oct. 2006.

[50] D. Chen, E. H. Jordan, and M. Gell, “The Solution Precursor Plasma Spray Coatings: Influence of Solvent Type,” *Plasma Chem. Plasma Process.*, vol. 30, no. 1, pp. 111–119, Nov. 2009.

[51] H. Kaβner, R. Vaβen, and D. Stöver, “Study on instant droplet and particle stages during suspension plasma spraying (SPS),” *Surf. Coat. Technol.*, vol. 202, no. 18, pp. 4355–4361, Jun. 2008.

[52] F.-L. Toma, G. Bertrand, D. Klein, C. Coddet, and C. Meunier, "Nanostructured photocatalytic titania coatings formed by suspension plasma spraying," *J. Therm. Spray Technol.*, vol. 15, no. 4, pp. 587–592, Dec. 2006.

[53] L. Pawlowski, "Finely grained nanometric and submicrometric coatings by thermal spraying: A review," *Surf. Coat. Technol.*, vol. 202, no. 18, pp. 4318–4328, Jun. 2008.

[54] B. W. Robinson *et al.*, "Suspension plasma sprayed coatings using dilute hydrothermally produced titania feedstocks for photocatalytic applications," *J Mater Chem A*, vol. 3, no. 24, pp. 12680–12689, 2015.

[55] S. Mueller, E. W. Llewellin, and H. M. Mader, "The rheology of suspensions of solid particles," *Proc. R. Soc. Lond. Math. Phys. Eng. Sci.*, vol. 466, no. 2116, pp. 1201–1228, Apr. 2010.

[56] Z. Wang, Z. Ni, D. Qiu, G. Tao, and P. Yang, "Characterization of stability of ceramic suspension for slurry introduction in inductively coupled plasma optical emission spectrometry and application to aluminium nitride analysis," *J. Anal. At. Spectrom.*, vol. 20, no. 4, pp. 315–319, Mar. 2005.

[57] T. A. Ring, *Fundamentals of Ceramic Powder Processing and Synthesis*. Academic Press, 1996.

[58] R. G. Larson, *The Structure and Rheology of Complex Fluids*. OUP USA, 1999.

[59] D. Fairhurst, "An Overview of the Zeta Potential Part 3: Uses and Applications," 2013.

[60] D. Waldbillig and O. Kesler, "The effect of solids and dispersant loadings on the suspension viscosities and deposition rates of suspension plasma sprayed YSZ coatings," *Surf. Coat. Technol.*, vol. 203, no. 15, pp. 2098–2101, May 2009.

[61] R. Greenwood and K. Kendall, "Selection of Suitable Dispersants for Aqueous Suspensions of Zirconia and Titania Powders using Acoustophoresis," *J. Eur. Ceram. Soc.*, vol. 19, no. 4, pp. 479–488, Apr. 1999.

[62] Y. H. Wang, X. Q. Liu, and G. Y. Meng, "Dispersion and stability of 8 mol.% yttria stabilized zirconia suspensions for dip-coating filtration membranes," *Ceram. Int.*, vol. 33, no. 6, pp. 1025–1031, Aug. 2007.

[63] A. U. Khan, A. U. Haq, N. Mahmood, and Z. Ali, "Rheological studies of aqueous stabilised nano-zirconia particle suspensions," *Mater. Res.*, vol. 15, no. 1, pp. 21–26, Feb. 2012.

[64] L. Pawlowski, "Suspension and solution thermal spray coatings," *Surf. Coat. Technol.*, vol. 203, no. 19, pp. 2807–2829, Jun. 2009.

[65] L. Pawlowski, "Suspension and solution thermal spray coatings," *Surf. Coat. Technol.*, vol. 203, no. 19, pp. 2807–2829, Jun. 2009.

[66] S. Kozerski *et al.*, "Preliminary study on suspension plasma sprayed ZrO2 + 8 wt.% Y2O3 coatings," *J. Eur. Ceram. Soc.*, vol. 31, no. 12, pp. 2089–2098, Oct. 2011.

[67] S. Kozerski, L. Pawlowski, R. Jaworski, F. Roudet, and F. Petit, “Two zones microstructure of suspension plasma sprayed hydroxyapatite coatings,” *Surf. Coat. Technol.*, vol. 204, no. 9–10, pp. 1380–1387, Jan. 2010.

[68] J. Fazilleau, C. Delbos, V. Rat, J. F. Coudert, P. Fauchais, and B. Pateyron, “Phenomena Involved in Suspension Plasma Spraying Part 1: Suspension Injection and Behavior,” *Plasma Chem. Plasma Process.*, vol. 26, no. 4, pp. 371–391, Apr. 2006.

[69] A. Killinger, R. Gadow, G. Mauer, A. Guignard, R. Vaßen, and D. Stöver, “Review of New Developments in Suspension and Solution Precursor Thermal Spray Processes,” *J. Therm. Spray Technol.*, vol. 20, no. 4, pp. 677–695, Mar. 2011.

[70] F.-L. Toma *et al.*, “Comparative study on the photocatalytic behaviour of titanium oxide thermal sprayed coatings from powders and suspensions,” *Surf. Coat. Technol.*, vol. 203, no. 15, pp. 2150–2156, May 2009.

[71] P. Blazdell and S. Kuroda, “Plasma spraying of submicron ceramic suspensions using a continuous ink jet printer,” *Surf. Coat. Technol.*, vol. 123, no. 2–3, pp. 239–246, Jan. 2000.

[72] R. Vaßen, H. Kaßner, G. Mauer, and D. Stöver, “Suspension Plasma Spraying: Process Characteristics and Applications,” *J. Therm. Spray Technol.*, vol. 19, no. 1–2, pp. 219–225, Nov. 2009.

[73] P. Fauchais, M. Vardelle, S. Goutier, and A. Vardelle, “Key Challenges and Opportunities in Suspension and Solution Plasma Spraying,” *Plasma Chem. Plasma Process.*, vol. 35, no. 3, pp. 511–525, Nov. 2014.

[74] A. Ozturk and B. M. Cetegen, “Modeling of axially and transversely injected precursor droplets into a plasma environment,” *Int. J. Heat Mass Transf.*, vol. 48, no. 21–22, pp. 4367–4383, Oct. 2005.

[75] R. Etchart-Salas *et al.*, “Influence of Plasma Instabilities in Ceramic Suspension Plasma Spraying,” *J. Therm. Spray Technol.*, vol. 16, no. 5–6, pp. 857–865, Oct. 2007.

[76] P. Mohanty, J. Stanisic, J. Stanisic, A. George, and Y. Wang, “A Study on Arc Instability Phenomena of an Axial Injection Cathode Plasma Torch,” *J. Therm. Spray Technol.*, vol. 19, no. 1–2, pp. 465–475, Dec. 2009.

[77] H. Gotô and I. Atsuya, “Stabilization of the plasma-jet flame and determination of aluminium and boron in steel,” *Fresenius Z. Für Anal. Chem.*, vol. 240, no. 2, pp. 102–110, Mar. 1968.

[78] Z. Duan and J. Heberlein, “Arc instabilities in a plasma spray torch,” *J. Therm. Spray Technol.*, vol. 11, no. 1, pp. 44–51, Mar. 2002.

[79] K. Bobzin *et al.*, “Modelling and diagnostics of multiple cathodes plasma torch system for plasma spraying,” *Front. Mech. Eng.*, vol. 6, no. 3, pp. 324–331, May 2011.

[80] M. Hrabovsky, “Thermal Plasma Generators with Water Stabilized Arc,” *Open Plasma Phys. J.*, vol. 2, no. 1, pp. 99–104, 2009.

[81] M. Hrabovsky, “Water-stabilized plasma generators,” *Pure Appl. Chem. - PURE APPL CHEM*, vol. 70, no. 6, pp. 1157–1162, 1998.

[82] S. Raghu, G. Goutevenier, and R. Gansert, “Comparative study of the structure of gas-stabilized and water-stabilized plasma jets,” *J. Therm. Spray Technol.*, vol. 4, no. 2, pp. 175–178, Jun. 1995.

[83] T. Kavka, J. Gregor, O. Chumak, and M. Hrabovsky, “Effect of arc power and gas flow rate on properties of plasma jet under reduced pressures,” *Czechoslov. J. Phys.*, vol. 54, no. 3, pp. C753–C758, Mar. 2004.

[84] J. Jeništa, M. Bartlová, and V. Aubrecht, “Performance of water and hybrid stabilized electric arcs: the impact of dependence of radiation losses and plasma density on pressure,” *Czechoslov. J. Phys.*, vol. 56, no. 2, pp. B1224–B1230, Oct. 2006.

[85] C. Delbos, J. Fazilleau, V. Rat, J. F. Coudert, P. Fauchais, and B. Pateyron, “Phenomena Involved in Suspension Plasma Spraying Part 2: Zirconia Particle Treatment and Coating Formation,” *Plasma Chem. Plasma Process.*, vol. 26, no. 4, pp. 393–414, Apr. 2006.

[86] A. Ganvir, “Microstructure and Thermal Conductivity of Liquid Feedstock Plasma Sprayed Thermal Barrier Coatings,” University West, Trollhattan, Sweden, 2016.

[87] R. Stevens, *An introduction to zirconia: written for Magnesium Elektron.* Twickenham, Middx: Magnesium Elektron Ltd., 1986.

[88] X. Q. Cao, R. Vassen, and D. Stoever, “Ceramic materials for thermal barrier coatings,” *J. Eur. Ceram. Soc.*, vol. 24, no. 1, pp. 1–10, Jan. 2004.

[89] C. Pascual and P. Durán, “Subsolidus Phase Equilibria and Ordering in the System ZrO2-Y2O3,” *J. Am. Ceram. Soc.*, vol. 66, no. 1, pp. 23–27, Jan. 1983.

[90] C. Viazzi, J.-P. Bonino, F. Ansart, and A. Barnabé, “Structural study of metastable tetragonal YSZ powders produced via a sol–gel route,” *J. Alloys Compd.*, vol. 452, no. 2, pp. 377–383, Mar. 2008.

[91] H. G. Scott, “Phase relationships in the zirconia-yttria system,” *J. Mater. Sci.*, vol. 10, no. 9, pp. 1527–1535.

[92] W. B. Gong, C. K. Sha, D. Q. Sun, and W. Q. Wang, “Microstructures and thermal insulation capability of plasma-sprayed nanostructured ceria stabilized zirconia coatings,” *Surf. Coat. Technol.*, vol. 201, no. 6, pp. 3109–3115, Dec. 2006.

[93] K. Haberko and R. Pampuch, “Influence of Yttria content on phase composition and mechanical properties of Y-PSZ,” *Ceram. Int.*, vol. 9, no. 1, pp. 8–12, Jan. 1983.

[94] L. M. Lopato and E. R. Andrievskaya, “Reaction of Cerium Oxide with Zirconium and Yttrium Oxides at 1250°C,” *Powder Metall. Met. Ceram.*, vol. 41, no. 1–2, pp. 63–71.

[95] L. M. Lopato and E. R. Andrievskaya, “Interaction of Cerium Oxide with Hafnium, Zirconium, and Yttrium Oxides at 1500°C,” *Powder Metall. Met. Ceram.*, vol. 40, no. 7–8, pp. 405–413, Jul. 2001.

[96] G. Di Girolamo, C. Blasi, A. Brentari, and M. Schioppa, “Microstructure and thermal properties of plasma-sprayed ceramic thermal barrier coatings,” *ENEA Mag.*, no. 1–2, 2013.

[97] S. Y. Park, J. H. Kim, M. C. Kim, H. S. Song, and C. G. Park, “Microscopic observation of degradation behavior in yttria and ceria stabilized zirconia thermal barrier coatings under hot corrosion,” *Surf. Coat. Technol.*, vol. 190, no. 2–3, pp. 357–365, Jan. 2005.

[98] S. Sodeoka, M. Suzuki, T. Inoue, K. Ueno, and S. Oki, “Thermal and mechanical properties of plasma sprayed ZrO2-CeO2-Y2O3 coatings,” *Proc. 9th Natl. Therm. Spray Conf. Therm. Spray-Pract. Solut. Eng. Probl.*, pp. 295–302, 1996.

[99] P. Sokołowski, L. Pawłowski, D. Dietrich, T. Lampke, and D. Jech, “Advanced Microscopic Study of Suspension Plasma-Sprayed Zirconia Coatings with Different Microstructures,” *J. Therm. Spray Technol.*, vol. 25, no. 1–2, pp. 94–104, Sep. 2015.

[100] P. Sokołowski, L. Łatka, L. Pawłowski, A. Ambroziak, S. Kozerski, and B. Nait-Ali, “Characterization of microstructure and thermal properties of YCSZ coatings obtained by suspension plasma spraying,” *Surf. Coat. Technol.*, vol. 268, pp. 147–152, Apr. 2015.

[101] T. Wriedt, “Mie Theory: A Review,” in *The Mie Theory*, W. Hergert and T. Wriedt, Eds. Springer Berlin Heidelberg, 2012, pp. 53–71.

[102] Praxair Surface Technologies, “Model SG-100 Plasma Spray Gun Operator’s Manual,” 2011.

[103] Oerlikon Metco, “Atmospheric Plasma Spray Solutions,” 2014.

[104] A. Ravaux, “Réalisation et étude de dépôts composites multi-échelle élaborés par projection plasma pour applications tribologiques à hautes températures,” University of Limoges, Limoges.

[105] Northwest Mettech Corp, “Axial III™ Spray System - Advanced Coating Solutions.”

[106] S. Nishikawa and S. Kikuchi, “The Diffraction of Cathode Rays by Calcite,” *Proc. Imp. Acad.*, vol. 4, no. 8, pp. 475–477, 1928.

[107] T. Maitland and S. Sitzman, “Backscattering Detector and EBSD in Nanomaterials Characterization,” in *Scanning Microscopy for Nanotechnology*, W. Zhou and Z. L. Wang, Eds. Springer New York, 2006, pp. 41–75.

[108] B. K. P. Horn, “Shape from Shading: A Method for Obtaining the Shape of a Smooth Opaque Object from One View,” MIT Artificial Intelligence Laboratory, MIT/LCS/TR-79, 1970.

[109] P. Sokołowski *et al.*, "The microstructural studies of suspension plasma sprayed zirconia coatings with the use of high-energy plasma torches," *Surf. Coat. Technol.*, vol. submitted for a publication.

[110] L. C. Thomas, "Why Modulated DSC®? ; An Overview and Summary of Advantages and Disadvantages Relative to Traditional DSC," TA Instruments Technical Paper, 2005.

[111] R. A. Lombardia, "LFA for Thermal Diffusivity and Conductivity of Metals, Ceramics and Polymers," NETZSCH-Gerätebau GmbH, Branch Office Barcelona, Spain.

[112] J. A. Cape and G. W. Lehman, "Temperature and Finite Pulse-Time Effects in the Flash Method for Measuring Thermal Diffusivity," *J. Appl. Phys.*, vol. 34, no. 7, pp. 1909–1913, Jul. 1963.

[113] T. Baba and N. Taketoshi, "Analysis of Thermal Diffusion in Multi-layer Thin Films by a Response Function Method," presented at the Proceedings of Eurotherm 57, Poitiers, France, 1998, pp. 285–292.

[114] B. K. Jang, M. Yoshiya, N. Yamaguchi, and H. Matsubara, "Evaluation of thermal conductivity of zirconia coating layers deposited by EB-PVD," *J. Mater. Sci.*, vol. 39, no. 5, pp. 1823–1825.

[115] "ASTM E92-82," ASTM, Easton, Annual Book of ASTM Standards, 1.03 ASTM, 1996.

[116] G. D. Quinn, P. J. Patel, and I. Lloyd, "Effect of Loading Rate Upon Conventional Ceramic Microindentation Hardness," *J. Res. Natl. Inst. Stand. Technol.*, vol. 107, no. 3, pp. 299–306, Jun. 2002.

[117] W. C. Oliver and G. M. Pharr, "An improved technique for determining hardness and elastic modulus using load and displacement sensing indentation experiments," *J. Mater. Res.*, vol. 7, no. 6, pp. 1564–1583, Jun. 1992.

[118] R. B. King, "Elastic analysis of some punch problems for a layered medium," *Int. J. Solids Struct.*, vol. 23, no. 12, pp. 1657–1664, Jan. 1987.

[119] M. Dao, N. Chollacoop, K. J. Van Vliet, T. A. Venkatesh, and S. Suresh, "Computational modeling of the forward and reverse problems in instrumented sharp indentation," *Acta Mater.*, vol. 49, no. 19, pp. 3899–3918, Nov. 2001.

[120] J. M. Antunes, L. F. Menezes, and J. V. Fernandes, "Three-dimensional numerical simulation of Vickers indentation tests," *Int. J. Solids Struct.*, vol. 43, no. 3–4, pp. 784–806, Feb. 2006.

[121] M. Troyon and L. Huang, "Correction factor for contact area in nanoindentation measurements," *J. Mater. Res.*, vol. 20, no. 3, pp. 610–617, Mar. 2005.

[122] D. Chicot *et al.*, "Influence of tip defect and indenter shape on the mechanical properties determination by indentation of a TiB2–60%B4C ceramic composite," *Int. J. Refract. Met. Hard Mater.*, vol. 38, pp. 102–110, May 2013.

[123] S. Bec, A. Tonck, J.-M. Georges, E. Georges, and J.-L. Loubet, “Improvements in the indentation method with a surface force apparatus,” *Philos. Mag. A*, vol. 74, no. 5, pp. 1061–1072, Nov. 1996.

[124] M. Y. N’jock *et al.*, “A criterion to identify sinking-in and piling-up in indentation of materials,” *Int. J. Mech. Sci.*, vol. 90, pp. 145–150, Jan. 2015.

[125] J. C. Hay, A. Bolshakov, and G. M. Pharr, “A critical examination of the fundamental relations used in the analysis of nanoindentation data,” *J. Mater. Res.*, vol. 14, no. 6, pp. 2296–2305, Jun. 1999.

[126] P. Fauchais and A. Vardelle, “Solution and Suspension Plasma Spraying of Nanostructure Coatings,” in *Advanced Plasma Spray Applications*, H. Salimi Jazi, Ed. InTech, 2012.

[127] A. Ganvir, N. Curry, S. Björklund, N. Markocsan, and P. Nylén, “Characterization of Microstructure and Thermal Properties of YSZ Coatings Obtained by Axial Suspension Plasma Spraying (ASPS),” *J. Therm. Spray Technol.*, vol. 24, no. 7, pp. 1195–1204, Jun. 2015.

[128] J.-F. Bisson, D. Fournier, M. Poulain, O. Lavigne, and R. Mévrel, “Thermal Conductivity of Yttria–Zirconia Single Crystals, Determined with Spatially Resolved Infrared Thermography,” *J. Am. Ceram. Soc.*, vol. 83, no. 8, pp. 1993–1998, Aug. 2000.

[129] R. P. Ingel and D. L. Iii, “Lattice Parameters and Density for Y2O3-Stabilized ZrO2,” *J. Am. Ceram. Soc.*, vol. 69, no. 4, pp. 325–332, Apr. 1986.

[130] D. Taylor, “Thermal expansion data: II binary oxides with the fluorite and rutile structures MO2 and the antifluorite structure M2O,” *Trans. J. Br. Ceram. Soc.*, no. 83, 1984.

[131] P. Sokołowski *et al.*, “Thermophysical properties of zirconia coatings obtained using suspension with different plasma spray torches,” *Surf. Coat. Technol.*, vol. submitted for a publication.

[132] T. M. V. R. de Barros, R. C. Santos, A. C. Fernandes, and M. E. M. da Piedade, “Recent Advances in Thermal Analysis and CalorimetryAccuracy and precision of heat capacity measurements using a heat flux differential scanning calorimeter,” *Thermochim. Acta*, vol. 269, pp. 51–60, Dec. 1995.

[133] D. R. Askeland, P. P. Fulay, and W. J. Wright, *The Science and Engineering of Materials, SI Edition*. Cengage Learning, 2011.

[134] G. Di Girolamo, C. Blasi, A. Brentari, and M. Schioppa, “Microstructure and thermal properties of plasma-sprayed ceramic thermal barrier coatings — it,” *Energ. Ambiente E Innov.*, vol. 1–2, pp. 69–76, 2013.

[135] C. C. Berndt and H. Herman, “Anisotropic Thermal Expansion Effects in Plasma-Sprayed ZrO2-8%-Y2O3 Coatings,” in *Proceedings of the 7th Annual Conference on*

Composites and Advanced Ceramic Materials: Ceramic Engineering and Science Proceedings, W. Smothers, Ed. John Wiley & Sons, Inc., 1983, pp. 792–801.

[136] J. Ilavsky, G. G. Long, A. J. Allen, L. Leblanc, M. Prystay, and C. Moreau, "Anisotropic microstructure of plasma-sprayed deposits," *J. Therm. Spray Technol.*, vol. 8, no. 3, pp. 414–420.

[137] A. S. M. Ang and C. C. Berndt, "Investigating the anisotropic mechanical properties of plasma sprayed yttria-stabilised zirconia coatings," *Surf. Coat. Technol.*, vol. 259, Part C, pp. 551–559, Nov. 2014.

[138] W. D. C. Jr and W. D. Callister William D., *Materials Science and Engineering: An Introduction, 7th Edition Wiley Plus Set*. John Wiley & Sons, Limited, 2007.

[139] I. Sevostianov and M. Kachanov, "Anisotropic thermal conductivities of plasma-sprayed thermal barrier coatings in relation to the microstructure," *J. Therm. Spray Technol.*, vol. 9, no. 4, pp. 478–482.

[140] E. Le Bourhis, "Appendix 3: Thermal Expansion and Elasticity," in *Glass*, Wiley-VCH Verlag GmbH & Co. KGaA, 2007, pp. 271–274.

[141] C. H. Lee, H. K. Kim, H. S. Choi, and H. S. Ahn, "Phase transformation and bond coat oxidation behavior of plasma-sprayed zirconia thermal barrier coating," *Surf. Coat. Technol.*, vol. 124, no. 1, pp. 1–12, Feb. 2000.

[142] P. J. Huang, J. J. Swab, P. J. Patel, and W. S. Chu, "Evaluation of CeSZ Thermal Barrier Coatings for Diesels - Thermal Spray Society," presented at the International Thermal Spray Conference: Surface Engineering via Applied Research, 2000, pp. 1179–1183.

[143] D. R. Clarke and S. R. Phillpot, "Thermal barrier coating materials," *Mater. Today*, vol. 8, no. 6, pp. 22–29, Jun. 2005.

[144] B. D. Sartwell and R. McPherson, "A review of microstructure and properties of plasma sprayed ceramic coatings," *Surf. Coat. Technol.*, vol. 39, pp. 173–181, Dec. 1989.

[145] D. D. Hass, A. J. Slifka, and H. N. G. Wadley, "Low thermal conductivity vapor deposited zirconia microstructures," *Acta Mater.*, vol. 49, no. 6, pp. 973–983, Apr. 2001.

[146] C. B. Carter and M. G. Norton, *Ceramic Materials: Science and Engineering*. Springer Science & Business Media, 2007.

[147] L. Wang *et al.*, "Influence of pores on the thermal insulation behavior of thermal barrier coatings prepared by atmospheric plasma spray," *Mater. Des.*, vol. 32, no. 1, pp. 36–47, Jan. 2011.

[148] P. Carpio *et al.*, "Correlation of thermal conductivity of suspension plasma sprayed yttria stabilized zirconia coatings with some microstructural effects," *Mater. Lett.*, vol. 107, pp. 370–373, Sep. 2013.

[149] L. Łatka, D. Chicot, A. Cattini, L. Pawłowski, and A. Ambroziak, “Modeling of elastic modulus and hardness determination by indentation of porous yttria stabilized zirconia coatings,” *Surf. Coat. Technol.*, vol. 220, pp. 131–139, Apr. 2013.

[150] R. S. Lima, A. Kucuk, and C. C. Berndt, “Bimodal distribution of mechanical properties on plasma sprayed nanostructured partially stabilized zirconia,” *Mater. Sci. Eng. A*, vol. 327, no. 2, pp. 224–232, Apr. 2002.

APPENDIX

Paper 1 - published in Surface and Coatings Technology

Paper 2 - published in Surface and Coatings Technology

Paper 3 - published in Journal of Thermal Spray Technology

Paper 4 - under review in Surface and Coatings Technology

Paper 5 - under review in Surface and Coatings Technology

PAPER 1

Characterization of microstructure and thermal properties of YCSZ coatings obtained by suspension plasma spraying

Paweł Sokołowski
(Wrocław University of Technology, Wrocław, Poland; University of Limoges, Limonges, France)

Leszek Łatka, Andrzej Ambroziak, Stefan Kozerski
(Wrocław University of Technology, Wrocław, Poland)

Lech Pawłowski, Benoit Nait-Ali
(University of Limoges, Limonges, France)

Published: Surface and Coatings Technology,
Volume 268, April 2015, pp. 147–152

Printed with permission

Surface & Coatings Technology 268 (2015) 147–152

http://dx.doi.org/10.1016/j.surfcoat.2014.10.006

CHARACTERIZATION OF MICROSTRUCTURE AND THERMAL PROPERTIES OF YCSZ COATINGS OBTAINED BY SUSPENSION PLASMA SPRAYING

P. Sokołowski [a,b], L. Łatka [a], L. Pawłowski [b], A. Ambroziak [a], S. Kozerski [a], B. Nait-Ali

[a] *Wrocław University of Technology, Wyb. Wyspiańskiego 27, Pl-50371 Wroclaw, Poland*
[b] *SPCTS, University of Limoges, 12 Rue Atlantis, UMR CNRS 7315, F-87068 Limoges, France*

The paper describes the procedure of determination of thermal properties (thermal diffusivity and thermal conductivity) of yttria/ceria stabilized zirconia coatings. The coatings were deposited by suspension plasma spraying method using SG-100 torch. The commercial powder with a chemical composition ZrO2 + 24 wt.% CeO2 + 2.5 wt.% Y2O3 was used and coatings were sprayed onto stainless steel substrates. The suspensions consisted of zirconia powder, water, ethanol and small addition of dispersant. The design of spray experiments included the following variable process parameters: (i) spray distance; and (ii) torch scan linear speed. The microstructure of coatings was determined by scanning electron microscopy (SEM) and X-ray diffraction (XRD). The phase composition and the crystallite size of coatings were estimated by Rietveld method. The different methods were used to find out the thermal properties values up to 573 K. Firstly, thermal diffusivity of YCSZ coatings was determined by using a commercial setup and the obtained results were used to calculate the values of thermal conductivity. Then, to check the validity of the measurements and calculations, the simulations of laser flash experiment were made using COMSOL Multiphysics software. The least square method enabled to find the optimized value of thermal conductivity. Finally, the use of another setup enabled to find out the thermal transport properties in the temperature up to 873 K.

Keywords: *suspension plasma spraying, zirconia coatings, thermal barrier coatings, thermal diffusivity, thermal conductivity*

1. Introduction

Thermal barrier coatings (TBC) are important elements of gas turbine technology applied mainly in aviation industry [1,2]. Two different reasons of their application can be distinguished. First is the possibility of extending lifetime at the same operating temperatures. The second one is the rise of the operating temperature resulting in better turbine efficiency.

The turbine blades work in demanding conditions and increasing of temperature inside gas turbine causes further increasing of requirements for TBC's materials [3]. Consequently, the research of new deposition technologies and new materials has been continuing [4].

A part of them is research of new material for overlay coatings which includes the rare earth zirconates having also additions of elements like gadolinium, lanthanum, ytterbium or cerium [5–7]. On the other hand, new technologies have been developed to produce the coatings with improved parameters. One of these technologies is suspension plasma spraying (SPS). The SPS process may enable modifying the microstructure of coatings, e.g. thickness, porosity, morphology, etc. [8–10].

The presented experiments are devoted to yttria and ceria stabilized zirconia (YCSZ) coatings produced by SPS method. The previous studies on this material showed that YCSZ can work in higher temperatures and is characterized by higher resistance to high temperature corrosion than YSZ [11–13]. The present study focuses on the thermal transport properties of YCSZ coatings.

2. Experimental material

The commercial powder Metco 205NS (YCSZ) prepared by spray drying and heat treatment was used to produce coatings by SPS method. The initial volume-surface mean diameter of this powder was equal to d_{vs} = 38 μm. The powder was crushed mechanically to decrease the particles sizes. The mechanical ball milling was realized with the use of moliNEx system (NEZTSCH, Germany), the zirconia balls used as grinding medium and ethanol as cooling medium. Finally the powders were sieved prior to suspension formulation.

After milling process resulting powder had a mean size equal to dvs = 3.91 μm and monomodal sizes' distribution. The distribution was measured with the use of laser diffraction technique (Partica LA-950V2, Horiba). Moreover, SEM micrographs of the milled powder (Fig. 1) showed finely grained particles, confirming the granulometry tests.

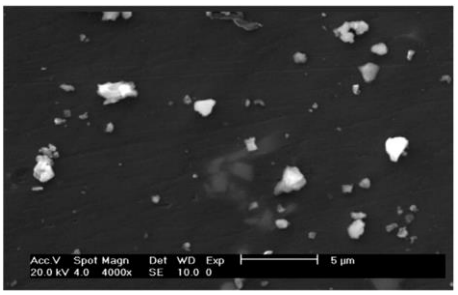

Fig. 1. SEM image (secondary electrons) of Metco 205NS powder after milling process.

The suspension used to spray experiments consisted of 20 wt.% of milled zirconia powder with 40 wt.% of distillated water and 40 wt.% of ethanol. The dispersant agent, phosphate ester (Beycostat C213, CECA), was added to prevent particles agglomeration. The zeta potential measured using Zetasizer Nano ZS (Malvern, England) of these suspensions was equal to $\zeta = -6.2$ mV. The value is relatively low.

3. Experimental methods

3.1. Spray process

Plasma spraying process was performed using a SG-100 torch (Praxair S.T., Indianapolis, In, USA) installed on a 5-axis IRB-6 robot of ABB (Zürich, Switzerland). The working gas mixture of Ar + H2 (45+5 slpm) and electric power of 40kWwere used. The experiments were made using 2k (k=2) full factorial design, where the variable parameters were robot scan speed (from 300 mm/s and 500 mm/s) and spray distance (from 40 mm and 60 mm). The suspension feed rate was of about 39 g/min. The suspension was introduced via internal injection mode using a continuous-stream injector (with an internal diameter of 0.5 mm) installed inside the anode-nozzle of the plasma torch. The suspension spraying was performed in order to obtain coatings with a thickness up to 70 μm. The operational spray parameters are collected in Table 1.

Stainless steel 304L cylinders (diameter 25mmand thickness about 8 mm) were used as the substrate material. They were sand blasted using corundum grit (F36 according to the FEPA standards) under a pressure of 0.04 MPa and cleaned in ethanol before spray process. Furthermore the thickness of substrates was controlled before and after spraying to ensure the same deposition conditions for all samples and finally of thermal transport properties measurements also.

3.2. Coating characterization

The basic characterization of coatings, including the determination of their thicknesses, was made with the use of the light microscopy (Nikon Eclipse LV100). The procedure of thickness measurement was as follows—for each sample 3 regions were chosen and in each region 5 local thicknesses measurements were made. Finally, the average value for each region and the average value for these 3 regions were calculated.

Table 1. Variable spray parameters and the values of thickness and porosity of coatings

Run	Scan velocity [mm/s]	Spray distance [mm]	Range of maximal surface temperature [°C]	Thickness [μm]	Thickness, standard deviation [μm]	Porosity [%]
1	300	40	668–736	53	2.9	21.5
2	500	40	509–643	90	8.1	18.7
3	400	50	453–603	78	1.6	20.3
4	300	60	422–563	101	2.7	15.1
5	500	60	393–474	88	1.1	20.6

The morphology of obtained ceramic coatings YCSZ was characterized with the scanning electron microscope Philips 515 (Eindhoven, Netherlands) using a secondary electron detector. The micrographs were made on the top of surfaces and on the cross-sections of the coatings. To estimate the porosity of coatings SEM images were taken at 10,000 × magnification. Then, the images were edited using ImageJ free software for the porosity calculations.

The phase composition was estimated by X-ray diffraction analysis using a D8-Bruker apparatus (Bruker AXS, Karlsruhe, Germany) with Cu-Kα1 radiation. The measurements were made in the wide range of 2θ angles from 15° to 120°. The phases were identified using Diffrac+Eva software. The quantitative analysis of coating composition was made with the use of Rietveld method. In the same way the lattice parameters of coatings were determined.

3.3. Thermal diffusivity measurements

Thermal diffusivity of YCSZ coatings was determined by using laser flash method. It is one of the most popular methods that enable thermal diffusivity characterization, where the bottom side (the substrate) of the sample is heated by energy pulse and the change of the temperature versus measurement time is collected by the detector on the top of the sample (the TBC coating). The sample is coated few times with the thin graphite layers prior to measurements to increase signal-noise ratio and provide good quality of analysis.

During the research two devices LFA 447 and LFA 427 both of Netzsch, Germany, were used. The LFA 447 setup, equipped in a xenon lamp allowed analyzing the coatings up to 573 K. The use of LFA 427, which used the laser as the heat source enabled obtaining the values of thermal diffusivity in higher temperatures. Because the measurements were made with the use of the coatings attached directly to the substrates (without the intermediate layer), the measurements in this case were made up to 873 K to avoid the effect of the difference of linear expansion coefficients. The chosen range of the temperature did not require the use of shielding gas or vacuum—the measurements were made in the air in both cases. The two measuring systems required also two different sample shapes, for LFA 447 it was necessary to prepare 25 mm discs and for LFA 427 10 mm squares. Moreover the setups have installed the same kind of infrared detector—InSb. Finally the 2-layer numerical model was developed to determine thermal diffusivity of the coatings. The model included corrections resulting from: (i) heat losses; (ii) pulse duration, and (iii) contact resistance between substrate and zirconia coating.

3.4. Thermal conductivity calculations

To calculate thermal conductivity of sprayed coatings, it was necessary to determine the values of: (i) thickness, (ii) density, (iii) specific heat, (iv) thermal dilatation, and (v) thermal diffusivity for each layer of material.

The thickness of coatings was found in using observation of the cross-section with the optical microscope. The density values were corrected for porosity basing on following expression:

$$\rho = \rho_0 \cdot (1 - P) \quad (1)$$

where: ρ_0 is the density of tetragonal phase ZrO_2, equal to 6050 kg/m^3 and P is porosity.

Specific heat for alloys or composites was calculated from Kopp-Neumann law, which has the following form:

$$c_p = \sum_{i=1}^{n} (c_{pi} \cdot f_i) \quad (2)$$

where:

c_{pi} – specific heat of compound forming alloy;
f_i – atomic fraction of molecule

Finally, thermal diffusivity values were found from the LFA measurements. More details about the description of thermal conductivity calculations and material data are reported elsewhere [14].

3.5. Numerical analysis of thermal transport properties

In order to confirm the experimental data obtained from thermal diffusivity and conductivity determinations the authors used the numerical simulation. The simulation was made with the use of Comsol Multiphysics software and the "Heat transfer" mode. The "axial symmetry" numerical model concerned a sample composed of 2 layers, including substrate and coating and one additional virtual layer corresponding to TCR (thermal contact resistance) layer (Fig. 2). The model simulated the experiment of laser flash leading to the determination of thermal diffusivity. The temperature – time response, being a result of simulation, was collected in a point on the top of coating surface.

The most important conditions, which were used to simulate the conditions of real measurements made by laser flash method, were divided in the following stages:

- heating of samples – heat flux was imposed on the back face of sample (side of substrate) ad was determined by equation (3):

$$-n \cdot (-k\nabla T) = q_0 + h(T_{ext} - T) \quad (3)$$

where n is normal vector of the boundary pointing out from the domain, $-k\nabla T$ is conductive flux vector, q_0 is heat flux from external source (xenon lamp), h is heat transfer coefficient, T is currently temperature and finally T_{ext} is an external temperature. In addition, it was also assumed that the energy pulse of xenon lamp was rectangular with regard to time and of relatively short duration compared to the half-rise time during the measurements of thermal diffusivity (pulse time $t_p << t_{0.5}$). In this experiment t_p was equal to 0.18 ms.

- cooling of samples – was supposed to result from natural convection. The heat exchange coefficient equations for horizontal samples, cooled in air, can be calculated from e.g. the well-known *Newton's Law for Cooling*.

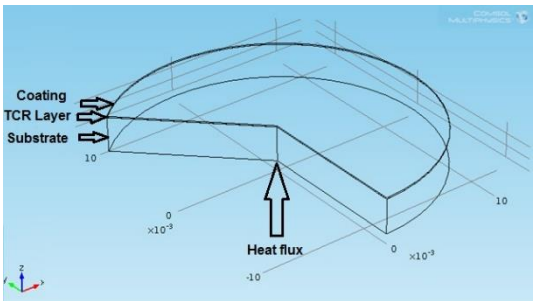

Fig. 2. Schematic view of numerical model used in simulation in Comsol Multiphysics.

Finally, the least square method was used to fit the temperature – time curves obtained from simulation, to the experimental ones. The latter were the voltage evolutions collected by InSb infrared detector. When the best fitting was sought by the method of least squares the variable parameter was thermal conductivity of coating. The thermal conductivity values were change for each coating in the Comsol software as long as the highest correlation coefficients were found. The differences between experimental and theoretical values were calculated for all experimental points of diffusivity device in the range up to 10 t50 for each sample.

4. Results

4.1. Microstructure description

The values of average coatings thicknesses, which were obtained using optical microscope, are collected in Table 1. The values were in the range from 53μm to 101μm. The image analysis showed that the coatings were quite porous (porosity of about 20%). On the micrographs which were made on the top of surfaces and on the cross-sections of coatings by scanning electron microscopy, it was possible to observe typical for SPS method *two-zones* microstructure (Fig.3). It consisted of more or less molten large lamellas and small sintered particles of powder. Furthermore, the coatings were characterized by small number of microcracks. The interface between substrate and coatings did not show any discontinuities and other defects.

X-ray diffraction diagrams showed that the major phase is tetragonal ZrO_2 with a small quantity of monoclinic phase. The use of Rietveld method enabled determining the amount of these phases precisely and find the lattice parameters of coatings (Table 2). The results confirmed that in the coatings microstructure consisted of only small amount of monoclinic phase (about 5%) and the main phase is tetragonal ZrO_2 (about 95%).

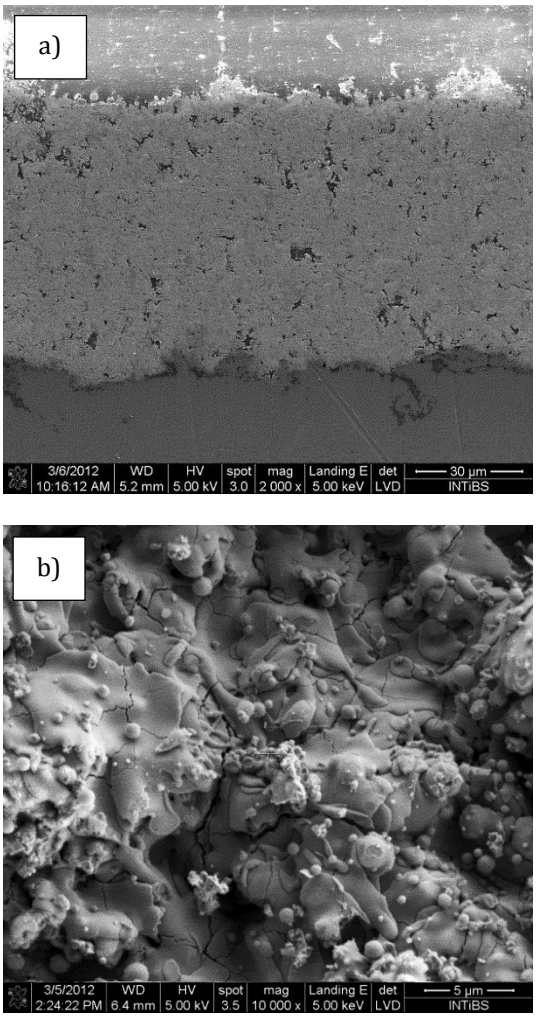

Fig. 3. SEM micrographs (secondary electrons) of cross-section (a) and surface (b) of YCSZ coatings sprayed in run no.3.

4.2. Thermal diffusivity of coatings

The results of thermal diffusivity for YCSZ coatings made using the LFA 447 set up are shown in Fig. 4a. Thermal diffusivity was in the range of 0.23 to $0.49 \cdot 10^{-6}$ [m^2/s] depending on the spray run. As it can be seen, the samples sprayed in the run no. 2 have the greatest diffusivity, whereas the samples sprayed in the run no. 1 have the lowest one. The values of thermal diffusivity were related to the porosity of coatings – if the porosity was higher the thermal diffusivity was lower. Only the samples sprayed in run no. 4 did not follow this correlation.

The results of measurements carried out in higher temperature with the use of LFA 427 equipment are shown in Fig.4b. The correlation between porosity and thermal diffusivity were the same as in low temperature measurements but the values of thermal diffusivity for all coatings were generally a little bit higher. The lowest value was $0.25 \cdot 10^{-6}$ [m^2/s] for RT and the samples sprayed in run no. 1 and the highest reached $0.47 \cdot 10^{-6}$[m^2/s] at higher temperatures for sample sprayed in run no. 2.

4.3. Thermal conductivity of coatings

With the use of thermal diffusivity measurements the essential parameter - thermal conductivities of coatings were calculated. The values of thermal conductivity obtained for the temperature up to 573K were in the range from 0.46 to 1.07 W/(m·K) (Fig.5a). While the calculations performed for the LFA 427 (up to 873K) measurements showed the values in the range from 0.51 to 1.22 W/(m·K) (Fig.5b). However when comparing the values from both devices only up to 573K the differences were even smaller. For higher temperatures the calculated values of thermal conductivity increased faster because there was a greater change of other important thermal parameters like specific heat, thermal dilatation etc. But it was possible to see the same trend like in thermal diffusivity diagrams – the values strongly depended on the porosity of the coatings.

4.4. Verification of thermal transport properties measurements

The numerical verification of thermal transport properties of YCSZ coatings were made based on the LFA 447 measurements. The comparison of experimental and numerical signal curves is showed on Fig. 6. We can observe that the experimental and numerical signal curves are very similar, the differences can be observed only in the part of curve related to the cooling of samples. Values of thermal conductivity of YCSZ coatings with values of the best fitting the experimental and simulated results are presented in Table 3. The values of correlation coefficients (R^2) determined using least squares method were very high, in the range from 0.9777 to 0.9920.

Table 2. Results of quantitative analysis and lattice parameters using Rietveld refinement

Sample	Tetragonal zirconia			Monoclinic zirconia		
	content, wt.%	*a*,Å	*c*,Å	content, wt.%	*a*,*b*,Å	*c*,Å;*γ*, °
YCSZ-1	95.0	3.6406	5.2172	5.0	5.161 5.246	5.284 99.04
YCSZ-2	96.1	3.6403	5.2168	3.9	5.150 5.256	5.281 99.06
YCSZ-3	95.9	3.6382	5.2159	4.1	5.155 5.209	5.333 99.14
YCSZ-4	95.4	3.6404	5.2176	4.6	5.172 5.251	5.280 99.03
YCSZ-5	95.9	3.6402	5.2166	4.1	5.162 5.261	5.279 99.06

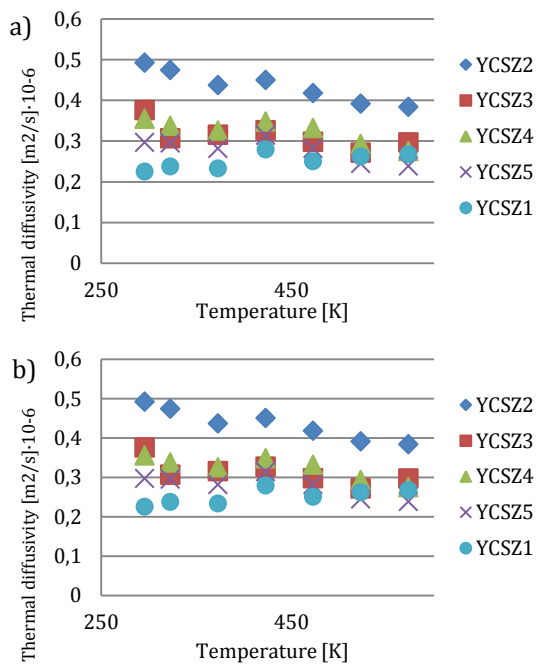

Fig. 4. Thermal diffusivity of coatings determined with the use of a) LFA 447 and b) LFA 427 set ups.

5. Discussion

Ceramic thermal barrier coatings are currently produced using physical vapor deposition method mainly with high energetic electron beam (EB-PVD) or atmospheric plasma spraying (APS) [15]. This paper shows that SPS method is also very interesting process for TBC applications offering different type of coatings' microstructure and improved parameters in comparison to conventional processes.

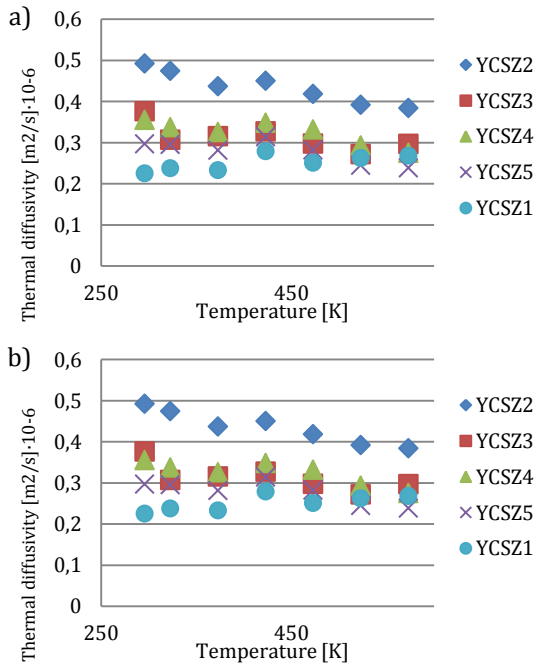

Fig. 5. Thermal conductivity values for YCSZ coatings determined based onto measurements of thermal diffusivity made using LFA 447 (a) and LFA 427 (b).

The microstructural investigations showed that the coatings were characterized by finely grained microstructure with some small lamella and a small amount of microcracks. Similar way of suspension plasma sprayed coatings microstructure formation was observed by e.g. Kozerski et al. [16]. The interface between substrate and coating did not show any discontinuities and other defects. Furthermore, the SPS method allowed producing coatings with different amount of pores, which can also be controlled by spray parameters [14, 17].

The studies devoted to thermal transport properties proved that YCSZ can be an good alternative for typical YSZ coatings. The coatings were characterized by comparable values of thermal diffusivity and conductivity as the YSZ coatings produced also with SPS method with similar operational parameters [14], when Cao et al. reported that the zirconia coatings with the addition of CeO_2 can be characterized by even better thermal transport properties values than well-known yttria stabilized zirconia coatings [5]. For the most porous YCSZ coatings the values of thermal conductivity were lower than 0.75 W/(m·K) up to 873K. The small values of thermal conductivity are the result of the micro-porosity observed in the coatings. Raghavan et al. analyzed the relationship between the porosity and TBC properties and confirmed the influence of micro-porosity on thermal conductivity values [18]. A small difference of thermal diffusivity values measured with two commercial set-ups can be explained by different energy sources installed in the devices. The heat was generated by xenon lamp in LFA 427 system and LFA 447 used the laser pulse. The laser system was much more advance and provided more stable measurements. Moreover the different LFA systems required different shapes of the samples. The dimensions of samples were very carefully checked but it could have a small influence on the measurement also. Finally the numerical analysis made using *Comsol software* showed that despite the use of some material data taken from literature the measurements were consistent. Furthermore using numerical methods it was possible quickly simulate real phenomena with acceptable accuracy.

Table 3. Thermal conductivity of YCSZ with values of the best fitting the experimental results and simulated ones

Temperature *T* [K]	Thermal conductivity [W/m·K] Correlation coefficient R^2				
	YCSZ-1	*YCSZ-2*	*YCSZ-3*	*YCSZ-4*	*YCSZ-5*
298	0,50	0,95	0,75	0,85	0,60
R^2	0,9896	0,9868	0,9878	0,9838	0,9878
323	0,50	0,95	0,70	0,80	0,65
R^2	0,9907	*0,9870*	0,9891	0,9853	0,9900
373	0,50	0,95	0,70	0,85	0,65
R^2	0,9919	*0,9847*	0,9859	0,9811	0,9880
423	0,55	1,00	0,75	0,90	0,65
R^2	0,9920	*0,9831*	0,9847	0,9795	0,9889
473	0,55	1,00	0,70	0,90	0,70
R^2	0,9906	*0,9809*	0,9839	0,9777	0,9851
523	0,60	0,95	0,70	0,80	0,65
R^2	0,9914	*0,9835*	0,9861	0,9794	0,9857
573	0,60	0,95	0,70	0,80	0,65
R^2	0,9909	*0,9856*	0,9870	0,9815	0,9870

6. Conclusions

The studies were conducted to examine the microstructure and thermal transport properties of relatively new kind of zirconia coatings (yttria/ceria stabilized zirconia) deposited by suspension plasma spraying method.

The research started from preparation and examination of spraying precursor. The solid phase in the suspension with a main size of 3.9 μm was obtained by milling coarse Metco 205NS powder. The liquid phase in the suspension was a mixture of distilled water and ethanol, in 1:1 ratio. The plasma spray parameters were optimized by varying the spray distance and torch scan linear speed.

Thanks to use of various spraying parameters it was possible to achieve microstructure of coatings with different porosity. The porosity of the samples was found to be in the range of 15–21.5%. The microstructural investigations allowed finding typical for SPS coatings' manufacturing method *two-zones* microstructure with a small amount of microcracks and without any other defects.

The essential properties of thermal barrier coatings, so thermal diffusivity and thermal conductivity was measured and analyzed with the use of commercial NanoFlash systems, in two temperature ranges, from RT up to 573K and from RT up to 873K. The coatings were characterized by very low thermal conductivity values (even 0.5W/(m·K)). Furthermore the numerical analysis was prepared using *Comsol Multiphysics* software to confirm the thermal transport properties measurements.

However, the YCSZ coatings have to be characterized using thermomechanical tests like thermal shock resistance or hot corrosion resistance. These kinds of studies will be carried out in the next part of authors' researches.

References

[1] R.A. Miller, Current status of thermal barrier coatings – an overview, Surf. Coat. Technol., 30 (1987), 1.

[2] N.P. Padture, M. Gell, and E.H. Jordan, Thermal Barrier Coatings for Gas-Turbine Engine. Applications, Science 296 (2002), 280.

[3] T. Roberts, The structure and stability of high temperature intermetallic phases for application within coating systems, PhD Thesis, Cranfield University, November 2009

[4] U. Schulz, Some recent trends in research and technology of advanced thermal barrier coatings, Aerosp. Sci. Technol., 7 (2003), 73.

[5] X.Q. Cao, R. Vassen, and D. Stöver , Ceramic materials for thermal barrier coatings, J. Eur. Ceram. Soc., 24 (2004), 1.

[6] J. Yu, H. Zhaoa, S. Tao, X. Zhou, C. Ding, Thermal conductivity of plasma sprayed $Sm_2Zr_2O_7$ coating, J. Eur. Ceram. Soc., 30 (2010), 799.

[7] A. Rauf, Q. Yu, L. Jin, C. Zhou,Microstructure and thermal properties of nanostructured lanthana-doped yttria-stabilized zirconia thermal barrier coatings by air plasma spraying, Scr. Mater., 66 (2012), 109.

[8] E. H. Jordan, L. Xie, M. Gell, N. P. Padture, B. Cetegen, A. Ozturk, X. Ma, J. Roth, T. D. Xiao, P. E. C. Bryant, Superior thermal barrier coatings using solution precursor plasma spray, J. Therm. Spray Technol.,13 (2004), 57.

[9] A. Bacciochini, E. Brousse, J. Ilavsky, G. Montavon, A. Denoirjean, S. Valette, P. Fauchais., Quantification of void networks ofas-sprayed and annealed nanostructured yttria-stabilized zirconia (YSZ) deposits manufactured by suspension plasma spraying, Surf. Coat. Technol., 202 (2010), 683.

[10] S. Kozerski, L. Łatka, L. Pawlowski, F. Cernuschi, F. Petit, C. Pierlot, H. Podlesak, J. P. Laval, Preliminary study on suspension plasma sprayed ZrO_2+ 8 wt.% Y_2O_3 coatings, J. Eur. Ceram. Soc., 31 (2011), 2089.

[11] W.A. Kaysser, M. Peters, K. Fritscher, U. Schulz, Processing, Characterization and Testing of EB-PVD Thermal Barrier Coatings. In: AGARD Report 823, Thermal Barrier Coatings, NATO Neuilly-sur-Seine, Paris, AGARD, 1998.

[12] S. Y. Park, J. H. Kim, M. C. Kim, H. S. Song, C. G. Park, Microscopic observation of degradation behavior in yttria and ceria stabilized zirconia thermal barrier coatings under hot corrosion, Sur. Coat. Technol., 190 (2005), 357.

[13] G. Di Girolamo, C. Blasi, A. Brentari, M. Schioppa, Microstructure and thermal properties of plasma-sprayed ceramic thermal barrier coatings, Raport of Italian National Agency for New technologies: Energry and Sustainable Economic Development, 2013.

[14] L. Latka, L. Pawlowski, S. Valette, B. Pateyron, J.P. Lecompte, A. Denoirjean, A. Cattini, R. Kumar, Thermal diffusivity and conductivity of yttria stabilized zirconia coatings obtained by suspension plasma spraying, Sur. Coat. Technol., 208 (2012), 87.

[15] H. Xu and H. Guo (editors), Thermal barrier coatings, Edited by, Woodhead Publishing Limited, 2011.

[16] S. Kozerski, L. Pawlowski, R. Jaworski, F. Roudet, F. Petit, Two zones microstructure of suspension plasma sprayed hydroxyapatite coatings, Sur. Coat. Technol., 204 (2010), 1380.

[17] P. Fauchais, G. Montavon, Latest developments in suspension and liquid precursor thermal spraying, J. Therm. Spray Technol., 19 (2010), 226.

[18] S. Raghavan, H. Wang, R. B. Dinwiddie, W. D. Porter, M. J. Mayo, The effect of grain size, porosity and yttria content on the thermal conductivity of nanocrystalline zirconia, , Scr. Mater. 39 (1998) 1119.

PAPER 2

The key process parameters influencing formation of columnar microstructure in suspension plasma sprayed zirconia coatings

Paweł Sokołowski

(Wrocław University of Technology, Wrocław, Poland; University of Limoges, Limonges, France)

Stefan Kozerski, Andrzej Ambroziak

(Wrocław University of Technology, Wrocław, Poland)

Lech Pawłowski

(University of Limoges, Limonges, France)

Published: Surface and Coatings Technology,

Volume 260, September 2014, pp. 97–106

Printed with permission

Surface & Coatings Technology 260 (2014) 97–106

http://dx.doi.org/10.1016/j.surfcoat.2014.08.078

THE KEY PROCESS PARAMETERS INFLUENCING FORMATION OF COLUMNAR MICROSTRUCTURE IN SUSPENSION PLASMA SPRAYED ZIRCONIA COATINGS

Paweł Sokołowski [a,b], Stefan Kozerski [b], Lech Pawłowski [a], Andrzej Ambroziak [b]

[a] *SPCTS, UMR CNRS 7315, University of Limoges, 12, rue Atlantis, 87068 Limoges, France*
[b] *Faculty of Mechanics, Wrocław University of Technology, ul. Łukasiewicza 5, 50-371Wrocław, Poland*

The paper discusses the screening of experimental variables leading to formation of a columnar microstructure in suspension plasma sprayed zirconia coatings. These variables tested in 12 experimental runs included: (i) 2 types of zirconia powder; (ii) 4 concentration of solids in suspensions; (iii) 4 substrate preparationmethods; and (iv) 2 plasma spray setups. Two different, commercially available, powders were used to formulate the suspensions. Yttria and ceria stabilized zirconia of composition ZrO2 + 24 wt.% CeO2 + 2.5 wt.% Y2O3 (YCSZ) was milled the decrease the particles sizes. The yttria stabilized zirconia of composition ZrO2 + 14 wt.% Y2O3 (14YSZ) was used as received. The coatings were deposited on 304L stainless steel substrates which had the surface prepared by: (i) grid blasting; (ii) grinding; (iii) turning; and (iv) laser treatment. The 3D topographies of substrates' surfaces were characterized and their roughnesses were measured. The suspensions were plasma sprayed using the following plasma torches: SG-100 of Praixair and Triplex of Sulzer-Metco. The microstructure of powders and coatings was analyzed by optical microscopy, scanning electron microscopy (SEM) and field emission scanning electron microscopy (FE-SEM) as well as by X-ray diffraction. The columnar microstructure was formed in coatings sprayed with both plasma setups sprayed using finer 14YSZ powder suspensions. The substrate surface preparation as well as low concentration of solids in suspension promoted their formation. Rietveld method was applied to determine the quantity of different phases in the structure of coatings and to calculate the lattice parameters. The YCSZ coatings crystallized in mainly tetragonal phasewith a small content of monoclinic phase. The 14YSZ crystallized in cubic phase. Finally, the thermal diffusivity of coatings was characterized up to 523 K with the use of laser flash method and thermal conductivities of coatings were determined. The conductivities were in the range from 0.6 to 1.1 W/(mK) depending on temperature for YCSZ and 14YSZ coatings.

Keywords: *thermal barrier coatings, suspension plasma spraying, yttria stabilized zirconia, ceria stabilized zirconia, columnar microstructure of coatings*

1. Introduction

The microstructure of suspension plasma sprayed coatings results from the particularities of process such as e.g. liquid feedstock which includes small, nano- or submicrometric solids and, on the other hand, from a very short spray distance. Typically, the coatings contain large lamellas formed from the solids agglomerated in-flight and small grains which remained at the periphery of plasma jet and form a two-zone microstructure [1]. The small grains may sinter due to the heat flux coming from plasma torch [2]. The coatings contain also usually a network of fine pores which may reduce their thermal conductivity [3–5]. Low thermal conductivity is an important advantage in the application of stabilized zirconia as thermal barrier coatings (TBC). The TBCs must however withstand many thermal shocks in service and the best adapted microstructure to achieve this specification is a columnar one in which crystal grains grow up perpendicularly to the interface. Such microstructure is formed in the films condensed from saturated vapors e.g. in the process called electron beam physical vapor deposition (EBPVD) which is described in many references [6–8]. An important drawback of EBPVD processes is a capital cost of coatings' equipment being many times greater than that of suspension plasma spraying (SPS) equipment. This difference in the capital cost was one of the motivations to realize the research on the columnar structure in stabilized zirconia coatings using SPS processes. The studies initiated a few years ago focused on: (i) relationship between suspension formulation and the microstructure of YSZ coatings obtained by SPS [9]; (ii) the effect of rare-earth additives on thermal transport properties of zirconia coatings [10]; and more recently (iii), the formation of columnar structure in suspension plasma sprayed Mg–Al–spinel coatings [11]. The present study focuses on screening of key process parameters favorable to form the columnar microstructure. Consequently, the SPS zirconia coatings were suspension sprayed using different initial powders including yttria and ceria as zirconia main stabilizers with two different plasma spray setups. Moreover, the suspensions were formulated using 4 different solid phase concentrations ranging from 2.5 to 20 wt.% of solid. Finally, the coatings were sprayed onto substrates having surfaces of different morphology. Basing onto the analysis of obtained results, a simplified description of the mechanism of columns formation was made.

2. Experimental methods

2.1. Suspension formulation

The first of used powderwasMetco 205NS having composition ZrO_2+24wt.% CeO_2+2.5 wt.% Y_2O_3 (YCSZ). The granulometric tests of the powder use the laser diffraction setup of type LA-950V2 of Horiba (Kyoto, Japan). The volumemean diameters of the initial coarse powder were equal to d_{v50} = 39.6 μm. The morphology of the powder, characterized using SEM type Philips XL30 (Eindhoven Netherlands), is presented in Fig. 1a. The initial powder was milled up using the MoliNEx setup of Netzsch (Selb, Germany) using zirconia balls having a 2mmdiameter, ethanol as cooling medium and Beycostat C123 as dispersant. The mean diameter of powder particles decreased down to d_{v50} = 696 nm and the milled powder morphology is shown in Fig. 1b. The second used powder was yttria stabilized zirconia powder, ZrO_2+14 wt.% Y_2O_3 (14YSZ) of Tosoh (Tokyo, Japan). The mean diameter was equal to d_{v50} = 398 nm and its morphology observed using FE-SEM of JSM-7400F of Jeol (Tokyo, Japan) is shown in Fig. 2. The XRD phase analysis made using Bruker D8 Advance setup (Billerica, MA, USA) enabled to find out that 14YSZ powder crystallized as yttrium zirconium oxide identified using file no. 01-078-5501 of the JCPDS database. The phase composition of YCSZ powder enabled to find three different phases identified with the help of the JCPDS database:

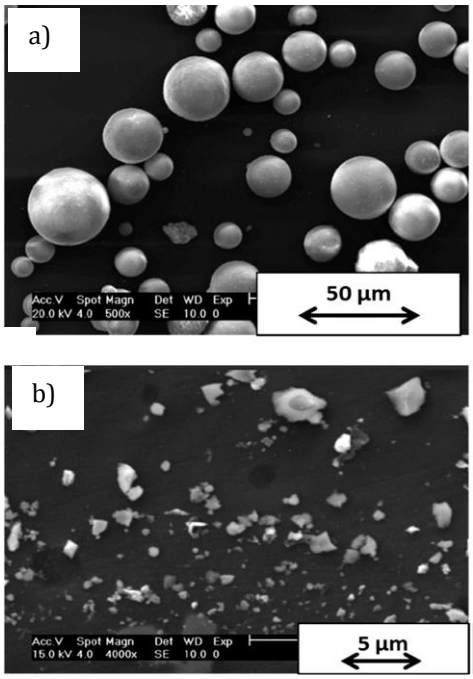

Fig. 1. SEM micrographs (secondary electrons) of 205NS Metco powder: (a)—initial powder; (b)—powder after milling (b).

- tetragonal phase of cerium yttrium zirconium oxide identified using file no. 04-013-9723;
- monoclinic phase of ZrO2–Baddeleyite identified using file no. 00-037-1484;
- cubic phase of cerium yttrium oxide identified using file no. 04-016-4629.

The suspensions of water and ethanol in ratio 1:1 with different content of solid phase were prepared, in wt.%: 2.5; 5; 10; and 20. The dispersant agent was added to suspension to prevent the agglomeration and sedimentation. The zeta potential measurements enabled to find the values of ζ = 82.5 mV for the suspension with 14YSZ powder (the suspension had pH = 4.8) and ζ = −12.9 mV for YCSZ powder suspension (pH = 6.8).

2.2. Substrate preparation

Stainless steel 304L discs of diameter 25 and thicknesses of 10 or of 2 mm were used as substrates. The substrates' surfaces were prepared using: (i) grid blasting; (ii) grinding; (iii) turning; and (iv) laser treatment. White corundum with the particles size ranging between 500 and 600 μm was used for grid blasting of substrates. Grinding was performed with the use of SiC abrasive paper (grit size 320). The laser treatment was realized using Duetto picosecond laser of Time-Bandwidth Products (Zürich, Switzerland). The substrates were cleaned up in the ultrasonic bath of ethanol prior to spraying. The 3D views of substrates topographies were made confocal microscope type Lext OLS4000 of OLYMPUS (Tokyo, Japan) and are presented in Fig. 3. Finally, the roughness of the substrate surfaces was measured with the use of the profilometer type FormTalysurf 120L of Rank Taylor Hobson (Leicester, England) and the results were as follows:

- grid-blasting: Ra=5.50 μm, Rz = 32.4 μm;
- grinding: Ra=0.07 μm, Rz=0.6 μm;
- laser treatment: Ra=3.6 μm, Rz=17.6 μm;
- turning: Ra=0.54 μm, Rz=3.06 μm.

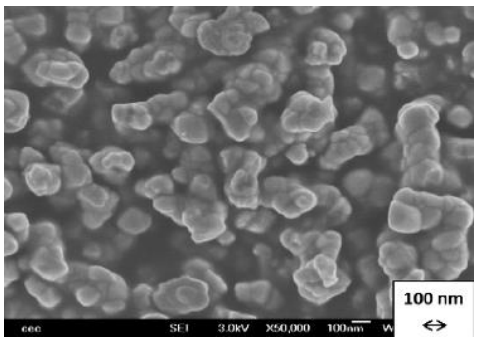

Fig. 2. FE-SEM micrograph (secondary electrons) of Tosoh powder.

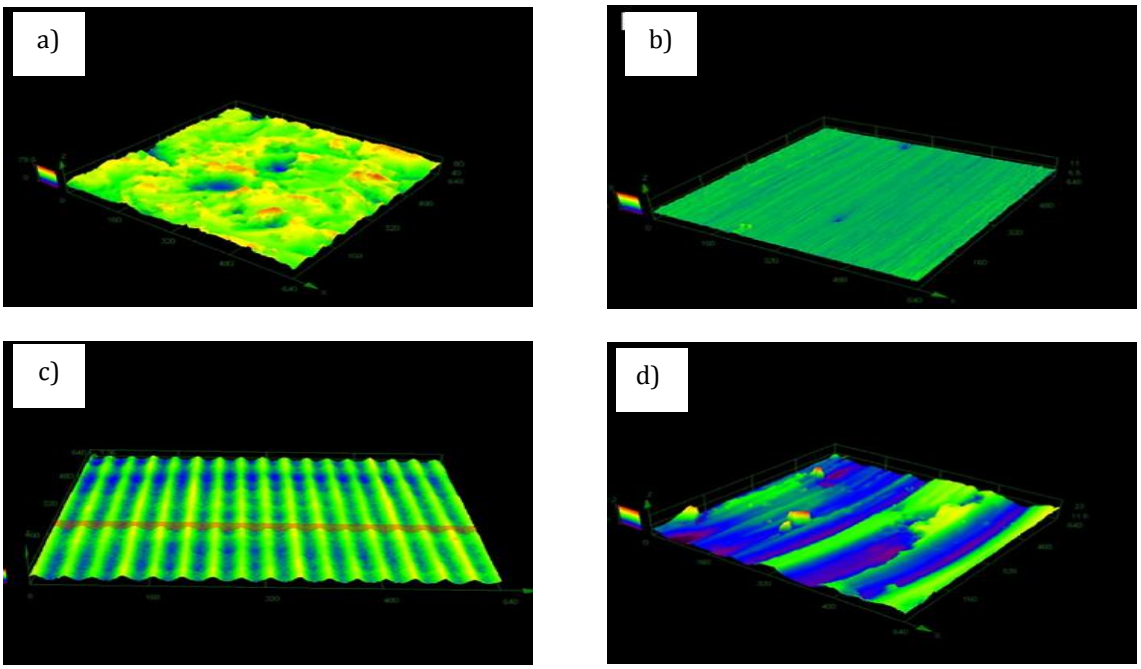

Fig. 3. Topography of substrates used to deposit coatings: (a)—grid-blasted; (b)—grinded, (c)—laser treated; (d)—turned.

2.3. Plasma spraying

The coatings were plasma sprayed using two spray installations. The first one included the torch SG-100 of Praxair (Indianapolis, IN, USA) with an internal injector, mounted on a 5-axis robot as described in details elsewhere [3]. The second installation used was equipped in three cathode Triplex torch of SulzerMetco (Wohlen, Switzerland). The temperature of coatings at spraying was controlled using a pyrometer IN 5 Plus of LumaSense Technologies (Santa Clara, CA, USA). The operational spray parameters are collected in Table 1. The spray experiments were designed with the use of the following variables: (i) powder type; (ii) concentration of solid in suspension; and (iii) substrates' surface preparation. The detailed design is shown in Table 2.

2.4. Coating characterizations

The thickness of the coatings was estimated using metallographic cross-sections of samples observed with optical microscope Eclipse LV100 of Nikon (Tokyo, Japan). The mean thickness of the coatings was found from 18 measurements in different regions of the coatings. The procedure of this measurement was as follows: 3 regions were chosen for and in each sample and 6 local thicknesses were measured in each region. Finally, a mean value was calculated. The porosity was estimated with the use of software Image J. The morphology of the coating surface and sections were observed using SEM XL 30 and the phase analysis was made using Bruker D8 diffractometer using CuKα1 radiation in the range of 2θ angles from 15° to 120°. The phases were identified using Diffrac + Eva software. The quantitative analysis of coatings was carried out by the Rietveld method with the use of Topas V4.1 software.

Table 1. Operational spray parameters.

Process parameters	Torch SG-100 of Praxair	Torch Triplex of Sulzer-Metco
Electric power, kW	40	45
Working gases composition	Ar + H_2	Ar
Working gases flow rate, slpm	45 + 5	70
Spray distance, mm	40	70
Torch speed velocity, mm/s	500	1000
Number of scans	Depends on experimental run. After each scan the spraying was interrupted until temperature dropped down to 40 °C	Depends on experimental run. When coating's temperature reached 500 °C the spraying was interrupted until temperature dropped down to 150 °C
Distance between the neighboring torch passes, mm	3	10
Suspension injector type	Nozzle inside the torch	Nozzle outside the torch
Nozzle injector internal diameter, mm	0.50	0.15
Static pressure in suspension container, MPa	0.05	1.3

Table 2. Design of spray experiments and thickness and porosity of coatings.

Run no.	Powder material	Sample description	Concentration of solid in suspension [wt.%]	Type of plasma torch	Substrate preparation	Thickness, average; standard deviation, µm	Porosity average and standard deviation, %
1	14YSZ	ST21	2.5	SG-100	Grit-blasting		
	14YSZ	ST22	2.5	SG-100	Laser treatment	66;4	21.4;2.7
	14YSZ	ST23	2.5	SG-100	Grinding		
2	14YSZ	ST51	5	SG-100	Grit-blasting		
	14YSZ	ST52	5	SG-100	Laser treatment	83;9	18.3;2.3
	14YSZ	ST53	5	SG-100	Grinding		
3	14YSZ	ST101	10	SG-100	Grit-blasting		
	14YSZ	ST102	10	SG-100	Laser treatment	116;14	15.2;1.4
	14YSZ	ST103	10	SG-100	Grinding		
4	YCSZ	SC21	2.5	SG-100	Grit-blasting		
	YCSZ	SC22	2.5	SG-100	Turned	55;3	19.0;2.2
	YCSZ	SC23	2.5	SG-100	Grinding		
5	YCSZ	SC51	5	SG-100	Grit-blasting		
	YCSZ	SC52	5	SG-100	Turned	105;4	15.5;1.5
	YCSZ	SC53	5	SG-100	Grinding		
6	YCSZ	SC101	10	SG-100	Grit-blasting		
	YCSZ	SC102	10	SG-100	Turned	96;7	13.2;0.9
	YCSZ	SC103	10	SG-100	Grinding		
7	14YSZ	TT51	5	Triplex	Grit-blasting		
	14YSZ	TT52	5	Triplex	Laser treatment	80;5	16.0;1.0
	14YSZ	TT53	5	Triplex	Grinding		
8	14YSZ	TT101	10	Triplex	Grit-blasting		
	14YSZ	TT102	10	Triplex	Laser treatment	77;2	13.1;0.8
	14YSZ	TT103	10	Triplex	Grinding		
9	14YSZ	TT201	20	Triplex	Grit-blasting		
	14YSZ	TT202	20	Triplex	Laser treatment	91;2	11.8;0.9
	14YSZ	TT203	20	Triplex	Grinding		
10	YCSZ	TC51	5	Triplex	Grit-blasting		
	YCSZ	TC52	5	Triplex	Turned	74;2	18.0;2.2
	YCSZ	TC53	5	Triplex	Grinded		
11	YCSZ	TC101	10	Triplex	Grit-blasting		
	YCSZ	TC102	10	Triplex	Turned	91;2	15.9;1.6
	YCSZ	TC103	10	Triplex	Grinded		
12	YCSZ	TC201	20	Triplex	Grit-blasting		
	YCSZ	TC202	20	Triplex	Turned	148;7	12.4;1.2
	YCSZ	TC203	20	Triplex	Grinded		

Finally, thermal diffusivity of 14YSZ and YCSZ coatings was measured by laser flash technique using setup LFA 447 of Netzsch (Selb, Germany). Both sides of samples were coated with graphite prior to the measurements in order to provide better absorption and emission of radiative energy. The measurements were made in the temperature range between room temperature (RT) to 523 K. The measurements were made with the use of the coatings sprayed on the grit-blasted substrates and the 2-layer model was developed to determine thermal diffusivity of the coatings. The corrections resulting from: (i) heat losses; (ii) pulse duration, and (iii) contact resistance were included in the model used for calculations. To calculate the thermal diffusivity of ceramic coatings, it was necessary to know the values of their thicknesses as well as the thermal diffusivity values of the steel. Such material data as density in RT, as well as thermal dilatation and specific heat in all temperatures used in measurements had to be known for substrate (stainless steel 304L) and ceramic coatings. The porosity of ceramic coatings, P, was used to correct the density following the expression:

$$\rho_{300} = \rho_0 \cdot (1 - P) \quad (1)$$

where ρ_0 is density in RT being equal to 6050 kg/m^3 for dense tetragonal phase of ZrO_2 and to 5830 kg/m^3 for dense cubic phase of ZrO_2 [12,13]. The specific heat, c_p(T), and thermal dilatation values, $\Delta L/L\ (T)$, were taken from literature separately for tetragonal and cubic ZrO_2 [14–16], which were the main phases in YSZ and YCSZ

coatings (according to XRD analysis of phase composition of coatings). The values of specific heat for alloys or composites were recalculated from Kopp-Neumann law. Finally, the data for calculating thermal diffusivity of coatings are collected in Table 3. The values of specific heat, thermal dilatation and thermal diffusivity of stainless steel substrate were taken from literature [17–19]. Thermal diffusivity of stainless steel 304L was also measured directly using our experimental setup. Knowing thermal diffusivity values, *a(T)*, thermal conductivity, *λ(T)* was calculated following the equation:

$$\lambda(T) = a(T)c_p(T)\frac{\rho_{300}}{1 + 3 \cdot \frac{\Delta L}{L}(T)} \qquad (2)$$

Table 3. Thermal dilatation and specific heat values used in calculations of thermal diffusivity of 14YSZ and YCSZ coatings [14–16].

Temperature [K]	14YSZ		YCSZ	
	Specific heat c_p [J/(kgK)]	Thermal dilatation ΔL/L[-]	Specific heat c_p [J/(kgK)]	Thermal dilatation ΔL/L[-]
298	515	8.5267×10^{-5}	427	3.4031×10^{-5}
323	540	2.5646×10^{-4}	441	2.0583×10^{-4}
373	580	6.8840×10^{-4}	465	5.5722×10^{-4}
423	610	1.1262×10^{-3}	485	9.1804×10^{-4}
473	630	1.6598×10^{-3}	501	1.2873×10^{-3}
523	655	2.0206×10^{-3}	514	1.6640×10^{-3}

3. Results

3.1. Microstructural characterization

The phase analysis in the coatings sprayed using 14YSZ powder indicates only cubic zirconia (Fig. 4a). This phase remains unchanged at coating deposition. The YCSZ coatings were modified at spraying and the cubic phase present in initial powder was not detected in obtained coatings (Fig. 4b). The Rietveld analysis shows the lattice parameters of phases obtained in all experimental runs (Table 4).

3.1.1. Morphology of coating suspension formulated using 14YSZ powder

3.1.1.1. Torch SG-100. The coatings had a two-zone-microstructure with large molten lamellas and fine unmolten particles. The morphologies of coatings sprayed using suspension having a concentration of 2.5wt.% of solid are shown in Fig. 5. The coatings sprayed have a columnar microstructure for all type of substrate surface preparation even including polished substrate (see Fig. 5c). The columnar structure is visible also for the suspension of greater i.e. 5 wt.% concentration (Fig. 6); however, the columns are much less visible while grinded substrate was used. Finally, the increase of suspension concentration up to 10 wt.% resulted in formation of the columnar microstructure only in coatings sprayed onto the laser treated surface (Fig. 7 b). The porosity of coatings decreases from about 21% at lowest suspension concentration of 2.5 wt.% down to about 15% at the suspension concentration of 10 wt.% (see Table 2).

3.1.1.2. Torch Triplex. The coatings sprayed using suspension having 10 wt.% of solid phase were generally dense and the columnar microstructure is visible only for the laser treated substrate (Fig. 8b). The coatings sprayed using 20 wt.% suspension did not indicate any columnar structure. The porosity of the coatings is lower than that sprayed using SG-100 torch and decreases from about 16% to about 12% with increasing suspension concentration.

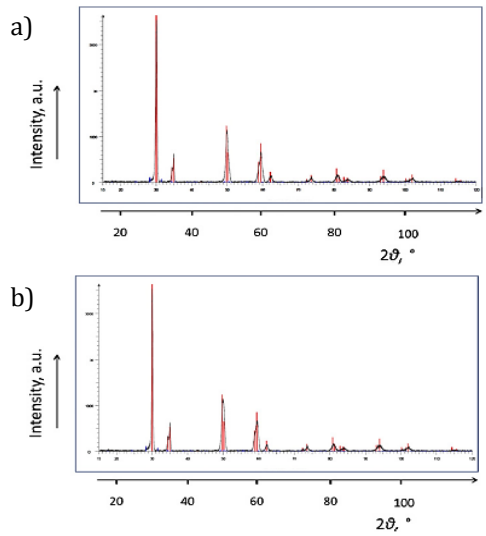

Fig. 4. X-ray diffraction diagram of typical coating sprayed using: (a) sample TT102 obtained using 14YSZ powder suspension containing cubic zirconia identified using 00-030-1468 1484 file of the JCPDS data base; (b) sample TC202 obtained using YCSZ powder containing suspension tetragonal and monoclinic zirconia identified using 04-013-9723 and 04-004-4339 files of the JCPDS data base.

3.1.2. Morphology of coating suspension formulated using YCSZ powder

The application of suspension with the use of coarse YCSZ powder resulted in coatings which do not have a columnar structure independent on suspension concentration and torch type. The examples of microstructures obtained with torch SG-100 and Triplex are shown in Figs. 9 and 10 respectively. The increase in suspension concentration results in the increase in coating density and in fewer defects and fewer pores (see Fig. 10). The coating porosity is lower for coatings sprayed using suspension formulated using YCSZ powder than that formulated using 14YSZ one and for that sprayed using Triplex torch than that sprayed using SG-100 one (see Table 2). Consequently, the lowest porosity of about 12% was reached for coatings sprayed using suspension of concentration 20 wt.%, YCSZ powder and Triplex torch.

Table 4. Rietveld analyses of phase's content and lattice parameters in coatings sprayed in all experimental runs

YCSZ coatings							14YSZ coatings		
Sample	Tetragonal phase			Monoclinic phase			Sample	Cubic phase	
	Content, wt.%	a, Å	c, Å	Content, wt.%	a, b, Å	c, Å; γ, °		Content, wt.%	a, Å
SC22	97.45	3.6401	5.2133	2.55	5.1570 5.2601	5.2590 99.165	ST22	100	5.1404
SC52	97.10	3.6406	5.2160	2.90	5.1532 5.2719	5.2551 99.064	ST52	100	5.1409
SC102	97.30	3.6382	5.2097	2.70	5.1535 5.2545	5.2574 99.090	ST102	100	5.1410
TC52	92.62	3.6351	5.2167	7.38	5.1884 5.2783	5.2077 98.799	TT52	100	5.1413
TC102	96.02	3.6358	5.2146	3.98	5.1867 5.2983	5.2033 98.834	TT102	100	5.1427
TC202	94.54	3.6353	5.2161	5.46	5.1932 5.2993	5.2046 98.818	TT202	100	5.1434

3.2. Thermal conductivity of sprayed coatings

The thermal conductivity of coatings sprayed using suspension formulated using fine 14YSZ powder is shown in Fig. 11a. The conductivity is lower for the coatings sprayed using SG-100 torch than that sprayed using Triplex one and decreases with concentration of solid in suspension. Similar observations can be made for the coatings made using suspension formulated using YCSZ powder. Finally, the thermal conductivity of coatings sprayed using suspension including 14YSZ powder is slightly lower than that sprayed using YCSZ powder suspension for similar suspension concentrations.

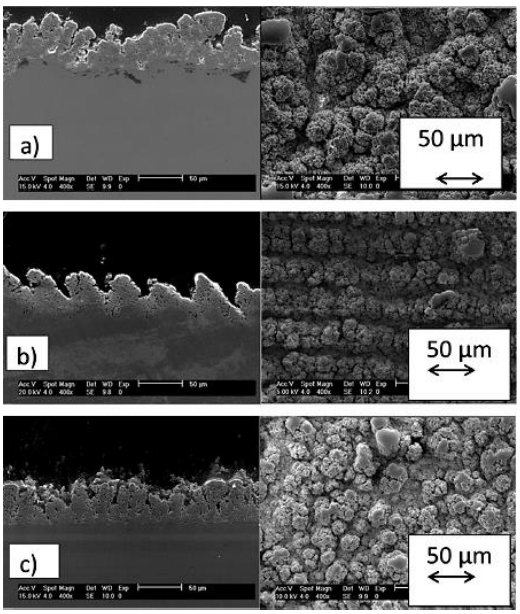

Fig. 5. SEM (secondary electrons) micrographs of cross-sections (left side) and surfaces (right side) of coatings suspension including 2.5 wt.% of 14YSZ solid phase sprayed using SG-100 torch onto substrates prepared by: (a)—sand blasting, sample ST21; (b)—laser treatment, sample ST22; (c)—grinding, sample ST23.

4. Discussion

The thermal conductivity of tested samples was determined to be in the range of 0.6 to 1.1 W/(mK). The lowest conductivity values were obtained for the samples sprayed using well stabilized suspension having small concentration of 14YSZ powder using SG-100 torch obtained in the spray run ST22 (Fig. 11a). Similar conductivity values were obtained for YCSZ sprayed using Triplex torch in spray run TC52 (see Fig. 11b). The conductivity values are comparable to those obtained for the suspension sprayed 8YSZ described elsewhere [3]. The low values of conductivity results from: (i) high porosity of coatings and, in particular, from the presence of fine pores; (ii) bad contacts between the grains; and (iii) from the presence of small, unmolten grains being sintered with the other and discussed elsewhere [1,2].

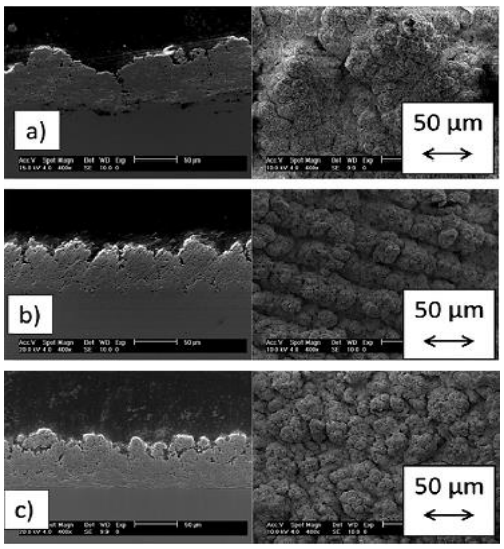

Fig. 6. SEM (secondary electrons) micrographs of cross-sections (left side) and surface (right side) of coatings suspension including 5 wt.% of 14YSZ solid phase sprayed using SG-100 torch onto substrates prepared by: (a)—sand blasting, sample ST51; (b)—laser treatment, sample ST52; (c)—grinding, sample ST53.

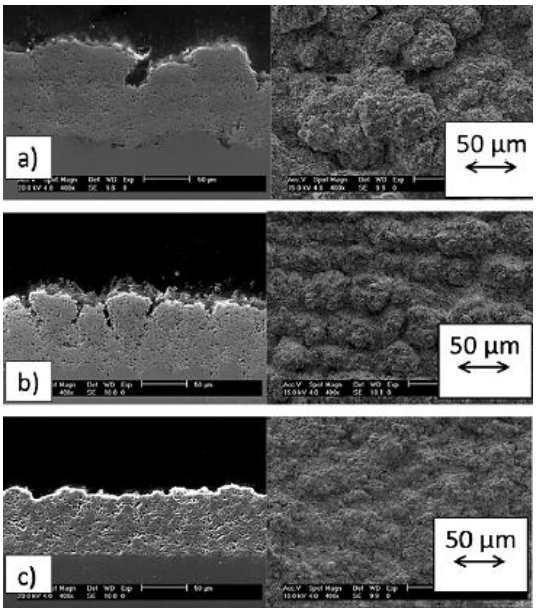

Fig. 7. SEM (secondary electrons) micrographs of cross-section (left side) and surfaces (right side) of coatings suspension including 10 wt.% of 14YSZ solid phase sprayed using SG-100 torch onto substrates prepared by: (a)—sand blasting, sample ST101; (b)—laser treatment, sample ST102; (c)—grinding, sample ST103.

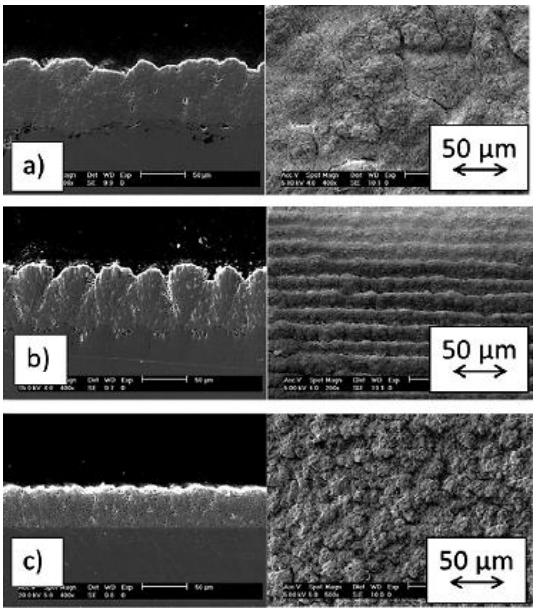

Fig. 8. SEM (secondary electrons) micrographs of cross-section (left side) and surfaces (right side) of coatings suspension including 10 wt.% of 14YSZ solid phase sprayed using Triplex torch onto substrates prepared by: (a)—sand blasting, sample TT101; (b)—laser treatment, sample TT102; (c)—grinding, sample TT103.

The columnar microstructure was formed in the samples: ST22, ST23, ST52, ST102, and TT102. All the samples were sprayed using 14YSZ powder being a finer one. Consequently, only fine powder formulated suspension enabled formation of the columnar microstructure independent of the torch used. The substrate surface preparations methods resulting in the formation of the columnar microstructure are as follows:

- laser treated substrate coated with the help of the SG-100 torch (ST22 and ST52 shown in Figs. 5b and 6b respectively) and with the help of the Triplex torch (sample TT102 shown in Fig. 8b);
- machined substrate sprayed using 14YSZ suspension with the SG-100 torch (sample ST102 shown in Fig. 7b);
- grinded substrate coated with the help of the SG-100 torch (sample 23 shown in Fig. 5c).

Finally, low concentration of fine solids in suspension promoted the formation of the columnar microstructure. The greatest concentration among the tested ones resulting in such microstructure was 10 wt.% of solids suspension sprayed onto the laser treated substrate. The obtained experimental results enable a design of a simplified a mechanism of formation of the columnar microstructure.

The fine solid particles arriving on the substrate may adhere to the substrate or move radially parallel to the substrate suspended in a working gas. The behavior of particles results from the equilibrium of two forces shown in Fig. 12, i.e.: (i) the force acting on a particle which can be assumed to be drag force,[1] F_D, by the gas moving radially; and (ii) force of adhesion, FA, keeping the particle attached to the substrate. The drag force can be expressed under simplified assumption that particles moves in Stokes regime as follows:

$$F_D = 3\eta_g \pi d_p (v_g - vp) \qquad (3)$$

in which η_g is the viscosity of gas acting on particle, d_p is the particle diameter, vg is the velocity of gas equal to v_g = 600 m/s [2] and v_p is the particle velocity. Supposing that the velocity of the particle is about a half of the velocity of gas, v_p=0.5v_g, what corresponds roughly to the calculations made for fine hydroxyapatite particles in the numerical simulation presented elsewhere [20], and that the viscosity of working gas composed of plasma forming gases and products of suspension liquids evaporation is equal to η_g= 6× 10^{-5} kg/(ms), the drag force for different particles diameters is represented in Fig. 13. The adhesion force, F_A, can be approximated by a critical force measured at scratch test, i.e. the force applied when indenter reaches the coating's interface with the substrate. The values of critical force were measured to be in the range of 9 to more than 30 N in suspension plasma sprayed 8YSZ coatings [3] and 10 to 17 N for suspension plasma sprayed TiO_2 coatings [21]. The very rough comparison of two forces acting on small particles shows that generally $F_A \geq F_D$ what means that the particles adhere to the substrate at impact. The explication of columnar microstructure formation may be given by the presence of small unmolten particles which remain on the periphery of the jet and arrive on the substrate with much lower velocity than the particles which has the trajectory in the middle of the jet (Fig. 14).

[1] A more realistic model should take into account thermophoresis force [20].

[2] The value corresponds to the working gas temperature of 3000 K calculated in the jet axis at the spray distance 40mm and at the power input to the gas of 30 kWbeing lower than that used in the present study. More details are shown in the study [20].

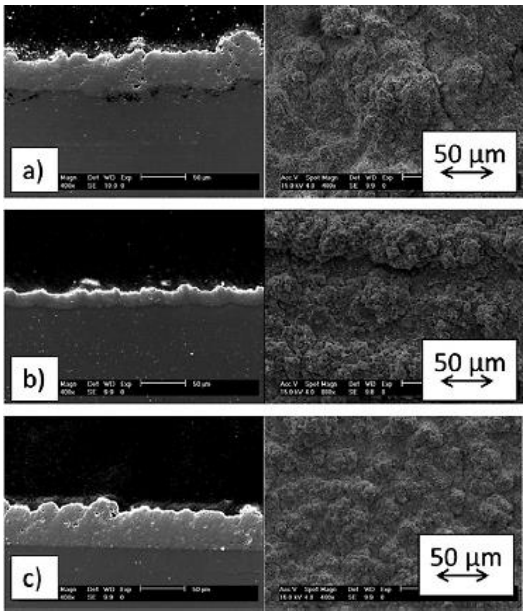

Fig. 9. SEM (secondary electrons) micrographs of cross-section (left side) and surfaces (right side) of coatings suspension including 2.5 wt.% of YCSZ solid phase sprayed using SG-100 torch onto substrates prepared by: (a)—sand blasting, sample SC21; (b)—machining, sample SC22; (c)—grinding, sample SC23.

These slow particles may be easily accelerated by the working gas moving radially with regard to the torch axis, parallel to the substrate. For these particles $F_D > F_A$ and they move parallel to the growing coating surface until they meet an irregularity on this surface to which they may adhere. Such irregularities were formed at substrate preparation by laser treatment, sand blasting or machining. The following torch passes bring new charge of particles contributing in forming the islands growing as the columns as shown in Fig. 15. However, a question remains how was it possible to form a columnar structure (sample ST23 shown in Fig. 5 c) on a grinded substrate having a smooth surface shown in Fig. 3b? The answer results from the superposition of many process parameters of the spray processes synthesized graphically in Fig. 16. The suspension used to spray this sample was having a small concentration of solids (2.5 wt.%) and was well stabilized (zeta potential, ζ = 82.5 mV) i.e. the fine solids were well separated. Moreover the SG-100 setup was having a large diameter of injector (ID = 0.5 mm) and the droplets issuing from the injector were large too. These two factors may be synthesized by showing a large droplet with a few solids inside as shows it the right side of Fig. 16. The fine solids in large droplets were distant and some of them remain separated after evaporation of liquid from the droplet. These got molten and accelerated in the plasma jet and impacted on the substrate and adhered to it. The mechanism of adhesion of these small splats could have been their mechanical anchorage to the nano-irregularities of the smooth substrate. In that way the irregularities on the grinded surface became greater and greater. Finally, their size was great enough to start the mechanism of columnar growth shown in Fig. 15.

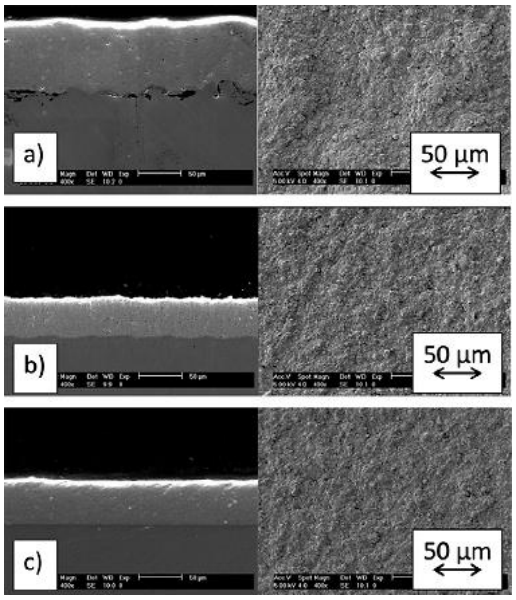

Fig. 10. SEM (secondary electrons) micrographs of cross-section (left side) and surfaces (right side) of coatings suspension including 10 wt.% of YCSZ solid phase sprayed using Triplex torch onto substrates prepared by: (a)—sand blasting, sample TC101; (b)—machining, sample TC102; (c)—grinding, sample TC103.

5. Conclusion

The screening of some suspension plasma spraying process parameters influencing the formation of the columnar microstructure in zirconia coatings was carried out. The following experimental variables were used in 12 experimental runs: (i) powders in suspensions and their concentration; (ii), substrate preparation methods; and (iii) plasma spray equipment. The powders included yttria and ceria stabilized zirconia of composition ZrO2 + 24 wt.% CeO2 + 2.5 wt.% Y2O3 and ZrO2 + 14 wt.% Y2O3. The coatings were deposited on the 304L substrates having the surface prepared by: (i) grid blasting; (ii) grinding; (iii) turning; and (iv) laser treatment. The plasma torches used were: SG-100 and Triplex. The microstructure of the coatings was analyzed using scanning electron microscopy (SEM) and (FE-SEM) as well as the X-ray diffraction. Rietveld method was applied and enabled to determine that the 14YSZ samples crystallized as tetragonal zirconia and the YCSZ included major tetragonal phase and monoclinic zirconia as the minor one. Finally, the thermal conductivity of coatings was characterized up to 523 K with the use of laser flash method and it was found to be in the range of 0.6 to 1.1 W/(mK). The columnar microstructure was formed in the samples with both spray setups. Such microstructure was possible to form using fine 14YSZ powder suspension depending on the suspension concentration. Lower concentration promoted, generally, the formation of columns. The columnar microstructure when using coarse YCSZ powder was formed only with the laser treated substrate surface. The other substrate surface preparations methods resulting in the formation of the columnar microstructure were machining and turning. Surprisingly, it was found out that the spraying of such low concentration suspension as 2.5 wt.% of fine 14YSZ solids on a smooth, grinded substrate resulted in the formation of columnar microstructure.

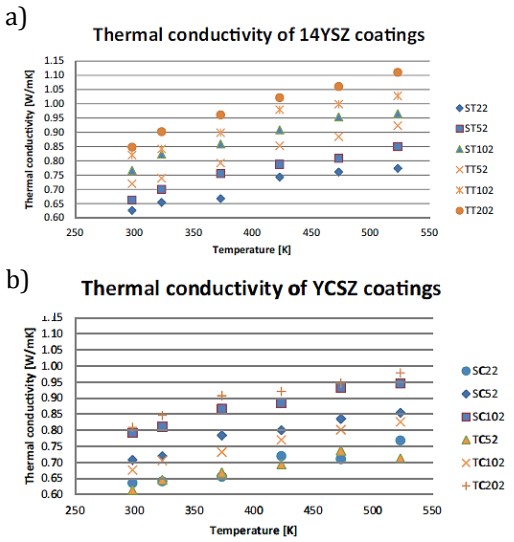

Fig. 11. Thermal conductivity of coatings sprayed using suspensions formulated with: (a)—14YSZ powder; (b)—YCSZ powder.

The simple model explaining the formation of the columnar microstructure was described. The future studies will concern the creation of more precise numerical model of interaction of fine solids with the working gas moving parallel to the substrate. The measurements of thermal conductivity at higher temperatures, thermal shock resistance and mechanical properties of the samples sprayed using optimized spray parameters should be also carried out.

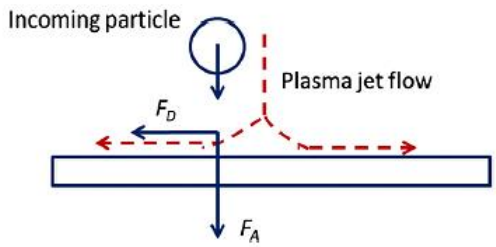

Fig. 12. Schematic representation of forces acting on a particles arriving on substrate or on previously deposited coating.

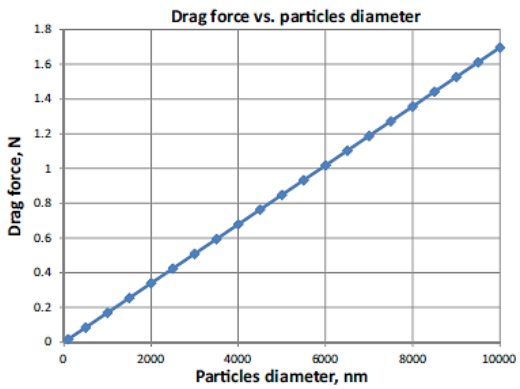

Fig. 13. Drag force vs. particles diameter for a simplified model developed following the data from our previous study [20].

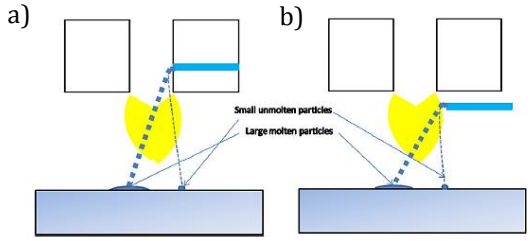

Fig. 14. Possible trajectories of droplets/particles during plasma spraying with the use of: (a) internal, injection (SG-100 torch); (b) external injection (Triplex torch).

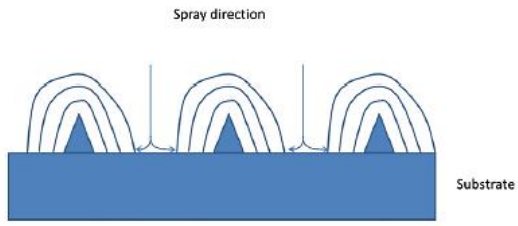

Fig. 15. Mechanism of the columnar structure formation at suspension spraying on the roughened substrate having surface with many irregularities (inspired by [9]).

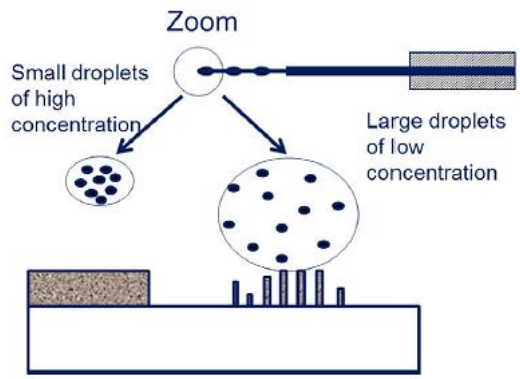

Fig. 16. Mechanism of the columnar structure formation in sample ST23 having a grinded surface as shown in Fig. 5c. The large droplet on the right side of the figure corresponds to the low concentration of a stable suspension (having great zeta potential).

Acknowledgments

The help of David Jech,MSc Eng from Brno University of Technology in spray experiments and in coatings' characterization is thankfully acknowledged. Dr. Alain Denoirjean of SPCTS helped with the very useful discussions. The paper reviewers helped considerably in eliminating the paper's imperfections. The bilateral Polonium program financed by French government covered the travels fees of the researchers from France and from Poland realized during this study. Drs Richard Mayet and Jean-Paul Laval helped in X-ray diffraction investigations.

References

[1] S. Kozerski, L. Pawłowski, R. Jaworski, F. Roudet, F. Petit, Surf. Coat. Technol. 204 (2010) 1380–1387.

[2] L. Łatka, S.B. Goryachev, S. Kozerski, L. Pawłowski, Materials 3 (7) (2010) 3845–3866.

[3] S. Kozerski, L. Łatka, L. Pawłowski, F. Cernuschi, F. Petit, C. Pierlot, H. Podlesak, J.-P. Laval, J. Eur. Ceram. Soc. 31 (2011) 2089–2098.
[4] K. VanEvery, M.J.M. Krane, R.W. Trice,W. Porter, H.Wang, M. Besser, D. Sordeletz, J. Ilavsky, J. Almer, Int. J. Appl. Ceram. Technol. 8 (6) (2011) 1382–1392.
[5] L. Łatka, A. Cattini, L. Pawłowski, S. Valette, B. Pateyron, J.-P. Lecompte, R. Kumar, A. Denoirjean, Surf. Coat. Technol. 208 (2012) 87–91.
[6] D.R. Clarke, M. Oechsner, N.P. Padture, MRS Bull. 37 (10) (2012) 891–897.
[7] R. Vaßen, M.O. Jarligo, T. Steinke, D.E. Mack, D. Stöver, Surf. Coat. Technol. 205 (2010) 938–942.
[8] R. Krishnamurthy, D.J. Srolovitz, Acta Mater. 57 (2009) 1035–1048.
[9] K. VanEvery,M.J.M. Krane, R.W. Trice, H.Wang, W. Porter,M. Besser, D. Sordelet, Jan Ilavsky, J. Almer, J. Therm. Spray Technol. 20 (4) (2011) 814–828.
[10] S. Gong, K. VanEvery, H. Wang, R.W. Trice, J. Eur. Ceram. Soc. 34 (2014) 1243–1253.
[11] N. Schlegel, S. Ebert, G. Mauer, R. Vaßen, ITSC 2014, Barcelona, Spain, DVS-Berichte, volume 302, ISBN: 978-3-87155-574-9, May 21-23, 2014, pp. 113–118.
[12] F. Cernuschi, P.G. Bison, S. Marinetti, P. Scardi, Acta Mater. 56 (16) (2008) 4477–4488.
[13] K.E. Wilkes, R.B. Dinwiddie, R.S. Graves, Thermal Conductivity 23, CRC Press, 1996.
[14] L.B. Pankratz, Thermodynamic Properties of Elements and Oxides, U. S. Bureau of Mines Bulletin, 1982. 672.
[15] Y. Takeda, H.Y. Tu, H. Sakaki, N. Imanishi, O. Yamamoto,M.B. Philips, N.M. Sommes, J. Electrochem. Soc. 144 (1997) 2810–2816.
[16] H. Miyazaki, J. Therm. Anal. Calorim. 98 (2009) 343–346.
[17] R.J. Jenkins, R.W. Westover, The Thermal Diffusivity of Stainless Steel Over the Temperature Range 20 C to 100 C, USNRDL TR-484, 1960. 1–13.
[18] A.P. Miller, A. Cezairliyan, High Temp. - High Press. 23 (1991) 205–214.
[19] W. Poessnecker, U. Gross, High Temp. - High Press. 34 (1) (2002) 1–8.
[20] B. Pateyron, L. Pawłowski, N. Calve, G. Delluc, A. Denoirjean, Surf. Coat. Technol. 214 (2013) 86–90.
[21] R. Jaworski, L. Pawłowski, F. Roudet, S. Kozerski, F. Petit, Surf. Coat. Technol. 202 (2008) 2644–2653.

PAPER 3

Advanced Microscopic Study of Suspension Plasma-Sprayed Zirconia Coatings with Different Microstructures

Paweł Sokołowski

(Wrocław University of Technology, Wrocław, Poland; University of Limoges, Limonges, France)

Lech Pawłowski

(University of Limoges, Limonges, France)

Dagmar Dietrich, Thomas Lampke

(Chemnitz University of Technology, Chemnitz, Germany)

David Jech

(Brno University of Technology, Brno, Czech Republic)

Published: Surface and Coatings Technology,

Volume 260, September 2014, pp. 97–106

Printed with permission

Journal of Thermal Spray Technology 25(1-2) (2016) 94–104

DOI: 10.1007/s11666-015-0310-7

ADVANCED MICROSCOPIC STUDY OF SUSPENSION PLASMA SPRAYED ZIRCONIA COATINGS WITH DIFFERENT MICROSTRUCTURES

Paweł Sokołowski [a,b], Lech Pawłowski [a], Dagmar Dietrich [c], Thomas Lampke [c], David Jech [d]

[a] *University of Limoges, Limoges, France*
[b] *Wroclaw University of Technology, Wroclaw, Poland*
[c] *Chemnitz University of Technology, Chemnitz, Germany*
[d] *Brno University of Technology, Brno, Czech Republic*

The main goal of the paper is to study the differences of two microstructures that can be obtained using suspension plasma spraying technology: (i) columnar one; and, (ii) lamellar, two-zone microstructure. The optimization of spray parameters was made and then the advanced microstructural studies were performed. The work was focused on zirconia stabilized by yttria (YSZ, ZrO2 + 14 wt. % Y2O3) and both by yttria and ceria (YCSZ, ZrO2 + 24 wt. % CeO2 + 2.5 wt. % Y2O3) which are most frequently used as thermal barrier coatings (TBC). Moreover, two types of microstructure were achieved using two different plasma torches, namely SG-100 of Praxair and Triplex of Oerlikon Metco. The microstructure of prepared coatings was analyzed using electron microscopy (SEM) after optimization of the spray parameters. The conventional SEM microscope with secondary electrons detector (SE) and back scattered electrons one (BSE) were used. The energy dispersive spectroscopy (EDS) was performed to analyze the chemical composition. By electron backscatter diffraction (EBSD) grain shape, size and crystal orientation were determined. The analysis enabled the discussion of the coatings growth mechanism. Finally, the Shape From Shading (SFS) technique was applied to recreate and to analyze 3D views of coatings' topographies.

Keywords: *Yttria Stabilized Zirconia, Ytria-Ceria Stabilized Zirconia, Thermal Barrier Coatings, Suspension Plasma Spraying, Columnar Microstructure, Two-Zone Microstructure, Electron Back-Scatter Diffraction*

1. Introduction

Suspension plasma spraying (SPS) is a modification of atmospheric plasma spraying (APS) processes. The complexity of SPS results from the necessity of controlling the phenomena related to the use of liquid suspension instead of dry powder [1, 2]. Thanks to the use of suspension, the submicrometric or nanometric size solids can be introduced to the plasma jet. The resulting coatings are very finely grained [3, 4].

The window of optimal SPS process parameters is narrow. The changes in spray conditions results in different coatings' morphologies. Kozerski et al. [5] described the mechanism of formation of *two-zone* microstructure, which is typical for suspension plasma spraying process. The coatings contained dense zones with well melted lamellas and the zones with irregularly distributed, more or less sintered small particles can be observed. The formation of *two-zone* microstructure resulted from the small sizes of solid and from different trajectories in plasma jet. More recently, many researches were conducted to analyze the possibilities of producing *columnar like* microstructure using SPS technology. VanEvery et al. [6] proved that using axial injection of precursor the columnar microstructure can be produced. The same effect was achieved by Sokołowski et al. [7] for radially injected suspensions by changing the amount of the solid phase in the suspension and/or by appropriate preparation of the substrate surface morphology. The effect of the columnar structure formulation was explained by the deviation of hot gas trajectory near the substrate material. In the studied cases the *columnar like* microstructure occurred only in the coatings sprayed using suspension containing very fine particles.

The columnar microstructure is useful for thermal barrier coatings since it may improve the thermo-mechanical properties and, in particular, thermal shock resistance [8, 9]. On the other hand, the fine grained lamellar microstructure containing a great number of submicrometer and nanometer pores can significantly decrease thermal conductivity of coatings [10, 11]. The present paper focuses on the analysis of the microstructure of the coatings and the manufacturing technology aiming production of columnar like microstructures as well as lamellar ones.

2. Experimental procedure

2.1. Feedstock Preparation

The suspensions used in the spray process were prepared using two zirconia powders having different: (i) chemical composition; and (ii) particles size. The YSZ powder was manufactured by Tosoh (Kyoto, Japan) and had composition of ZrO_2 + 14 wt. % Y_2O_3. The granulometry tests (DLS method, Zetasizer Nano-ZS, Malvern Instruments) showed that the volume mean diameter was equal to d_{V50}=398nm. The powder

was used as manufactured (Fig. 1). The second powder, noted as YCSZ, had the trade name Metco205NS and a composition of ZrO_2 + 24 wt. % CeO_2 + 2.5 wt. % Y_2O_3 (YCSZ). The initial size of YCSZ powder was equal to dv_{50}= 39.6μm. The powder was crushed mechanically using ball milling (moliNEx system, NETZSCH). The mechanical treatment allowed decreasing of powder's size (Fig. 2). The granulometry tests (DLS method, Partica LA-950V2, Horiba) showed that the volume mean diameter was equal to d_{v50}= 696nm.

The suspensions including YSZ and YCSZ were formulated with different fractions of solid phase were prepared. The fractions were torch specific: 2.5 wt. %, 5 wt. %, 10 wt. % of powder for SG-100 torch and 5 wt. %, 10 wt. % and 20 wt. % of powder for Triplex torch. The greater concentration of solid resulted from higher electric power input to Triplex torch. The liquid phase in suspension included water and ethanol in ratio 1:1 and small quantity of dispersant agent (Beycostat C213, CECA, France). The details of feedstock preparation are shown elsewhere [7, 12].

2.2. Spray Experiments

The zirconia coatings were produced using two spray set-ups equipped with different plasma torches (SG-100 and Triplex) and the deposition parameters were optimized separately for each torch [7]. Moreover, the influence of the substrate topography on the coatings' microstructure was tested. The topographies were generated with: (i) grit blasting; (ii) grinding; (iii) turning; and (iv) laser treatment. All substrates were cleaned in the ultrasonic bath in ethanol prior to spraying.

Finally, fours variables occurred in the spray experiments: (i) type of powder; (ii) concentration of solid phase in suspension and (iii) substrate topography; (iv) torch type. As a result 12 spray experiments were performed for each torch type and 36 different coatings were sprayed (Table 1).

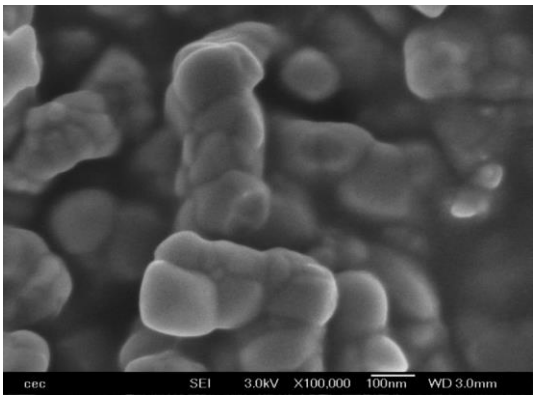

Fig. 1. SEM morphology (secondary electrons) of YSZ powder

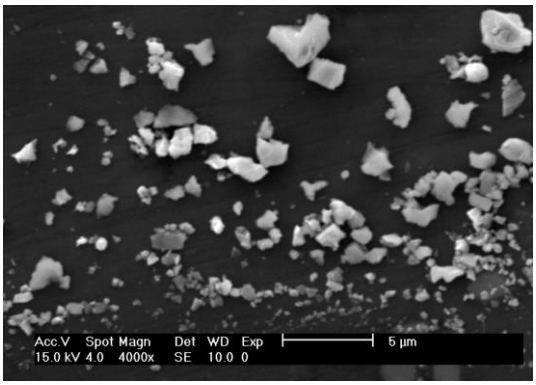

Fig. 2. SEM morphology (secondary electrons) of YCSZ powder particles after milling

2.3. Microstructure Characterization

The metallographic preparation of specimens for advanced microscopic studies was carried out using the conductive bakelite resin with carbon filler (Polyfast Struers). The samples were then grinded and polished - also with the final polishing with colloidal silica oxides (OPS Struers). The samples were cleaned in ethanol, dried and coated with very thin layer of a carbon layer.

The observations were carried out using two different microscopes: (i) Leo 1455VP (Carl Zeiss GmbH) with Metek EDS detector of EDAX was used for SEM observations and EDS measurements; (ii) Neon 40ESB (Carl Zeiss GmbH) with DigiView EBSD camera was used for SEM and EBSD investigations.

The EBSD examination of the coatings' microstructure was made with the following parameters:

- step size of 100nm;
- beam voltage 15kV with an aperture 60μm;
- scan speed of 6-10 points per second.

The obtained data were then analyzed using OIM Analysis 6.1 software. The filtering of the data to minimize the effect of some noises, which are unavoidable for this type of analysis, was made based on two types of filters – *confidence index* (CI>0.12) or *image quality* (IQ).

The coating topography was characterized by *Shape From Shading* method (Phenom G2 pro, Eindhoven, The Netherlands). By using four different local 2D images of the sample and well-known shadowing effect [13] the 3D views of coatings surfaces were recovered. Then the topography profiles could be observed and analyzed [Fig.3]. Finally the influence of substrate topography and spray process parameters on the coating substrate and roughness was investigated. In this case, non-contact laser confocal microscopy method was applied (Olympus, LEXT OLS4000 3D Laser Measuring Microscope, Tokyo, Japan).

Table 1 Design of experiment and nomenclature of sprayed coatings (highlighted lines correspond to columnar like coatings) [7]

Run	Powder material	Concentration of powder in the suspension [%]	Plasma torch	Substrate preparation	Sample
	YSZ-Tosoh	**2.5**	**SG-100**	**Grit-blasting**	**ST21**
1	**YSZ-Tosoh**	**2.5**	**SG-100**	**Laser treatment**	**ST22**
	YSZ-Tosoh	**2.5**	**SG-100**	**Grinding**	**ST23**
	YSZ-Tosoh	5	SG-100	Grit-blasting	ST51
2	**YSZ-Tosoh**	**5**	**SG-100**	**Laser treatment**	**ST52**
	YSZ-Tosoh	5	SG-100	Grinding	ST53
	YSZ-Tosoh	10	SG-100	Grit-blasting	ST101
3	**YSZ-Tosoh**	**10**	**SG-100**	**Laser treatment**	**ST102**
	YSZ-Tosoh	10	SG-100	Grinding	ST103
	YCSZ	2.5	SG-100	Grit-blasting	SC21
4	YCSZ	2.5	SG-100	Turning	SC22
	YCSZ	2.5	SG-100	Grinding	SC23
	YCSZ	5	SG-100	Grit-blasting	SC51
5	YCSZ	5	SG-100	Turning	SC52
	YCSZ	5	SG-100	Grinding	SC53
	YCSZ	10	SG-100	Grit-blasting	SC101
6	YCSZ	10	SG-100	Turning	SC102
	YCSZ	10	SG-100	Grinding	SC103
	YSZ-Tosoh	5	Triplex	Grit-blasting	TT51
7	YSZ-Tosoh	5	Triplex	Laser treatment	TT52
	YSZ-Tosoh	5	Triplex	Grinding	TT53
	YSZ-Tosoh	10	Triplex	Grit-blasting	TT101
8	YSZ-Tosoh	10	Triplex	Laser treatment	TT102
	YSZ-Tosoh	10	Triplex	Grinding	TT103
	YSZ-Tosoh	20	Triplex	Grit-blasting	TT201
9	YSZ-Tosoh	20	Triplex	Laser treatment	TT202
	YSZ-Tosoh	20	Triplex	Grinding	TT203
	YCSZ	5	Triplex	Grit-blasting	TC51
10	YCSZ	5	Triplex	Turning	TC52
	YCSZ	5	Triplex	Grinded	TC53
	YCSZ	10	Triplex	Grit-blasting	TC101
11	YCSZ	10	Triplex	Turning	TC102
	YCSZ	10	Triplex	Grinded	TC103
	YCSZ	20	Triplex	Grit-blasting	TC201
12	YCSZ	20	Triplex	Turning	TC202
	YCSZ	20	Triplex	Grinded	TC203

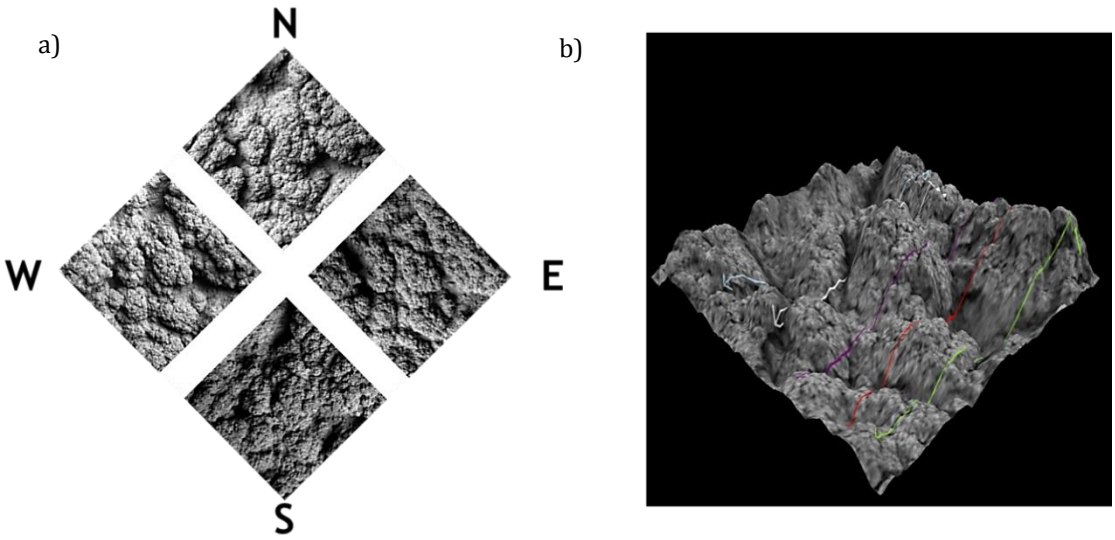

Fig. 3. *Shape From Shading* technique: (a) reconstruction of coating surface, (b) 3D view of coating

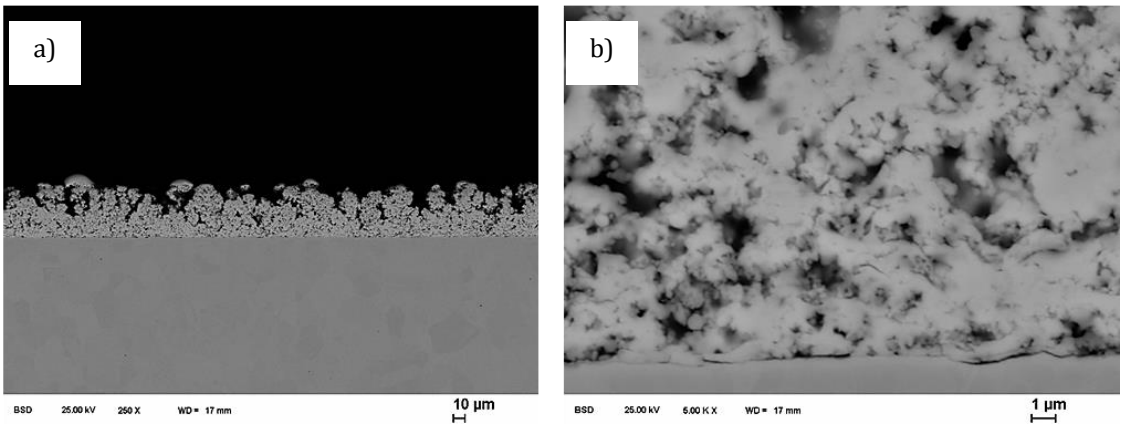

Fig. 4. SEM microstructure (backscattered electrons) of ST23 coatings under magnification of 2509 (a) and 50009 (b)

3. Results

3.1. EDS Chemical Analysis

The first part of a larger study done on the samples produced as shown in Table 1 contains a basic microstructure characterization and is presented elsewhere (Ref 7). Consequently, to complete the previous studies, the chemical analysis of coatings using Energy Dispersive Spectroscopy was carried out.

The EDS analysis of samples sprayed using suspension including YSZ powder showed that the spraying did not introduce the modification in the chemical composition. The content of the elements in the coating microstructure was as follows: (i) 25-30 wt. % of oxygen, (ii) 14-18 wt. % of yttrium; and (iii) 53-58 wt. % of zirconium what corresponds to the initial composition of YSZ-Tosoh powder used to prepare the suspension ((i) 25 wt. % of oxygen; (ii) 11 wt. % of yttrium; and (iii) 64 wt. % of zirconium).

The YCSZ coatings consisted of about: (i) 18-23 wt. % of oxygen; (ii) 15-18 wt. % of cerium; (iii) 5-6 wt. % of yttrium; and (iv) 56-63% of zirconium. This composition is similar to the initial one which corresponds to (i) 21 wt. % of oxygen; (ii) 20 wt. % of cerium; (iii) 2 wt. % of yttrium; and (iv) 47% of zirconium.

3.2. Columnar-Like Coatings

Table 1 shows the process parameters resulting in columnar like microstructures. The microstructure was achieved for both plasma set-ups, different kinds of substrates' surface topographies and only for fine grained YSZ powder. A typical columnar like microstructure cross-section for ST23 coating is shown in Fig. 4a. This sample was particularly interesting because of numerous perpendicular columns having irregular shape, size and height which were created onto smooth, grinded, substrate surface. The size of pores was nanometric to submicrometric.

The interface between coating and grinded substrate did not include the delamination of coating and any cracks (Fig. 4b). However, after having the cut sample and placing it into conductive resin, some single discontinuities could have been observed.

The orientation and size of crystal grains in the ST23 coatings were tested using EBSD analysis. The sample had very finely grained microstructure (Fig. 5). It was possible to observe that finer grains occurred near to the substrate. The top of the coatings consisted of a few very big grains which were very different comparing to the rest of the coating microstructure. These grains could have been formed by a few droplets of the suspension which leaked out from the injector and fell at the top of a hot sample at the end of the spray process. Three different pole figures {001}, {011} and {111} were composed to observe the main crystallite directions. The differences between these orientations were very small and it was not possible to distinguish any preferred directions of columns growth. The main volume grain size was near 600 nm - almost two times bigger than the initial powder particle size. However, the main number grain was of 300 nm and below, which was close to initial particle powder size.

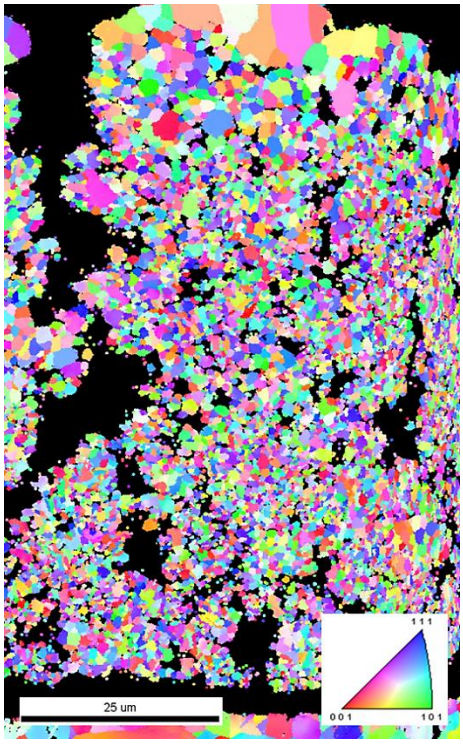

Fig. 5. EBSD image (inverse pole figure) of ST23 sample

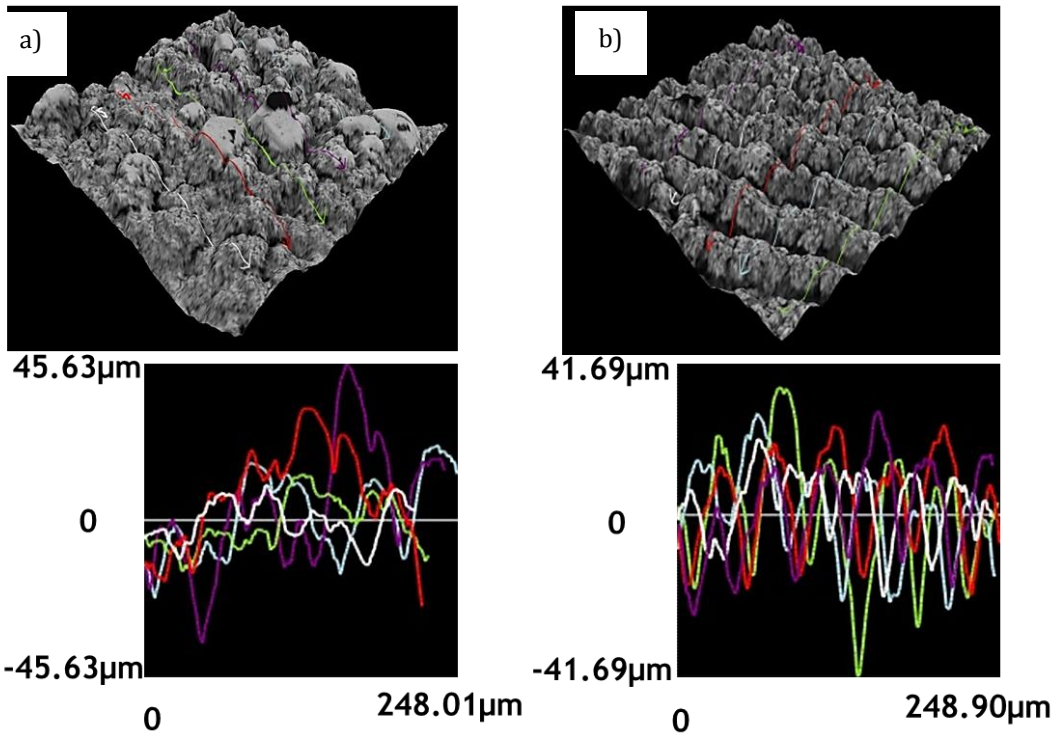

Fig. 6. Topography of coatings having columnar microstructure (SFS method): irregular, cauliflower like, surface of ST23 coatings created at grinded surface (a) and very regular coating ST52 created at laser treated substrate

The coatings surface topography analysis enabled to find out that ST23 coating was the roughest one when taking into account the small initial roughness of substrate surface (Fig. 6a). Consequently, the value of Ra = 7.9 lm and Rz = 51.2 lm was measured for the coating surface and Ra = 0.1 lm and Rz = 0.6 lm for the substrate, respectively. Another coating having columnar microstructure was ST52 (Fig. 7a). The substrate topography, achieved by laser treatment, influenced the coating morphology. The columnar microstructure was formed in the way that each ''peak'' corresponded to a column and above the ''valleys'' the longitudinal pores were formed. The coatings were also denser than sample ST23, because of the use of two times greater suspension concentration. However, a big amount of larger micropores was also observed. Near the top of the coating, the microstructure was very fine grained as observed with the SEM (Fig. 7b).

The EBSD measurement area was chosen in a way that the ''peaks and valleys'' were analyzed simultaneously (Fig. 8). The measurements showed that the growth mechanism of coating was not the same in the two analyzed regions of the sample. Consequently, the grains, which were deposited above the peaks of the substrate (see no. 2 on Fig. 8a), were rather spherical. On the other hand, the grains solidified between the peaks were more deformed, i.e., thin and perpendicular to the substrate surface (see no. 1 on Fig. 8a). The longitudinal shape of the grains may suggest that coatings have a texture. Because of these differences in the grains morphology, an additional EBSD maps in these two regions of the sample were analyzed (Fig. 8b). But the observed differences between different grain orientations were in fact very small and it was not possible to find any preferred directions of crystal growth. The grain size distribution showed that the grains with the size of about 600 nm covered the largest area fraction of samples (see Fig. 9a). On the other hand, a great number of small grains with the size of about 250-300 nm were found out (see Fig. 9b). Moreover, the grains which solidified above the peaks of substrate, had slightly smaller size.

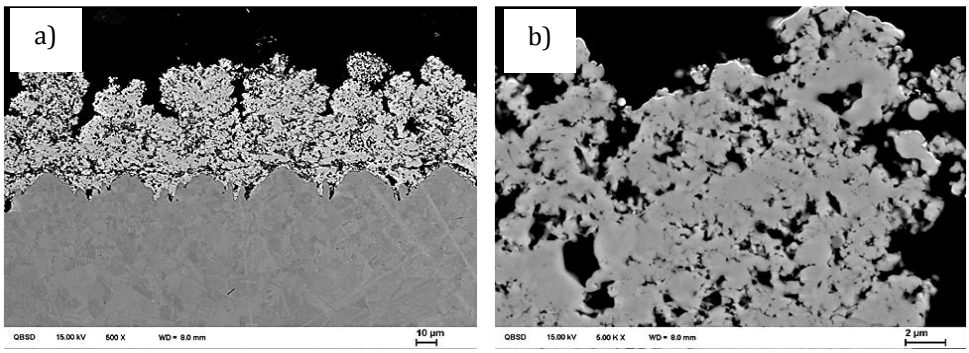

Fig. 7. SEM microstructure (back scattered electrons) of ST52 coatings with magnification of 500x (a) and 5000x (b)

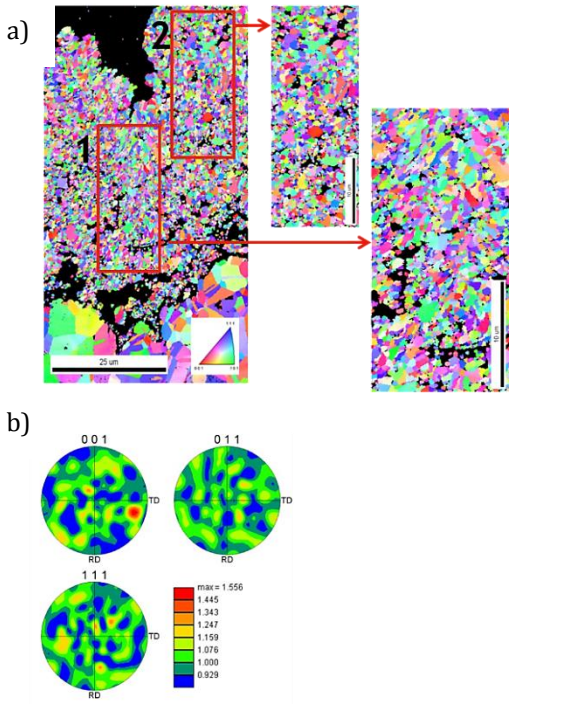

Fig. 8. EBSD map showing the grains of ST52 coating and their crystallographic orientation (a), and texture analysis performed in area 2 (b)

SFS enabled to find the cauliflower-like surface morphology in samples with columnar-like structure. The coatings sprayed onto laser-treated substrates had very regular surface. The coating profile was very similar to that of the substrate prior to spraying (Fig. 6b). However, the roughness of coating can be characterized by Ra = 7.4 lm and Rz = 43.5 lm, which was still around two times bigger than that measured on the laser-treated substrate prior to spraying (Ra = 3.6 lm and Rz = 17.6 lm).

3.3. Lamellar Coatings

The lamellar microstructure was observed, i.e., for YCSZ coatings prepared using Triplex torch and suspension having 10 wt.% of solid phase. The microstructure of these coatings was much denser than in columnar-like coatings (Fig. 10a).

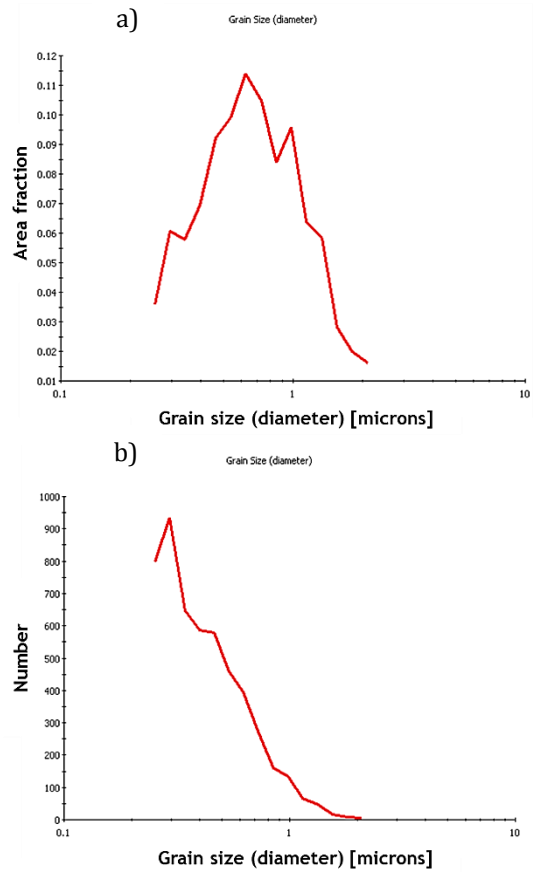

Fig. 9. The volume (a) and number (b) distribution of the grain size in ST52 coating microstructure

The presence of cerium could be noticed as bright fields in Fig. 10(b). Finally, it was found that the substrate preparation process did not influence this type of coating microstructure. The EBSD investigation visualized the thin columns inside the lamellas, especially near the substrate (Fig. 11). The grain size examination, carried out for the TC102 sample, enabled to find the main size of about 450 nm, and the number distribution was less than 300 nm (see Fig. 12a and b).

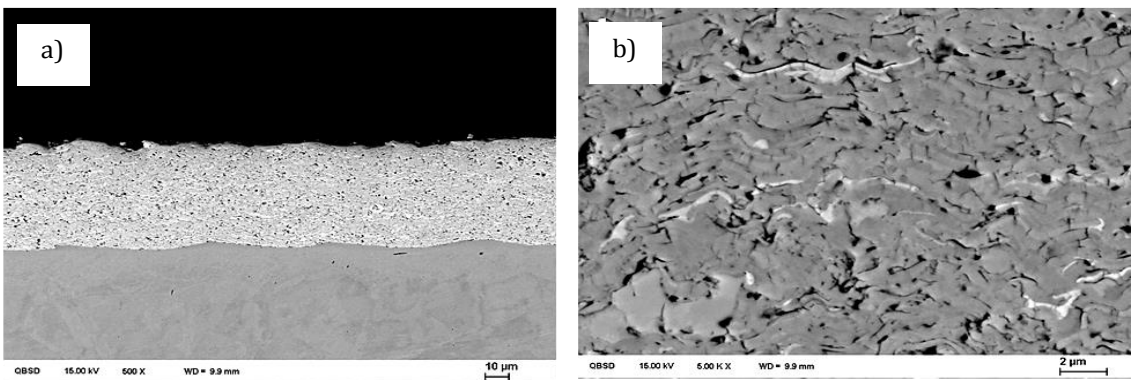

Fig. 10. SEM micrographs (back scattered electrons) of the TC102 sample with 500x (a) and 5000x magnification (b)

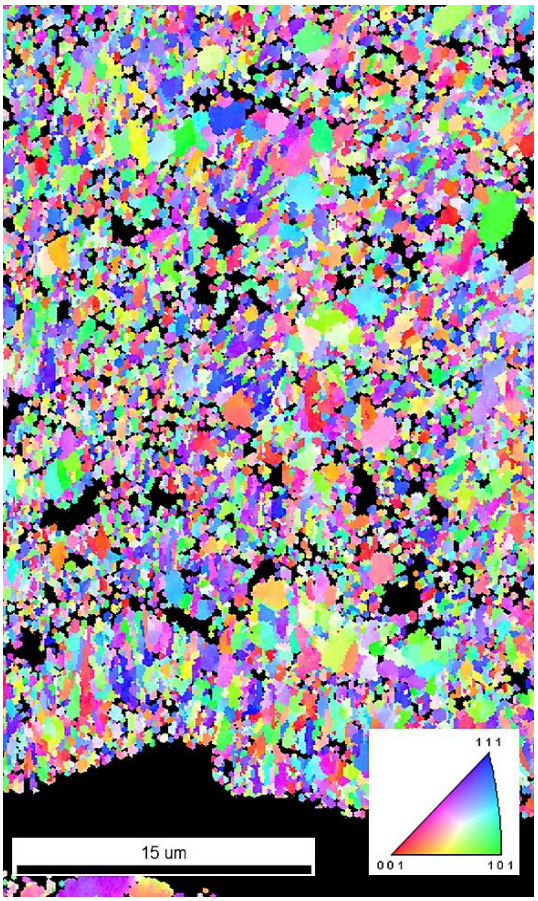

Fig. 11. EBSD map (inverse pole figure) of TC102 coating

The coatings surface was much smoother comparing to the coatings having columnar structure but also smoother with regard to other samples deposited using fine YSZ powder (Fig. 13). The single peaks on the surface profile could also be observed as a result of coarser particles that are present on coating surface. The SEM observations were confirmed by roughness measurements. The surface of TC102 sample was characterized by R_a = 3.2 lm and R_z = 23.2 lm. Furthermore, a decrease of roughness parameters with an increase in suspension concentration could be observed, especially for Triplex torch.

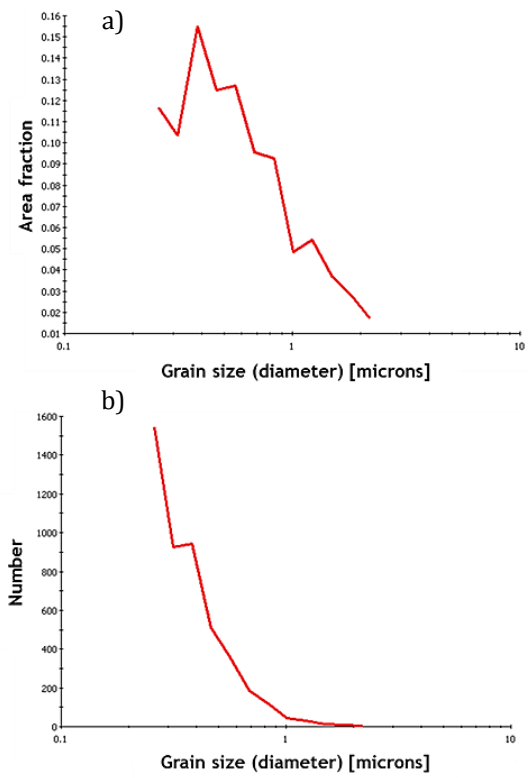

Fig. 12. The volume (a) and number (b) crystal grain size distribution of lamellar (TC102) sample

4. Discussion

The experiments were carried out in order to better understand the formation of the columnar and lamellar microstructures of suspension plasma-sprayed zirconia coatings but also to observe main differences between these microstructures. The coatings' growth mechanisms in SPS process were also investigated (Ref 14-16).

The coatings having columns were heterogeneous in terms of porosity, shape and size of grains, and the surface topography. Contrarily, the coatings with lamellas had fine-grained microstructure, regular distribution of micropores, and smooth surface.

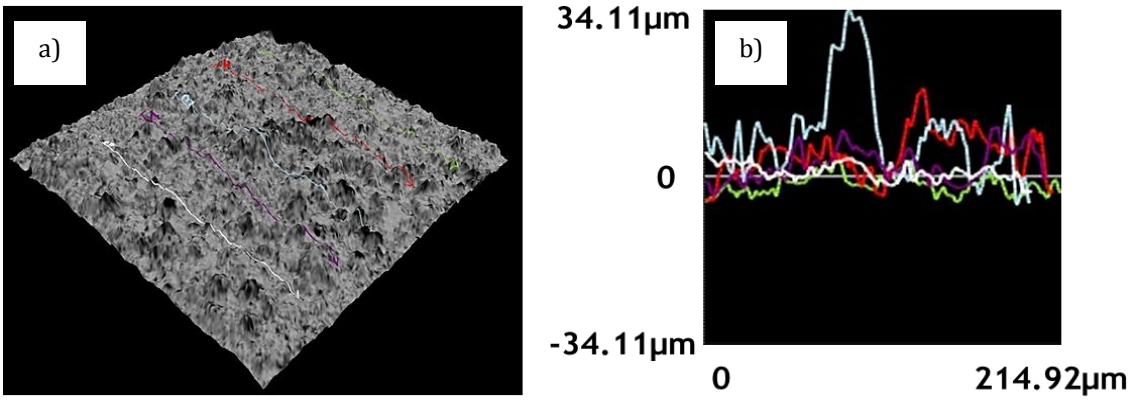

Fig. 13. Shape From Shading method applied to sample TC102: 3D view (a) and topography profile (b)

These differences were caused by the hot gas fluctuations in contact with the substrate surface. The irregular columns could be created by the particles which followed the hot gas swirls and adhered mainly

to the peaks of substrate or previous deposits forming columnar-like microstructure. The effect was strengthened by morphology of substrate surface and fine size of powder particles Fig. 14 (Ref 6, 7). The EBSD maps confirmed previous analyses and explanations. Another issue related to the behaviour of powder particles that came into a contact with substrate resulted from equilibrium of forces (Ref 7, 17): (i) F_D—drag force pushing fine solids and (ii) adhesion force F_A keeping the particles on the substrate surface. Consequently, the particles could stick directly to the substrate or move parallel to it depending on which of these forces dominated. The relation $F_A > F_D$ is valid for larger particles transported close to the axis of plasma jet. But inside the coatings, the fractions of fine, unmelted, grains were noticed also. These zones were generated by particles that moved in external and colder regions of plasma. For these particles, the balance of forces changed and, consequently, FD > FA. Subsequently, they moved perpendicular to jet axis and adhered to an irregularity they meet on their way (Fig. 15). This mechanism connected with small amount of solid phase in the suspension, and low number of particles in the suspension droplet coming from the injector allows columns growing even when the substrate is smooth. This will be possible only if single irregularities (''roots'') on the substrate surface will be created. Then the procedure will be similar as in the case of laser-treated substrate but as the result, much more irregular coatings will be formed (Fig. 16). Finally, the mechanism of columnar growth may be related to shadowing effect discussed elsewhere (Ref 6, 18). The growth of coating was rather an effect of intense accumulation of powder particles on surface peaks, than on its shadowed parts. This resulted in formation of columns or long, perpendicular to the substrate, pores, respectively (Fig. 14).

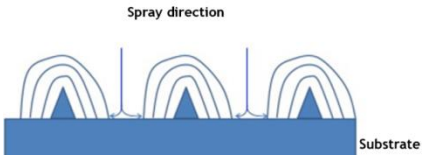

Fig. 14. Growth-up mechanism of columnar like coatings through plasma fluctuations and shadowing effect (inspired by [6, 7])

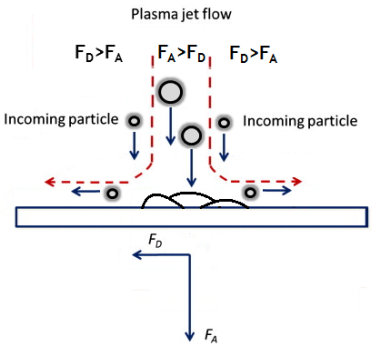

Fig. 15. The behavior of powder particles that come into a contact with substrate or previous deposits (inspired by [7])

However, it should be stressed up that despite many attempts, it was not possible to achieve so regular columnar structure using SPS similar to that obtained with the physical vapour deposition (PVD) technology (Ref 19, 20). This can be explained by the fact that the particles used in SPS have a size many orders of magnitude greater than the atoms or molecules forming islands which become the columns during PVD processes.

The growth of lamellar microstructure resulted from suspension injection into the plasma and the phenomena occurring thereafter in the plasma jet Fig. 17 (Ref 5). This type of coating occurred mainly when the suspension had 10-20 wt.% of solid phase. As the injection systems in two plasma torches were different, there were some differences in morphologies of obtained coatings. The smaller and more concentrated droplets were injected into the plasma flux in Triplex setup, and as a result, more homogeneous coating was formed.

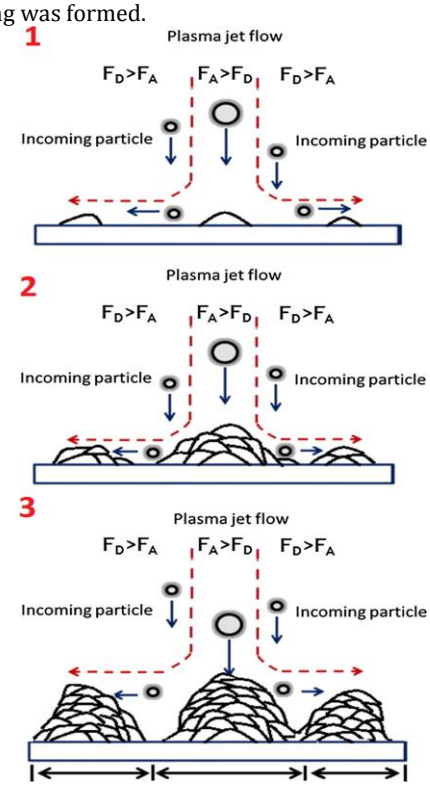

Fig. 16. The schematic illustration of columns formation on smooth surfaces for suspension containing low concentration of solid phase: 1—irregularly distributed single splats create single ''roots'' for columns; 2—particle trajectory depending on FA and FD (FD > FA preferred because of particle size); 3—continuous growth of columns supported by shadowing effect

On the other hand, all mentioned coatings were formed using the same process—SPS—so among many differences, they showed also many similarities. Firstly, it was possible to observe, smaller or larger, completely randomly oriented lamellae and surrounding them micropores inside all columnar-like coatings. Furthermore, thin and longitudinal (columnar-like) grains inside big, flattened, lamella were observed, when analyzing coatings having lamellar microstructure like TC102.

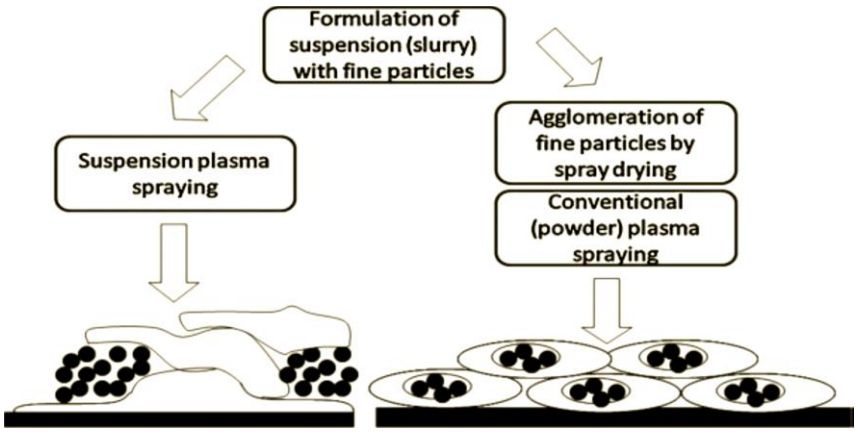

Fig. 17. The mechanism of formation conventional two-zone lamellar structure using Suspension Plasma Spraying method (Ref 5)

5. Conclusions

Advanced microstructural studies using scanning electron microscopy (SEM), energy dispersive x-ray diffraction
(EDS), electron beam scattering diffraction (EBSD), and finally SFS method were used to characterize suspension plasma-sprayed zirconia coatings having different microstructures.

The research showed that the amount of solid phase used during suspension formulation had important influence on the microstructure of coatings, especially on porosity and topography of the coating surface. When using small amount, the porous and rough coatings were achieved. With the increase of solid phase amount, the porosity of coatings was decreasing. A similar effect was observed when the particles of powders with different size
were used.

The differences in coating microstructure were observed also depending on which plasma torch was used during spray process. SG-100 of Praxair seemed to give more possibilities in producing coatings having different microstructures. At the same time, coatings deposited by Triplex of Oerlikon Metco were much more homogenous in term of porosity and coating topography.

The EDS analysis proved that the spray process did not influence the chemical composition of coatings. The concentration of the elements in coatings microstructure was close to that observed in initial powders.

The EBSD analysis proved that the suspension plasma sprayed coatings were composed of grains with random crystal orientation. The effect was related to the topography of the coatings as could be observed for coatings deposited on the laser-treated substrates. The analysis of the crystal grain size of coatings showed that their size is comparable or smaller than that of initial powders.

The SFS technique was used to recreate and to analyse 3D views of coatings_ topographies. The investigations showed that the suspension composition, powder particle size, and substrate preparation can be an important factor influencing coating topography. The roughness analysis was carried by non-contact laser confocal microscopy and proved correlations that were observed with the use of SFS method.

In future work, the studies of thermal and thermomechanical properties will be realized in order to verify what kind of coating microstructure is more beneficial for TBC_s applications. For some applications, especially as thermal barrier coatings, the coatings having columnar microstructure seem to be more advantageous. The main benefit is high resistance for thermal shocks, which improves the sprayed coating in-service time (Ref 21). However, due to the fine-grained microstructure with the regular distributed micropores in the lamellar coating microstructure, the thermal transport is significantly reduced. The influence of the coatings microstructure on thermal conductivity was discussed previously (Ref 12, 22, 23). Therefore, the selection of adequate coatings microstructure for desired application has to be a compromise.

Acknowledgments

This research received support from the Grant Sonata, UMO-2013/11/D/ST8/03400, awarded to the Faculty of Mechanical Engineering at the Wroclaw University of Technology by the National Science Centre (Poland). French Embassy in Poland enabled the stay of Paweł Sokołowski at University of Limoges in frame of joint PhD ‘‘Cotutelle’’ program which is realized in cooperation between France and Poland. The Polonium program attributed by the French Embassy in Poland helped in financing the visits of Polish researchers in France.

References

[1] F. Gitzhofer, E. Bouyer, and M.I. Boulos, ‘‘Suspension Plasma Spraying’’, US Patent 5,609,921, 3 Nov 1997

[2] 2. P. Fauchais, R. Etchart-Salas, V. Rat, J.F. Coudert, N. Caron, and K. Wittmann-Te´ne` ze, Parameters Controlling Liquid Plasma Spraying: Solutions, Sols or Suspensions, J. Therm. Spray Technol., 2008, 17, p 31-59

[3] 3. R. Vaßen, H. Kaßner, G. Mauer et al., Suspension Plasma Spraying: Process Characteristics and Applications, J. Therm. Spray Technol., 2010, 19, p 219-225

[4] 4. S. Kozerski, L. Pawłowski, R. Jaworski, R. Francine, and F. Petit, Two Zones Microstructure of Suspension Plasma Sprayed Hydroxyapatite Coatings, Surf. Coat. Technol., 2010, 204, p 1380-1387
[5] 5. S. Kozerski, L. Łatka, L. Pawłowski, F. Cernuschi, F. Petit, C. Pierlot, H. Podlesak, and J.P. Laval, Preliminary Study on Suspension Plasma Sprayed ZrO2 + 8 wt.% Y2O3 Coatings, J. Eur. Ceram. Soc., 2011, 31, p 2089-2098
[6] 6. K. VanEvery, M.J.M. Krane, R.W. Trice, H. Wang, W. Porter, M. Besser, D. Sordelet, J. Ilavsky, and J. Almer, Column Formation in Suspension Plasma-Sprayed Coatings and Resulting Thermal Properties, J. Therm. Spray Technol., 2011, 20(4), p 817-828
[7] 7. P. Sokołowski, S. Kozerski, L. Pawłowski, and A. Ambroziak, The Key Process Parameters Influencing Formation of Columnar Microstructure in Suspension Plasma Sprayed Zirconia Coatings, Surf. Coat. Technol., 2014, 260(15), p 97-106
[8] 8. R. Vaßen, H. Guo, and D. Stover, Manufacture and Properties of Segmented Thermal Barrier Coatings, Proceedings of the 29th International Cocoa Beach Conference & Exposition, D. Zhu, W.M. Kriven, Ed., Jan 23-28, 2005 (Cocoa Beach, FL), Ceramic Engineering and Science Proceedings, Vol 26(38), p 37-450
[9] 9. N. Curry, K. VanEvery, T. Snyder, and N. Markocsan, Thermal Conductivity Analysis and Lifetime Testing of Suspension Plasma-Sprayed Thermal Barrier Coatings, Coatings, 2014, 4(3), p 630-650
[10] 10. E. Garcia, P. Miranzo, R. Soltani, and T.W. Coyle, Microstructure and Thermal Behavior of Thermal Barrier Coatings, J. Therm. Spray Technol., 2008, 17(4), p 478-485
[11] 11. B. Nait-Ali, K. Haberko, H. Vesteghem, J. Absi, and D.S. Smith, Thermal Conductivity of Highly Porous Zirconia, J. Eur. Ceram. Soc., 2006, 26(16), p 3567-3574
[12] 12. P. Sokołowski, L. Łatka, L. Pawłowski, A. Ambroziak, S. Kozerski, and B. Nait-Ali, Characterization of Microstructure and Thermal Properties of YCSZ Coatings Obtained by Suspension Plasma Spraying, Surf. Coat. Technol., 2015, 268(25), p 147-152
[13] 13. B.K.P. Horn, ''Shape from Shading: A Method for Obtaining the Shape of a Smooth Opaque Object from One View,'' Ph.D. thesis, Massachusetts Institute of Technology, 1970
[14] 14. H. Kassner, R. Siegert, D. Hathiramani, R. Vassen, and D. Stoever, Application of Suspension Plasma Spraying (SPS) for Manufacture of Ceramic Coatings, J. Therm. Spray Technol., 2008, 17(1), p 115-123
[15] 15. L. Łatka, S.B. Goryachev, S. Kozerski, L. Pawłowski, and T. Lampke, Buildup Mechanisms of Suspension Plasma Sprayed ZrO2 + 8 wt.% Y2O3 Coatings, Thermal Spray 2011: Proceedings of the International Thermal Spray Conference and Exposition, Sept 27-29, 2011 (Hamburg, Germany), DVS Media, 2012, p. 104-109
[16] 16. Z. Tang, H. Kim, I. Yaroslavski, G. Masindo, Z. Celler, and D. Ellsworth, Novel Thermal Barrier Coatings Produced by
[17] Axial Suspension Plasma Spray, Thermal Spray 2011: Proceedings of International Thermal Spray Conference and Exposition, Sept 27-29, 2011 (Hamburg, Germany), DVS Media, 2012, p 571-576
[18] 17. B. Pateyron, L. Pawłowski, N. Calve, G. Delluc, and A. Denoirjean, Modeling of phenomena occurring in plasma jet during suspension spraying of hydroxyapatite coatings, Surf. Coat. Technol., 2013, 214(15), p 86-90
[19] 18. G. Mauer, A. Hospach, N. Zotov, and R. Vaßen, Process conditions and microstructures of ceramic coatings by gas phase deposition based on plasma spraying, J. Therm. Spray Technol., 2013, 22(2-3), p 83-89
[20] 19. A. Guignard, Development of Thermal Spray Processes with Liquid Feedstocks, Forschungszentrum Ju¨ lich GmbH Zentralbibliothek, Verlag, Energie & Umwelt/Energy & Environment, Vol 141, 2012
[21] 20. U. Schulz, K. Fritscher, and M. Peters, EB-PVD Y2O3- and CeO2/Y2O3-Stabilized Zirconia Thermal Barrier Coatings-Crystal Habit and Phase Composition, Surf. Coat. Technol., 1996, 82, p 259-269
[22] 21. W.A. Kaysser, M. Peters, K. Fritscher, and U. Schulz, Characterization and Testing of EB-PVD Thermal Barrier Coatings, AGARD Report 823, Thermal Barrier Coatings, NATO Neuillysur-Seine, Paris, AGARD, 1998
[23] 22. P. Carpio, Q. Blochet, B. Pateyron, L. Pawłowski, M.D. Salvador, A. Borrell, and E. Sanchez, Correlation of Thermal Conductivity of Suspension Plasma Sprayed Yttria Stabilized Zirconia Coatings with Some Microstructural Effects, Mater. Lett., 2013, 107, p 370-373
[24] 23. D.S. Smith, A. Alzina, J. Bourret, B. Nait-Ali, F. Pennec, N. Tessier-Doyen, K. Otsu, H. Matsubara, P. Elser, and U.T. Gonzenbach, Thermal Conductivity of Porous Materials, J. Mater. Res., 2013, 28(17), p 2260-2272

PAPER 4

The microstructural studies of suspension plasma sprayed zirconia coatings with the use of high-energy plasma torches

Paweł Sokołowski

(Wrocław University of Technology, Wrocław, Poland; University of Limoges, Limonges, France)

Per Nylen

(University West, Trollhättan, Sweden)

Radek Musalek

(Institute of Plasma Physics CAS, Prague, Czech Republic)

Leszek Łatka, Stefan Kozerski

(Wrocław University of Technology, Wrocław, Poland)

Dagmar Dietrich, Thomas Lampke

(Chemnitz University of Technology, Chemnitz, Germany)

Lech Pawłowski

(University of Limoges, Limonges, France)

Under review in Surface and Coatings Technology

Printed with permission

THE MICROSTRUCTURAL STUDIES OF SUSPENSION PLASMA SPRAYED ZIRCONIA COATINGS WITH THE USE OF HIGH-ENERGY PLASMA TORCHES

Paweł Sokołowski [a,b], Per Nylen [c], Radek Musalek [d], Leszek Łatka [a], Stefan Kozerski [a], Dagmar Dietrich [e], Thomas Lampke [e], Lech Pawłowski [b]

[a] *Wroclaw University of Science and Technology, ul. Łukasiewicza 5, 50-371 Wrocław, Poland*
[b] *University of Limoges, 12 rue Atlantis, 87068 Limoges, France*
[c] *University West, Gustava Melins Gata 2, 461 86 Trollhättan, Sweden*
[d] *Institute of Plasma Physics CAS, v.v.i., Za Slovankou 3, 18200 Prague, Czech Republic*
[e] *Chemnitz University of Technology, D-09107 Chemnitz, Germany*

The presented studies are focused on the microstructure characterization of zirconia-based coatings deposited by two types of high-energy plasma torches: (i) Axial III; and, (ii) hybrid version of Water-Stabilized Plasma (WSP) torch. The suspensions were formulated using solid dispersed phase of: (i) zirconia stabilized with 14 wt.% of Y_2O_3 and (ii) zirconia stabilized with 24 wt.% of CeO_2 + 2.5 wt.% of Y_2O_3 and continuous phase of water with ethanol. The spray process parameters were optimized for each plasma set-up individually. The in-flight observations (shadowgraphy) were performed to optimize the injection of the liquid feedstock into the plasma jet. Then the coating's morphology and coating/substrate interface were characterized using conventional light microscopy and scanning electron microscopy (SEM). The results showed that through the change of deposition parameters various coatings microstructures could be obtained, in particular columnar and two-zones structures. The EDS/EDX and XRD studies showed that there was no significant change in chemical/phase composition of zirconia material before and after spraying. Electron Backscatter Diffraction (EBSD) method allowed to analyze the grain size in the coating microstructure as well as crystallographic orientation of individual grains. The results showed that coatings were characterized by submicrometric microstructure what corresponded to the size of powder particles used to formulate suspension. No texture was observed in the coatings microstructure. The surface topography analysis which was performed by confocal scanning laser microscopy (CSLM) and Shape From Shading (SFS) technique proved the great influence of suspension concentration on the coating structure.

Keywords: *water-stabilized plasma (WSP), gas-stabilized plasma (GSP), suspension injection, columnar microstructure, two-zones microstructure, electron backscatter diffraction*

1. Introduction

The surface of an object plays a major role in the engineering. The surface is the place exposed to the stresses resulting from mechanical, thermal or tribological interactions. Such interactions occur in many industries such as automotive, aerospace, power or machinery etc. [1–3]. For example the power and fuel efficiency of gas turbines are currently limited by the properties of materials that are used for parts fabrication, especially by the insufficient resistance to high temperatures caused by the fuel combustion process [4]. That is why Thermal Barrier Coating systems (TBC's) are in common use in the aviation industry. The main reason why the coating industry has been growing very fast in recent decades results from the economic considerations. In accordance to analysis by Matthews [5], the UK coating industry was worth over £ 10.8bn. But at the same time it affected the products being worth over £ 140bn. Afterwards, thermal spraying and powder coatings themselves were priced over £ 1bn. This clearly shows that coating industry is an important part of the production worldwide.

One of the latest and extensively studied coating methods is the Suspension Plasma Spraying (SPS). This process is derived from conventional powder plasma spraying and was invented in order to deposit fine grained feedstock that cannot be applied by APS [6,7]. Currently, Suspension Plasma Spraying seems to be one of the most versatile methods among thermal spray processes. It includes many important deposition parameters that can influence coating's microstructure. The latter can be influenced by:

- torch position and dynamics (spray distance, scan speed, scan off-set studied by Łatka et al. [8]);
- suspension injection (injection mode, injection angle, feed rate etc. [9,10);
- suspension properties (powder size and rheological properties of suspension investigated by e.g. Rampon et al. [11]);
- substrate preparation and temperature [12,13];
- plasma properties related to type of torch that are presented in this study;
- and many others.

In our previous works [12,14] the application of low-energy plasma torches (SG-100 and Triplex) for Suspension Plasma Spraying was presented and discussed in details. In this work, the two different high-energy plasma spray torches (called Axial III and WSP-H 500) were tested for a production of stabilized zirconia coatings having various microstructures. The present paper is focused on microstructural fea-

tures and zirconia-based coating formation mechanisms in Suspension Plasma Spraying.

2. Materials and methods

2.1. Powders and suspensions characterization

Yttria-stabilized zirconia (YSZ) and yttria/ceria-stabilized zirconia (YCeSZ) powders were used for suspension formulation. The properties of solid phase were as follows:

- YSZ - the submicrometer-sized powder produced by Tosoh (Tosoh TZ-8YS, Tokio, Japan) and having a chemical composition of ZrO_2 + 14 wt.% Y_2O_3. The powder had fully cubic structure according to the XRD and Rietveld analysis[12]. The powder particle size (Zetasizer Nano ZS, Malvern Instruments Ltd, Worcestershire, UK) was dv_{10}=0.36 µm, dv_{50}=0.53 µm, and dv_{90}=0.95 µm. The morphology analysis performed by scanning electron microscopy showed irregular microstructural features of YSZ powder. The powder grains formed longitudinal and heterogeneous aggregates (the SEM micrographs of YSZ powder particles showed elsewhere [14]).
- YCeSZ - the powder produced by Oerlikon Metco having a chemical composition of ZrO_2 + 24 wt.% CeO_2 + 2.5 wt.% Y_2O_3 (Metco 205NS, Oerlikon Metco, Switzerland). The XRD studies showed that powder had complex phase composition (mostly tetragonal but the appearance of cubic and monoclinic components was observed also)[12]. In fact, the powder was originally designed for conventional Powder Plasma Spraying, so the particles were micrometer-sized and spherical in the as-produced state. For the purpose of Suspension Plasma Spraying the powder was pre-treated according to previously established methodology. The 3-hours mechanical ball-milling process (moliNEx, Netzsch, Selb, Germany), performed in an ethanol bath, allowed to obtain submicrometer-sized YCeSZ powder particles. The laser granulometry of crushed powder showed monomodal size distribution, where dv_{10}=0.41 µm, dv_{50}=0.75 µm, and dv_{90}=1.80 µm (Horiba Partica LA-950V, Kyoto, Japan). The final powder particles were angular but non-agglomerated (see YCeSZ powder SEM micrographs here [15]).

Each formulated suspension was a mixture of: (i) solid particles, (ii) solvent and (iii) surfactant. Three different loads of YSZ and YCeSZ powders were used for a suspension formulation (10, 20 and 30 wt.%). As a result six various mixtures were tested for spraying. Ethanol and water were mixed in ratio 1:1 and used as a solvent each time. In order to stabilize suspensions and increase their rheological properties, the surfactant Beycostat C213 (CECA, La Garenne-Colombes, France) was added. The whole procedure of suspension preparation was similar as showed in the previous studies, where less concentrated suspensions (2.5, 5, 10 wt.% of solid) were sprayed by using low-energy plasma torches[12]. The most important features of precursors used for spraying are summarized in Table 1.

Table 1 The characteristic of liquid feedstock used for SPS

Suspension details	Powder dv_{10} (µm)	Powder dv_{50} (µm)	Powder dv_{90} (µm)	Suspension concentration (wt.% of solid)	Solvent type	Chemical agent
YSZ based suspension	0.36	0.53	0.95	10 ; 20 ; 30	water/ethanol(50:50)	Beycostat C213
YCeSZ based suspension	0.41	0.75	1.80	10 ; 20 ; 30	water/ethanol(50:50)	Beycostat C213

2.2. Substrate preparation

Besides the suspension concentration, another variable in the coating preparation process was a substrate topography. Three different procedures were applied in order to create surfaces having different roughness and features. Grit-blasted substrates were having the highest roughness (Ra=7.8 µm) and very irregular surface. Laser-treated substrates were still having medium roughness (Ra=3.2 µm) but the surface peaks were this time distributed very regularly (see Fig. 1b). The laser pre-treatment was used to create fine grooves at the steel substrate (one-dimensional linear pattern). The grinded substrates were the smoothest ones (Ra=0.5 µm). All substrates were manufactured from 2 mm thick 304L stainless steel coupons. The surface profiles (Form Talysurf 120l, Taylor Hobson Ltd, Leicester, UK) are showed in Fig. 1.

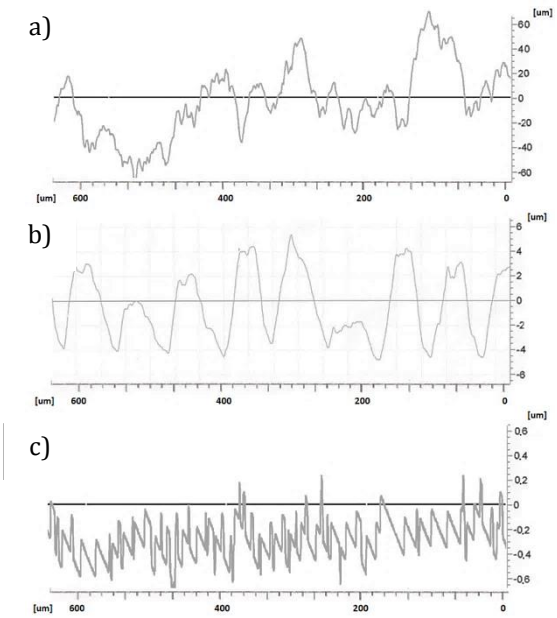

Fig. 1. The substrates' surface roughness profiles: (a) grit-blasted, (b) laser-treated (c) and grinded

2.3. Spray process description

The spray process was realized with the use of two different high-energy plasma torches called Axial III (Mettech, North Vancouver, Canada) and WSP-H 500 (ProjectSoft HK a.s., Hradec Kralove, Czech Republic together with the Institute of Plasma Physics CAS, Prague, Czech Republic). Both plasma torches were much different in the term of their constructions, operating rules, feedstock injection etc. Consequently, all spray parameters had to be set individually for WSP-H 500 and Axial III plasma torches and are presented in Tab. 2. The optimized deposition parameters were similar for all suspensions concentrations.

Table 2 Details of spray processes performed by using WSP-H 500 and Axial III plasma torches

Torch	WSP-H500	Axial III
Process parameters, units	Values	Values
Electric power, kW	~150	~120
Working gases composition	Ar + H_2O decomposition products*	Ar + H_2 + N_2
Total plasma gases flow rate, slpm	15 of Ar + H_2O decomposition products*	245
Stand-off distance, mm	100	75
Relative torch scan speed velocity, mm/s	~900	~1000
Offset between plasma torch passes, mm	30	5
Nozzle injector internal diameter, mm	0.35	0.50
Suspension injection system	Pneumatic system; continuous stream injector	Peristaltic pomp; continuous stream injector
Suspension injection rate, ml/min	90-100#	45
Injector type	Nozzle outside the torch, injection realized radially	Nozzle inside the torch, injection realized axially

* Hydrogen, oxygen and OH groups were formed from the water vortex ionization during the torch operation (the torch consumed 2-3 liters of water per hour of torch operation)

** Depending on the optimized feeding pressure

The configuration of both spray set ups was as follow: the plasma torch was mounted on an arm of 6-axis industrial robot, whereas the substrates were mounted on a rotational carousel. The linear movement of the robot arm determined the spraying path and the offset between consecutive plasma torch passes. Afterwards, the rotation of the carousel corresponded to the plasma torch scan speed. The arrangement of spray set-ups is presented in Fig. 2.

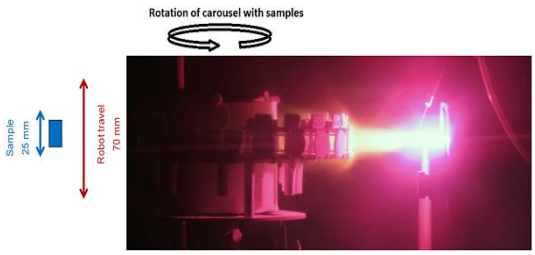

Fig. 2. The configuration of spray set-ups (example for WSP-H 500 plasma torch)

As mentioned previously, the presented studies were a continuation of wider research plan. The microstructural features of zirconia coatings sprayed by two low-energy plasma torches can be found here [12,14]. In this work another two different and high-power plasma torches were applied. The detailed characteristics (summarized in Table 2) of both set-ups were as follows:

- WSP-H 500 plasma torch - the latest hybrid version of water stabilized plasma torch (WSP) operating with dual (both gas and water) stabilization modes. It uses a very low working gas flow rate (only 15 slpm of Ar). In addition, the torch consumes about 2 liters of water per hour of torch operation. The water is partially decomposed into hydrogen, oxygen and OH groups and these gases form also the plasma jet. But the torch provides at the same time a high arc power (150 kW) resulting in much higher temperature and enthalpy of plasma than in gas stabilized units [16]. The partial stabilization with Ar also provides a benefit of increased plasma density when compared to the previous WSP torches without hybrid stabilization, which may be also used for suspension spraying [17]. This is expected to provide more effective momentum transfer on the fragmented liquid.

The suspension transportation was realized using conventional pneumatic system. The feeder was equipped with magnetic stirrer also. The slurry was introduced to the plasma jet by the external injection mode. The optimization of appropriate injection angle and pressure was done by application of SprayCam system (Control Vision Inc., Sahuarita, USA). The shadow graphy method was also used for a visualization of the liquid feedstock stream break-up and drop fragmentation in the plasma jet. The injection pressure was adjusted in the range of 3 to 3.2 bars depending on the powder material and suspension preparation. This corresponded to the suspension flow rate of 90 to 100 ml/min.

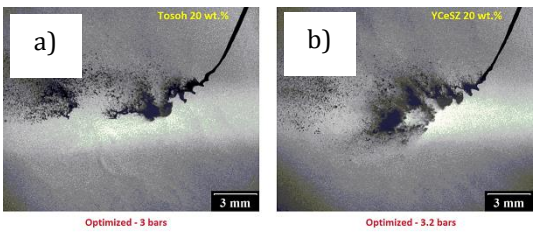

Fig. 3. The optimization of suspension injection pressure by using shadowgraphy (SprayCam)

- Axial III plasma torch - the multi-cathode and gas-stabilized plasma torch. During the coating deposition, the total arc power of 120 kW (40kW per each cathode-anode pair) was used. The plasma gases of Ar + H_2 + N_2 were chosen as a mixture providing high temperature and enthalpy of plasma jet, which is important when spraying refractory materials. The total gas flow was 245 slpm.
  The suspension transportation was realized by the NanoFeed system dedicated for Axial III. The system was equipped with peristaltic pump and mass flow controller. The suspension injection rate was set as 45ml/min. The suspension was mixed during spraying by internal mechanical stirrer. Moreover, Axial III enabled fully axial suspension injection so the optimization of the injection point was not necessary here. The liquid slurry was introduced directly in the center of three separated plasma jets, which joint into one in a common exit nozzle of the torch. This is the only one commercially available plasma torch with such design.

2.4. Coating microstructure characterization

The characterization of zirconia coatings was made by light-microscopy observation (Nikon Eclipse LV100, Tokyo, Japan), which was used to measure the thickness of coatings. Five measurements in three different parts of coating cross-section (15 values at all) were taken to calculate the average thickness. The aimed thickness of both kinds of zirconia coatings was 150μm.

Then, the SEM and EDS studies were performed using Philips XL30 microscope (Eindhoven, Netherlands) equipped with energy-dispersive spectrometer (Oxford Instruments, Oxfordshire, UK). Scanning Electron Microscopy observations allowed to analyze the morphology of coatings. The surface and cross-sectional observations were performed as well. The SEM micrographs were used also to calculate the porosity of coatings. The image editing made by Image J software was done in at least five different regions of each coating (for coatings deposited onto grit-blasted substrates, Table 3). The energy-dispersive spectroscopy studies were done in order to qualitatively evaluate the chemical composition of the coatings.

The phase composition analysis of deposited coatings was performed by the XRD method using Bruker D8 Advance diffractometer (Billerica, MA, USA). The measurements were carried out under Bragg-Brentano geometry with Cu Kα1 radiation and at 2θ in the range 15–120° with step 0.03°. The collected diffractograms were analyzed with dedicated Diffrac+ EVA Software using reference patterns from JCPDS-ICDD database.

The microstructural-crystallographic studies were followed by the electron back-scattered diffraction analysis. First, the selection of appropriate coating area was done under SEM Neon 40ESB (Carl Zeiss GmbH). Then, the area was scanned by DigiView EBSD camera (EDAX Inc, New Jersey, USA). The coating cross-section was measured with a step size in the range of 100-150nm and scan speed of 6 to 10 points per second depending on the test area. The data collection and analysis was done by OIM Analysis 6.1 software provided by EDAX. By using the EBSD method, the detailed orientation of grains, grain shape and grain size was investigated.

Finally, the analysis of the coating surface topography was performed. The roughness of the samples was evaluated with non-contact confocal laser scanning microscopy (Olympus LEXT OLS4000, Tokyo, Japan). The free-surface of the coatings was also investigated by using Shape From Shading method. The 3D views of the coating surfaces reconstructed by SFS gave another insight on the surface profile and morphology. The 3D models were created automatically due to the assembling of four local SEM micrographs which were taken by symmetrically located BSD detectors (Phenom G2 pro, Phenom-World B.V., Eindhoven, The Netherlands). The other information about SFS procedure are given in [14].

3. Results

3.1. Coatings sprayed by WSP-H 500 plasma

3.1.1. Morphology of coatings

<u>YSZ</u>

The thickness of YSZ coatings sprayed by the hybrid water-stabilized plasma torch was measured to be between 170 and 180 μm. The coatings had porosity ranging from 13 to 21% depending on the coating morphology (Table 3). Two different types of microstructures were observed when spraying submicrometer YSZ suspension. The first one was columnar-like structure with typical vertical (intercolumnar) voids. The width of separated columns was not uniform, usually having a few tenths of micrometers. The columnar-like coatings were having also the highest closed porosity among all produced samples. The single pores were usually rounded and irregularly distributed in the coating structure. The typical size of the single pores was submicrometric, whereas the clusters of pores reached the total size of several micrometers. Those coatings were having also typical "cauliflower" surface (Fig. 3 a, b). The columnar-like coatings were achieved only for the fine grained YSZ powder and suspension having the lowest content of solid phase (10 wt.%). Those coatings were produced for all three kinds of substrate topographies that were prepared. Furthermore, it should be stressed that the columnar-like coatings were successfully achieved also on flat, grinded, substrate. In this case the coating-substrate interface did not show also any signs of delamination.

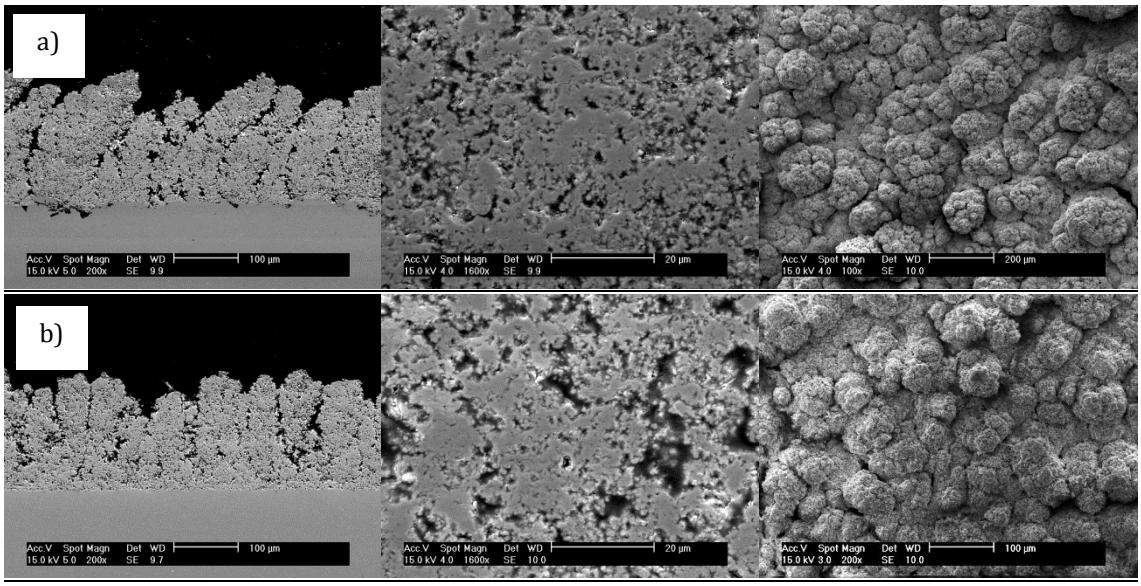

Fig. 4. The morphology of columnar-like YSZ coatings sprayed by WSP-H500 torch: (a) WT101 sample sprayed onto grit-blasted substrate, (b) WT103 sample sprayed onto grinded substrate

The coatings sprayed by using more concentrated YSZ suspensions (20-30 wt.% concentration) were characterized by much denser and so called *two-zones* microstructures. The coatings had porosity in the range of 13 to 16% and the porosity decreased when the suspension concentration increased. The size of closed pores was similar as in case of columnar-like YSZ coatings. The single vertical cracks were observed also within the coating structure, especially for grit-blasted substrates. In the case of the coatings sprayed onto polished or laser treated steel coupons, the single delamination began to occur at the coating-substrate interface. But the coatings were much more homogeneous. The majority of the coating structure consisted of well melted lamellas. However, the single aggregations of fine, sintered or unmelted, powder particles occurred (marked by arrows on Fig. 4 a, b). The coating surface was also smoother than in case of columnar-like coatings. This was observed especially when spraying 30 wt.% concentrated suspensions.

YCeSZ

The YCeSZ coatings were 145 to 186 μm thick depending on the spray run. Afterwards, the calculated average porosity of coatings ranged from 13 to 14% only. Similarly, as in the case of YSZ coatings, the number of pores decreased with the increase in the solid content in the suspension. The coatings sprayed using 10 wt.% suspension showed single clusters of pores, which were almost perpendicular to the substrate surface (see Fig. 5a). The use of more concentrated suspensions (30 wt.% of powder) caused that pores seemed to become more separated and much finer.

But at the same time, single microcracks appeared as well. This was observed especially for grinded or laser treated substrates, in which the local delamination was formed also at the coating-substrate interface.

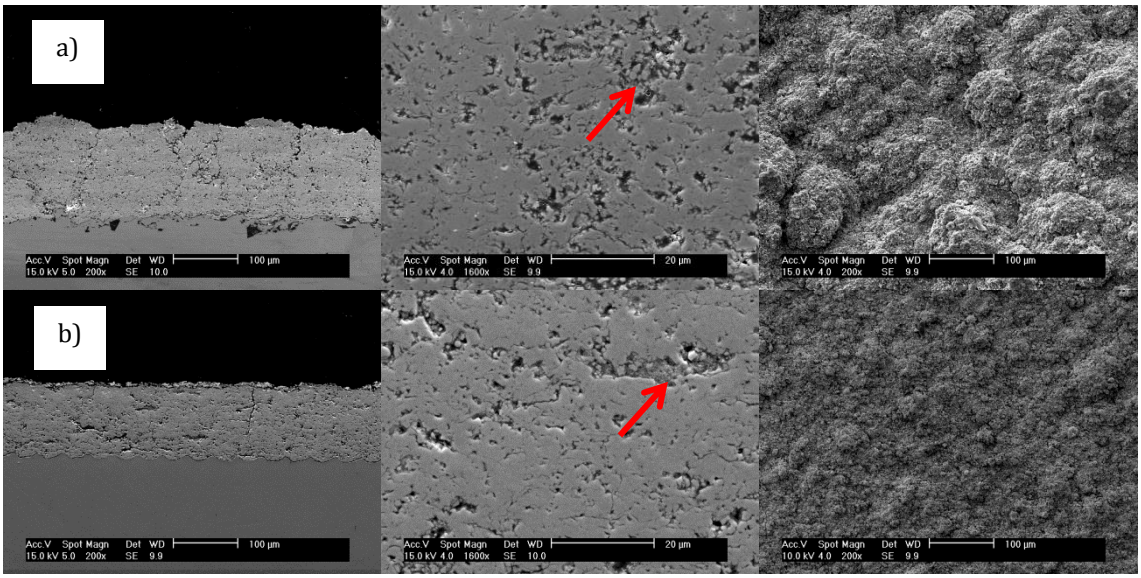

Fig. 5. The example of dense YSZ structures sprayed by WSP-H 500 torch: (a) WT201 sample sprayed onto grit-blasted substrate, (b) WT302 sample sprayed onto laser treated substrate

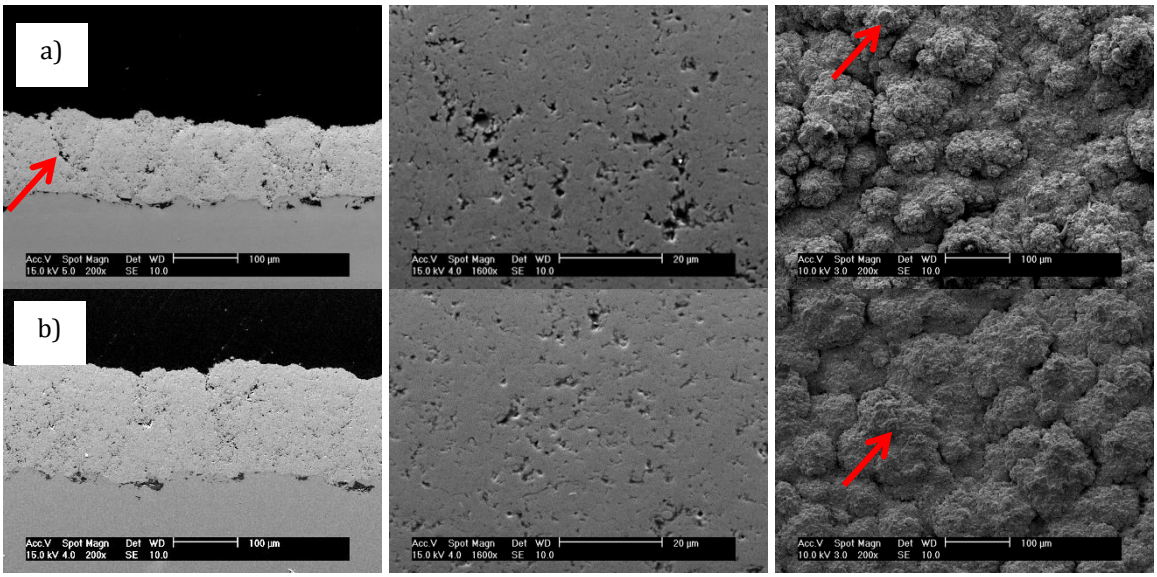

Fig. 6. The dense YCeSZ structures sprayed by WSP-H 500 torch: (a) WC101 sample sprayed onto grit-blasted substrate, (b) WC301 sample sprayed onto grit-blasted substrate

But despite the wider distribution of powder particles size than in case of YSZ, the YCeSZ coatings seemed to be much more homogeneous and better heat-treated in a plasma jet. All coatings showed well-melted lamellar microstructure. The single powder aggregates were observed only on the coating surface (marked by arrows on Fig. 5 a, b). The surface micrographs showed also the fine-grained structure of YCeSZ coatings.

3.1.2. Electron back-scatter diffraction analysis

The electron back-scatter diffraction method was used as an advanced method for the microstructural effects investigations. Thanks to the application of EBSD it was possible to see the orientation and shape of grains in the coating structure. In the case of columnar-like coatings (coating WT102 from Fig. 6 a-c was taken as a representative sample), the orientation of the grains was very random. Moreover, the coating consisted of two different types of grains. The first ones were more spherical and were deposited above the substrate peaks. Those peaks were formed by the laser treatment. The other grains had deformed shape and were no longer rounded. Those grains were more longitudinal (labelled by arrows on Fig. 6 b) and were formed between the substrate patterns. The columnar coatings sprayed onto grit-blasted or grinded substrates did not show the mentioned dual nature of crystals - all of them were nearly rounded. Moreover, the columnar-like coatings were characterized by the highest number of porosity. The pores were also visible on the EBSD map after filtering of the data. Furthermore, the EBSD analysis showed that the analyzed coating consisted mostly of grains of about 0.86 μm (volume-based analysis, see Fig. 6c). But at the same time, there were many very fine grains in the coating structure having the mean diameter of 0.43 μm (number-based analysis). The results corresponded well to the particle size of as-produced YSZ powder used for SPS spraying. The EBSD analysis of YCeSZ coating deposited by WSP-H 500 torch showed much more homogeneous structure than YSZ coatings. The shape of grains was much more uniform. A substantial area of the coating consisted of fine spherical grains. But several larger crystals could be seen also. This corresponded to the grain size plots. According to the volume-based distribution, the medium size of grains was equal to 0.65 μm. On the other hand, the number-based distribution suggested that coating was built mainly by finer grains having a diameter of 0.37 μm. This can be explained by the powder preparation method. The YCeSZ was milled prior to spraying, so many very fine powder particles were created. At the same time, some coarser powders were not milled properly (see powder size distribution in Table 1). Similarly as in case of columnar coatings, no preferred plane of crystal growth was found. The pore size was also significantly lower but the pore clusters were still detectable by EBSD after appropriate data filtering.

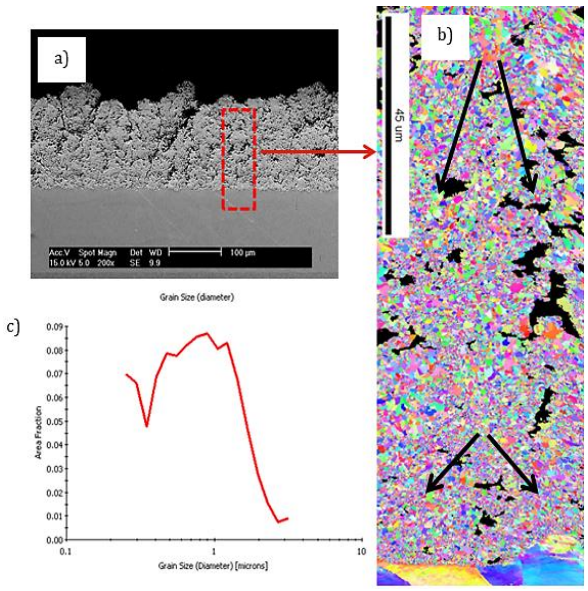

Fig. 7. The EBSD analysis of columnar-like WT102 sample sprayed by WSP-H 500 torch: (a) selection of area, (b) crystallographic orientation map and (c) grain size distribution (volume-based)

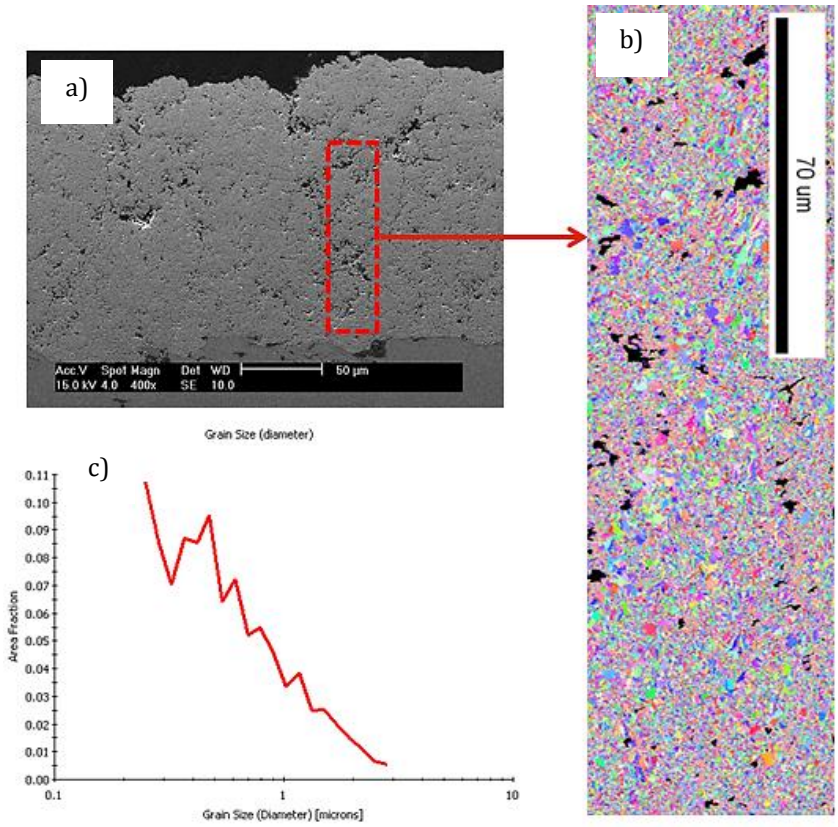

Fig. 8. The EBSD analysis of dense WC301 sample sprayed by WSP-H 500 torch: (a) selection of area, (b) EBSD map and (c) volume grain size distribution

3.1.3. Topography analysis

The results of roughness measurements that were carried by confocal scanning laser microscopy (CSLM) confirmed the previously observed microstructural features of the coatings. The most irregular surface was a domain of columnar-like coatings, which had even two times greater roughness than the other samples (see Table 3). Following, the coating roughness was highly influenced by the suspension concentration prepared for spraying. This phenomenon was observed for YSZ and YCeSZ powders as well. The higher amount of solid in suspension resulted in smoother and more uniform coating surface. Moreover, the substrate preparation was another important parameter affecting the coating structure. The highest Ra values of the coating surfaces were observed for the most irregular, grit-blasted, substrates. The coating roughness of coatings sprayed onto laser treated or grinded substrates was comparable.

Another observations were performed by Shape From Shading (SFS) method. The 3D models of the coating surfaces were reconstructed and investigated. This technique was found to be a very useful tool in order to analyze columnar-like coatings. By using SFS, the column high and width were easily measured. The width of columns was in a range of 70 to 90 µm.

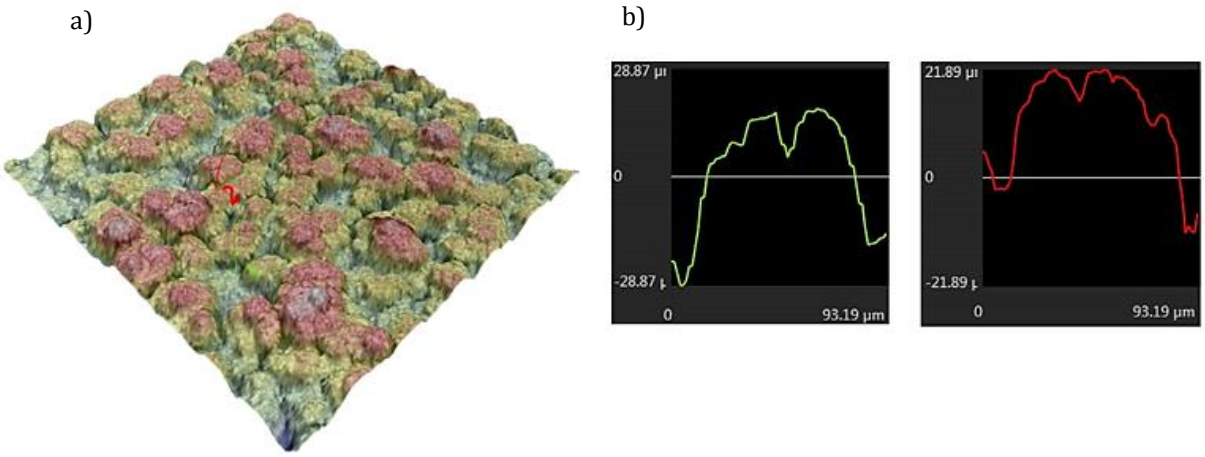

Fig. 9. The reconstruction of WT103 coating surface made by Shape From Shading technique: (a) 3D model, (b) the example of column width analysis

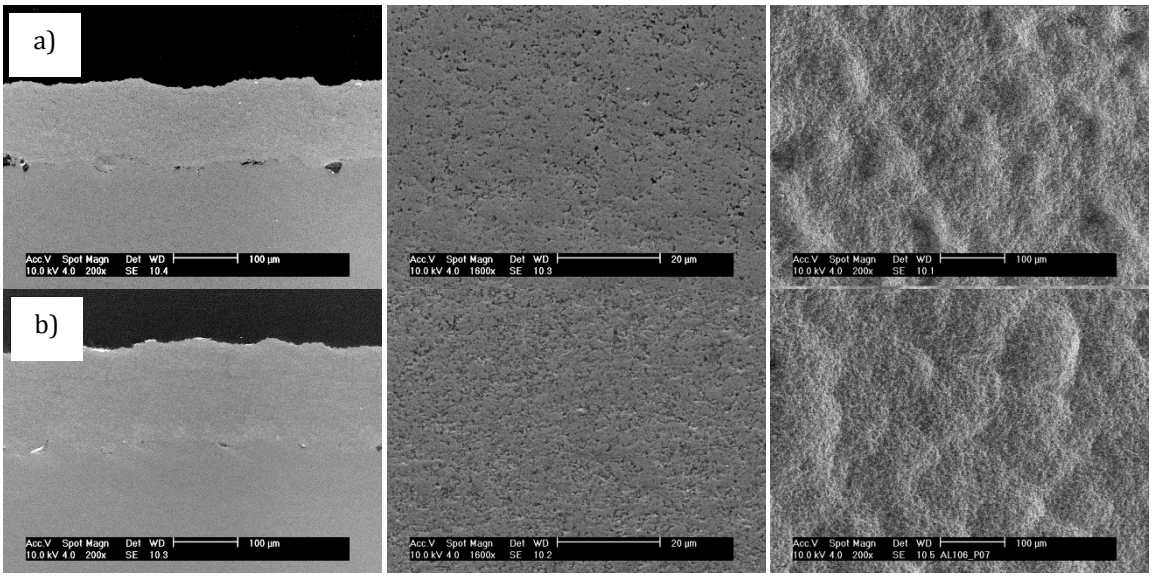

Fig. 10. The example of dense YSZ structures sprayed by Axial III plasma torch: (a) AT101 sample sprayed onto grit-blasted substrate, (b) AT301 sample sprayed onto grit-blasted substrate

3.2. Coatings sprayed by Axial III plasma torch

3.2.1. Morphology of coatings

YSZ

In an opposition to WSP-H 500 plasma torch, the YSZ coatings sprayed by using Axial III plasma torch were very similar in the term of porosity and morphology regardless to the deposition conditions. The columnar like microstructure was not achieved for Axial III torch even when spraying fine YSZ powder. The porosity of coatings was in the range of 10 to 16%. However, the pores had a very small diameter (hundreds of nanometers) and they were homogenously distributed in the whole coating structure (see Fig.9). The pores did not create bigger aggregates as in the case of coatings sprayed by the hybrid water-stabilized plasma torch. Moreover, the suspension concentration did not affect the coating structure and porosity (Table 3). Furthermore, the substrate preparation did not influence the coating morphology at all. The coating surface was wavy and confirmed a fine grained nature of YSZ coatings. The coating-substrate interface was free of defects. But in case of laser treated or grinded substrates, the bonding was much weaker. The coatings had a tendency to delaminate and much more careful metallographic preparation was needed. Finally, the columnar like microstructure was not achieved for Axial III torch even when spraying finer YSZ powder.

YCeSZ

The YCeSZ coatings sprayed by Axial III were the most dense and homogeneous among all produced layers (Fig.10). The porosity was around 5 % only (Table 3). The single pores were very fine, spherical and were not interconnected.

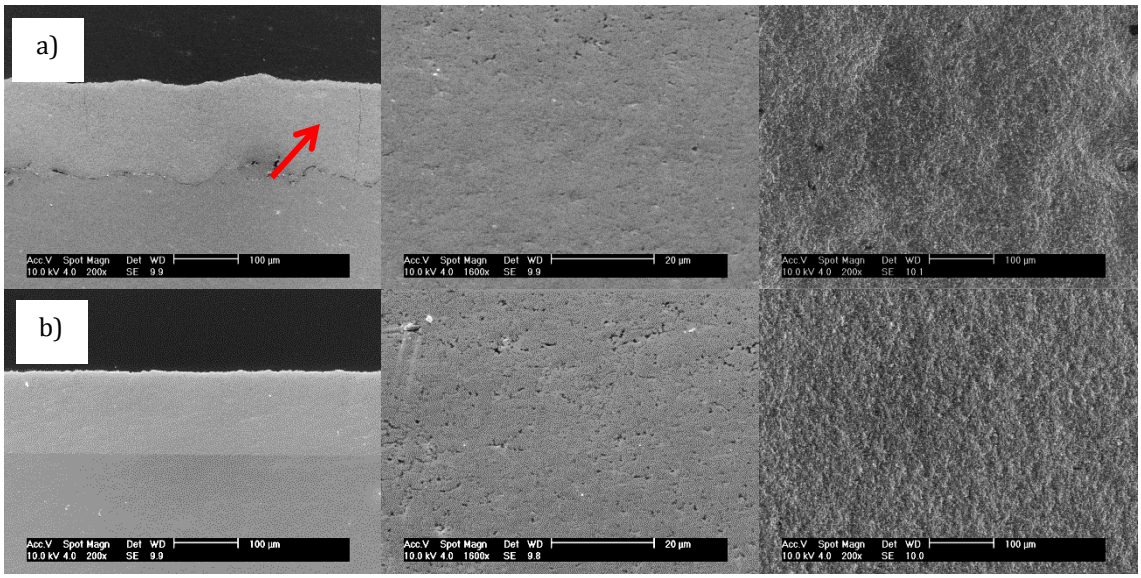

Fig. 11. The example of dense YCeSZ structures sprayed by Axial III plasma torch: (a) AC101 sample sprayed onto grit-blasted substrate, (b) AC303 sample sprayed onto grinded substrate

Table 3 The details of spray process performed by using WSP-H 500 and Axial III plasma torches

			WSP-H 500 torch			Axial III torch		
Powder	Suspension concentrat. [%]	Substrate*	WSP-H 500 sample	Porosity [%]	Roughness Ra; St.dev. [µm]	Axial III sample	Porosity [%]	Roughness Ra; St.dev. [µm]
YSZ	10	GB	WT101	21.0	14.1; 1.6	AT101	10.3	4.5; 0.5
YSZ	10	LT	WT102	-	6.4; 0.8	AT102	-	1.9; 0.2
YSZ	10	G	WT103	-	9.7; 0.3	AT103	-	2.0; 0.3
YSZ	20	GB	WT201	16.3	6.0; 0.4	AT201	16.1	3.9; 0.6
YSZ	20	LT	WT202	-	3.9; 0.4	AT202	-	1.8; 0.2
YSZ	20	G	WT203	-	3.7; 0.4	AT203	-	1.6; 0.1
YSZ	30	GB	WT301	13.1	3.9; 0.6	AT301	15.8	3.1; 0.5
YSZ	30	LT	WT302	-	3.3; 0.2	AT302	-	1.9; 0.2
YSZ	30	G	WT303	-	4.2; 0.4	AT303	-	1.7; 0.2
YCeSZ	10	GB	WC101	11.3	9.0; 1.5	AC101	5.2	2.4; 0.4
YCeSZ	10	LT	WC102	-	3.1; 0.1	AC102	-	2.1; 0.3
YCeSZ	10	G	WC103	-	6.2; 0.6	AC103	-	1.9; 0.2
YCeSZ	20	GB	WC201	12.2	6.3; 0.4	AC201	5.2	2.6; 0.2
YCeSZ	20	LT	WC202	-	3.5; 0.5	AC202	-	1.9; 0.2
YCeSZ	20	G	WC203	-	4.9; 1.1	AC203	-	1.8; 0.3
YCeSZ	30	GB	WC301	7.9	6.7; 0.7	AC301	5.6	2.5; 0.4
YCeSZ	30	LT	WC302	-	3.1; 0.4	AC302	-	2.0; 0.2
YCeSZ	30	G	WC303	-	3.3; 0.5	AC303	-	2.0; 0.3

*GB - grit-blasted, LT - laser treated, G – grinded

The single vertical cracks in YCeSZ coating structure (AC101, labelled by arrow on Fig. 10a) were also observed. But the coatings adhered to the laser treated and grinded substrates much better than in case of YSZ coatings (Fig.10b). The coating-substrate interface was found to be a defect-free. The influence of the feedstock and substrate preparation on the coating structure was observed to be not so pronounced as in the case of hybrid water-stabilized plasma torch. Furthermore, the surface investigations showed that the coatings were very smooth (almost flat, see Fig. 10a, c) and fine grained.

3.2.2. Electron back-scatter diffraction analysis

The EBSD studies confirmed that YSZ coatings deposited by Axial III torch had a very fine grained and uniform structure. The inverse pole figure (IPF) presented in Fig. 10b showed the homogeneous shape and size of grains. Even the use of laser treated substrates did not affect the grain morphology. The longitudinal grains (as in the columnar-like coatings for sample WT102) were not observed. The volume-based mean grain size was of about 0.80 µm (Fig. 10c) and number-based mean size of 0.57 µm. The difference was not that significant as for WSP-H, which also suggest much more uniform grain size. Furthermore, the pores size and pores number was too small to be revealed by the electron back-scatter diffraction analysis with a step size of 100 nm.

A similar results of EBSD analysis were obtained for coatings sprayed using YCeSZ powders. The coatings were very dense and homogeneous, which could be seen on the grains orientation map. Only a slight dispersion in the grain size and grain morphology appeared. The results of grain size measurements were as follows: d_{v50}=0.81 µm and d_{n50}=0.39 µm. But as stated previously for hybrid WSP coating, this wider distribution was a consequence of powder milling needed for suspension preparation. Similarly as in the case of dense YSZ coatings, a very fine porosity of coatings was not revealed on EBSD maps.

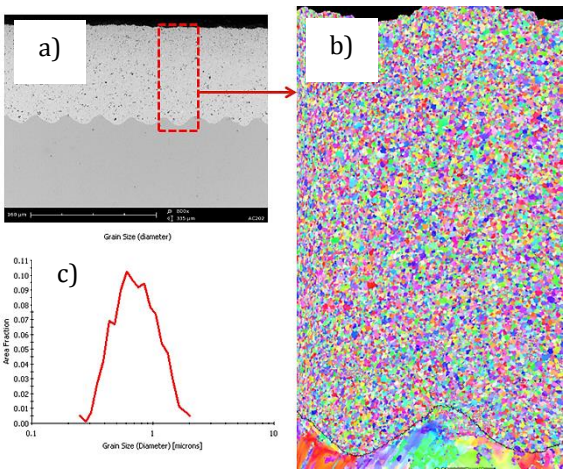

Fig. 12. The EBSD analysis of dense AT102 sample sprayed by Axial III torch: (a) selection of area, (b) grains orientation map and (c) grain size distribution

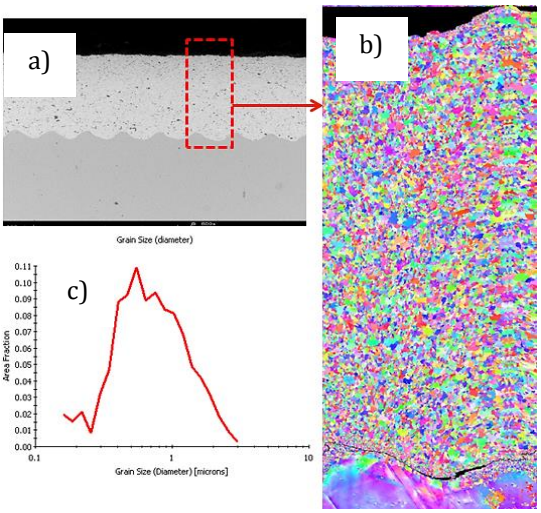

Fig. 13. The EBSD analysis of dense AC202 sample sprayed by Axial III torch: (a) selection of area, (b) crystallographic orientation map and (c) grain size distribution

3.2.3. Topography analysis

The coatings sprayed by Axial III system were much more homogeneous in comparison to those produced by WSP-H 500 plasma torch. It was clearly visible also when comparing the surface roughness of both sets of coatings produced by two torches. In the case of YSZ coatings produced by Axial III, the roughness was even up to 3 times lower, whereas for YCeSZ coatings usually up to 2 times lower.

For YSZ coatings, an influence of the substrate preparation on the surface roughness was observed. The coatings sprayed onto grit-blasted substrates were characterized by almost two times greater Ra value than coatings deposited on laser-treated or grinded substrate. On the other hand, the effect of substrate preparation and suspension concentration on the coating roughness was negligible in the case of YCeSZ coatings. The difference in roughness was very low. All YCeSZ coatings were characterized by Ra in range of 1.8 μm up to 2.6 μm.

Shape From Shading method was not applied for coatings sprayed by Axial III. There was no need to reconstruct 3D models by SFS method because the coatings had almost flat surface with negligible asperities.

3.3. Phase and chemical composition of the coatings sprayed by WSP-H 500 and Axial III torches

The results of XRD and EDS studies are presented together as there was no significant difference between both torches.

The phase composition of YSZ and YCeSZ coatings was almost not changing when comparing to the raw powder material and deposited coatings. According to X-Ray diffraction analysis, the YSZ coatings were characterized by fully-cubic structure, whereas YCeSZ coatings crystalized in tetragonal lattice with a small contribution of monoclinic ZrO_2. The XRD plots were not presented as they were very similar as in case of samples sprayed by low-energy plasma torches and can be seen here [12].

The analysis performed by Energy Dispersive Spectroscopy method also did not show any important difference in the chemical composition of coatings. The content of elements in the coating structure was as follows:

- For YSZ coatings: (i) 13-17 wt.% of yttrium; (ii) 56-60 wt.% of zirconium and (iii) 23-28 wt.% of oxygen,
- For YCeSZ coatings: (i) 3-5 wt.% of yttrium; (ii) 16-20 wt.% of cerium; (iii) 58-63 wt.% of zirconium and (iv) 20-22 wt.% of oxygen.

The results of EDS studies were very similar for all studied coatings. The composition of coatings corresponded also to the composition of initial powder materials. The percentage chemical composition of raw YSZ and YCeSZ powders was calculated and discussed previously here [14].

4. Discussion

The use of two high-energy plasma torches for suspension spraying allowed to successfully produce YSZ and YCeSZ coatings as well. However, the WSP-H 500 and Axial III plasma torches enabled to obtain much various coatings in terms of their microstructures. According to the presented study, the substantial differences in the coating morphology, porosity and surface topography were achieved.

During spraying by hybrid water-stabilized plasma torch, there was a possibility to obtain coatings characterized by different microstructures - starting from columnar up to very dense two-zones structures. On the other hand, the coatings deposited by the Axial III system were very homogeneous with much lower porosity, especially in the case of YCeSZ. At the same time, none of the deposition conditions used for the Axial III torch resulted in deposition of columnar-like coatings. The explanation of this difference seems to be the difference in the design and operation principles of both systems:

- plasma characteristics: the dual stabilization mode in WSP-H 500 torch enables producing of plasma jet having much higher power, enthalpy, temperature and velocity when comparing to conventional gas-stabilized torches [18]. This means, that the generated droplets of liquid feedstock can be well heat-treated. The fragmentation of droplets in the plasma jet is also effective. However, the suspension was injected radially at the distance of 30 mm downstream from the torch nozzle, where the plasma flow is more turbulent due to its interaction with surrounding atmosphere, which can explain more heterogeneous morphology of the deposited coatings,
- injection mode: if the injection is realized fully axially (as for Axial III torch), then the suspension can be introduced exactly in the same direction as the plasma flow occurs. Furthermore, the dispersion angle of the particles travelling in the plasma jest is very narrow. This means also that there is much smaller number of particles travelling in the plasma periphery. Additionally, the particles flow together in a small space of narrow plasma jet [19,20]. As a result, the mechanism of fragmentation of injected stream into fine droplets maybe less intensive than in the case of radial injection mode with much more pronounced shearing of the liquid. Afterwards, all those phenomena cause that powder particles can easily interact

with one another in the plasma jet. Consequently, the particles can form bigger aggregates. Moreover, it was presented already [12,14] that the interactions between: (i) powder particles and plasma jet as well as (ii) plasma particles and substrate are influenced by the adhesion and drag forces (called F_A and F_D respectively). For bigger particles travelling in the core of plasma jet $F_A>F_D$ and for smaller moving in the plasma periphery $F_D>F_A$. For the outlined conditions, the adhesion force seems to be much bigger than drag force. As a result, the molten particles having narrower distribution of temperature and velocity hit the substrate and formulate dense and homogeneous structures (see Fig. 12).

Moreover, the columnar-like coatings were not observed for Axial III even for the laser-treated substrate. The regular peaks of these substrates significantly promote the growth of columns as they intensify the shadowing effect. This was observed in our previous studies [12] and discussed in details by VanEvery et al. [21]. But the characteristic deformations of grains (see for example sample WT102 and longitudinal grains in the coating structure) did not occur in coatings sprayed by Axial III torch. This proves that the particles travel mostly in the hot regions of plasma and did not follow the plasma swirls.

The key process parameter, which can be especially important in the case of Axial III torch, is the powder particle size. As presented by Curry et al. [22], the decrease in the powder particle size promotes the growth of the columnar coatings. The smaller the particles are, the harder for them to maintain the trajectory in the center of plasma jet. The particles travelling in the plasma periphery seem to be therefore needed for a deposition of columnar coatings. In this study the both powders were submicrometer ones. They seem to be to coarse, especially for axial injection mode, as the particles cannot reach the plasma periphery and follow the plasma swirls.

The feedstock preparation can be another important point when discussing the SPS coatings growth-up mechanisms. The suspension optimization and selection of the appropriate dispersant agent was done based on zeta potential measurements [12]. But this is not the only one parameter, which gives the information about the colloid behavior. Another phenomena, like sedimentation velocity or viscosity may play a substantial role in the spray process. Furthermore, the two used experimental set-ups had two different suspension transportation and mixing systems. So the suspension could be also subjected to various phenomena before being injected to the plasma flame. So the influence of suspension transportation should be considered also.

Another interesting issue is the deposition rate during the spray process depending on the powder material but also on the suspension preparation (content of the solid phase). The results for the presented study are showed on Fig. 13. Please note that different sample-torch trajectories had to be used for the WSP-H torch than for the Axial III in order to prevent overheating of the samples and the sample holder. As the result, the deposition rates in terms of thickness increase per deposition pass are only informatory and not mutually comparable for both torches. However, regardless to the setup, the deposition rate of up to 2 μm/pass was achievable. It can be clearly seen that the deposition rate is in both cases influenced by the suspension preparation and powder material. Coatings are formed much faster when more concentrated suspensions were used. The dependency between the deposition rate and suspension concentration is almost linear. The results also show that there are differences in the deposition rate when powders having various morphologies and part icle size distributions are sprayed. Furthermore, it seems that axial injection mode is less sensitive to the differences in powder particle size (see Fig. 13b). Finally, the deposition efficiency plot proves that SPS may be a very effective technology for a production of fine-grained coatings and can be very competitive with other technologies, like for example vapor deposition methods.

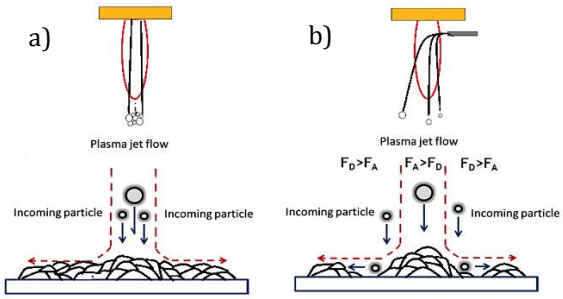

Fig. 14. The coating formation for: (a) axial injection (case of Axial III) and (b) radial injection (case of WSP-H 500) (inspired by [14,20,21])

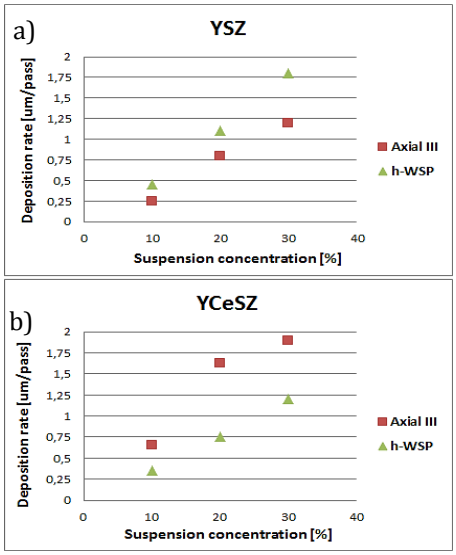

Fig. 15. The deposition rate for both spraying platforms when spraying (a) YSZ and (b) YCeSZ coatings

5. Conclusions

In this study the application of two high-energy plasma torches (called Axial III and WSP-H 500) for Suspension Plasma Spraying was analyzed and discussed. The application of both spraying set-ups allowed deposition of YSZ and YCeSZ coatings from ethanol-water mixture-based suspensions. The deposition of coatings with various microstructures was achieved: the coating characterized by the columnar-like morphology and the porous lamellar structures as well as coatings with very dense microstructure.

The microstructural studies showed an important influence of selected spray variables on the coating micro-

structure. The suspension concentration was one of the crucial parameters affecting the coating morphology and the surface topography. The lower the solid load content was, the coatings were more heterogeneous and their surface more rough. Furthermore, only the lowest concentration of YSZ powder allowed producing columnar coatings. The suspensions with greater powder particles created more dense and homogeneous structures. EBSD studies confirmed also a strong correlation between the feedstock particle size and grain size in the coating structures. The fine-grained microstructures of zirconia-based coatings were also revealed using back-scatter electron diffraction. Laser confocal scanning microscopy (CSLM) showed that there was also strong correlation between the substrate preparation and the coating roughness. Finally, the Shape From Shading was found to be a sufficient method for the quantitative analysis of coatings having columnar-like structure.

The findings in this study shed light on the application of high-power plasma torches for the purpose of Suspension Plasma Spraying. In order to deeply understand the coating growth-up mechanisms another tests are planned. The use of less viscous ethanol suspensions and the application of nanometer-sized powders are the most important ones. This allows better understand the dependences between the coating microstructure and spraying conditions.

Acknowledgements

The help of Stefan Bjorklund and Jonas Olsson (University West, Sweden) as well as Marek Janata, Jiri Kotlan and Jan Medricky (Institute of Plasma Physics, Czech Republic) within the spraying process is thankfully acknowledged. French Embassy in Poland enabled the stay of Paweł Sokołowski at University of Limoges in frame of joint PhD ''Co-tutelle'' program. The part of work realized by the Polish team work was financed by the National Science Centre (Poland) in frame of grant Sonata, UMO-2013/11/D/ST8/03400. The spraying of coatings realized at IPP Prague was supported by the grant GA15-12145S "Physical aspects of plasma spray deposition from liquid feedstock".

References

[1] D. Zhu, H.-T. Lin, Y. Zhou, Advanced Ceramic Coatings and Materials for Extreme Environments: Ceramic Engineering and Science Proceedings, Volume 32, John Wiley & Sons, 2011

[2] M. Wieland, M. Merklein, Wear Behavior of Uncoated and Coated Tools under Complex Loading Conditions, Tribol. Ind. (2012) 11–17

[3] S.C. Cha, A. Erdemir, Coating Technology for Vehicle Applications, Springer, 2015.

[4] D.R. Clarke, M. Oechsner, N.P. Padture, Thermal-barrier coatings for more efficient gas-turbine engines, MRS Bull. 37 (2012) 891–898. doi:10.1557/mrs.2012.232

[5] A. Matthews, The UK surface engineering market, Trans. IMF. 89 (2011) 69–70. doi:10.1179/174591911X12976865501110

[6] F. Gitzhofer, E. Bouyer, M.I. Boulos, Suspension plasma spray, US5609921 A, 1997. http://www.google.com/patents/US5609921 (accessed May 1, 2016)

[7] J. Karthikeyan, C.C. Berndt, J. Tikkanen, J.Y. Wang, A.H. King, H. Herman, Preparation of nanophase materials by thermal spray processing of liquid precursors, Nanostructured Mater. 9 (1997) 137–140. doi:10.1016/S0965-9773(97)00037-8

[8] L. Łatka, A. Cattini, L. Pawłowski, S. Valette, B. Pateyron, J.-P. Lecompte, R. Kumar, A. Denoirjean, Thermal diffusivity and conductivity of yttria stabilized zirconia coatings obtained by suspension plasma spraying, Surf. Coat. Technol. 208 (2012) 87–91. doi:10.1016/j.surfcoat.2012.08.014

[9] S. Kozerski, L. Pawlowski, R. Jaworski, F. Roudet, F. Petit, Two zones microstructure of suspension plasma sprayed hydroxyapatite coatings, Surf. Coat. Technol. 204 (2010) 1380–1387. doi:10.1016/j.surfcoat.2009.09.020

[10] A. Killinger, R. Gadow, G. Mauer, A. Guignard, R. Vaßen, D. Stöver, Review of New Developments in Suspension and Solution Precursor Thermal Spray Processes, J. Therm. Spray Technol. 20 (2011) 677–695. doi:10.1007/s11666-011-9639-8

[11] R. Rampon, O. Marchand, C. Filiatre, G. Bertrand, Influence of suspension characteristics on coatings microstructure obtained by suspension plasma spraying, Surf. Coat. Technol. 202 (2008) 4337–4342. doi:10.1016/j.surfcoat.2008.04.006

[12] P. Sokołowski, S. Kozerski, L. Pawłowski, A. Ambroziak, The key process parameters influencing formation of columnar microstructure in suspension plasma sprayed zirconia coatings, Surf. Coat. Technol. 260 (2014) 97–106. doi:10.1016/j.surfcoat.2014.08.078

[13] A. Joulia, W. Duarte, S. Goutier, M. Vardelle, A. Vardelle, S. Rossignol, Tailoring the Spray Conditions for Suspension Plasma Spraying, J. Therm. Spray Technol. 24 (2014) 24–29. doi:10.1007/s11666-014-0184-0

[14] P. Sokołowski, L. Pawłowski, D. Dietrich, T. Lampke, D. Jech, Advanced Microscopic Study of Suspension Plasma-Sprayed Zirconia Coatings with Different Microstructures, J. Therm. Spray Technol. 25 (2015) 94–104. doi:10.1007/s11666-015-0310-7

[15] P. Sokołowski, L. Łatka, L. Pawłowski, A. Ambroziak, S. Kozerski, B. Nait-Ali, Characterization of microstructure and thermal properties of YCSZ coatings obtained by suspension plasma spraying, Surf. Coat. Technol. 268 (2015) 147–152. doi:10.1016/j.surfcoat.2014.10.006

[16] M. Hrabovsky, Water-stabilized plasma generators, Pure Appl. Chem. - PURE APPL CHEM. 70 (1998) 1157–1162. doi:10.1351/pac199870061157

[17] R. Mušálek, G. Bertolissi, J. Medřický, J. Kotlan, Z. Pala, N. Curry, Feasibility of suspension spraying of yttria-stabilized zirconia with water-stabilized plasma torch, Surf. Coat. Technol. 268 (2015) 58–62. doi:10.1016/j.surfcoat.2014.07.069

[18] M. Hrabovský, Generation of thermal plasmas in liquid-stabilized and hybrid dc-arc torches, Pure Appl. Chem. 74 (2002). doi:10.1351/pac200274030429

[19] P. Fauchais, A. Vardelle, Solution and Suspension Plasma Spraying of Nanostructure Coatings, in: H. Salimi Jazi (Ed.), Adv. Plasma Spray Appl., InTech, 2012. http://www.intechopen.com/books/advanced-plasma-spray-applications/solution-and-suspension-plasma-spraying-of-nanostructure-coatings (accessed August 25, 2016)

[20] A. Ganvir, Microstructure and Thermal Conductivity of Liquid Feedstock Plasma Sprayed Thermal Barrier Coatings, University West, 2016

[21] K. VanEvery, M.J.M. Krane, R.W. Trice, H. Wang, W. Porter, M. Besser, D. Sordelet, J. Ilavsky, J. Almer, Column Formation in Suspension Plasma-Sprayed Coatings and Resultant Thermal Properties, J. Therm. Spray Technol. 20 (2011) 817–828. doi:10.1007/s11666-011-9632-2

[22] N. Curry, K. VanEvery, T. Snyder, J. Susnjar, S. Bjorklund, Performance Testing of Suspension Plasma Sprayed Thermal Barrier Coatings Produced with Varied Suspension Parameters, Coatings. 5 (2015) 338–356. doi:10.3390/coatings503033

PAPER 5

Thermophysical properties of zirconia coatings obtained using suspension with different plasma spray torches

Paweł Sokołowski

(Wrocław University of Technology, Wrocław, Poland; University of Limoges, Limonges, France)

Stefan Björklund

(University West, Trollhättan, Sweden)

Radek Musalek

(Institute of Plasma Physics CAS, Prague, Czech Republic)

Rolando T. Candidato Jr., Lech Pawłowski,), Benoit Nait-Ali, David Smith

(University of Limoges, Limonges, France)

Under review in Surface and Coatings Technology

Printed with permission

THERMOPHYSICAL PROPERTIES OF ZIRCONIA COATINGS OBTAINED USING SUSPENSION WITH DIFFERENT PLASMA SPRAY TORCHES

Paweł Sokołowski [a,b], Stefan Björklund [c], Radek Musalek [d], Rolando T. Candidato Jr. [b], Lech Pawłowski [b], Benoit Nait-Ali [b], David Smith [b]

[a] *Wroclaw University of Science and Technology, ul. Łukasiewicza 5, 50-371 Wrocław, Poland*
[b] *University of Limoges, 12 rue Atlantis, 87068 Limoges, France*
[c] *University West, Gustava Melins Gata 2, 461 86 Trollhättan, Sweden*
[d] *Institute of Plasma Physics CAS, v.v.i., Za Slovankou 3, 18200 Prague, Czech Republic*

The paper describes a production of various ceramic top coats of Thermal Barrier Coatings (TBC) by Suspension Plasma Spraying (SPS). The spray process realized with different plasma torches allowed obtaining coatings having different microstructures. The microstructures influenced the thermal transport properties of TBC's.

The study analyses the thermal transport properties of yttria and yttria with ceria stabilized zirconia coatings, i.e. YSZ and YCeSZ, respectively. The powders used to formulate the suspension were submicrometric in size. The spray processes were realized with the use of three different plasma spray torches: (i) SG-100; (ii) Axial III and (iii) hybrid WSP torch. The deposition parameters were designed for each plasma torch separately. The microstructure of coatings was then analyzed using Optical and Scanning Electron Microscopy i.e. OM and SEM, respectively. The thermophysical properties of the coatings such as density, specific heat and thermal dilatation were measured using gas pycnometry, calorimetry and dilatometry methods respectively. The collected data were used, together with thermal diffusivity found with the use of Laser Flash Analysis (LFA) method, to calculate the thermal conductivity of the deposits. Thermal conductivity values were validated values with the use of a so called response function method.

Keywords: *Thermal Barrier Coatings (TBC), Suspension Plasma Spraying, thermal conductivity, specific heat, thermal dilatation, response function method*

1. Introduction

The important element of gas turbines quality and efficiency are Thermal Barrier Coatings mostly used in the aviation industry. Still, commonly used are still two-layer TBC's developed in the late 1970-ties [1,2]. This type of TBC includes oxidation resistant metallic bondcoat and thermally insulating ceramic topcoat [3,4]. The complex structure of multilayer systems and severe working condition in gas turbines causes many operational and material problems such as thermally grown oxides (TGO) layer control, calcia-magnesia-alumina-silicate (CMAS) attack behavior, thermal shock and hot corrosion resistances, etc. That makes the TBC system life-time difficult to predict [5,6].

Another unresolved and very important issue determining the development of multilayer TBC's technology is the possibility to achieve high thermal insulation properties associated with high fatigue resistance [7]. Both properties are highly influenced by the microstructure of ceramic topcoat layer. The heat conduction through the solid materials, which is the key property in the case of current TBC's, is limited by the porosity of coating. The size of pores and its distribution as well as their shape need to be known and controlled also. Furthermore, the coatings' internal defects, such as cracks or voids, may also significantly reduce heat flow through the coating [8,9]. On the other hand, the requirements concerning the microstructure of coatings having high cyclic fatigue resistance are very different. The columnar microstructure resulting in low in-plane elastic modulus would be recommended in this case. This kind of microstructure allows and easy accommodation of strains generated during cyclic compression and tension of TBC system. The main source of strains is the thermal expansion mismatch between metallic bondcoat and ceramic top coat. This mismatch can be slightly reduced by porosity and brick-wall microstructure of plasma sprayed coatings [10–12].

Suspension Plasma Spraying enables obtaining the coatings with microstructure useful for both mentioned properties of TBC's. In fact, the microstructure combines the most valuable features of vapor deposited films, e.g. using EB-PVD and of atmospheric plasma sprayed (APS) coatings using coarse powders. Firstly, the obtaining of columnar-like microstructure with controlled width is possible [13]. On the other hand, the SPS coatings are very porous and pores size is submicrometer or even nanometer [14].

In this work, the careful analysis of thermal transport properties of Suspension Plasma Sprayed zirconia coatings having various microstructures was carried out. Two coatings morphologies were identified, namely, *columnar-like* and *two-zones microstructure* and related to the spray conditions. The thermophysical properties of the coatings having these microstructures were evaluated.

2. Materials and methods

2.1. Spray process description

Two different powders (having different chemical composition and particle size) were used to formulate suspension for spray processes:

- yttria fully stabilized zirconia, YSZ, powder (ZrO_2 + 14 wt.% Y_2O_3, TZ-8YS, Tosoh, Japan) having main particle size $d_{v50} \cong 400$ nm and cubic structure;
- both yttria/ceria stabilized zirconia, YCeSZ, (ZrO_2 + 24 wt.% CeO_2 + 2.5 wt.% Y_2O_3, Metco 205NS, Oerlikon Metco, Switzerland) having main particle size $d_{v50} \cong 700$ nm and mixed tetragonal-monoclinic-cubic structure.

YSZ powder was used as-produced whereas commercial YCeSZ powder was designed for conventional powder plasma spraying and the powder particles were to coarse for SPS. Therefore, Metco 205NS powder was mechanically crushed in order to obtain submicrometer powder particles. Well-known ball-milling method was used to decrease the size of powders. The final morphology of both powders is presented in Fig. 1.

Afterwards, the powders were formulated in a water/ethanol (50 vol. %/50 vol. %) based suspensions. The suspensions had various content of solid being in the range of 2.5 up to 30 wt. %, depending on type of torch and operational spray parameters. Suspensions were homogenized, stabilized by the addition of dispersant agent (Beycostat C213, CECA). All details regarding powder characterization (powder particle size distribution, chemical/phase composition, morphology analysis) and suspension formulation method are shown elsewhere [15].

The coatings were prepared in multiple-parameters spray process experiments in which the influence of important spray parameters on internal microstructure and build-up mechanism of coatings was investigated (please, see [16,17] to know more details about spraying and plasma torches characteristics). The modification of: (i) powder material; (ii) suspension concentration; (iii) substrate topography; and finally, (iv) plasma torch resulted in spraying of coatings having very different microstructures. In total, 72 different spray runs were carried out using YSZ and YCeSZ based suspensions. The selection was carried out and the coatings having opposite microstructural features, namely:

- columnar-like or lamellar;
- homogeneous or heterogeneous;
- dense or very porous microstructure,

were selected for thermophysical properties characterization. The key spray process variables are presented in Table 1.

Due to the fact that the investigations were performed at relatively high temperatures, all coatings were sprayed onto temperature-resistant nickel super alloy (Inconel 600, UNS N06600). The substrates were 2mm thick and were sand-blasted and cleaned in ultrasonic bath in ethanol prior to the spraying.

Table 1 The key process parameters used to produce coatings

Torch	Injector	Injection angle	Electric power [kW]	Arc stabilization mode	Plasma forming gases
SG-100	Internal	Radial	Low (40kW)	Gas	$Ar+H_2$
Axial III	Internal	Axial	High (120kW)	Gas	$Ar+H_2+N_2$
WSP-H 500	External	Radial	High (150kW)	Water	$Ar+H_2O$ decomposition products [3]

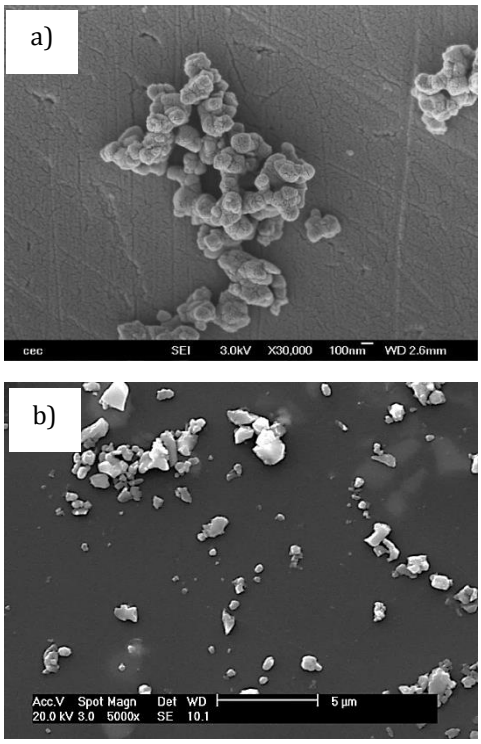

Fig. 1. Yttria stabilized zirconia (a) and yttria/ceria stabilized zirconia (b) powder used for spraying

2.2. Microstructure characterization

The microstructure of zirconia coatings selected for thermophysical properties investigations was carefully characterized. Thickness of coatings was determined with the use of the metallographic cross-sections with the help of light microscope (Nikon Eclipse LV100, Tokyo, Japan), whereas their morphology was characterized by Scanning Electron Microscopy (Philips XL30, Amsterdam, Netherlands) using the detectors of secondary electrons (SE) and back-scattered ones (BSD). The observations were carried out on the cross-sections of coatings and on their surfaces. The porosity of coatings was determined basing on SEM micrographs. The total area of pores was calculated in the ImageJ software using at least

[3] Hydrogen, oxygen and OH groups as a products of decomposition of water vortex inside a torch during the torch operation

five coating micrographs taken in the different regions of samples (see Table 2). More advanced microstructural studies of YSZ and YCeSZ zirconia coatings, which were sprayed according to the design of experiments (DoE) are shown elsewhere [16,17].

Table 2 Thickness and porosity measurements together with the samples description (coatings selected for thermophysical properties investigations)

Sample name	Thickness [µm]	Standard deviation [µm]	Porosity [%]	Standard deviation [%]
ST21	66.1	3.7	21.4	2.7
AT101	139.0	2.5	10.3	1.7
WT101	176.0	30.8	21.0	3.2
WT201	165.6	9.9	16.3	3.6
WT301	179.2	10.0	13.1	1.6
SC51	105.2	3.8	15.5	1.5
SC101	96.5	7.5	13.2	0.9
AC201	168.6	4.5	5.2	0.8
AC301	186.6	5.1	5.6	0.1
WC101	145.4	11.3	10.2	1.2

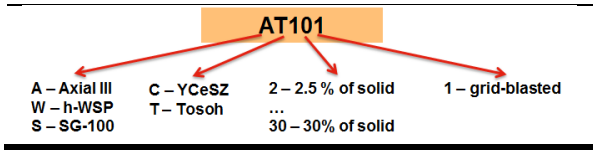

2.3. Density measurements

The gas pycnometer method was applied (AccuPyc II 1340 Pycnometer, Micromeritics, USA) to determine the coatings densities. This technique enables measuring very precisely volume of materials. Then, after having found the mass of samples, the density of materials was calculated. The internal porosity of materials may influence the values of volume measured by a pycnometer. To estimate the effect of closed porosity, the densities of: (i) raw powders, (ii) ball-milled powders (YCeSZ); and, (iii) mechanically crushed coatings, were determined and compared. Helium was used as a working gas in pycnometric measurements. For each powder 10 measurements were performed and then average value was calculated (see Table 3). The powders were dried before pycnometer test. The density of Inconel 600 substrate was determined using the same procedure.

2.4. Specific heat capacity investigations

Two different approaches were used in order to examine specific heat of coating materials. Firstly, differential scanning calorimetry (DSC) was applied. The measurements were carried out in the following different temperature ranges using with different set-ups:

- range from 40°C up to 200°C (Setaram C80, France). The use of 3D Calvet sensor in form of a ring, which surrounds the whole sample, allowed determining c_p value with the highest level of accuracy here. An increased capacity of the crucible enabled to measure between 10 to even 20 g of the coating material. The heating rate was set as 0.2 °C/min;
- range from 30°C up to 500°C (TA Instruments Q1000, USA). The measurements were performed in modulated DSC mode (called MDSC, where the modulation was ± 1°C every 100 s) as it enhances the sensitivity of measurements and separates properties of material from its thermal history. This mode is often used also for complex materials [18]. The standard hermetic, crimped, alumina pan was used. With this kind of crucible it was possible to measure from 5 to 8 g of coating material in a form of powder. The specific heat of Inconel 600 was measured using this set-up also. In the case of nickel super alloy a small cube was inserted in alumina pan. Furthermore, nitrogen was used as a cell purge gas here.

For the purpose of c_p measurements both zirconia coatings (YSZ and YCeSZ) were delaminated and crushed. This allows good filling of DSC crucibles and improved heat flow through the material. Both calorimeters were also calibrated using sapphire samples prior to c_p investigations. All powders were dried prior to the measurements.

In order to know specific heat capacity values of coatings in higher temperature range Kopp's law (known also as "rule of mixture") was applied. Based on the chemical composition of coatings the c_p values were calculated using the following formula:

$$c_p(T) = \sum_{i=1}^{n} c_{pi}(T) \cdot f_i \qquad (1)$$

Where c_{pi} is specific heat of the i-th compound forming alloy [J/(kg·K)], f_i denotes the mass or atomic fraction the i-th constituent [%], and n - the total number of constituents [-]. The general chart was plotted with c_p values determined using both DSC measurements and theoretical values obtained by Kopp's law. Then, the behavior of curves was evaluated in order to see if there is any correlation between the results.

2.5. Thermal dilatation determination

The thermal expansion elongation of coating material was measured. First, the coating was attempted to be removed from the substrate and then cut into the desired sample shape from the coating material. However, due to the small thickness of the coatings sprayed by SPS and their high adhesion to the substrate, this approach was not succeeded. Consequently, the coatings for the dilatometric measurements were sprayed by conventional APS method using coarse powders. YCeSZ had the same chemical composition as the powder used for SPS. The YSZ powder used for APS had lower Y_2O_3 content (8 wt. % instead of 8 mol. %). The thickness of APS sprayed coatings was about 2 mm and they were sprayed onto coupons having the diameter of 25 mm. Their microstructure is shown in Fig. 2a. Dilatometry measurements were performed first on 2 mm samples. The size of samples was limited by the thickness

of coatings. The thermal expansion was investigated in two different configurations - horizontally (parallel to the substrate) and vertically (perpendicular to the surface) as shows it Fig. 2b. It was done to evaluate the expected anisotropy of thermal expansion in the coatings. It must be however underlined that length of the sample influences the accuracy of CTE measurements. So the 10 mm long samples were prepared also and measured in order to validate obtained values (measurements were conducted only in horizontal position here due to the dimensions of coatings). The dilatometry test was also performed for Inconel 600. The 10 mm long substrate samples were investigated and the procedure was the same as in the case of zirconia coatings.

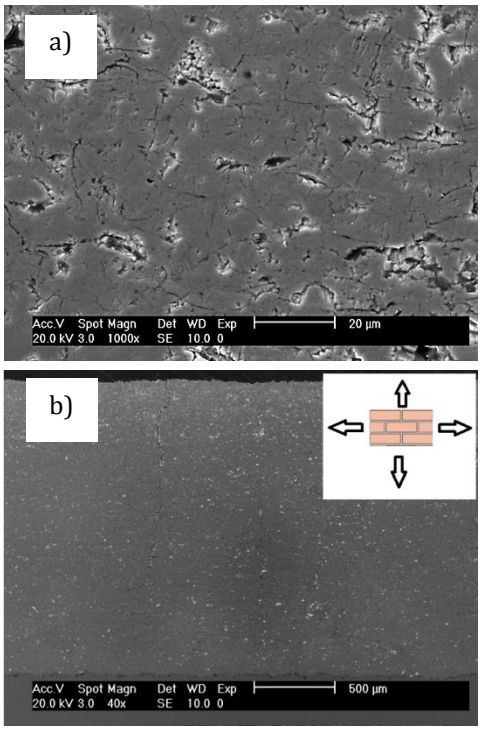

Fig. 2. The example of APS sprayed coating (YSZ) used for thermal expansion measurements: microstructure (a) and the configuration of the dilatometry measurements according to the coating (b)

The measurements were performed using push-rod dilatometer (Netzsch DIL 402 C, Germany). The thermal expansion was measured during heating and cooling as well. The temperature cycle was as follows: room temperature (RT) – 1200 °C – RT. The measurements were performed in the argon atmosphere. Both heating and cooling rate were equal to 2 °C/min. The testing procedure was as follows: (i) determination of correction values for dilatometer by measuring alumina standard sample, (ii) appropriate measurements of zirconia coatings and determination of thermal elongation by dedicated Proteus® software.

2.6. Thermal diffusivity and thermal conductivity determination

Laser flash analysis (LFA) using set-up of Netzsch LFA 427 (Germany) was applied to measure thermal diffusivity of the substrate and of selected zirconia coatings. The set-up was equipped with laser source that generated the heat impulse applied to the rear sample side (metallic substrate) and an InSb detector to observe the temperature change on the ceramic coating surface. The measurements were carried out starting from RT up to 1000°C (YSZ coatings and Inconel 600) or up to 800°C (YCeSZ coatings) and were done in argon atmosphere. The samples were coated with the graphite aerosol spray prior to measurements to improve emission and absorption properties of samples, avoid reflectivity of metallic substrate and finally increase the signal-noise ratio.

Thermal diffusivity of Inconel 600 was found with the use of Cowan model (see Fig. 3) [19]. The diffusivity value was helpful in analyzing thermal diffusivity of zirconia coatings. The sample composed of coating with substrate was considered as two-layer system. The diffusivity of coating material was found using the model by taking into account the corrections resulting from heat losses, pulse duration. The thermal contact resistance between the coating and substrate was not considered.

Afterwards, having thermal diffusivity values, thermal conductivity of coatings was calculated using following formula:

$$\lambda(T) = \alpha(T) \cdot c_p(T) \cdot \frac{\rho_{300}}{1+3\frac{\Delta L}{L}(T)} \qquad (2)$$

where α (T) is thermal diffusivity [m^2/s], ρ_{300} is apparent density in ambient temperature [kg/m^3], and $\Delta L/L$(T) is thermal expansion.

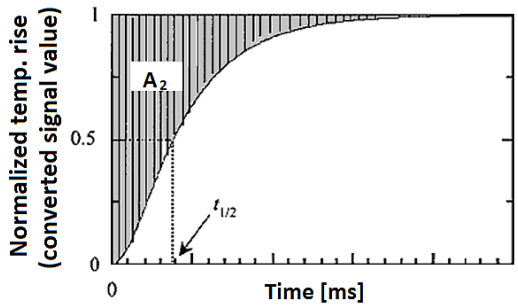

Fig. 3. Graphical interpretation of areal heat diffusion time based on LFA signal curves and $t_{1/2}$ (half time) used for analysis of Inconel substrate using Cowan model

As the measurement by laser flash method of multi-layer systems may lead to many errors, the verification of obtained thermal conductivity values is useful. An approach, chosen in this study, is called „response method" and was proposed firstly by Baba et al. [20]. The method bases on the signal curve obtained from LFA measurements. In this study, the signal curves were normalized first: the initial temperature was defined as "0" and the maximum temperature was "1". This allowed comparing all signal curves. Afterwards the "areal heat diffusion time" (see Fig. 3) was calculated. The size of this area is influenced by the thermophysical properties of the system which is subjected to the heat flux. Finally, having exact properties of substrate and both zirconia coatings as well, thermal conductivity of the coatings was calculated using proposed equation [21]:

$$\lambda_2 = \frac{d_2^2 C_{p2}\rho_2(3d_1C_{p1}\rho_1+d_2C_{p2}\rho_2)}{6A_2(d_1C_{p1}\rho_1+d_2C_{p2}\rho_2)-d_1^2C_{p1}\rho_1(d_1C_{p1}\rho_1+3d_2C_{p2}\rho_2)/\lambda_1} \quad (3)$$

Where A_2 is the surface area corresponding to thermal diffusion time (see Fig. 3), d_1, d_2 are the substrate and coating thicknesses [m], λ_1 is thermal conductivity of substrate [W/(m·K)] and the subscripts 1 corresponds to substrate and 2 – to coating.

Finally, the values of thermal conductivity obtained experimentally and analytically were compared and analyzed.

3. Results and discussion

3.1. Microstructure of coatings

Ten of the most distinctive samples of YSZ and YCeSZ from the extensive spraying plan (72 spraying conditions) were selected for the thermophysical properties measurements. The criterion of choice was to the samples having different porosity level, internal microstructure and surface topography.

YSZ coatings, presented in Fig. 4, had different microstructure and porosity. The use of the suspension formulated with finely grained powders and different solid phase content associated with various spray setups allowed obtaining coatings having porous *columnar microstructure* and, on the other hand, very dense microstructure. The coatings porosity varied between 21.4% (ST21) and 13.1% (WT301). But the size of pores and their distribution varied in all YSZ coatings. Dense coatings (like AT101 and WT301) were characterized by regularly distributed pores in the coating structure. The porosity in the coatings ST21 and WT101 is heterogeneous and the pores distribution is very random. Some of the coatings, namely that obtained in run WT201, exhibited vertical cracks. It should be added that the lower- and upper-limit values of porosity of coatings were obtained with the lowest and highest suspension concentration, respectively. Some more discussion about the microstructure of coatings can be found elsewhere [16,17].The microstructure of YCeSZ samples is presented in Fig. 5. The *columnar-microstructure* could be not created, due to the greater size of powder particles used for suspension preparation (more details are shown elsewhere [16]). Only coatings with fine lamellar structure were obtained. The observed porosities were very different starting from 15.5% for sample SC51 up to 5.2% for sample AC201. The porosity and distribution of pores and their size were again strongly influenced by the suspension concentration used for spraying. The shape and size of pores was more heterogeneous when the total porosity was greater (samples SC51 and WC101). The pores were more regular and homogeneously distributed for dense coatings. This effect was observed mostly when the high-power plasma torches were used (as Axial III or WSP-H 500).

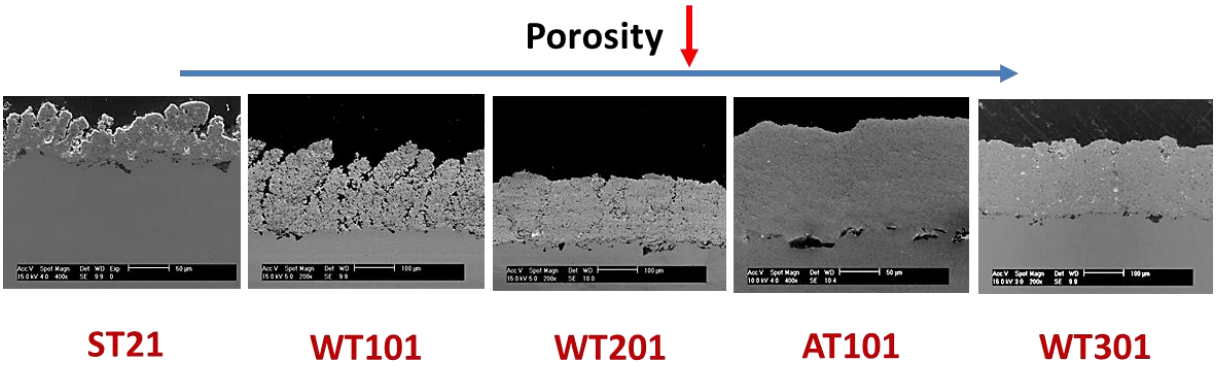

Fig. 4. Micrographs of YSZ coatings selected for thermal transport properties measurements. From the left: ST21, WT101, WT201, AT101, WT301 (the order according to the decrease in porosity)

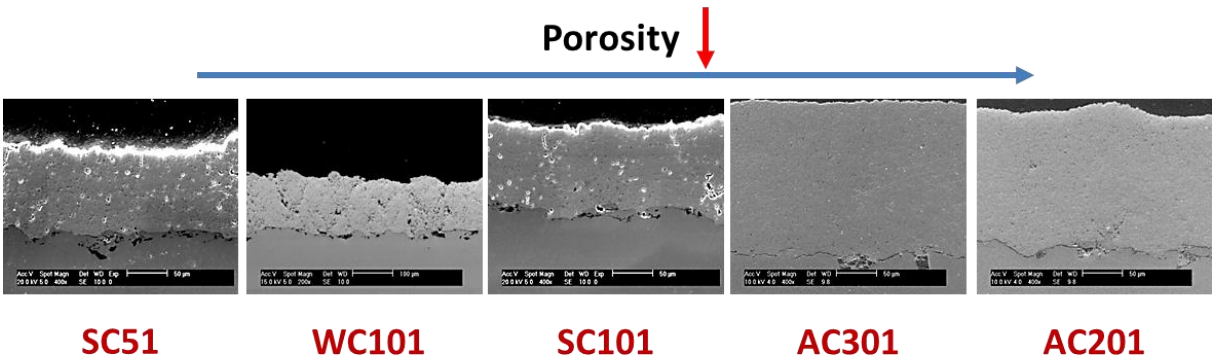

Fig. 5. Micrographs of YCeSZ coatings selected for thermal transport properties measurements. From the left: SC51, WC101, SC101, AC201, AC301 (the order according to the porosity decrease)

3.2. Thermophysical properties

One of the key properties necessary for thermal diffusivity and thermal conductivity investigations is the value of bulk density of coating. Based on this value the apparent density in ambient temperature (ρ_{300}) can be calculated. The pycnometric measurements showed that the values of coatings' densities were significantly higher than the density of powders that were used for spraying. The greatest difference was observed in the case of YCeSZ. The smallest density (5.507 g/cm^3) was recorded for the coarse, as-produced, YCeSZ powder. Metco 205NS powder is produced by spray-drying followed by heat treatment and the resulting powder particles are often hollow inside. After milling the hollows could have been opened and the density of fine powder was greater. Finally, after spraying and crushing of coating, the porosity even more reduced and the bulk density was estimated. The measured values of bulk coating density were very similar to the values reported in the literature [22]. The density of stabilized zirconia was influenced by the type of stabilizer and by its content. The density can be approximated by the rule of mixtures. The density of ZrO_2 is equal to 6200 kg/m^3 (according to the X-ray density of the cubic phase found from the elementary cell's dimension and mass using ASTM pattern 27-997), of Y_2O_3 is 5031 kg/m^3 (using X-ray density of cubic phase ASTM pattern 25-1200) and that of CeO_2 is equal to 7647 kg/m^3 [23,24]. This assumption was in agreement with measured YSZ coating density but the theoretical value for YCeSZ would be higher due to the CeO_2 content having greater mass. However, more precise approach taking into account the complex phase composition and atomic arrangements in the crystal structure should be used to define theoretical density of YCeSZ more precisely.

Table 3 The results of density measurements

	Average density value [g/cm^3]	Standard deviation [g/cm^3]
YSZ-powder as-produced	6.000	0.004
YSZ-crushed coating[4]	6.099	0.005
YCeSZ-powder as-produced	5.507	0.003
YCeSZ-powder after milling	5.825	0.005
YCeSZ-crushed coating*	6.108	0.009
Inconel 600	8.415	0.003

The specific heat of coatings was investigated empirically (in low temperatures) and extrapolated for high temperatures according to Kopp's law. The general chart presenting c_p values of YSZ and YCeSZ determined using both DSC measurements and values obtained by Kopp's law is presented in Fig. 6. The important point was to observe the trend of all curves and difference in c_p values. The difference between the obtained results was not greater than 10%. The curve of specific heat vs. temperature calculated by the rule of mixtures was between two curves obtained experimentally. This was particularly true for YSZ coatings, where the value found from Kopp's law constituted almost an average value between the c_p values measured different experimental set-ups. The difference between the values obtained using two calorimeters can be associated with e.g. various operational procedures and the difference in quantity of materials that was measured. The study of de Barros et al. [25] indicates that the sample mass has a significant effect on c_p values found using modulated DSC set-up. The precision of measurements get lower with decreasing samples' mass. It should be mentioned here also, that there is many other factors that can affect DSC measurements precision (e.g. related to the instrument itself, sample characteristics, calibration method and standard material etc.). A slight effect can be assigned also to the structure of the material, like grain size, crystallographic structure, dislocation density etc. [26]. Due to the high sensitivity of DSC method the results was satisfactory, especially when comparing to the literature data found in Ref. [27]. Finally, it was concluded in the view in all c_p results, that specific heat values calculated using Kopp's law are precise enough. Consequently, these values were used for thermal diffusivity and conductivity evaluation at high temperatures.

Another thermophysical property examined in this study was thermal dilatation of coatings prepared by plasma spraying of powder instead of suspension. The microstructure of SPS sprayed coatings is comparable to the APS ones for dense structures [28]. Both types of coatings include many lamellas formed by molten powder particles creating brick-wall structure. The biggest difference concerns the size of lamellas (that are much greater in case of APS) and *the columnar-like* microstructure of some coatings is produced by SPS. But the approach seems to be much more accurate than measuring the thermal dilatation of bulk zirconia.

The measurable anisotropy of $\Delta L/L$ values was found in zirconia coatings (Fig.7). This effect was observed previously in powder plasma sprayed coatings by e.g. Berndt et al. [29]or Ilavsky et al. [30]. This phenomenon can be influenced by a few factors, the most important among them are as follows:

- *brick-wall* like structure i.e. lamellar layered structure combined with the complex network of voids and pores preferentially oriented according to the spraying conditions [31];
- multiphase composition of coatings [32].

[4] this value was taken for apparent coating density calculations, where $\rho_{300} = (1\text{-P})\cdot \rho$, P being porosity

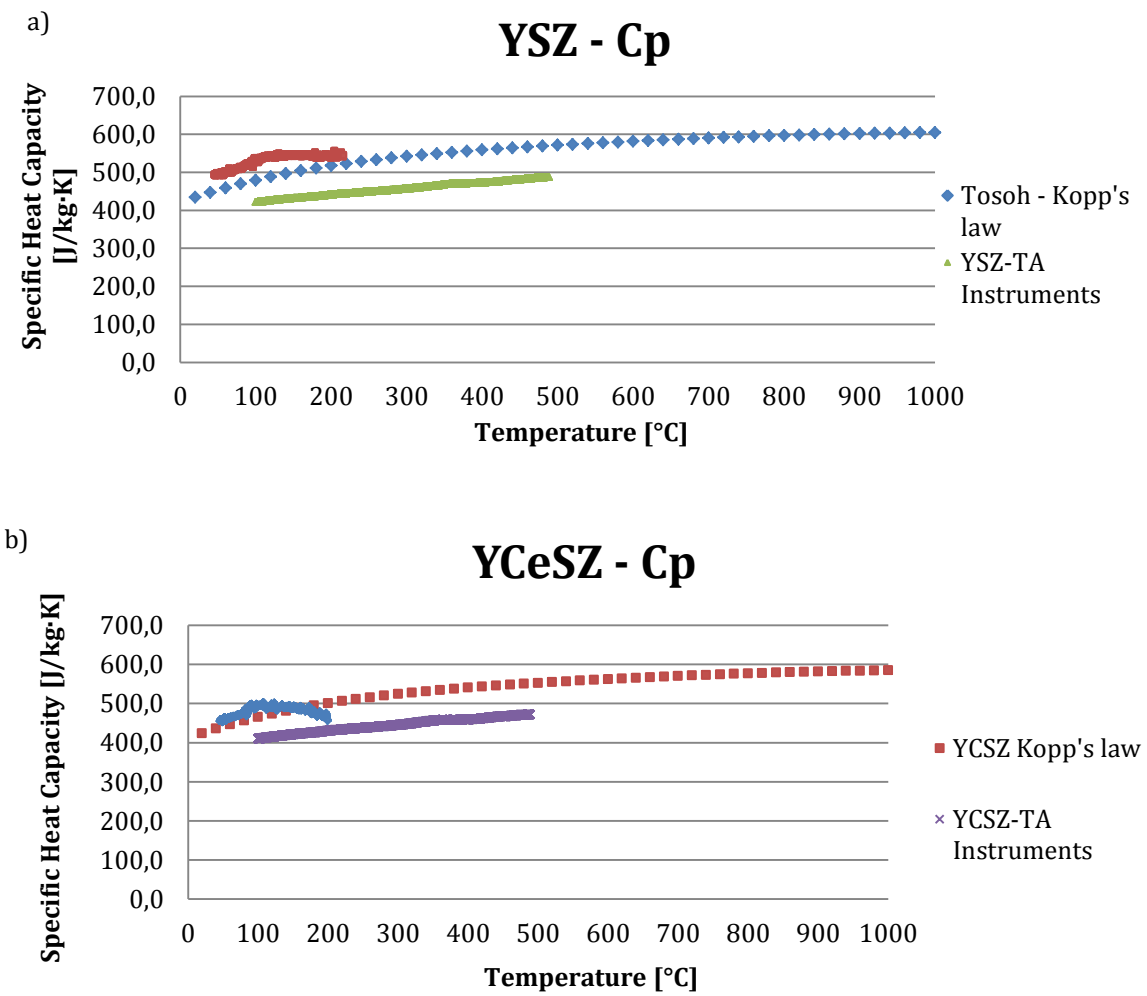

Fig. 6. Specific heat capacity values of YSZ (a), YCeSZ (b)

Based on the results, both coatings showed lower values of thermal expansion in a vertical direction (according to the spraying direction). As there was not that many studies focused on anisotropy of thermal expansion of plasma sprayed coatings, the phenomena can be analyzed based on mechanical properties, like stiffness or elastic modulus. Sevostianov and Kachanov [33] proposed the expression of "inverse anisotropy", where the elastic modulus and stiffness of coatings were higher in normal direction to the substrate material. This was explained by the scattering of pores orientation in the thermally sprayed coatings. Consequently, the materials having higher stiffness present a lower thermal expansion coefficient [34]. On the other hand, there is many studies, was observed that the elastic modulus may be even two times bigger in horizontal direction, parallel to the coating surface than in the direction perpendicular to the coating's surface [30,31]. This phenomenon still needs more studies to be fully understood. Finally, the $\Delta L/L$ values that were measured perpendicularly to the substrate material were taken for thermal transport properties investigations in our study (according to the heat flux flow).

The difference in thermal dilatation values during cooling and heating cycle was also observed. As the $\Delta L/L$ was anisotropic, consequently the dimensional changes were not distributed in a uniform way in the coating material. As a consequence microcracks could have been generated during heating and the thermal dilatation values during cooling changed. This effect was very strong for YCeSZ samples, which are more fatigue-resistant than YSZ. Another reason of the differences could have been associated to the very short length of the sample (only 2 mm) and to the instabilities during measurements. This observation is confirmed by the fact that the measurements of 10mm long sample did not show so big differences in thermal dilatation.

The measured values were in a good agreement with literature values of thermal expansion for both zirconia systems. The results of many studies suggesting that YCeSZ exhibits slightly bigger expansion than YSZ were also confirmed, especially when comparing the values determined perpendicularly to the substrate [27,35,36]. Furthermore, the data obtained for Inconel 600 (only 10-15% higher than YSZ and YSZ) were in good agreement with the literature data and values given by the nickel super alloy manufacturer.

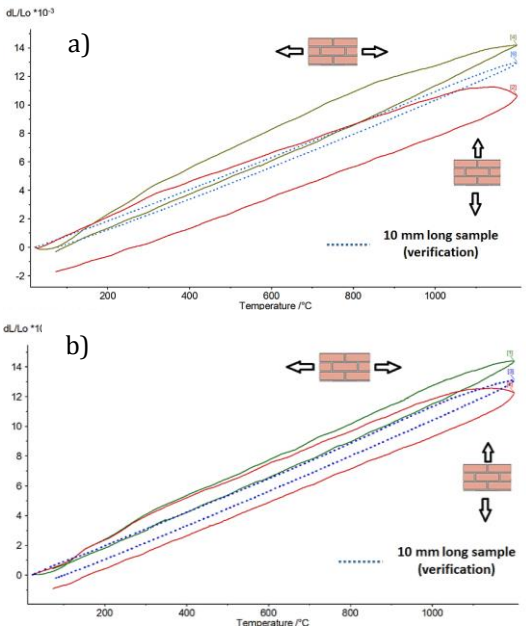

Fig. 7. Thermal expansion values of YSZ (a) and YCeSZ (b)

3.3. Thermal transport properties

The obtained values of thermal conductivity were in a range of 0.63 and 0.99 [W/m·K] for YSZ samples and between 0.82 and 1.37 [W/m·K] in the case of YCeSZ. Thermal conductivity was influenced by the coatings' porosity and their microstructure. The samples ST21 and WT101 had the highest porosity and the lowest thermal conductivity values. In the case of YCeSZ coatings the correlation is less apparent. The mallest λ values had sample AC301 at low temperatures. This sample had very low measured porosity. Low conductivity can be attributed to very fine pores. On the other hand and at high temperatures, the samples having highest porosity had the lowest thermal conductivity as well.

It was clearly visible that ytrria stabilized zirconia coatings showed much lower thermal conductivity in a whole range of temperatures comparing to yttria with ceria stabilized ones. Our previous studies showed the thermal conductivity values of YSZ and YCeSZ much more similar [37]. It should be mentioned that the coatings presented in this study were produced on Inconel substrates and that many of them were deposited by different plasma spray torches (Axial III and WSP-H 500). Moreover, the increase of thermal conductivity values at high temperatures, especially samples characterized by high porosity, was observed for a few samples as e.g. ST21 or WT101. This effect could have been caused by the radiative heat transport mechanism at high temperatures [38].

The values of thermal conductivity were much lower than that of bulk zirconia. This is typical for thermally sprayed coatings and was mentioned already in the literature [39]. But the values were also significantly lower than the reported values of EB-PVD columnar-like zirconia coatings. The coatings produced by vapor deposition methods have more homogenous and uniform microstructure but, on the other hand, they have longitudinal pores which may hamper the heat flow in the direction parallel to the substrate [40].

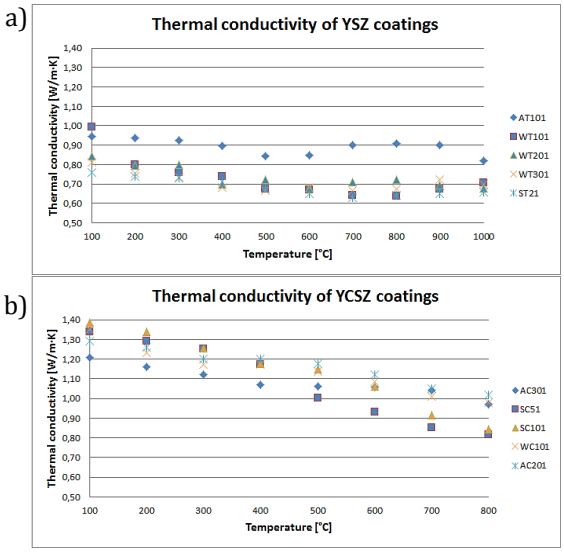

Fig. 8. Thermal conductivity values of YSZ (a) and YCeSZ coatings (b)

The following observations can be made with regard to the most important factors influencing low thermal conductivity values of SPS coatings:

- ***Porosity*** - thermal conductivity of gases is much lower than that of the ceramic materials (e.g. for air is 0.026W/m·K)[41]. So the pores can significantly decrease thermal conductivity of materials. But the shape, size, orientation and total volume of pores may also play an important here [9]. The pores parallel to the heat flow influence less thermal flux that the ones perpendicular to the flow. Furthermore, if the pores have some preferential orientation then thermal conductivity can be also anisotropic [33]. However, the quantitative analysis of pores morphology is difficult. The existing methods of direct porosity measurements, such as mercury intrusion porosimetry, are useful to find open porosity of coating. On the other hand, image analysis method is limited to a few cross-sections of one sample.
- ***Finely grained structure and scale effects*** – the mean free path of heat carriers is controlled by phonon-phonon interactions and depends on the material grain size, on the scattering by defects and on the crystallographic disorder. As described in details in our previous studies, both YSZ and YCeSZ coatings have submicrometer grain size of approximatively 500 nm [16]. Some other studies focused on SPS method used nano-suspensions, e.g. the work of Carpio et al. [42]. The size of grains would have the greatest effect on the heat flow if their size were similar size to the mean free path at phonon scattering. Consequently, thermal conductivity of such coating would drastically decreased [43]. The SPS sprayed coatings have high number of various defects that can scatter phonons and impede the heat flow[38]. Moreover, YSZ and YCeSZ ce-

ramics have internal point defects being oxygen vacancies resulting from incorporation of yttria or ceria into zirconia lattice. Finally, the implementation of big and heavy atoms (like Y or Ce) into the structure of ZrO_2 can influence thermal conductivity too [43].

The laser flash analysis (LFA) is a non-direct method of determining thermal diffusivity and has some limitations. That is why; the validation of results was made using response function method (see Fig. 9). One example of each type of coating is presented here in order to keep clarity of data. But the calculations were made for each sample in each temperature. The difference between thermal conductivity values usually did not exceed ±15%. In the case of coating WT101 and AC301, the difference was about ±20% in the lowest temperatures only. Thermal conductivity of WT101 obtained by LFA in 100°C seemed to be too high, whereas the empirical data for AC301 seemed to be too low in the temperatures between 100°C and 400°C. But generally, the results are very satisfactory and can provide an alternative to the verification of laser flash experiment by numerical simulation by finite elements method (FEM) in which the implementation of exact measurements conditions takes more time and the computations need long time. The response method is quite well-known actually and was applied to estimate thermal conductivity of different materials already. However, the FEM analysis gives more possibilities and more complex data, as in the case of our previous analysis [37].

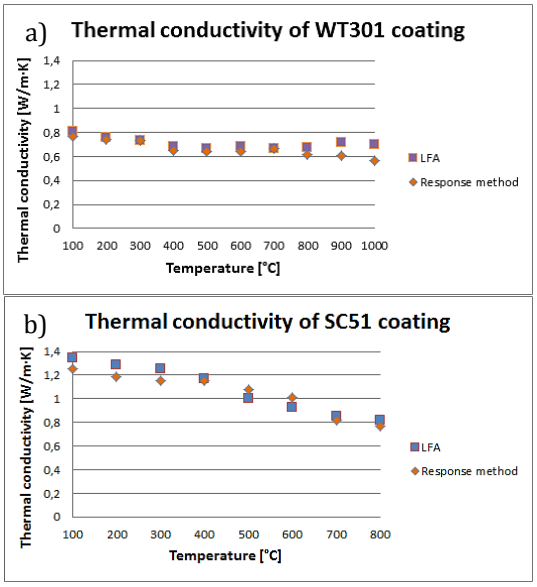

Fig. 9. Validation of thermal conductivity made by response function method. The examples for YSZ (a) and YCeSZ (b)

4. Conclusion

The main aim of the study was to characterize thermal transport properties of yttria stabilized zirconia and yttria/ceria stabilized zirconia coatings having various microstructures. The coatings had different porosity and morphology with *columnar-like* and *two-zones* microstructures. Furthermore, coatings were produced by Suspension Plasma Spraying using different spray set-ups (SG-100, Axial III and WSP-H 500).

In order to estimate thermal diffusivity and thermal conductivity of the coatings, their essential thermophysical properties were characterized and discussed first. The investigations of density showed that there is a significant difference between the values obtained for as-produced powders and crushed coatings. The analysis of specific heat capacity by DSC and rule of mixture proved that Kopp's law can be a sufficient method to evaluate *Cp* values in a wide temperature range. Whereas thermal expansion of coatings showed anisotropic appearance as the measurements were conducted in vertical and horizontal configuration. Then, thermal transport properties of zirconia coatings were analyzed using well-established LFA method. The thermal diffusivity and thermal conductivity values of the prepared SPS coatings were found to be strongly dependent on the porosity and the coating microstructure, which may be in a wide range controlled by the deposition conditions. It may be therefore expected that optimization of deposition conditions (including choice of plasma torch) may be used for tailoring of zirconia-based top coats for various potential applications. Finally, thermal conductivity values were successfully validated by the use of a so called response method, which can be an alternative for complex FEM methods.

Acknowledgements

The help of Dr. Stefan Kozerski and Dr. Leszek Łatka (both from Wroclaw University of Technology) within the spraying of zirconia coatings is thankfully acknowledged. French Embassy in Poland enabled the stay of Paweł Sokołowski at University of Limoges in frame of joint PhD "co-tutelle" program. The part of work carried out by Paweł Sokołowski was financed by the National Science Centre (Poland) in frame of grant Sonata, UMO-2013/11/D/ST8/03400. The deposition of coatings realized at IPP Prague was financed by the grant GA15-12145S "Physical aspects of plasma spray deposition from liquid feedstock".

References

[1] R.L. Jones, Thermal barrier coatings, in: K.H. Stern (Ed.), Metall. Ceram. Prot. Coat., Springer Netherlands, 1996: pp. 194–235. http://link.springer.com/chapter/10.1007/978-94-009-1501-5_8.

[2] R. Vaßen, M.O. Jarligo, T. Steinke, D.E. Mack, D. Stöver, Overview on advanced thermal barrier coatings, Surf. Coat. Technol. 205 (2010) 938–942. doi:10.1016/j.surfcoat.2010.08.151.

[3] G. Moskal, Thermal barrier coatings : characteristics of microstructure and properties, generation and directions of development of bond, J. Achiev. Mater. Manuf. Eng. Vol. 37 (2009) 323–331.

[4] U. Schulz, B. Saruhan, K. Fritscher, C. Leyens, Review on Advanced EB-PVD Ceramic Topcoats for TBC Applications, Int. J. Appl. Ceram. Technol. 1 (2004) 302–315. doi:10.1111/j.1744-7402.2004.tb00182.x.

[5] T. Sadowski, P. Golewski, Loadings in Thermal Barrier Coatings of Jet Engine Turbine Blades, Springer Singapore, Singapore, 2016.

http://link.springer.com/10.1007/978-981-10-0919-8.
[6] D.R. Clarke, and C.G. Levi, Materials Design for the Next Generation Thermal Barrier Coatings, Annu. Rev. Mater. Res. 33 (2003) 383–417. doi:10.1146/annurev.matsci.33.011403.113718.
[7] D. Stöver, C. Funke, Directions of the development of thermal barrier coatings in energy applications, J. Mater. Process. Technol. 92–93 (1999) 195–202. doi:10.1016/S0924-0136(99)00244-7.
[8] I.O. Golosnoy, A. Cipitria, T.W. Clyne, Heat Transfer Through Plasma-Sprayed Thermal Barrier Coatings in Gas Turbines: A Review of Recent Work, J. Therm. Spray Technol. 18 (2009) 809–821. doi:10.1007/s11666-009-9337-y.
[9] L. Wang, Y. Wang, X.G. Sun, J.Q. He, Z.Y. Pan, Y. Zhou, P.L. Wu, Influence of pores on the thermal insulation behavior of thermal barrier coatings prepared by atmospheric plasma spray, Mater. Des. 32 (2011) 36–47. doi:10.1016/j.matdes.2010.06.040.
[10] T. Troczynski, S. CockCroft, H. Wong, Thermal Barrier Coatings for Heat Engines, Key Eng. Mater. 122–124 (1996) 451–462. doi:10.4028/www.scientific.net/KEM.122-124.451.
[11] C. Giolli, A. Scrivani, G. Rizzi, F. Borgioli, G. Bolelli, L. Lusvarghi, Failure Mechanism for Thermal Fatigue of Thermal Barrier Coating Systems, J. Therm. Spray Technol. 18 (2009) 223–230. doi:10.1007/s11666-009-9307-4.
[12] R. Darolia, Thermal barrier coatings technology: critical review, progress update, remaining challenges and prospects, Int. Mater. Rev. 58 (2013) 315–348. doi:10.1179/1743280413Y.0000000019.
[13] R.C. Seshadri, S. Sampath, Characterization of the Deposition Formation Dynamics of Suspension Plasma Spray Coatings using In-Situ Coating Property Measurements, Proc. Int. Therm. Spray Conf. Shanghai PR China May 10 - 12 2016. (n.d.) 85–90.
[14] L. Pawlowski, Finely grained nanometric and submicrometric coatings by thermal spraying: A review, Surf. Coat. Technol. 202 (2008) 4318–4328. doi:10.1016/j.surfcoat.2008.04.004.
[15] P. Sokołowski, S. Kozerski, L. Pawłowski, A. Ambroziak, The key process parameters influencing formation of columnar microstructure in suspension plasma sprayed zirconia coatings, Surf. Coat. Technol. 260 (2014) 97–106. doi:10.1016/j.surfcoat.2014.08.078.
[16] P. Sokołowski, L. Pawłowski, D. Dietrich, T. Lampke, D. Jech, Advanced Microscopic Study of Suspension Plasma-Sprayed Zirconia Coatings with Different Microstructures, J. Therm. Spray Technol. 25 (2015) 94–104. doi:10.1007/s11666-015-0310-7.
[17] P. Sokołowski, P. Nylén, R. Musalek, D. Dietrich, T. Lampke, L. Łatka, S. Kozerski, L. Pawłowski, The microstructural studies of suspension plasma sprayed zirconia coatings with the use of high-energy plasma torches, Surf. Coat. Technol., submitted for publication (n.d.).
[18] L.C. Thomas, Why Modulated DSC®? ; An Overview and Summary of Advantages and Disadvantages Relative to Traditional DSC, TA Instruments Technical Paper, 2005.
[19] R.D. Cowan, Pulse Method of Measuring Thermal Diffusivity at High Temperatures, J. Appl. Phys. 34 (1963) 926–927. doi:10.1063/1.1729564.
[20] T. Baba, N. Taketoshi, Analysis of Thermal Diffusion in Multi-layer Thin Films by a Response Function Method, in: Eds; J. B. Saulnier, D. Lemonnier, and J. -P. Bardon, Poitiers, France, 1998: pp. 285–292.
[21] B.K. Jang, M. Yoshiya, N. Yamaguchi, H. Matsubara, Evaluation of thermal conductivity of zirconia coating layers deposited by EB-PVD, J. Mater. Sci. 39 (n.d.) 1823–1825. doi:10.1023/B:JMSC.0000016195.72123.77.
[22] J.-F. Bisson, D. Fournier, M. Poulain, O. Lavigne, R. Mévrel, Thermal Conductivity of Yttria–Zirconia Single Crystals, Determined with Spatially Resolved Infrared Thermography, J. Am. Ceram. Soc. 83 (2000) 1993–1998. doi:10.1111/j.1151-2916.2000.tb01502.x.
[23] R.P. Ingel, D.L. Iii, Lattice Parameters and Density for Y2O3-Stabilized ZrO2, J. Am. Ceram. Soc. 69 (1986) 325–332. doi:10.1111/j.1151-2916.1986.tb04741.x.
[24] D. Taylor, Thermal expansion data: II binary oxides with the fluorite and rutile structures MO2 and the antifluorite structure M2O, Trans. J. Br. Ceram. Soc. (1984).
[25] T.M.V.R. de Barros, R.C. Santos, A.C. Fernandes, M.E.M. da Piedade, Recent Advances in Thermal Analysis and CalorimetryAccuracy and precision of heat capacity measurements using a heat flux differential scanning calorimeter, Thermochim. Acta. 269 (1995) 51–60. doi:10.1016/0040-6031(95)02706-8.
[26] D.R. Askeland, P.P. Fulay, W.J. Wright, The Science and Engineering of Materials, SI Edition, Cengage Learning, 2011.
[27] G. Di Girolamo, C. Blasi, A. Brentari, M. Schioppa, Microstructure and thermal properties of plasma-sprayed ceramic thermal barrier coatings — it, Energ. Ambiente E Innov. 1–2 (2013) 69–76.
[28] S. Kozerski, L. Łatka, L. Pawlowski, F. Cernuschi, F. Petit, C. Pierlot, H. Podlesak, J.P. Laval, Preliminary study on suspension plasma sprayed ZrO2 + 8 wt.% Y2O3 coatings, J. Eur. Ceram. Soc. 31 (2011) 2089–2098. doi:10.1016/j.jeurceramsoc.2011.05.014.
[29] C.C. Berndt, H. Herman, Anisotropic Thermal Expansion Effects in Plasma-Sprayed ZrO2-8%-Y2O3 Coatings, in: W. Smothers (Ed.), Proc. 7th Annu. Conf. Compos. Adv. Ceram. Mater. Ceram. Eng. Sci. Proc., John Wiley & Sons, Inc., 1983: pp. 792–801. http://onlinelibrary.wiley.com/doi/10.1002/9780470320167.ch9/summary (accessed July 8, 2016).
[30] J. Ilavsky, G.G. Long, A.J. Allen, L. Leblanc, M. Prystay, C. Moreau, Anisotropic microstructure of plasma-sprayed deposits, J. Therm. Spray Technol. 8 (n.d.) 414–420. doi:10.1361/105996399770350368.
[31] A.S.M. Ang, C.C. Berndt, Investigating the anisotropic mechanical properties of plasma sprayed yttria-stabilised zirconia coatings, Surf. Coat. Technol. 259, Part C (2014) 551–559. doi:10.1016/j.surfcoat.2014.10.031.
[32] W.D.C. Jr, W.D. Callister William D., Materials Science and Engineering: An Introduction, 7th Edition Wiley Plus Set, John Wiley & Sons, Limited, 2007.
[33] I. Sevostianov, M. Kachanov, Anisotropic thermal conductivities of plasma-sprayed thermal barrier coatings in relation to the microstructure, J. Therm. Spray Technol. 9 (n.d.) 478–482. doi:10.1007/BF02608549.
[34] E. Le Bourhis, Appendix 3: Thermal Expansion and Elasticity, in: Glass, Wiley-VCH Verlag GmbH & Co. KGaA, 2007: pp. 271–274. http://onlinelibrary.wiley.com/doi/10.1002/9783527617029.app3/summary (accessed July 8, 2016).
[35] C.H. Lee, H.K. Kim, H.S. Choi, H.S. Ahn, Phase transformation and bond coat oxidation behavior of plasma-sprayed zirconia thermal barrier coating, Surf. Coat. Technol. 124 (2000) 1–12. doi:10.1016/S0257-8972(99)00517-4.
[36] P.J. Huang, J.J. Swab, P.J. Patel, W.S. Chu, Evaluation of CeSZ Thermal Barrier Coatings for Diesels - Thermal Spray Society, in: ASM International, 2000: pp. 1179–1183. http://www.asminternational.org/web/tss/materials-resources/-/journal_content/56/10192/CP2000ITSC1179/PUBLICATION;jsessionid=667CC961179707160114AF3138E2

0F1B?p_p_id=56_INSTANCE_0000&p_p_lifecycle=0&p_p_state=maximized&p_p_mode=view (accessed July 8, 2016).
[37] P. Sokołowski, L. Łatka, L. Pawłowski, A. Ambroziak, S. Kozerski, B. Nait-Ali, Characterization of microstructure and thermal properties of YCSZ coatings obtained by suspension plasma spraying, Surf. Coat. Technol. 268 (2015) 147–152. doi:10.1016/j.surfcoat.2014.10.006.
[38] D.R. Clarke, S.R. Phillpot, Thermal barrier coating materials, Mater. Today. 8 (2005) 22–29. doi:10.1016/S1369-7021(05)70934-2.
[39] B.D. Sartwell, R. McPherson, A review of microstructure and properties of plasma sprayed ceramic coatings, Surf. Coat. Technol. 39 (1989) 173–181. doi:10.1016/0257-8972(89)90052-2.
[40] D.D. Hass, A.J. Slifka, H.N.G. Wadley, Low thermal conductivity vapor deposited zirconia microstructures, Acta Mater. 49 (2001) 973–983. doi:10.1016/S1359-6454(00)00403-1.
[41] C.B. Carter, M.G. Norton, Ceramic Materials: Science and Engineering, Springer Science & Business Media, 2007.
[42] P. Carpio, E. Rayón, L. Pawłowski, A. Cattini, R. Benavente, E. Bannier, M.D. Salvador, E. Sánchez, Microstructure and indentation mechanical properties of YSZ nanostructured coatings obtained by suspension plasma spraying, Surf. Coat. Technol. 220 (2013) 237–243. doi:10.1016/j.surfcoat.2012.09.047.
[43] W.B. Gong, C.K. Sha, D.Q. Sun, W.Q. Wang, Microstructures and thermal insulation capability of plasma-sprayed nanostructured ceria stabilized zirconia coatings, Surf. Coat. Technol. 201 (2006) 3109–3115. doi:10.1016/j.surfcoat.2006.06.041.00